X-661-71-1
PREPRINT

COMPOSITION AND SPECTRA OF HIGH ENERGY COSMIC RAYS

A PROPOSAL FOR AN ORBITING LABORATORY FOR THE HEAO

JANUARY 1971

GSFC — GODDARD SPACE FLIGHT CENTER —
GREENBELT, MARYLAND

COMPOSITION AND SPECTRA OF HIGH ENERGY COSMIC RAYS

A PROPOSAL FOR AN ORBITING LABORATORY FOR THE HEAO

BY

J. F. ORMES

AND

V. K. BALASUBRAHMANYAN

NASA/GODDARD SPACE FLIGHT CENTER

T. BOWEN

UNIVERSITY OF ARIZONA

R. W. HUGGETT

LOUISIANA STATE UNIVERSITY

T. A. PARNELL

NASA/MARSHALL SPACE FLIGHT CENTER

AND

K. PINKAU

MAX PLANCK INSTITUT

The authors have been assisted in the preparation of this proposal by the following individuals:

C. J. CRANNEL, G. GUNTHER
W. V JONES, U. POLLVOGT, R. RAMATY,
M. J. RYAN, AND W. K. H. SCHMIDT

MAY 1970

CONTENTS

LIST OF ILLUSTRATIONS

ACKNOWLEDGMENTS

It is almost impossible to express proper appreciation to the many individuals who assisted directly and indirectly in the preparation of the proposal. Without their help, ideas and suggestions, it would have been a far more formidable task. It is hoped that those individuals will accept collectively our most sincere thanks.

In particular we would like to thank D. Fitzpatrick who wrote the Mechanical Section and his staff for their excellent job with the design studies; C. Cancro, H. White, D. Lokerson, J. Laws, and D. Stilwell for their electrical engineering support; L. Tyler for her assistance in Monte Carlo calculations; H. Schwille for his work with proportional counters; J. Watts for ion chamber resolution calculations; R. Ross and C. Ehrmann for advice regarding spark chambers; R. Price who has organized the figures and references; M. Ewing for her typing and patience with our corrections; and M. Becker and her staff for preparation.

We would especially like to thank F. B. McDonald for his ideas, suggestions and encouragement in writing this proposal and making viable an active program in experimental high energy astrophysics by his enthusiastic guidance and leadership.

COMPOSITION AND SPECTRA OF HIGH ENERGY COSMIC RAYS

A Proposal for an Orbiting Laboratory for the HEAO

ABSTRACT

The presently detectable galactic cosmic radiation extends in energy from about 10^7 eV to 10^{20} eV and in charge from Z = 1 to about 100. The energy region from 10^{10} to 10^{14} eV is a large but little studied segment of the cosmic ray spectrum. An experiment to investigate charged cosmic ray primaries in this energy range is proposed for the HEAO satellites. An instrument based upon our present balloon flight programs, has been designed to determine the intensities of protons, electrons, alpha particles, and heavier nuclei as a function of energy. With a satellite lifetime of one year, searches will be made for directional anisotropies and time variations of each component. These results will be used to study the cosmic ray source compositions, acceleration processes, propagation, and lifetime in the interstellar medium.

The experiment consists of three major sections: (a) charge identification, (b) trajectory definition and (c) energy measurement. The charge identification system uses two organic scintillators, a plastic Cerenkov radiator, an inorganic CsI scintillator, and a pulse ion chamber system. This redundancy of charge-sensitive detectors used in conjunction with the directional information provides

a measurement of the charge to within $z \pm 1/2$ through the iron region. Particle direction is determined by wire grid spark chambers and by scintillator wedges within the spectrometer itself. Energy is measured by an ionization spectrometer consisting of a tungsten-plastic scintillator sandwich ~5 interaction mean free paths thick. Throughout the energy range, the spectrometer determines energy to within ±15% which is considered adequate for meeting the scientific objectives. The spectrometer will be calibrated at 5×10^{11} eV at the National Accelerator Laboratory. Electrons will be separated from protons by the rapid development of the electromagnetic cascades in CsI scintillators at the top of the spectrometer. The payload will weigh 6000 lbs. with a geometric factor of 500 cm^2 ster for the spectrometer and 2500 cm^2 ster for the charge detection system. The data system will select events on a priority basis and generate 8×10^3 bits/sec. The entire electronics system will have redundant units for failsafe operation. Engineering design, data analysis plans, management aspects, possible second generation developments, and a description of the relevant scientific background are presented.

COMPOSITION AND SPECTRA OF HIGH ENERGY COSMIC RAYS

A Proposal for an Orbiting Laboratory for the HEAO

I. INTRODUCTION

A. SCIENTIFIC OBJECTIVES

High Energy Astrophysics is a new discipline which recognizes the interrelationship between studies in traditional optical astronomy and the new fields of radio, infra-red, x-ray and γ-ray astronomy and cosmic radiation. It is particularly appropriate that many of these fields should come together to participate in the High Energy Astronomy Observatory satellite.

In order to suggest some of the exciting results which may come from this satellite, the remarks of van de Hulst opening a talk before a colloquium in Bombay in 1968 are particularly appropriate (Daniel et al., 1968).

> "The astrophysicists are extremely clever in explaining things, in retrospect. They might have predicted stars - but of course they had seen them before. But they have not predicted the solar corona, solar flares, cosmic rays, magnetic fields, non-thermal radio emission, x-ray sources, quasars, pulsars - and there are many more things which have not been predicted. Actually, the word cosmic rays, at the time the name was given, was a curious double confession of ignorance - cosmic meaning that we did not know from where they were coming and rays meaning that we did not know what they were."

We now know what cosmic rays are, and we have begun to get a feeling for the kind of astrophysical information they can provide us. Cosmic rays have been observed with 10^9 times the energy of the most energetic particles which

can be accelerated by man made machines. These cosmic rays carry information about the most energetic processes which occur in nature. Their origin is quite possibly connected with the recently discovered pulsars, the neutron star remnants of supernova explosions or with the supernova explosions themselves; but the acceleration mechanism is not yet understood.

The galaxy is filled with $\sim 1\ eV/cm^3$ in cosmic rays and this is sufficient energy to play an important role in the structure and stability of the galaxy (Parker, 1965). Of particular interest is whether cosmic rays are confined to the galactic disk or whether they fill the elusive galactic halo. Some cosmic rays may pervade the local super cluster of galaxies or even fill all of intergalactic space.

A study of the details of the charge composition presents an exciting possibility of looking at a sample of material directly from a thermonuclear furnace. This aspect of the astrophysics of cosmic rays has become viable only recently with advances in experimental techniques which allow sufficient charge resolution to uniquely identify the cosmic rays up to iron and beyond. The modification of the charge spectrum in its interstellar travel is now being understood well enough to allow the source composition of cosmic rays to be derived.

The cosmic ray electrons are also of interest and are presently the subject of intensive study. Their spectra should reflect interactions with the 3° black-body

radiation (presumably left over from the primordial big bang), with the galactic magnetic fields, and with the intense infrared radiation recently discovered.

As can be seen from this all too brief discussion, the study of cosmic rays and the models for their origin, acceleration, and propagation is essential to the understanding of a wide range of cosmological phenomena.

During the past decade, the charge composition and energy spectra have been the subject of extensive studies at low energies. Figure I-1 shows some representative information available in the energy range 10^7 to 5×10^{10} eV. The models relating cosmic ray studies to astrophysical questions have been evolving from these low energy studies. However, the interpretations are confused by our lack of knowledge at higher energies. Many of the questions raised by these models can only be answered by an extension of detailed measurements above 10^{10} eV. An experiment to study the composition and spectra of the cosmic radiation between 10^{10} and 10^{14} eV is outlined in this proposal.

In this energy range the spectra are characterized by intensities

$$dN/dE = k/E^{\gamma} \quad (\text{where } \gamma \approx 2.5)$$

which decrease rapidly with increasing energy.

This is illustrated in Figure I-2 where the spectrum of all charged, nuclear particles is shown. At energies above 10^{13} eV, data are obtained from extensive

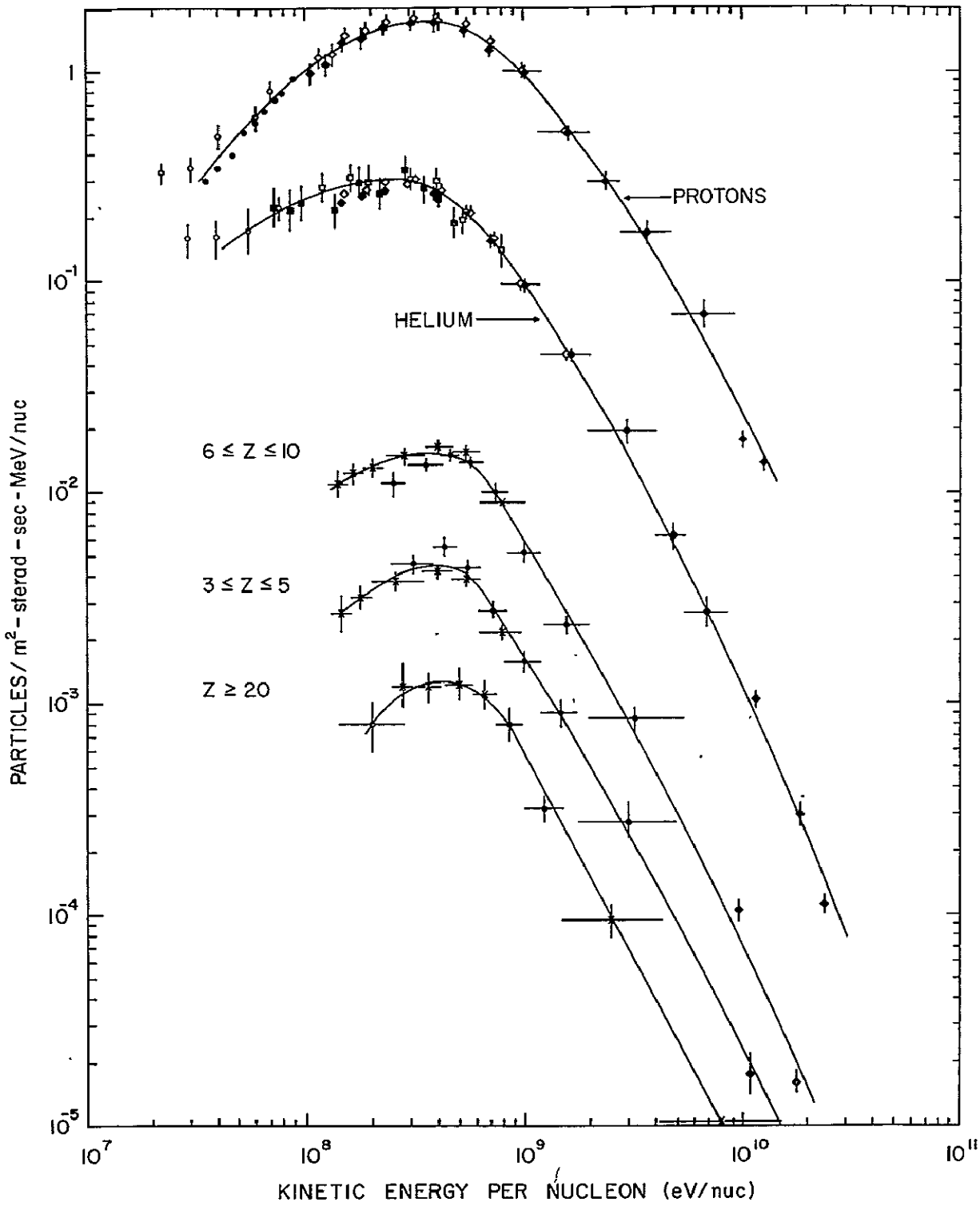

Figure I-1. Experimental data on the differential spectra for nucleons with charge Z = 1 through Z ≥ 20 in the energy range 10^7 to 5×10^{10} eV.

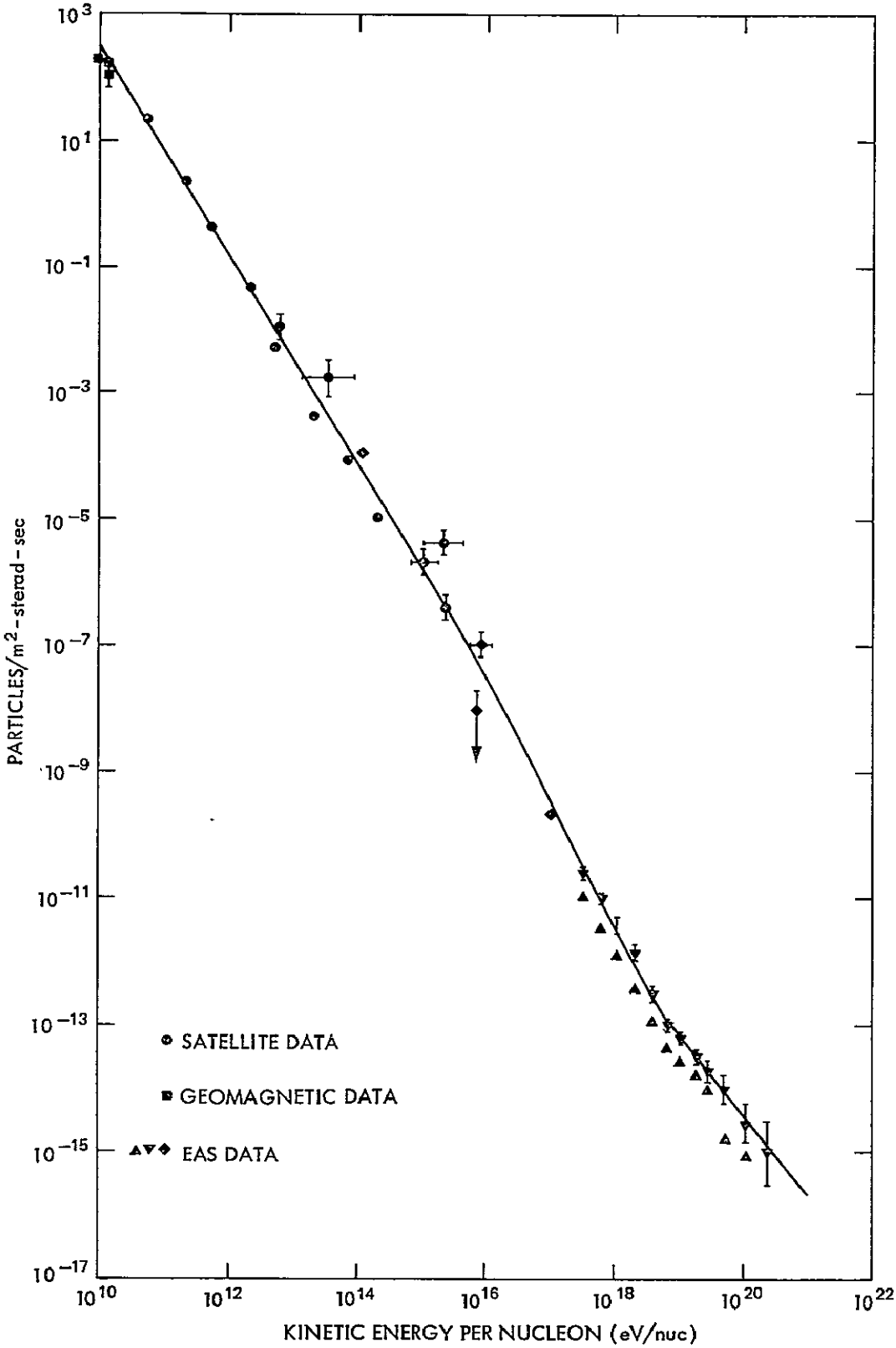

Figure I-2. Energy spectrum of all cosmic ray particles from 10^{10} to 10^{20} eV.

air shower measurements. Note the apparent steepening of the spectrum in the range 10^{14} to 10^{15} eV. This might be due to a transition between regions of galactic and extragalactic particles, or it could indicate a change in composition of the galactic primaries. Since particles of 10^{17} eV or more will escape from the galaxy quite readily, the highest energy particles are probably of extragalactic origin.

The energy region from 10^{10} to 10^{14} eV represents a little studied segment of the cosmic ray spectrum. The data which do exist in this energy range are shown in Figure I-3. The Russians (Grigorov et al., 1969) pioneered in this area on their series of "proton" satellites, utilizing an ionization "calorimeter" for energy measurement. Their experiment gives no directional information, however, and only identifies protons. Pinkau et al. (1969) have performed balloon experiments on the energy spectra of protons and alpha particles with improved techniques. Neither of these experiments provides information on the heavier nuclei. The emulsion results of Kaplon and Ritson (1952) and Lal (1953) are also shown, but there are large uncertainties in both the fluxes and energies in these measurements. More recent emulsion results from the Brawley stack by Koshiba et al. (1968) are available on the spectra of nuclei with $Z \geq 6$. As can be seen from the figure, large discrepancies exist between different measurements.

As shown in detail in subsequent sections, astrophysical questions can best be answered from a determination of both the charge and energy of each particle.

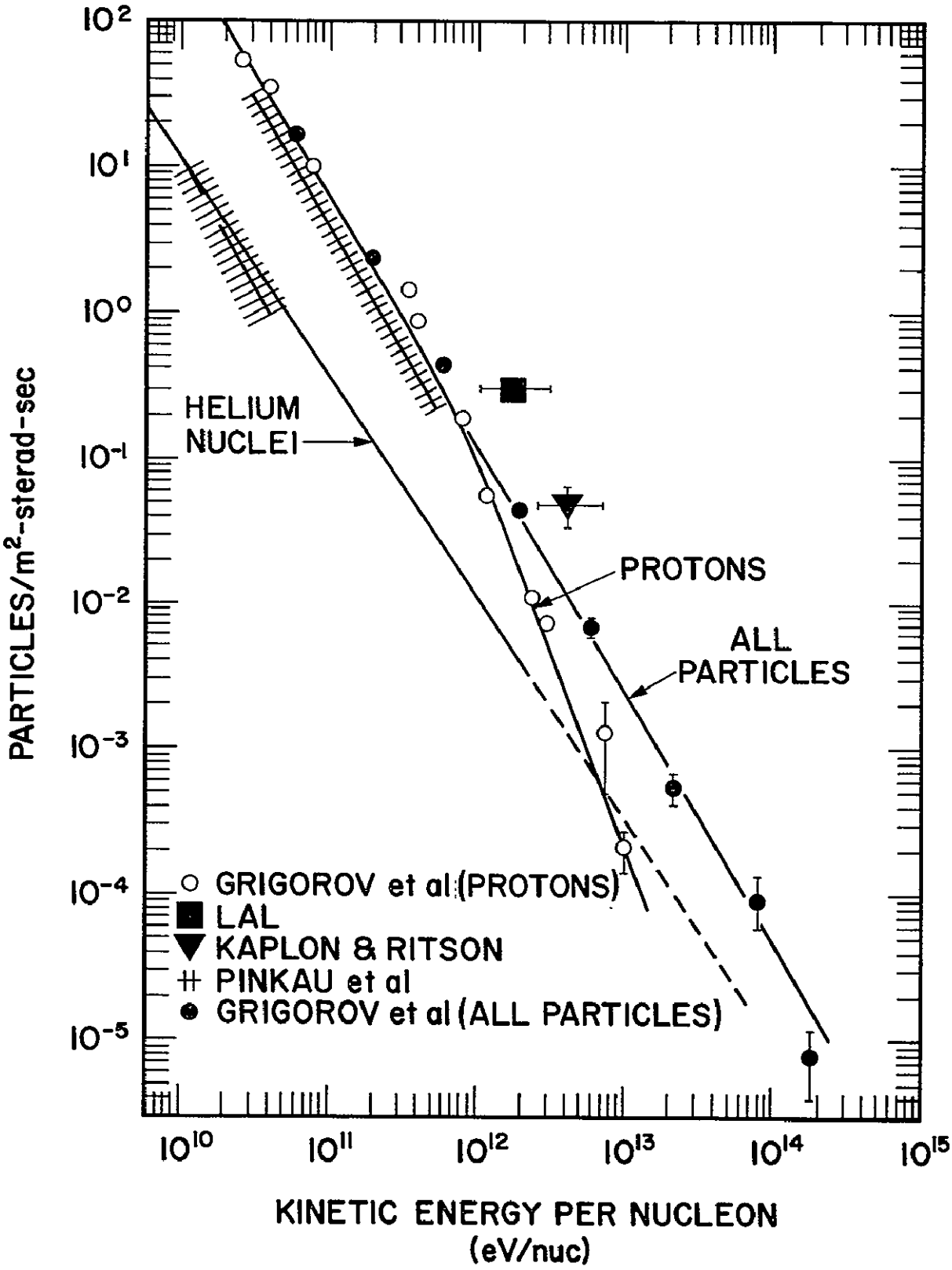

Figure I-3. Existing data on the energy spectrum of protons, Helium nuclei and all particles in the energy range $10^{10} - 10^{14}$ eV, the range to be studied in this experiment.

This objective is obtainable using state of the art techniques and represents an improvement and extension of the presently available measurements.

The primary objectives of the program are:

(1) to determine the energy distribution of the primary cosmic radiation from 10^{10} to 10^{14} eV;

(2) to determine the charge composition through iron and beyond; and

(3) to measure the electron spectrum for energies from 10^{10} to 10^{13} eV.

In addition, without any increased experimental complexity, it will be possible to use the data for studying anisotropies in the arrival direction of the incident electrons, protons, or heavier nuclei and for studying time variations at energies above 10^{10} eV.

B. EXPERIMENTAL TECHNIQUES

The objectives will be achieved by measuring (a) the charge, (b) the arrival direction, and (c) the energy of each incident particle. The measurements of these parameters over the entire range of energies and charges will all be made with a single instrument. This has the advantage of reducing effects due to systematic errors in determining the shape of the energy spectrum and in obtaining the relative fluxes of the different charge components. A schematic diagram of the proposed instrument is shown in Figure I-4.

The steep spectra of cosmic ray primaries are characterized by low fluxes at high energies. In Table I-1 the number of events expected from the proposed

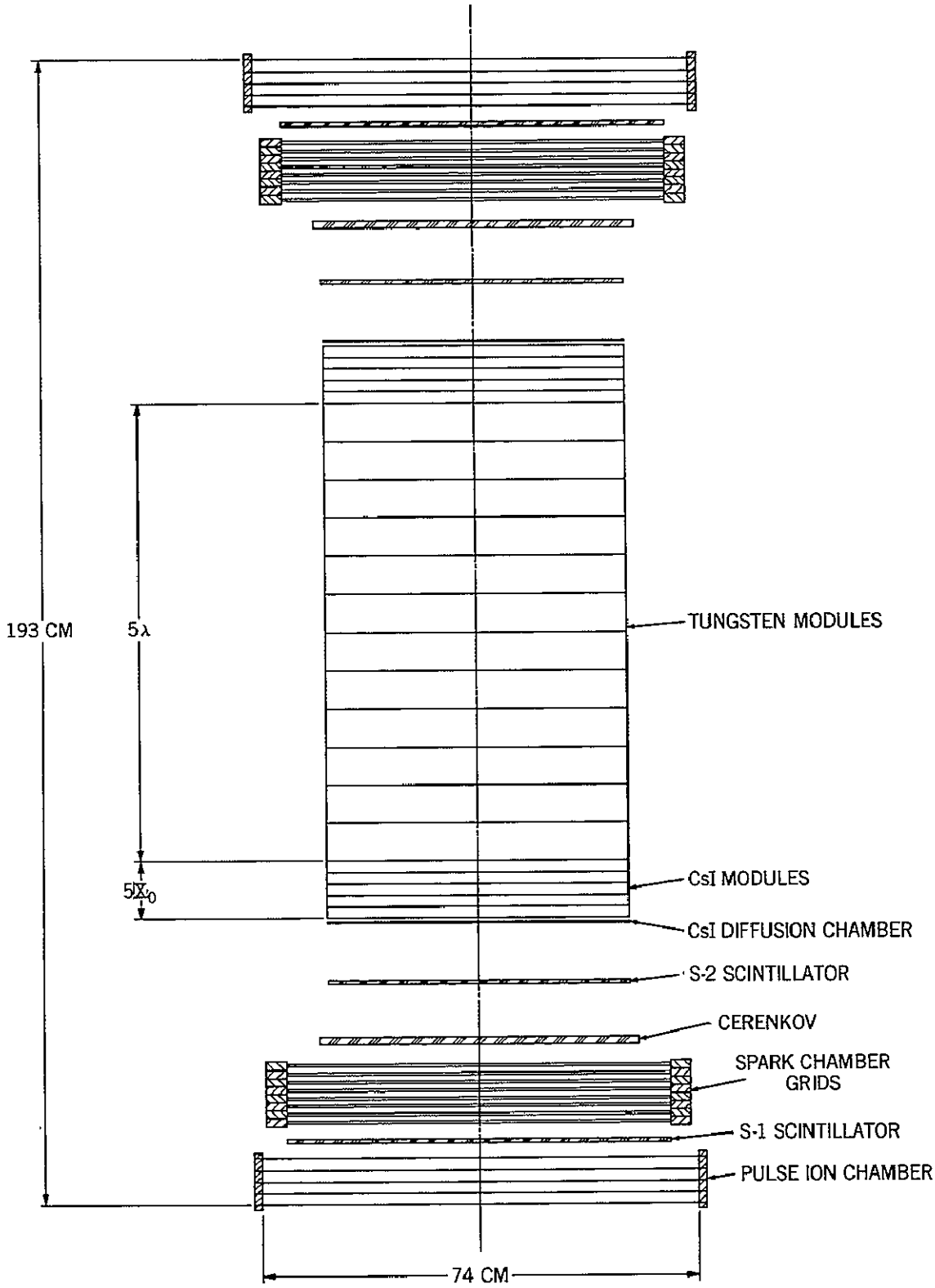

Figure I-4. Schematic cross section, high energy cosmic ray experiment.

Table I-1

EXPECTED TOTAL NUMBER OF EVENTS WITH

ENERGIES GREATER THAN E (eV/NUC)

Particle Type	10^{10} eV/nuc	10^{11}	10^{12}	10^{13}	10^{14}	10^{15}
Protons	2.5×10^{8}	6×10^{6}	1.6×10^{5}	4×10^{3}	80	2
Alphas	$\times10^{7}$	6×10^{5}	2×10^{4}	5×10^{2}	20	0.4
L ($3 \leq Z \leq 5$)	2×10^{5}	5×10^{3}	100	4		
M ($6 \leq Z \leq 9$)	6×10^{5}	1.6×10^{4}	400	10	0.2	
LH ($10 \leq Z \leq 14$)	2×10^{5}	7.5×10^{3}	100	4		
MH ($15 \leq Z \leq 19$)	2×10^{4}	600	14	0.4		
VH ($20 \leq Z \leq 29$)	6×10^{4}	1.6×10^{3}	40	1.0		
Electrons (Anand et al. (1968))	1.2×10^{7}	2.5×10^{5}	6×10^{3}	150	4	
Electrons (Marar et al. (1969))	5×10^{5}	5×10^{3}	50	0.6		

Geometrical Factor { Nucleons: 500 cm^2-ster; Electrons: 2000 cm^2-ster }

Satellite Lifetime 1 year

experiment are shown for various energies. The calculations were based on an exposure factor determined by the indicated geometry factors and a satellite lifetime of 1 year. The upper limits in energy are determined by statistical accuracy rather than by any limitation of the techniques employed.

Particle charge is measured by a combination of two plastic scintillators, a Cerenkov detector, a pulse ion chamber system, and CsI (T1) layers, all of which produce signals proportional to the square of the particle charge (Z^2) at relativistic velocities. Multiple measurements are used to eliminate background and to reduce the problem of statistical fluctuations in the signal output. Each detector is optimized for a certain charge range such that redundant measurements can be obtained over the range Z = 1 to 100.

The trajectory of each particle is determined by wire spark chambers or proportional counters and by wedge shaped scintillators in the ionization spectrometer. From calibrations, any variations of response with position and direction will be known enabling the desired charge resolution and energy accuracy to be attained. In addition, anisotropies in the arrival directions can be studied.

Energy of the particles is measured with the ionization spectrometer, which consists of alternating layers of dense material and plastic scintillators. Nucleons enter the spectrometer where they initiate nuclear cascades in which charged hadrons and neutral pions are produced. The neutral pions decay into gamma rays and subsequently develop electromagnetic cascades. The hadrons continue until they interact again, so that the process repeats itself until most of the energy is contained in electromagnetic cascades. The light signals from the scintillators are proportional to the total energy deposited through ionization loss in the scintillators

and hence to the energy of the incident particle. High energy electrons initiate electromagnetic cascades at their point of incidence on the spectrometer, and their total energy is also determined from the energy deposited in the scintillators.

The characteristic development of the cascades helps to distinguish between electrons and nuclear particles. The top of the spectrometer consists of 5 layers of CsI(Tl), each one-radiation length thick; the pulse height from each layer is recorded. Since all the energy deposited in this totally active section of the spectrometer is visible, the purely electromagnetic showers will be readily separated from those showers induced by protons masquerading as electrons.

The properties of the nuclear interactions at high energies can be studied for those nucleons which interact in the CsI(Tl) layers by observing the response of the individual layers of CsI(Tl) in conjunction with the response of the tungsten spectrometer.

These methods have been briefly outlined here, and are discussed in detail in the body of the proposal. It is shown that the proposed techniques are more than adequate to attain the stated objectives. Alternative techniques are discussed where appropriate with an attempt to show why the indicated choice was made.

C. STATE OF DEVELOPMENT

A start toward these objectives using balloon-borne instrumentation has been made by several groups. The complete objectives can be met only by a satellite experiment due to the following considerations:

(1) the very low fluxes demand large area detectors and long exposure times;

(2) the corrections for, and the background from, the overlying atmosphere are removed; and

(3) the energy measurement technique requires heavy payloads, which are at the limit of present day balloon technology.

A heavy-payload, scientific satellite such as the High Energy Astronomy Observatory (HEAO) provides an excellent opportunity to perform this experiment.

To take advantage of this ideal opportunity, groups at Max Planck Institute, Louisiana State University, Goddard Space Flight Center, Marshall Space Flight Center and The University of Arizona have agreed to collaborate in this effort. Each group brings a unique capability to the collaboration. The Max Planck Institute and Louisiana State University have considerable experience in experimentation using ionization spectrometers and spark chambers. They have flown an instrument on balloons and calibrated that instrument at the AGS at Brookhaven. They have also done extensive Monte Carlo calculations investigating the properties of ionization spectrometers. L.S.U. is also operating a large spectrometer at mountain altitudes. The Goddard group has considerable experience in studying the composition of the heavy nuclei. They are currently involved in flying a preliminary version of the proposed experiment on balloons.

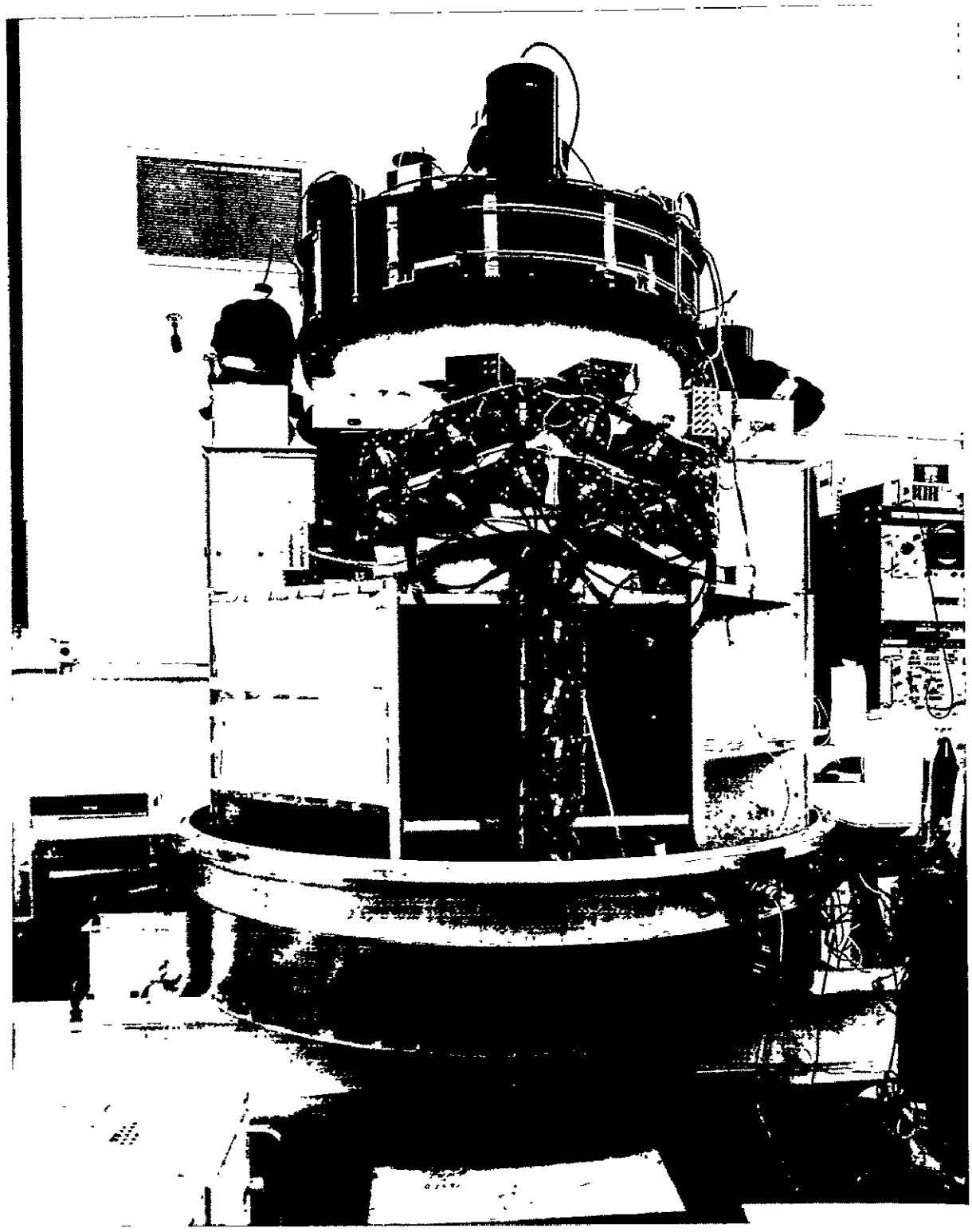

Figure I-5. Photograph of balloon engineering prototype.

Marshall Space Flight Center is working on large area gas filled ion chambers and proportional counters to be utilized in this experiment. The University of Arizona group is active in the area of high energy nuclear physics. They are presently involved in a mountain top experiment looking for fractionally charged "quarks."

This proposal is based upon the work of these several groups. A photograph of a balloon version of the experiment is shown in Figure I-5. It was built as an engineering prototype of a satellite version (see Appendix 3). Most of the subsystems have flown on balloons and have operated successfully. It will be calibrated at Brookhaven this summer and will be flown on a large balloon this fall. Critical existing items such as spark chambers, charge detectors, and electronic circuits are described where appropriate in the text. Based upon flight experience it should be possible to meet the rigid HEAO delivery schedules.

The project will be supervised by a council consisting of the six co-investigators. The principal investigator will act as chairman of this council. This Supervisory council will insure that the scientific objectives are met and will control the division of effort among the various groups. The responsibility for delivering the completed instrument will rest with the Goddard High Energy Cosmic Ray Group. The experiment will be built in modular form and integrated at Goddard Space Flight Center. The supervisory arrangements are discussed in more detail in a separate management proposal.

II. SCIENTIFIC BACKGROUND AND RELATED OBSERVATIONS

A. ENERGY SPECTRA

One of the most striking features of the cosmic radiation is the enormous range of energies over which cosmic ray primaries have been detected. Though models of the production mechanisms and transport processes of these particles have been devised, the observed energy spectra are by no means fully understood. In order to develop and test theoretical descriptions of the sources, acceleration mechanisms, and propagation, accurate knowledge of the shape of the energy spectra is particularly important.

At low energies, considerable spectral data are available from satellite and balloon experiments; these are shown in Figure II-1 (Fan et al., 1968; Hagge et al., 1968; Ormes and Webber, 1968). However, because of the effects of solar modulation, the interstellar energy spectra of cosmic rays have not been determined unambiguously at low energies. As a result, these data are difficult to use in interpreting models of cosmic ray production and interactions in the interstellar medium.

Above 10^{10} eV solar modulation should not be a problem in interpreting results. The presently available data are shown in Figure II-2. Over this wide range of energy, the differences in the techniques used to obtain data have made

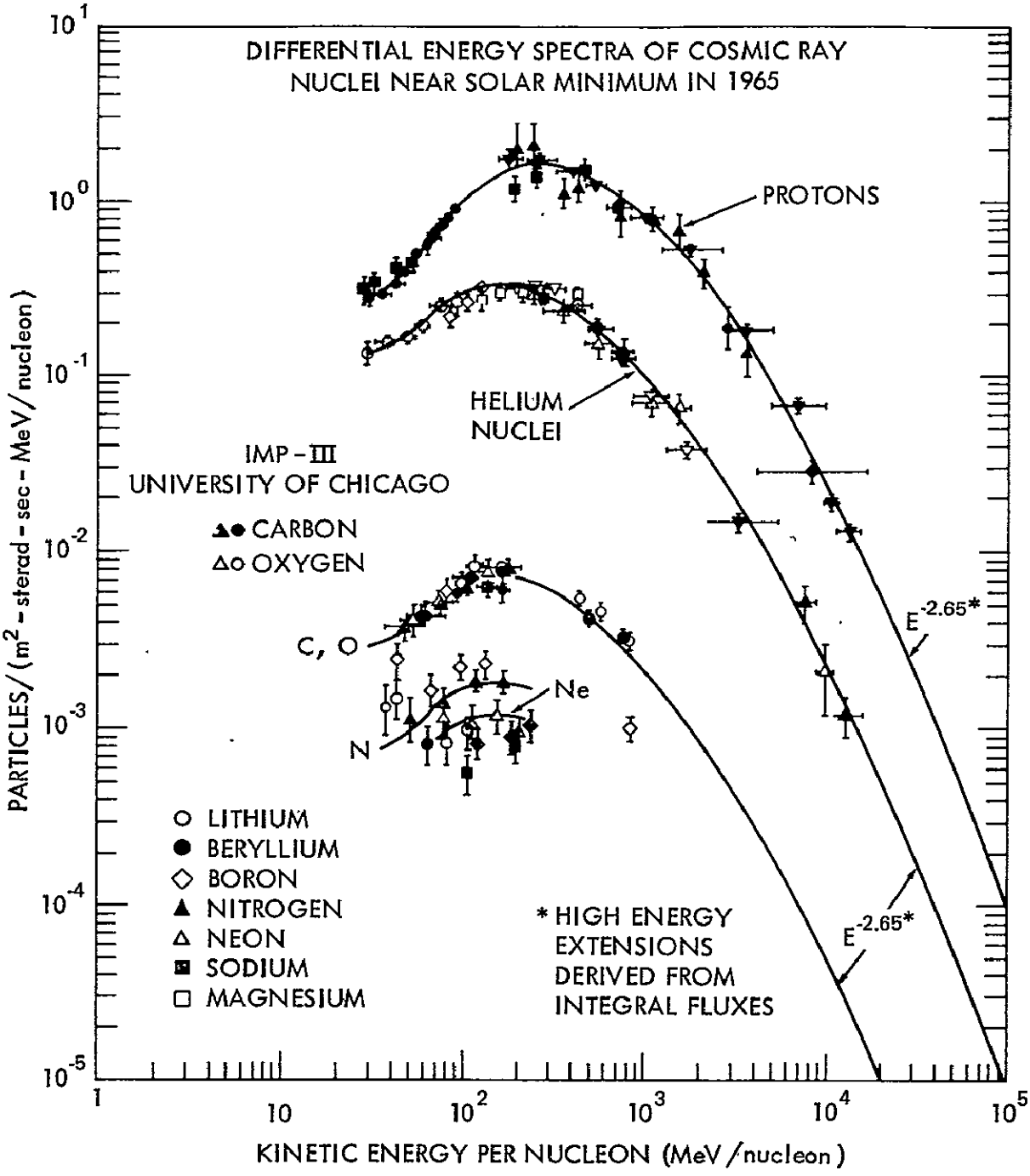
DIFFERENTIAL ENERGY SPECTRA OF COSMIC RAY NUCLEI NEAR SOLAR MINIMUM IN 1965
PROTONS
HELIUM NUCLEI
IMP - III
UNIVERSITY OF CHICAGO
CARBON
OXYGEN
C, O
Ne
N
LITHIUM
BERYLLIUM
BORON
NITROGEN
NEON
SODIUM
MAGNESIUM
* HIGH ENERGY EXTENSIONS DERIVED FROM INTEGRAL FLUXES
E^-2.65*
E^-2.65*
PARTICLES/(m^2 - sterad - sec - MeV/nucleon)
KINETIC ENERGY PER NUCLEON (MeV/nucleon)

Figure II-1.

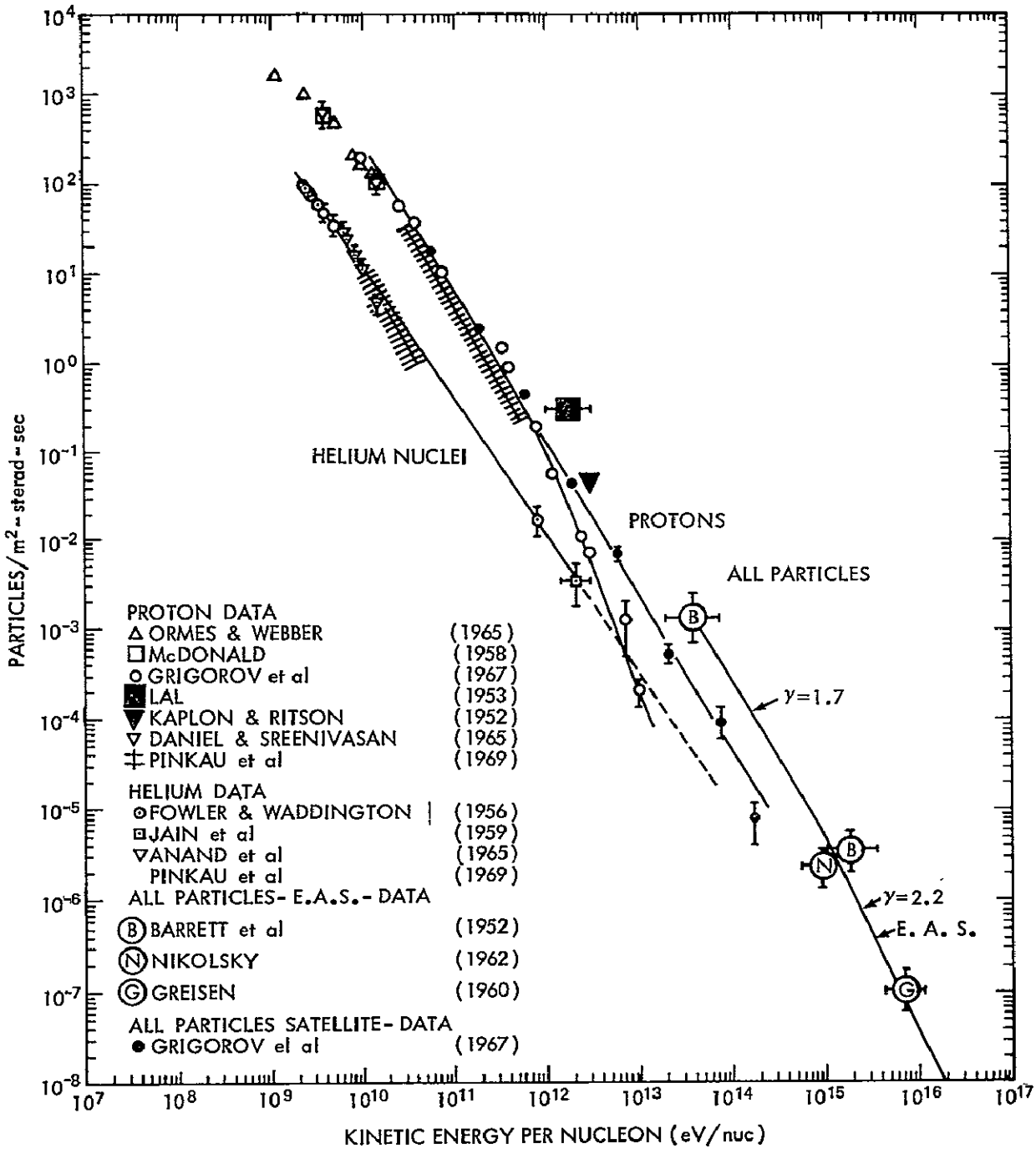

Figure II-2. Existing information on the energy spectrum up to 10^{16} eV. The discrepancies may be attributable to the different techniques used for the measurements.

intercomparisons uncertain. Near 10^{10} eV, the earth's magnetic field is used as a spectrometer. In the range 10^{10} to 10^{14} eV, the initial results have been obtained from nuclear emulsion experiments. More recently ionization spectrometers have provided more extensive data. Above 10^{14} eV, extensive air shower measurements are the only practical technique. Among these various data, there are large discrepancies.

The heavy nuclei are an important constituent of the cosmic rays, but very little direct information is available on these nuclei above 5×10^{10} eV. This is due primarily to the technical difficulty of measuring the low fluxes of these particles at high energies. The intensity is known to decrease rapidly with increasing energy, so that much larger equipment and much longer exposures are needed to extend the energy spectra.

Grigorov et al. (1969) on the "proton" series of satellites and Pinkau et al. (1969) with balloons have attempted to extend the measurements beyond 3×10^{10} eV using ionization spectrometers. The results of MPI-LSU are confined to protons and He nuclei and are consistent with a constant exponent of 1.75 for both components. For protons, the measurement extends from 30 to 500 GeV and the He nuclei from 10 to 40 GeV/nucleon. Grigorov's measurements resolve protons but do not identify any other charge components. His data extend up to $\sim 10^{13}$ eV for protons and $\sim 10^{14}$ eV for all particles. Grigorov's most recent results for protons are consistent with MPI-LSU's in the regions of overlap, but

indicate an unexpected change in the slope of the proton spectrum at 10^{12} eV. His spectrum for all particles continues with nearly constant exponent. These results have not been confirmed by any other direct measurement and are in sharp disagreement with the estimates of primary spectra and charge composition from extensive air shower (EAS) experiments (Rogers et al., 1969; Bradt et al., 1965; Brownlee et al., 1969; and Rappaport and Bradt, 1969). These EAS measurements indicate that a change in slope does not occur until about 10^{15} eV.

While EAS experiments are relatively insensitive to the detailed spectrum, they are consistent with a flux of cosmic ray primaries containing a mixture of a wide range of nuclei including protons. At energies above 10^{14} eV the EAS results are consistent with a charge composition similar to that below 10^{10} eV. The Brawley stack results, (Koshiba et al., 1968), indicate that up to 10^{11} eV/nucleon the spectra of the nuclei with $Z \geq 6$ is a power law with index 1.6 - 1.65, similar to that of the protons. However, Aizu et al. (1964) have published preliminary indications that at 10^{12} eV/nucleon the proportion of heavier nuclei to protons drops to 0.6 its value at the lower energies. Therefore, unambiguous measurements are needed at these energies to determine the relative fluxes of all the contributing charge components by consistent, direct charge-identification techniques.

The structure of the energy spectrum may be related to the number of sources which contribute to the local cosmic ray intensity. Thus the energies at which any changes occur in the slope of the energy spectrum are of particular

significance. F. Jones (1970) has shown that changes in spectral index take place very gradually with energy; a change of one power in the spectral index occurs, not as a sharp bend in the spectrum, but gradually over two or more decades in energy. Thus to be meaningful, measurements must be made over a wide range of energies. This has the further implication that the energy accuracy required to study the phenomena which result in changes of slope is rather moderate. These considerations favor the use of an ionization spectrometer rather than a device such as a magnetic spectrometer. The use of this type of instrument provides the optimum compromise between accuracy of energy measurement and geometry factor consistent with the experimental objectives.

Changes in slope may be associated with changes in composition. For the same total energy, particles of higher Z have lower rigidity and hence are more easily contained by magnetic fields. If spectral steepening is related to the escape mechanism, then the energy at which a spectral bend occurs should depend upon charge. On the other hand, in supernova theories of cosmic ray origin, nuclear photo-disintegration may destroy heavy nuclei at high energies causing a steepening in these spectra relative to the proton spectrum. Kinsey (1969) has studied the effects on the heavy nuclei of the mechanism in which particles are accelerated by plasma wave instabilities in supernova explosions (Colgate and White, 1963). The blue shifted photons in the outward moving shock wave would photo dissociate cosmic rays of high Z above 10^{12} eV/nucleon. This prediction is in contrast to the findings of Grigorov et al. (1969) who claim

that beyond 10^{12} eV, the heavy primaries become the dominant component of cosmic rays.

The "Proton" experiments were somewhat similar to the one proposed here. However, it is difficult to interpret their results for numerous reasons.

(1) The aperture of the apparatus was defined solely by scintillators and ionization counters. In balloon investigations with similar apparatus (Pinkau et al., 1969), a directional detector such as a spark chamber was found to be essential to define the solid angle properly.

(2) The telemetry capabilities of the proton satellites were apparently severely limited, so that counting losses occurred and large corrections had to be made to the results of Proton I and Proton II.

(3) The satellites tumbled in orbit, and the percentage of time that the earth shadowed the entrance aperture was only approximately known.

(4) The photomultipliers suffered a drift in sensitivity which was detected by a systematic change in counting rate.

(5) The ionization spectrometers were calibrated simply by scaling the measured energy lost by a singly charged, minimum ionizing particles rather than by using a known energy particle beam.

(6) Charge discrimination was limited to identifying protons as distinguished from the rest of the particles. The all particle spectrum is too heterogeneous to supply the information needed for astrophysical investigations.

The work of Pinkau et al. (1969) represents an important first step in overcoming these difficulties. Ormes et al. (1970) have described the efforts of the Goddard Group to extend these measurements to resolve the higher charge components.

The experiment proposed here will further these efforts with the instrument described in Section III. With a nominal lifetime of one year, and a geometrical factor of 500 cm^2ster, the proton spectrum can be measured to greater than 10^{14} eV and the heavy nuclei can be measured to 10^{13} eV. To extend the measurements significantly beyond these limits, an enormous increase in payload weight would be required because of the steep energy spectrum. The proposed experiment will determine the spectra up to the range where extensive air shower data are available. It will provide a check of Grigorov's results and add detailed charge composition information.

B. CHARGE COMPOSITION

The cosmic radiation has long been known to possess an over abundance of heavy nuclei with respect to the solar or "universal" abundance of elements. This has been postulated to be due either to a preferential acceleration of these nuclei or to the composition of the sources themselves. The latter is generally agreed to point strongly to supernova explosions as the source of these particles. These sources are believed to be the only ones energetically capable of keeping the galaxy full of cosmic rays. The recent discovery of pulsars, and

their identification as neutron star remnants of supernova explosions with magnetic fields as high $10^{12} - 10^{13}$ gauss, lends credence to this hypothesis. However, the mechanism for the acceleration of cosmic rays is still not understood.

During the past decade eccentric satellites enabling long exposure outside the magnetosphere and large balloons reaching to altitudes of a few gm/cm^2 have been used to provide detailed charge composition information in the energy range 30 Mev to 20 GeV. The most recent data are summarized in Figure II-3. This data is now sufficiently detailed to begin to provide information about the details of the thermonuclear processes which have produced the nuclei. The experimental situation at low energies is outlined and the information to be gained by its extension to high energies is considered.

Heavy nuclei are customarily divided into sub-groups based on the charge. These groups are the L nuclei (Li, Be, B), the M nuclei (C, N, O,), the LH nuclei (Z = 10 - 14), the MH nuclei (Z = 15 - 19) and the VH nuclei (Z = 20-30). The VVH or super heavy group include all nuclei above charge 30.

There is a very large abundance of the L nuclei in the cosmic rays relative to their universal abundances. It is believed that the L nuclei are absent in sources and that they are produced by spallation reactions in interstellar matter. Therefore, the L/M ratio of abundance is important because it gives a measure of the average amount of matter traversed by the M nuclei. In the assumption that the M nuclei pass through a slab, this matter is ~ 4.5 gm/cm^2.

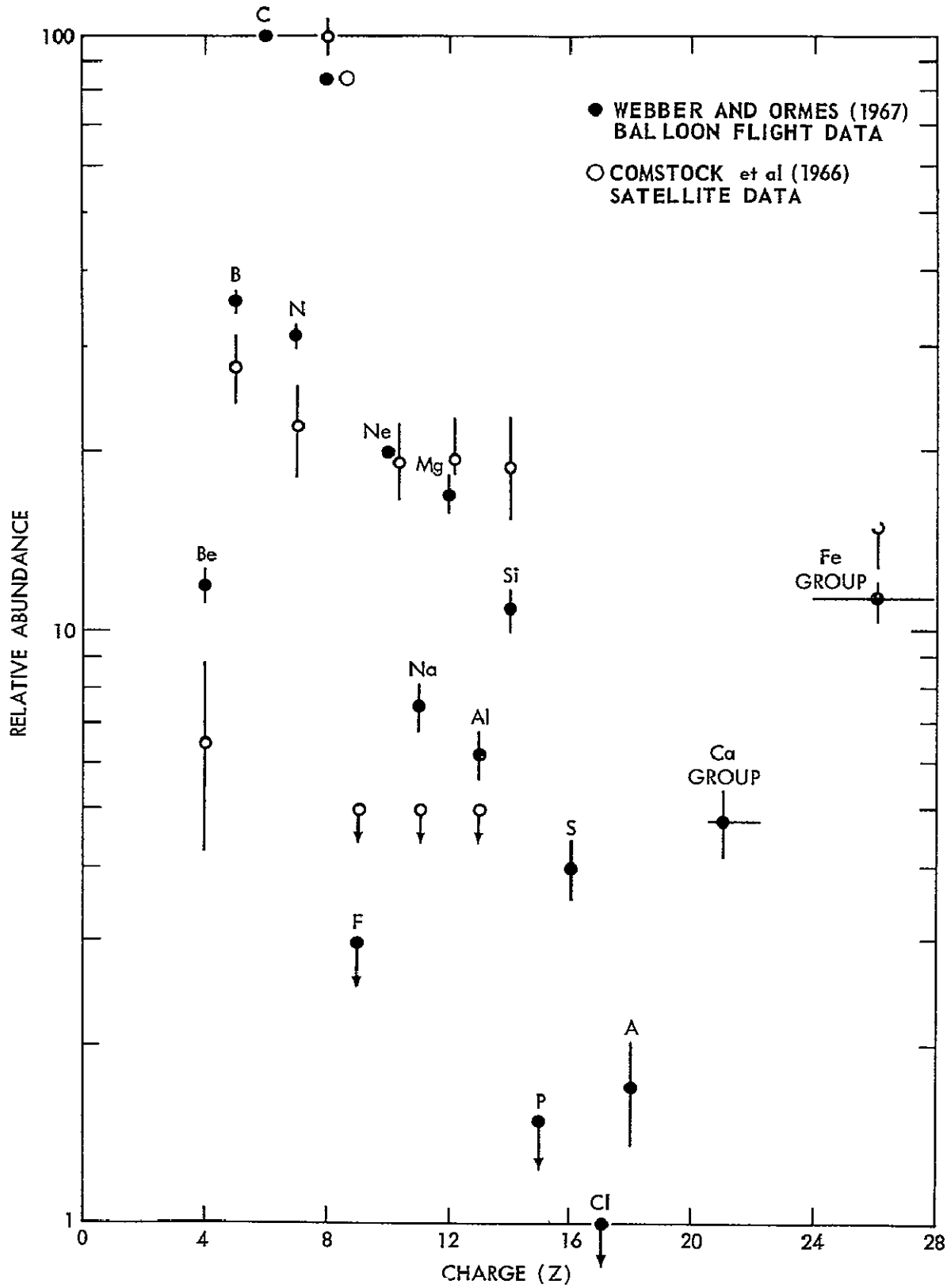

Figure II-3. Charge composition data obtained from satellite and balloon flight experiments.

Figure II-4 shows a summary of the latest L/M data from the Budapest Conference (Garcia-Munoz and Simpson, 1969; Lezniak, et al., 1969). Note that these data do not extend beyond 10 GeV. If the average material traversed depends upon energy then this should be reflected in a variation of the L/M ratio with energy. At higher energies particles should be subject to less magnetic scattering and hence might be expected to find their way out of the storage volume more rapidly.

In the L group, there are two radioactive nuclei, Be^{10} and Be^{7}. The effect of these nuclei on the relative L nuclei composition has been considered in detail most recently by Shapiro and Silberberg (1969). Be^{10} decays to B^{10} with a half life of 3×10^{6} years, and current data "suggest $T < 10^{7}$ years for the bulk of the cosmic ray nuclei." At higher energies the lifetime of Be^{10} should increase like particle energy due to the relativistic time dilation, so this should be reflected in an increase in Be/B ratio. The interpretation of this ratio is complicated by the presence of the radioactive nucleus Be^{7} which decays by electron capture (Lezniak et al., 1969). It is assumed that this nucleus would survive in the completely ionized state of a cosmic ray. However, recent measurements of the isotopic abundance of Be find that while Be^{7} makes up only 0.3 ± 0.1 of the Be nuclei at low energies (Garcia-Munoz and Simpson, 1969). Webber and Kish's results (1970) at higher energy show a predominance of Be^{7} over $Be^{9} + Be^{10}$. Roelof (1970) has suggested that these two results are consistent; however, serious solar modulation corrections still must be applied to

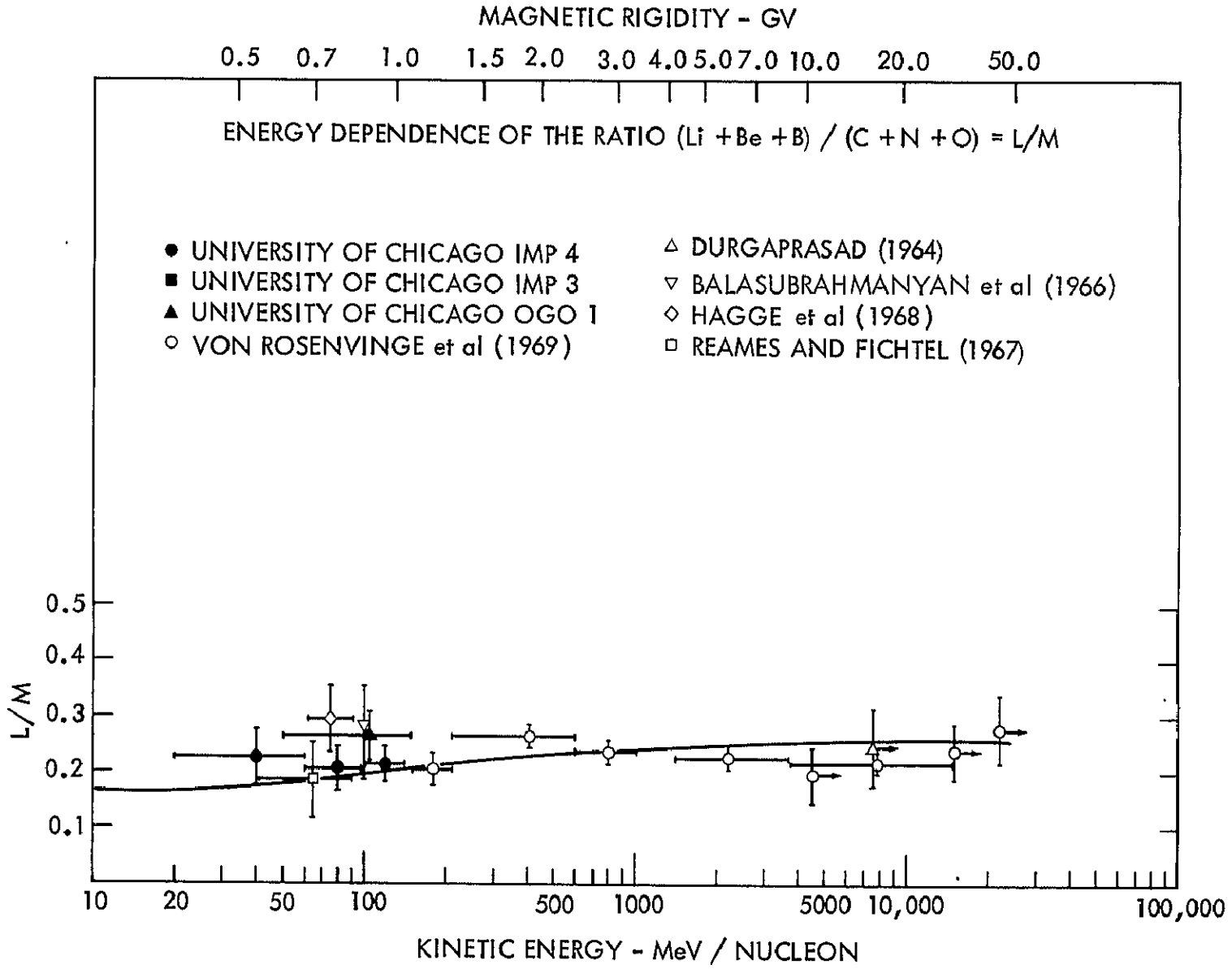
MAGNETIC RIGIDITY - GV
0.5 0.7 1.0 1.5 2.0 3.0 4.0 5.0 7.0 10.0 20.0 50.0
ENERGY DEPENDENCE OF THE RATIO (Li +Be +B) / (C +N +O) = L/M
UNIVERSITY OF CHICAGO IMP 4
UNIVERSITY OF CHICAGO IMP 3
UNIVERSITY OF CHICAGO OGO 1
VON ROSENVINGE et al (1969)
DURGAPRASAD (1964)
BALASUBRAHMANYAN et al (1966)
HAGGE et al (1968)
REAMES AND FICHTEL (1967)
L/M
0.5
0.4
0.3
0.2
0.1
10 20 50 100 500 1000 5000 10,000 100,000
KINETIC ENERGY - MeV / NUCLEON

Figure II-4.

the data making interpretation difficult. If a significant fraction of the Be^7 is found to have decayed it may indicate that the cosmic rays have spent a significant fraction of their lifetime in some region of high electron density, possibly the cosmic ray sources themselves (Webber, 1969). This data can be compared with the electron lifetime measurements to learn about the storage, diffusion, and leakage of the cosmic rays from the galaxy.

A precise knowledge of the relative abundances of the M nuclei is of importance as these abundance ratios should be little affected by solar modulation (C and O have the same A/Z, but Z^2 differs by factor of 1.8). The composition at the sources can be related to the thermonuclear processes which are producing the cosmic rays (von Rosenvinge, et al., 1969; Lezniak, et al., 1969). Some recent experimental evidence on the ratio of C/O (Teegarden et al., 1969, and Balasubrahmanyan et al., 1970) shown in Figure II-5 suggest variations of a factor of at least two over the low energy range. Clearly an extrapolation of this trend to higher energies would be important.

The most recent experiments with good charge resolution have found that the nitrogen abundance is less than 0.2 that of carbon or oxygen. This nucleus may be completely produced by spallation depending upon the exact fragmentation cross sections. At any rate its low abundance implies a low source abundance. This tends to rule out an equilibrium CNO cycle as controlling the composition in cosmic ray sources as this cycle results in nitrogen being the

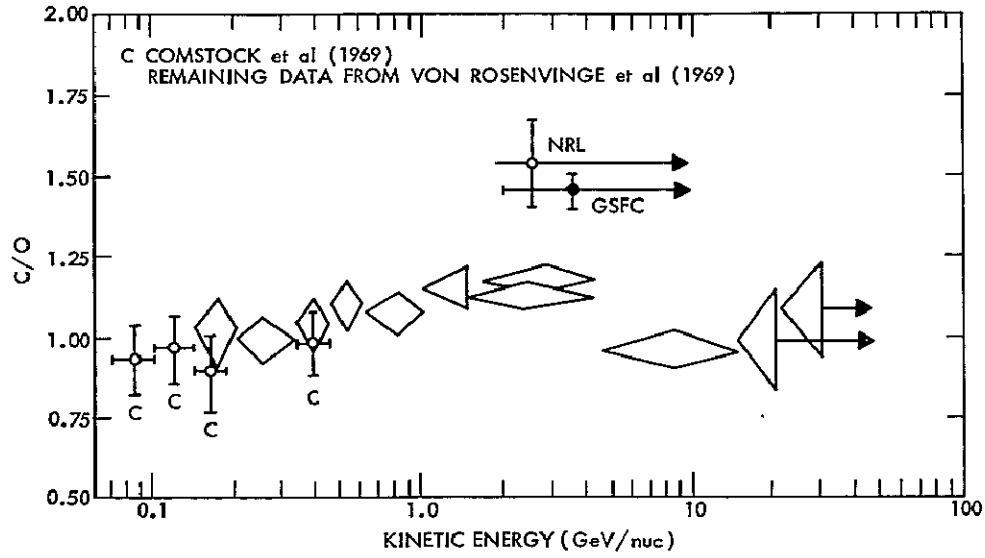

(a)

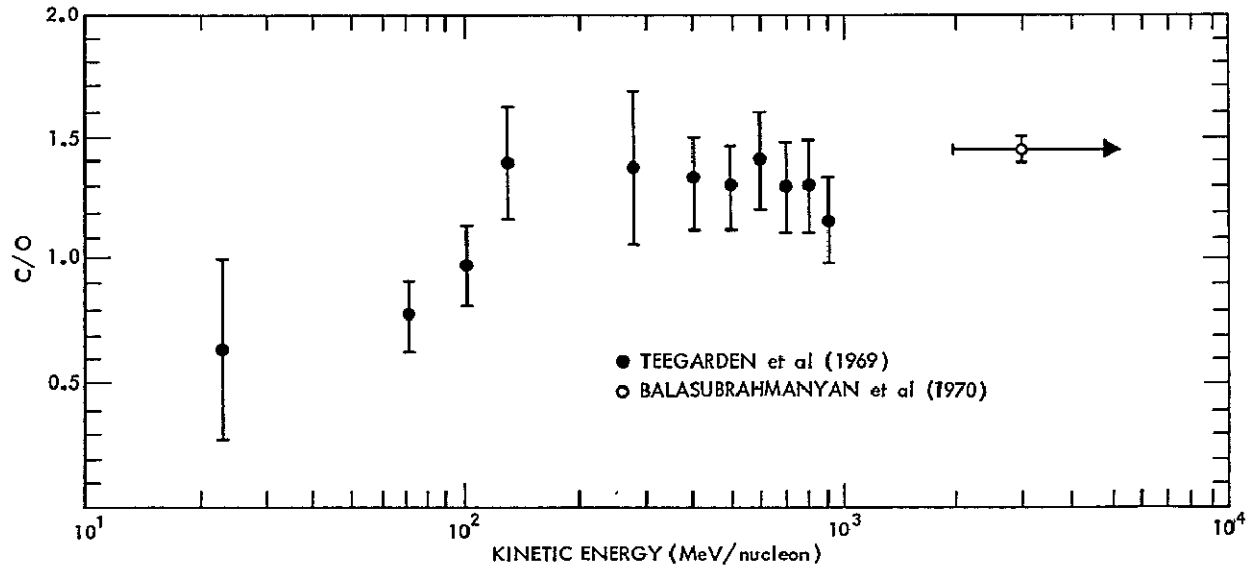

(b)

Figure II-5. Energy dependence of the carbon to oxygen ratio.

most abundant. This is an example of the kind of information about thermonuclear processes which can be gained from the study of the cosmic radiation.

In the LH region, the most striking feature is the relative absence of the nuclei of odd charges relative to those of even charges. These can be seen in the data summary from near solar minimum shown in Table II-1. (Webber and Ormes, 1967; Comstock, et al., 1966; O'Dell et al., 1969; and Meyer, 1969); more recent data obtained with the OGO satellite shows the same tendency. This is shown in Figure II-6 from Teegarden, et al., (1969).

Because of their low abundances, (0.1 of the LH group) the MH group has not been thoroughly investigated. The large collection area and long collection time of a satellite borne experiment would help remedy this situation. Data in this charge group are difficult to interpret. If the nuclei are spallation products they are probably second generation products of nuclei which began as iron, spallated down into the Z = 20-25 range, and then suffered a second reaction into the range 15 to 19. If this is so then the relative intensities should show a pronounced energy dependence. On the other hand, the abundance ratio MH/VH is similar to the universal abundance and so these nuclei may represent source composition.

The VH data are summarized in Figure II-7. These data are taken from von Rosenvinge (1970) and represent fluxes at the top of the atmosphere. Note that the data are based on only a few hundred events. The relative abundances

Table II-1

RELATIVE ABUNDANCE OF ELEMENTS IN THE COSMIC RADIATION

Element	IMP IV-OGO I (Garcia-Muñoz and Simpson) 1969 (50 - 300 MeV/nuc)	Gemini XI (O'Dell et al.) 1969 (> 1 GeV/nuc)	Balloon (Webber and Ormes) 1967 (200- 1000 MeV/nuc)
He	$4.2 \pm 0.6 \times 10^{3}$		
Li	$1.95 \pm 0.5 \times 10^{1}$		
Be^{4}	$6.5 \pm 2.2 \times 10^{0}$	$5.9 \pm 2.9 \times 10^{0}$	$8.8 \pm 2.4 \times 10^{0}$
B^{5}	$2.9 \pm 0.6 \times 10^{1}$	$3.0 \pm 0.4 \times 10^{1}$	$3.15 \pm 0.35 \times 10^{1}$
C^{6}	100 ± 6	$1.05 \pm 0.07 \times 10^{2}$	100
N^{7}	$2.55 \pm 0.2 \times 10^{1}$	$2.55 \pm 0.3 \times 10^{1}$	$2.6 \pm 0.4 \times 10^{1}$
O^{8}	100 ± 6	100 ± 10	$9.3 \pm 0.9 \times 10^{1}$
F^{9}	$1.7 \pm 0.2 \times 10^{0}$	$\leq 3.6 \times 10^{0}$	$< 3.75 \times 10^{0}$
Ne^{10}	$1.75 \pm 0.3 \times 10^{1}$	$2.35 \pm 0.35 \times 10^{1}$	$1.9 \pm 0.1 \times 10^{1}$
Na^{11}	$4.1 \pm 1.1 \times 10$	$< 3.6 \times 10^{0}$	$6.0 \pm 1.0 \times 10^{0}$
Mg^{12}	$2.3 \pm 0.1 \times 10^{1}$	$2.6 \pm 0.4 \times 10^{1}$	$1.75 \pm 0.05 \times 10^{1}$
Al^{13}	$3.4 \pm 0.4 \times 10^{0}$	$< 6.2 \times 10^{0}$	$5.6 \pm 0.6 \times 10^{0}$
Si^{14}	$1.7 \pm 0.3 \times 10^{1}$	$2.4 \pm 0.4 \times 10^{1}$	$1.4 \pm 0.3 \times 10^{1}$
P^{15}	$1.95 \pm 1.0 \times 10^{0}$		$< 1.5 \times 10^{0}$
S^{16}	$5.0 \pm 1.3 \times 10^{0}$		$4.0 \pm 0.45 \times 10^{0}$
$P\text{-}K^{17}$	$6.1 \pm 1.9 \times 10^{0}$	$1.05 \pm 0.27 \times 10^{1}$	$1.7 \pm 0.35 \times 10^{0}$
$Ca\text{-}Cr^{22}$	$7.6 \pm 1.8 \times 10^{0}$	$2.0 \pm 0.35 \times 10^{1}$	$4.8 \pm 0.65 \times 10^{0}$
(Fe group) $Mn\text{-}Ni^{26}$	$1.2 \pm 2.4 \times 10^{1}$		$1.3 \pm 0.15 \times 10^{1}$

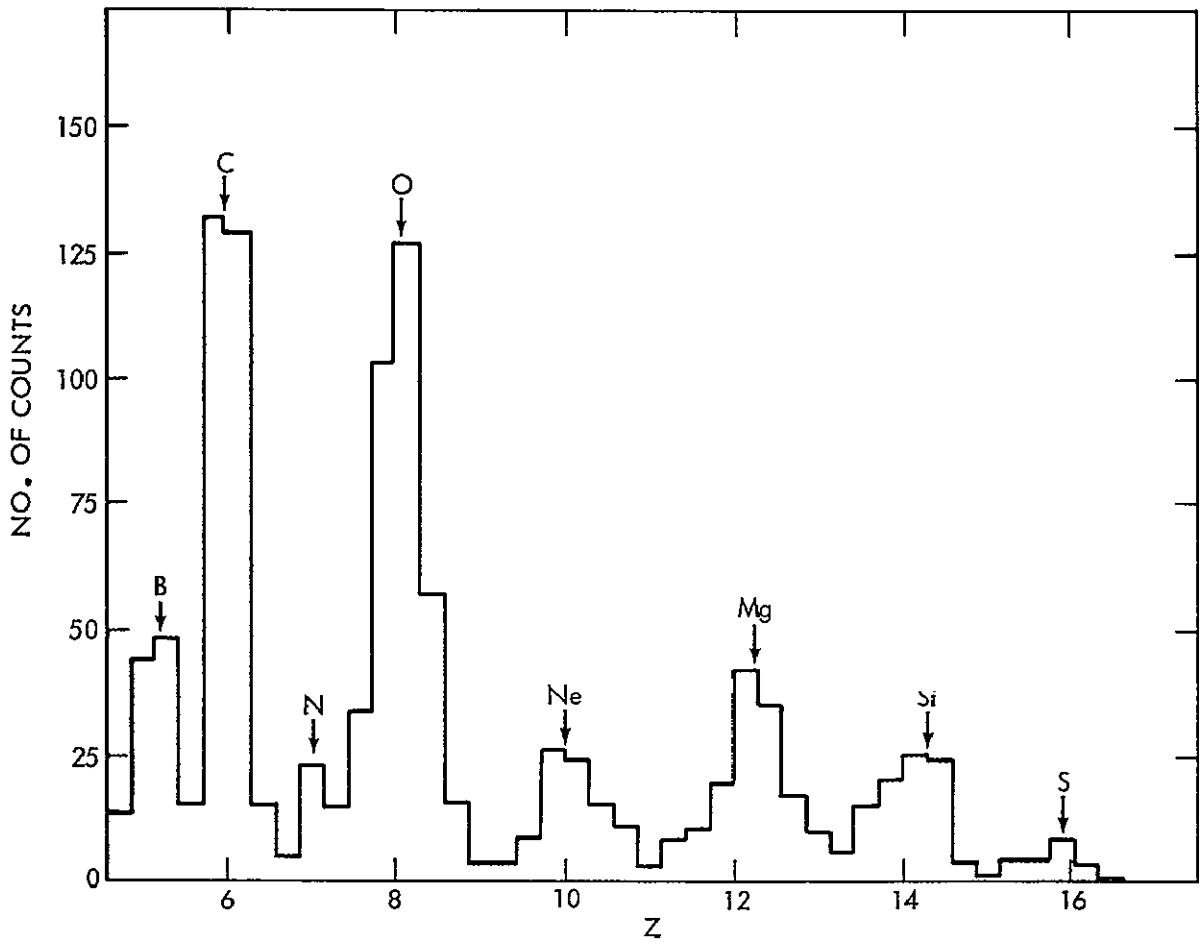

Figure II-6. Even-odd effect in the charge distribution of cosmic ray nuclei.

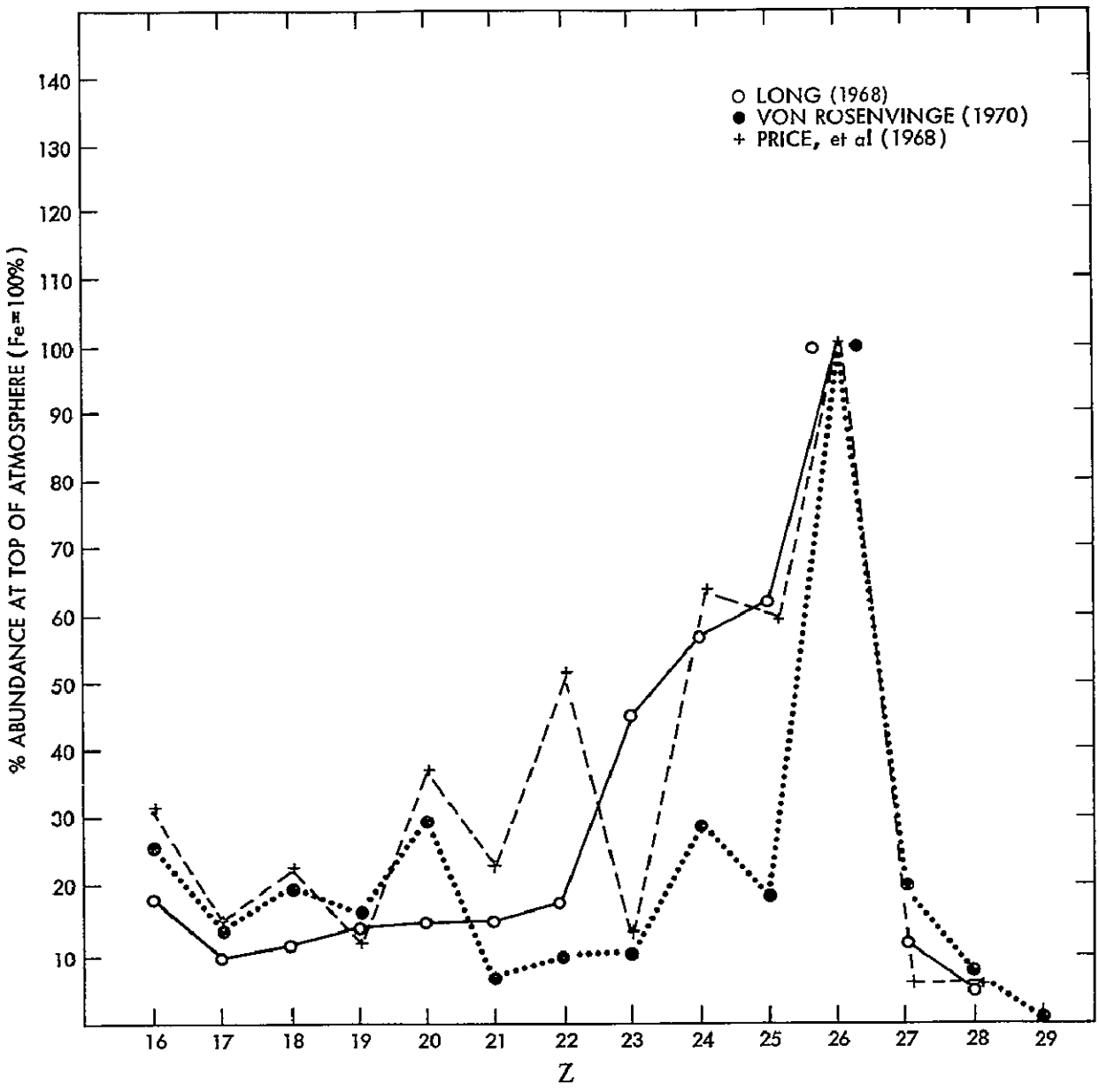

Figure II-7. Charge distribution of VH nuclei in cosmic rays.

of Mn, Cr, and Fe are still not known due to the lack of adequate change resolution.

This data can be analyzed in the same way as the L/M data by assuming that all the nuclei but iron are not significantly present at the source. In the slab approximation this VH data leads to a path length of 2.8 gm/cm^2, shorter than for the L nuclei. This can be understood as a shorter mean lifetime of the VH nuclei, due largely to the importance of interactions in the lifetime. The VH and L abundances can both be understood in terms of particles arriving at the solar system through an exponential distribution of path lengths in the interstellar matter. This means that on the average heavy nuclei are younger than light nuclei. This will be important when possible anisotropies are considered.

Following the discovery of fossil tracks of nuclei heavier than iron in meteorites by Fleischer et al. (1967), the composition of these VVH nuclei have been studied with emulsions and plastic detectors on balloons by Fowler et al. (1967) and Blanford et al. (1969). The experimental evidence is still too tentative to allow firm conclusions to be reached concerning the origin and propagation of these nuclei. The emulsion and plastic detectors have been flown on balloons requiring correction for fragmentation and ionization loss in the over lying atmosphere. The geomagnetic cut off at Palestine, Texas and absorbers in the emulsions have been used to determine that the nuclei were relativistic. Because the measured ionization loss is proportional to Z^2/v^2

energy losses in the atmosphere (changes in v) produce some uncertainty in the charge. In particular in the range Z = 30 to 33 the tail of the iron peak from the slower nuclei may introduce large errors.

The present models of supernova explosions indicate that the VVH nuclei may be built up by rapid neutron capture (r process) nucleosynthesis in the envelopes of these exploding stars (Burbidge et al., 1957). The results of Fowler et al., (1969) indicate peaks in the VVH spectrum at around Z = 52 and 76 as might be expected from an r process origin. Also, the transbismuth elements that apparently exist in the flux must be the result of the r process. In addition the existing data do not indicate a peak in the abundance spectrum at Z = 82. If slow neutron capture process is responsible for the observed VVH nuclei, a peak at Z = 82 should have been detected.

Fowler et al. (1967) and Blanford et al. (1969) have presented evidence for the existence of transuranic elements in cosmic rays. If confirmed, the presence of transuranic elements would be of interest not only concerning the origin of cosmic rays, but to nuclear theory as well (Myers et al., 1966; Meldner, 1967; and Nilson et al., 1969).

Because the interaction mean free path is very short, the VVH composition is strongly influenced by its passage through interstellar material. The composition that has been reported indicates that the VVH nuclei cannot have passed through more than 1 gm/cm^2 of material in a simple slab model (Fowler, 1970).

Even though only few hundred VVH nuclei have been identified, the results have already indicated the potential astrophysical importance of measurements in this charge range. However, no information is available on the VVH energy spectrum. In addition a simultaneous determination of the energy and charge is extremely important for increasing the reliability of the charge measurement (as discussed in a later section). It will also allow a measurement to be made of the relativistic rise of energy loss in gas counters for the heavy nuclei so that corrections to charge identification due to this effect can be evaluated. Energy measurements will be significant in looking for possible departures from the Z^2 dependence of the ionization loss (Doggett et al., 1957 and Semikoz, 1969).

Expected fluxes for VVH nuclei are given in Table II-2.

Table II-2

FLUXES AND NUMBER OF VVH NUCLEI TO BE SEEN IN ONE YEAR

Z	Flux Assumed > 5 GV Cutoff $(m^2 \text{ ster sec})^{-1}$	Number through Charge Module	Number with Energy Measurements	Number Within the Complete Spectrometer Aperture
"Fe Group"	4	4×10^6	10^6	4×10^5
$30 \leq Z \leq 35$	4×10^{-3}	4000	1000	400
$Z > 35$	4×10^{-4}	400	100	40
$Z > 45$	1.2×10^{-4}	120	30	12

C. ELECTRONS

Existing measurements of the cosmic ray electron spectrum cover the energy range from about 1 MeV to several hundred GeV. These measurements are shown in Figure II-8. Below a few GeV, the measured spectrum probably differs from the true interstellar electron spectrum due to solar modulation. Above ~10 GeV, the measured spectrum can be considered as representative of the galactic conditions.

Recent observations of the radio background in the range 0.4 to 6.5 MHz by Alexander et al. (1970) seem to suggest that the interstellar intensity of electrons of a few hundred MeV is larger by at least an order of magnitude than the intensity observed near the earth. They suggest that these observations imply either a large solar modulation of electrons at these energies or the existence of a gradient in the electron intensity in the region near the solar system.

The experimental data available above 10 GeV are shown in Figure II-9. A glance at this figure indicates the existence of serious discrepancies in the measurements. At the highest energies (around 300 GeV) statistical limitations may result in uncertainty of a factor of ~2 in the intensity. At energies around 10 GeV, where the errors are not dominated by statistics, the agreement is still not very good. For example, the intensities from the two similar emulsion experiments of Anand et al. (1968) and Marar et al. (1969) disagree by an order of magnitude. The early results seem to suggest that electrons have a spectral

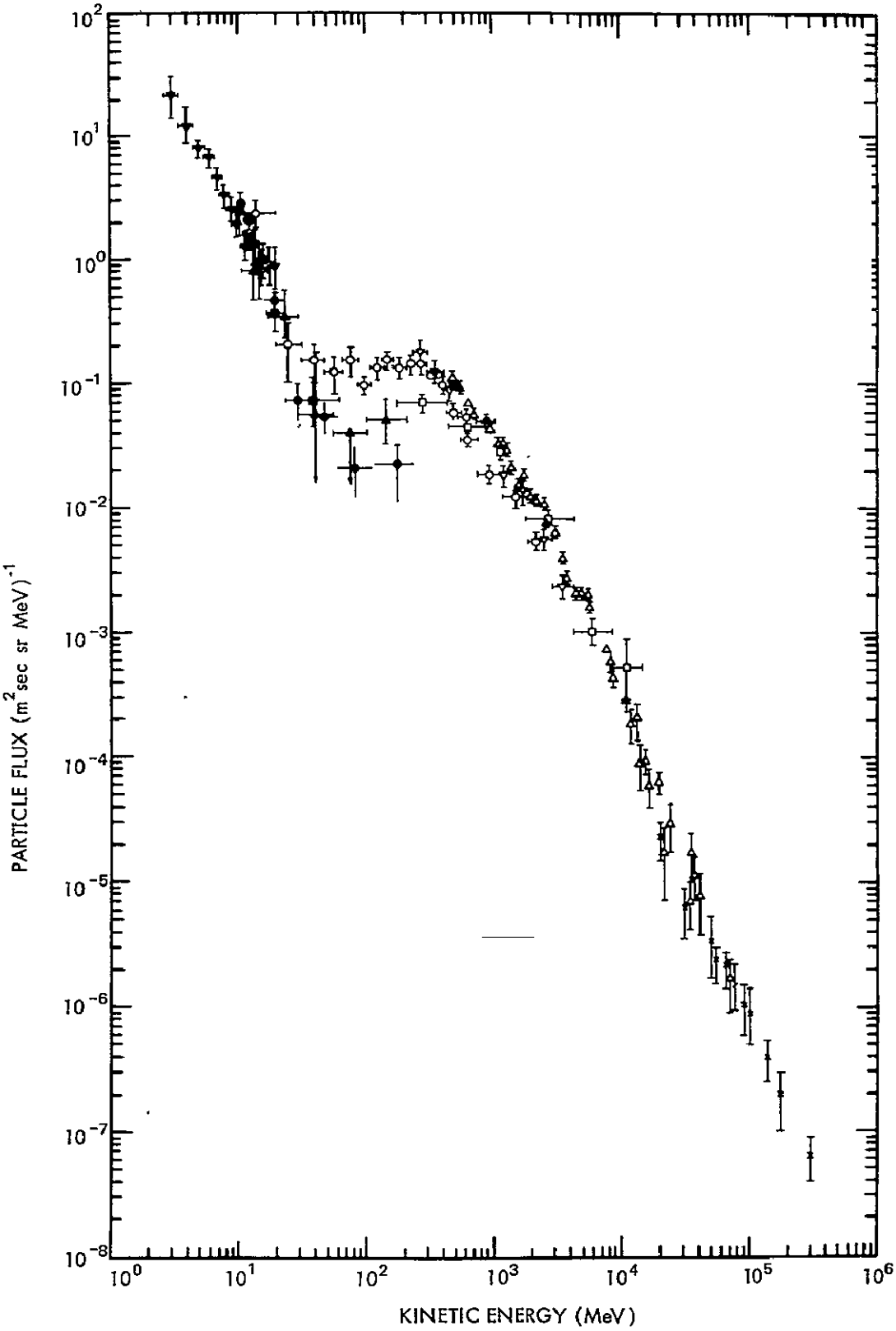

Figure II-8. Differential energy spectrum of cosmic ray electrons in the energy range $3 - 2 \times 10^5$ Mev.

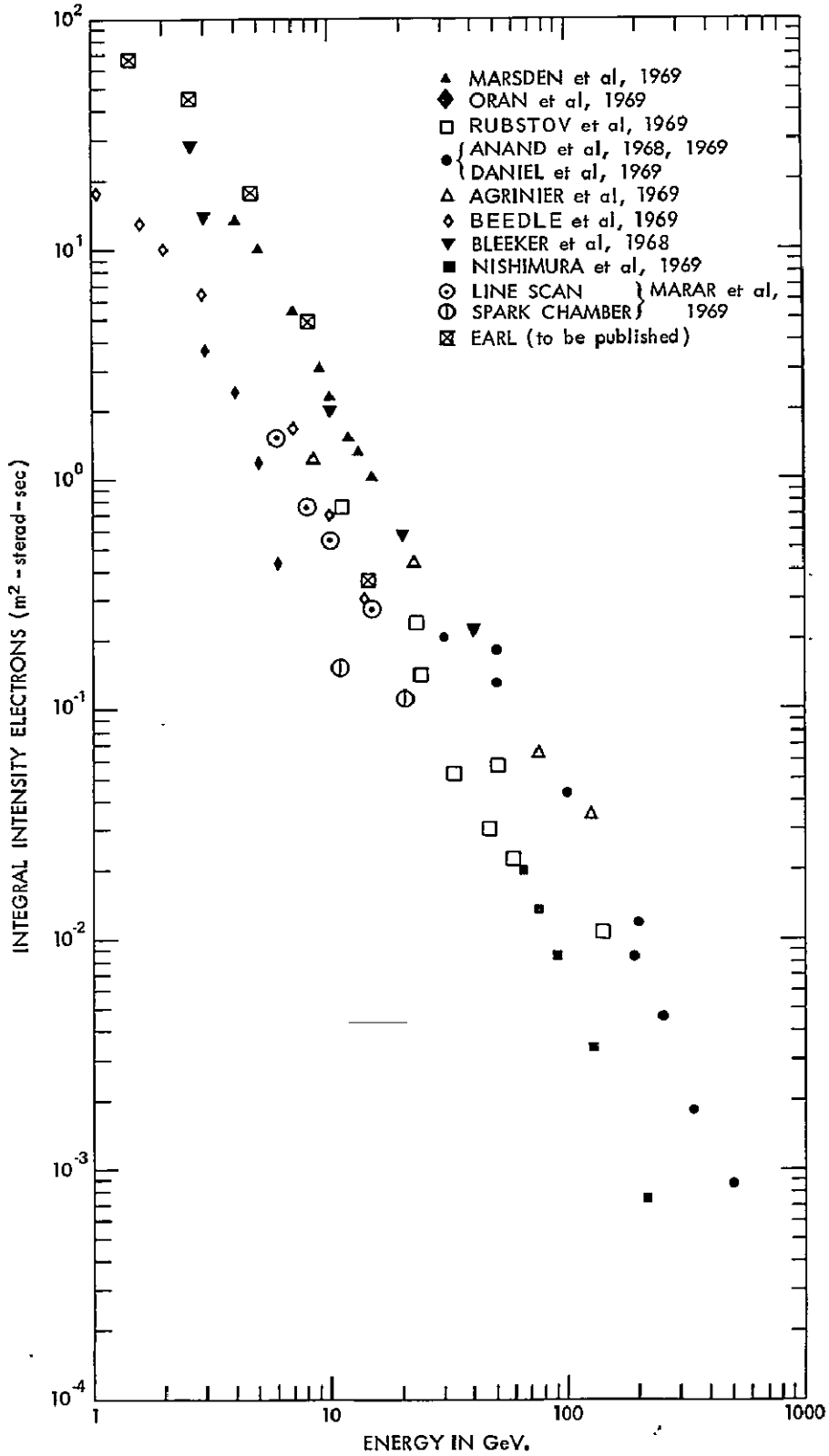

Figure II-9. Existing information on the integral energy spectrum of electrons in cosmic rays. Note the spread of the data.

index $\gamma \sim 2.5$ similar to protons, but with the present experimental situation one is not able to come to unambiguous conclusions (Earl, 1970).

The experimental difficulties are, in part, due to:

(1) corrections for atmospheric secondaries,

(2) proton interactions simulating electrons, and

(3) the errors in energy measurement.

In the case of a satellite, the correction due to the atmosphere does not arise, whereas the present balloon flight results may have some contribution from this effect. The proton interactions simulating electrons are particularly serious when the spectrometer does not have enough material to stop the electron cascades completely. The proton intensity is about 100 times the electron intensity and so it is necessary to design the experiment to have good discrimination between electrons and protons.

The seriousness of the problem is indicated in Figure II-10 which is from the balloon flight results of Silverberg et al. (1970). The Goddard instrument was calibrated with 18 GeV electrons at the Stanford Linear Accelerator Center (SLAC) and also flown in a balloon from Alamogordo, New Mexico, on 28 April 1969. The two histograms are distributions of a goodness of fit parameter. This parameter is obtained by comparing the data with expected electron cascades curves obtained in the calibration. The upper curve is a pure electron

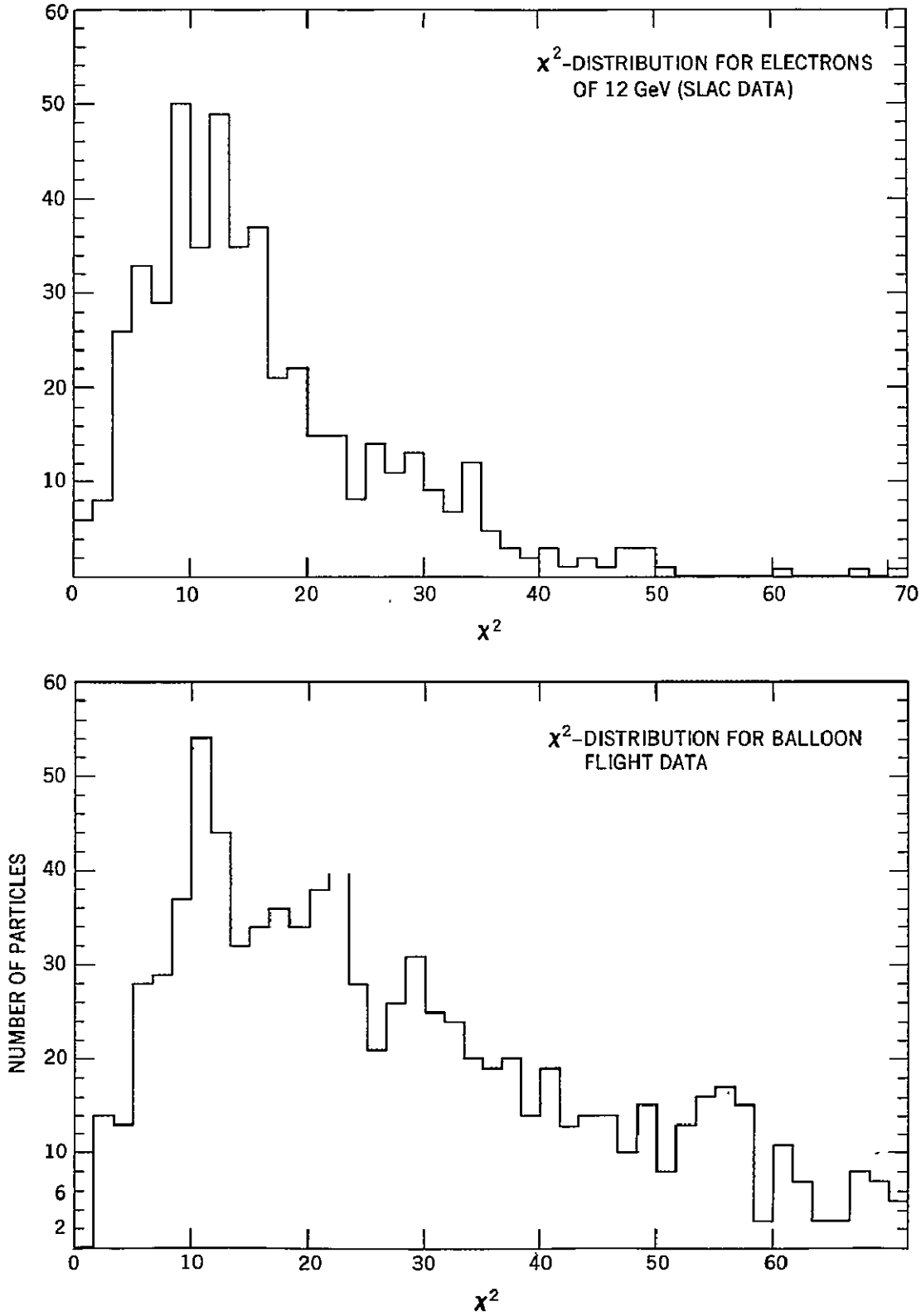

Figure II-10. χ^2 Distributions for electrons.

beam from the SLAC data and the lower curve is from balloon data. The same criteria for selecting data were applied in both cases. Other experimenters have used similar techniques (Earl, 1970, and Fanselow et al., 1970). It can be seen that, while the accelerator data distribution is peaked, the balloon flight data has a broad distribution with a flat pedestal. The pedestal is presumably due to the background protons. Unless the correction is evaluated accurately the resulting intensities of electrons could be in error. In the later section, details of the design features which help in achieving good discrimination for electrons against protons are described.

In order to eliminate systematic errors in measuring energy it is essential to calibrate the instrument with high energy accelerator electrons. This is because it is difficult to determine the minimum energy electron which participates in the shower development any other way. This manifests itself in a variation in measured response with incident angle and is not yet completely understood. (It may be responsible for some of the dispersion in the goodness of fit distribution from the flight data.) It is also desirable to expose the instrument to proton beams of various energies to correctly estimate the background protons contributing to the electron intensity. This can be done at a variety of energies in order to closely approximate the cosmic ray situation.

The study of the cosmic electron spectrum has a number of interesting astrophysical implications. The main reason for this is that at energies of a

few tens of GeV and above, depending on the galactic magnetic field and photon density in interstellar space, the lifetime of the electrons against synchrotron and Compton radiation losses is of the order of a few million years, comparable to the lifetime of the cosmic rays as obtained from the study of the nuclear fragmentation of C, N, O nuclei into Li, Be and B. For a power law injection spectrum of the electrons at their sources with spectral index γ, the observed spectrum should also be a power law with the same index γ up to an energy at which the radiation lifetime equals the cosmic ray lifetime. Above this energy the electron spectrum should steepen to $\gamma + 1/2$ and at higher energies to $\gamma + 1$. For known photon fields in interstellar space therefore, a detailed measurement of the cosmic electron spectrum up to a few hundred GeV would provide an independent determination of the cosmic ray lifetime. Such a determination would be of great importance for the origin and propagation of cosmic rays and would add to the information from the L/M ratio and the radioactive nuclei.

The interpretation of the high energy electron spectrum and the determination of the cosmic ray lifetime is seriously complicated by the present uncertainties in the experimental situation. On the one hand the interstellar photon intensities are poorly known, the main uncertainty resulting from the possible existence of a diffuse galactic photon flux in the submillimeter region (Shivanandan, et al., 1968) and on the other hand, the existing electron measurements are extremely uncertain. The high-energy electron measurements would therefore be of great significance not only for the determination of the cosmic

ray lifetime but also in the study of the interstellar photon densities. Large photon densities may be significant to more general problems such as the dynamics of the interstellar medium and the intergalactic matter. These electrons, via the inverse Compton interaction with background photons, may be responsible for the diffuse x-ray background. (Brecher and Morrison, 1969, O'Connell and Verma, 1969).

The electron measurements, which are an integral part of the proposed experiment, would contribute to the understanding of these areas of high-energy astrophysics. They will relate directly to the x-ray and γ-ray studies also proposed by other experimenters for the HEAO satellite.

D. ANISOTROPY

The measurement of the sidereal anisotropy of the cosmic rays, which is intimately connected to the streaming of the cosmic ray gas in interstellar space, is of decisive importance for understanding the origin and propagation of the cosmic radiation. It can be shown that for a net streaming velocity U, the sidereal anisotropy is given by

$$\delta = \frac{U}{V} (2 + \gamma)$$

where V is the particle velocity and γ the exponent of the differential spectrum. The measurements have to be done at a sufficiently high energy so that the radius of gyration of the particles is larger than the size of the solar cavity; otherwise, the disordered interplanetary magnetic fields will tend to diminish any existing

interstellar anisotropy. Most recently, Elliot et al. (1970) gave an upper limit on the sidereal anisotropy of $\sim 2 \times 10^{-4}$. This measurement is based on the underground muon intensity and is sensitive to the energy range of 10^{11} to 10^{12} eV. Even though these energies are not sufficiently large to completely eliminate the effects of the interplanetary fields, such a low anisotropy is suggestive of an extremely low streaming velocity of the cosmic rays in the galaxy. This leads to an apparent discrepancy with estimates of the cosmic ray lifetime as derived from the observed L/M ratio, because for such a low streaming velocity it becomes dynamically impossible for the cosmic rays to escape from the galaxy.

Ramaty et al. (1970) have recently investigated this problem in terms of a statistical model, which distributes cosmic rays randomly in space and time. They have shown that, even if fluctuations are taken into account, the high degree of cosmic ray isotropy can be best understood in terms of a long trapping time in the galactic disk. This implies that the lifetimes of the various nuclei are determined principally by nuclear interactions and not by escape and that these lifetimes decrease with increasing nuclear mass. The apparent discrepancy between isotropy and lifetime can then be readily understood, since the existing anisotropy measurements refer to the total cosmic ray flux which consists mainly of protons, while the lifetime estimates are based principally on the amount of matter traversed in interstellar space by nuclei in the M group. The implication of this is that even though the proton anisotropy may be quite low, the anisotropy of the heavier nuclei is probably larger and increases with

increasing nuclear mass. Because of this, the heavier nuclei should exhibit larger anisotropies which could in principle be detectable. However, even for iron the anisotropy may not be much larger than 10^{-2}

In addition, to the anisotropy associated with the outward streaming of the cosmic rays discussed above, the high energy electrons should exhibit an anisotropy which results from the preferential loss of transverse momentum due to synchrotron radiation (Earl and Lenchek, 1970). The expected electron anisotropy, however, depends on the randomizing effects of scattering of electrons by hydromagnetic waves in the interstellar medium which are presumably set up by the much larger flux of cosmic ray protons (Wentzel, 1969). The measurement of the electron anisotropy, therefore, would provide information on the completely unexplored area of wave particle interactions in the interstellar medium.

Previous measurements of anisotropy have all been made with sea level detectors which have wide opening angles. Extensive corrections for atmospheric effects are required in order to obtain reliable isotropy limits from these ground based observations. It would be most satisfying to check these results with a direct measurement above the atmosphere. In addition, if the scale sizes of the anisotropies are smaller than the angular aperture of the detectors, the effects being investigated would not appear. The directional resolution of the proposed experiment would be adequate to overcome these problems. Also, the possibility

of the low flux, high Z components having appreciable anisotropies compared to the more dominant proton component could not be studied in the previous experiments.

The extended lifetime of a satellite experiment which can accumulate reasonable statistics on measurements of the energies, charges, and directions of various components of the cosmic radiation, provides a unique possibility for making direct observations of the cosmic ray anisotropy. While no theoretical predictions of positive results have been made, little additional experimental effort is required to study this question. Direct reliable measurements can be made without the need for involved and indirect corrections necessary for the sea level data.

Statistical accuracy will be the dominant factor with which to contend. In this experiment, the measurement cannot be done at sufficiently high energies that interplanetary effects are completely negligible. For the VH nuclei an anisotropy of 10^{-3} could be detected correspond to a mean energy of about 10^{10} eV. For protons and He nuclei this limit can be reached at 10^{11} and 3×10^{10} eV respectively. Isotropy limits of 1% can be extended by another factor of 40 in energy. This will probably be the first direct study of this exciting problem. Once the techniques for this study are well established, the second generation development of the experiment (detailed later in the proposal) with geometry factors ~ 100 times the present experiment will be able to extend these results

to significant energy regions. Thus this attempt opens out a new area of research hitherto not accessible to direct study, with great possibilities in the future.

E. TIME VARIATIONS

Cosmic rays in their propagation in the interplanetary medium are subject to various types of modulation (both short and long term) which can reveal important information regarding the electromagnetic conditions in the solar system and propagation of cosmic rays. The studies will deal with

(1) Forbush decreases and recurrence phenomena which produce 27-day variations and

(2) diurnal and semidiurnal anisotropies.

All of these modulation effects become smaller in amplitude in the many GeV region, but underground muon intensity studies indicate that they are detectable up to energies ~100 GeV (Peacock et al., 1968).

The cosmic ray experiment proposed here has a counting rate of $\sim 3.6 \times 10^4$ counts/hour; a factor of two more than the IGY neutron monitors which have been extensively used for the study of these phenomena. In addition, these telescopes have several advantages which neutron monitors and underground muon telescopes do not have.

(1) Energy measurements are direct, and so energy dependence of the phenomena can be directly obtained;

(2) no corrections are required for atmospheric pressure and temperature changes; and

(3) the direction of each particle is measured directly so that features such as diurnal anisotropies can be studied in order to relate the temporal and spatial variations.

Forbush Decreases - 27 Day Variation. Thambyahpillai and Dutt (1965) have extended the study of Forbush decreases and 27 day variation to a few hundred GeV by studying the underground muon intensity. For the energies represented by the high latitude neutron monitors the spectral dependence for both Forbush decreases and 27 day variations are the same. But results of limited statistics at high energies seem to show that the two phenomena have a different spectral dependence. The difference in the spectral behavior could be related to the differences in the energy dependence of the propagation of the particles in the interplanetary medium.

Diurnal and Semi-Diurnal Anisotropies. Cosmic rays in the energy range 1 - 200 GeV exhibit diurnal anisotropy with an amplitude $\sim .4\%$ and a time of maximum around 1800 hours (McCracken and Rao, 1965). At times (particularly during Forbush decreases) the amplitude rises to 1 - 2% and persists over a number of days at this high value. The energy dependence is quite weak and the

effect has been detected with underground meson telescopes (Peacock et al. 1968; Cini-Castagnoli et al., 1968). The diurnal anisotropy can be understood as due to the partial co-rotation of particles with the sun with an azimuthal velocity of about 300 km/sec at the orbit of the earth (Parker, 1964; Axford, 1965). The underground measurements are limited by the atmospheric pressure and temperature effects for which important corrections must be made. Satellite measurements do not need these corrections and hence could provide a more sensitive and clear measurement of the energy dependence of the amplitude of this effect.

The semi-diurnal anisotropy has an amplitude of 0.1% and has been shown conclusively to exist by Ables et al. (1965). Here again the difficulty for ground based measurements of this effect has been the large atmospheric corrections to be applied. Ables et al. (1965), Patel et al. (1968), and Lietti and Quenby (1968) have shown that this effect, unlike the diurnal variation, has a positive spectral exponent in the many GeV region.

Both Subramanian and Sarabbai (1967) and Lietti and Quenby, (1968) have suggested that the second harmonic component of the daily variations is due to the particle density gradient in the plane perpendicular to the plane of the ecliptic. Assuming an Archimedes Spiral configuration for the interplanetary field, particles arriving along the sun's polar field lines suffer less modulation than those arriving in the ecliptic plane, thus giving rise to a cosmic ray

density gradient. The intensity increases away from the plane of the ecliptic. Therefore, viewing in a direction perpendicular to the interplanetary field, the detector samples particles arriving from heliolatitudes comparable to the gyroradius of the particle under consideration. Thus higher energies are related to higher heliolatitudes. Consequently, the study of this anisotropy as a function of energy could give information on the interplanetary magnetic field at the higher solar latitudes.

The HEAO satellite scans the whole sky once in about six months and hence the study of some of these modulation phenomena could be made to the extent permitted by the statistics of the measurements. Also in order to arrive at the true sidereal anisotropy these solar contributions and their variations have to be understood and eliminated. Thus in the course of the life of the satellite a large amount of useful information on the interplanetary medium could be collected and profitably studied in conjunction with similar ground based studies.

F. COMPLEMENTARY RESULTS WITH EXTENSIVE AIR SHOWER STUDIES

The flux of particles at energies above 10^{15} eV is so low that direct measurement of the charge composition and energy spectra is impossible at the present time. For example, an instrument of the type proposed here will be lucky to intercept 1 event with an energy above 10^{15} eV in a one-year exposure-time. So until effective techniques are developed to provide space-worthy detectors with much larger geometrical factors, studies of these rare particles will be

possible only with extensive air showers (EAS). High energy cosmic ray particles initiate these showers which are then developed in the atmosphere. Detectors which cover very large areas at sea level or on mountain tops sample the EAS to obtain estimates of the energy spectrum of the primary cosmic radiation. The results rely on extrapolations of charge composition, nuclear interaction characteristics and cascade development from meager data from nuclear emulsion studies at about 10^{12} eV.

The direct study proposed here will extend to energies of the order of 10^{14} eV at an expected counting rate of approximately 50 particles in a one-year exposure. Measurements of the interactions of these particles in the spectrometer will provide information concerning features of nuclear interactions at high energy. The lateral distribution and number of particles in a nuclear cascade at a depth of approximately 6 nuclear mean paths of matter, will be derived from the response of the directional detectors and ion chambers at the exit point of the showers.

The compact cascade showers developed in this instrument can be related to mountain top measurements of EAS through models in which the differences in both the decay probability of unstable particles and the multiple scattering of charged particles in the medium are suitably taken into account. The comparison will help to test the applicability of the shower models to predict and interpret the structure of nuclear cascades. Data from the measurements

proposed in this experiment can be compared with the parameters used in the Monte Carlo air shower simulations (Bradt and Rappaport, 1969). These interrelated data will improve the interpretation of the measurement data.

G. NUCLEAR PHYSICS

1. Using the Cosmic Ray Beam

Early cosmic ray studies were the source of many exciting developments in high energy physics. This is not surprising since the cosmic radiation was the first available source of high energy particles. Today the highest energy particles available are still the cosmic rays. As L. H. Smith (1967) has pointed out, an inviting possibility exists to someday use this beam to do nuclear physics experiments.

However there are several difficulties involved.

(1) The cosmic ray beam is isotropic and not controlled as in ground based accelerators. This produces unknown background problems and makes beam definition difficult.

(2) The cosmic ray fluxes are exceedingly low and in order to get meaningful statistics at particle energies above those at currently planned accelerators requires long observing times and large apparatus.

(3) To do the more interesting nuclear physics, complex, highly accurate apparatus is required to operate stably without repair in the severe space environment for long periods of time.

Consideration was given to using one end of the spectrometer for a nuclear physics experiment. One of the alternatives is described in Appendix 1. However it is felt that the potential results from such an experiment do not justify compromising the cosmic ray experiment. The addition of a nuclear physics

experiment would introduce greater complexity into the experimental apparatus and it would reduce the counting rates of the cosmic ray experiment by at least a factor of two. A brief outline of the reasoning follows.

P-P Interactions: The interactions of most immediate interest to elementary particle theorists would be proton-proton interactions. Of the many quantities which might be measured, the only two having a direct bearing on present-day theories which can be measured in a fairly simple apparatus are the total inelastic interaction cross section, $\sigma_{\text{inelastic}}$ (p-p), and the elastic differential scattering cross section, $d\sigma/dt$, in the forward diffraction region (t is the four-momentum transfer squared). Integration of the latter would give σ_{elastic} (p-p), which, when added to $\sigma_{\text{inelastic}}$, would provide the total cross section, σ_{total} (p-p). The behavior of all of these quantities at high energy is of considerable theoretical interest. They are expected to vary, at most, slowly with energy, so we may be guided by the cross sections at accelerator beam energies, where $\sigma_{\text{inelastic}}$ (p-p) $\approx$ 30 mb. and σ_{elastic} (p-p) $\approx$ 9 mb. Experimental considerations (see Appendix 1) limit the target layer thickness to the order of magnitude of 2 gm-cm^{-2} of hydrogen. With a total cross section of 39 mb, a high energy proton has a probability of .05 of having a p-p interaction. Assuming an effective geometric factor of 265 cm^2 ster, Table II-3 gives the estimated number of p-p interaction events which would be observed in one year at a variety of different energies. Table II-4 lists accelerator beam energies which will become available in the near future.

Table II-3

HEAO SATELLITE EXPERIMENT-1974

Energy lower limit (eV)	No. of p-p Interaction Events
10^{11}	1.6×10^5
10^{12}	4×10^3
10^{13}	80

Table II-4

ACCELERATOR BEAMS

Accelerator	Date Ready	Max. Beam Energy (eV)
Serpukov (U.S.S.R.)	Now	0.7×10^{11}
National Accelerator Laboratory (Batavia, Ill.)	1972	2×10^{11}
	Low beam current operation	5×10^{11}
CERN Proton Storage Rings (Geneva, Switzerland)	1972	1.7×10^{12}*

*Laboratory proton beam and cosmic ray proton energy which is equivalent to the 56 GeV center of mass system energy provided by the colliding beams.

At energies below 2×10^{12} eV the HEAO experiment cannot hope to compete with accelerator experiments. Since p-p cross sections vary slowly with energy, cosmic ray interactions can give new information only above 10^{13} eV. The poor statistics with which these interactions can be measured will seriously limit the usefulness of this type of study.

P-Nucleus Interactions: While proton-nucleus interactions are more complicated and less easy to interpret theoretically, there is some theoretical and practical interest in knowing, for example, how the total inelastic cross sections vary with energy. Since the CERN storage rings will produce only p-p collisions, the highest accelerator energies for the study of p-nucleus interactions will be 2×10^{11} eV in 1972 and 4×10^{11} eV several years later with the NAL accelerator.

Since one can readily provide targets for one end of the spectrometer with on the order of a nuclear interaction mean free path of thickness of such nuclei as carbon, iron, and lead, the number of p-nucleus interactions could be made a factor of 10 greater than the corresponding numbers listed in Table II-3 for p-p interactions; 4×10^4 events with $E > 10^{12}$ eV and 800 events with $E > 10^{13}$ eV would appear statistically interesting. However, our past experience attempting to make such measurements with a spectrometer in close proximity to the nuclear target material indicates that it is almost impossible to be sure of what is being measured. There are two sources of confusion. First some interactions occuring in the target layer have only a single charged secondary leaving the target and secondly, some primaries, whose first nuclear interaction is in the spectrometer, produce backward secondaries which are interpreted as though the interaction had occurred in the target material.

Selection biases can be reduced by using target materials which scintillate in order to more reliably locate interactions. Another method would be to use different target thickness and use a subtraction technique to reduce the biases. In the present experiment, the top section of the ionization spectrometer is a totally active CsI module arranged in layers of uniform thickness. However, it is not considered a reasonable alternative to add other target materials to this module. The complexity thereby introduced must be measured against the fact that one expects, at most, changes of 10 or 20% in cross section per decade of energy so that biases must be small and very insensitive to primary energy. Our opinion is that the potential results would not justify compromising the cosmic ray composition and spectra experiment by reducing its counting rates a factor of 2 or more and by introducing greater complexity into the experimental apparatus.

In spite of the above stated conclusion, it is possible that a very definitive nuclear interaction experiment using the cosmic ray beam may be proposed. If the scientific rewards from such an experiment warrant it, it may be necessary to reexamine this conclusion.

Assuming that a very fundamental and unique nuclear physics experiment is forthcoming then one may consider using the ionization spectrometer to provide the energy measurement for both the cosmic ray and nuclear physics experiments. It is of course, necessary for the two experiments to be compatible to each other,

and to the spacecraft in terms of mechanical constraints, information handling limitations etc. Though such a possibility is not foreseen, the coexperimenters of the high energy cosmic ray experiment are willing to consider any particular case on its merit.

2. Nuclear Physics Using the Spectrometer

A second important aspect of nuclear physics is related to this experiment through the principles of operation of the ionization spectrometer. The interaction cross sections, and other parameters such as the inelasticities and the multiplicities, all must be known in order to understand the way in which the spectrometer responds. By the same token, the spectrometer can be used to provide some information about these parameters both through the calibration program and from the flight data.

The nuclear physics which relates to the operation of the ionization spectrometer is discussed in this section.

a. Interaction Cross Sections

When the energy of the incident particle is known, the spectrometer can be used to obtain information about the nuclear interaction process. The amount of information which can be extracted from the cascade development is limited by the simplicity of construction necessitated by the requirements of space flight. However, the spectrometer is suitable for making measurements on the p-nucleus inelastic cross section. The measurements can be made by examining the distribution of depths at which the first interaction of the primary particle occurs.

It has been shown (Schmidt, 1969; Pollvogt, 1970; and W. V. Jones et. al., 1969) that it is impossible to carry out reliable measurements of the inelastic interaction cross section as a function of energy with a single slab of target material.

This is related to the fact that it is very difficult to define what is an interaction and where it has occured. However, Schmidt (1969) has used an arrangement similar to that proposed here to measure the interaction cross section in iron. He shows that sufficiently far from the boundaries of a stack of modules similar to the one proposed here, the slope of the exponential distribution of beginning points of cascades gives the mean free path of nuclear interaction. This technique will be used during the accelerator calibration exposures of the proposed spectrometer to measure the inelastic interaction cross section of protons in tungsten. Establishing the inelastic cross section is an important factor in determining how well the energy response at accelerator energies can be extrapolated to the highest cosmic ray energies.

Extensive work with the ionization spectrometer in cosmic ray experiments, largely at mountain altitudes, indicates that the nuclear interaction and electromagnetic cascade processes do not change their character in the 10^{10} to 10^{14} eV energy region. This conclusion is supported by results from nuclear emulsion stacks and extensive air shower experiments. The total inelastic nuclear interaction cross section remains roughly constant. If there is any change with

energy, most indications are that it rises only slightly as the energy increases, possibly due to coherent effects in complex nuclei. Any increase in the total inelastic cross section can help an ionization spectrometer of a given depth to work better, partially offsetting the need for more material at higher energy to absorb the same fraction of electromagnetic cascade energy.

It will be possible also to utilize the data from the proposed satellite experiment itself to confirm that the total inelastic nuclear interaction cross section behaves as expected. As in the case of the accelerator calibration this can be done by examining the distribution of depths at which the first interactions of the incident particles occur. Of course, there must be a means of energy measurement in order to select particles of a certain energy. Therefore, between the largest depth of sampling for interactions and the lower edge of the spectrometer there must be a sufficient amount of absorber to measure the energy. If at all sampling depths one uses for energy measurements an equal length of absorber, then the energy measurements will be done in the same way for each sampling depth. Thus for the purpose of cross section measurement the total depth of the spectrometer should be:

boundary layer + number of samplings of interactions + sufficient material to measure energy.

The boundary layer should be 1/2 interaction length (λ) (Schmidt, 1969). There could then be about four samplings, each approximately 1/2 interaction length apart. In the proposed experiment there remains 2.5 λ of material which

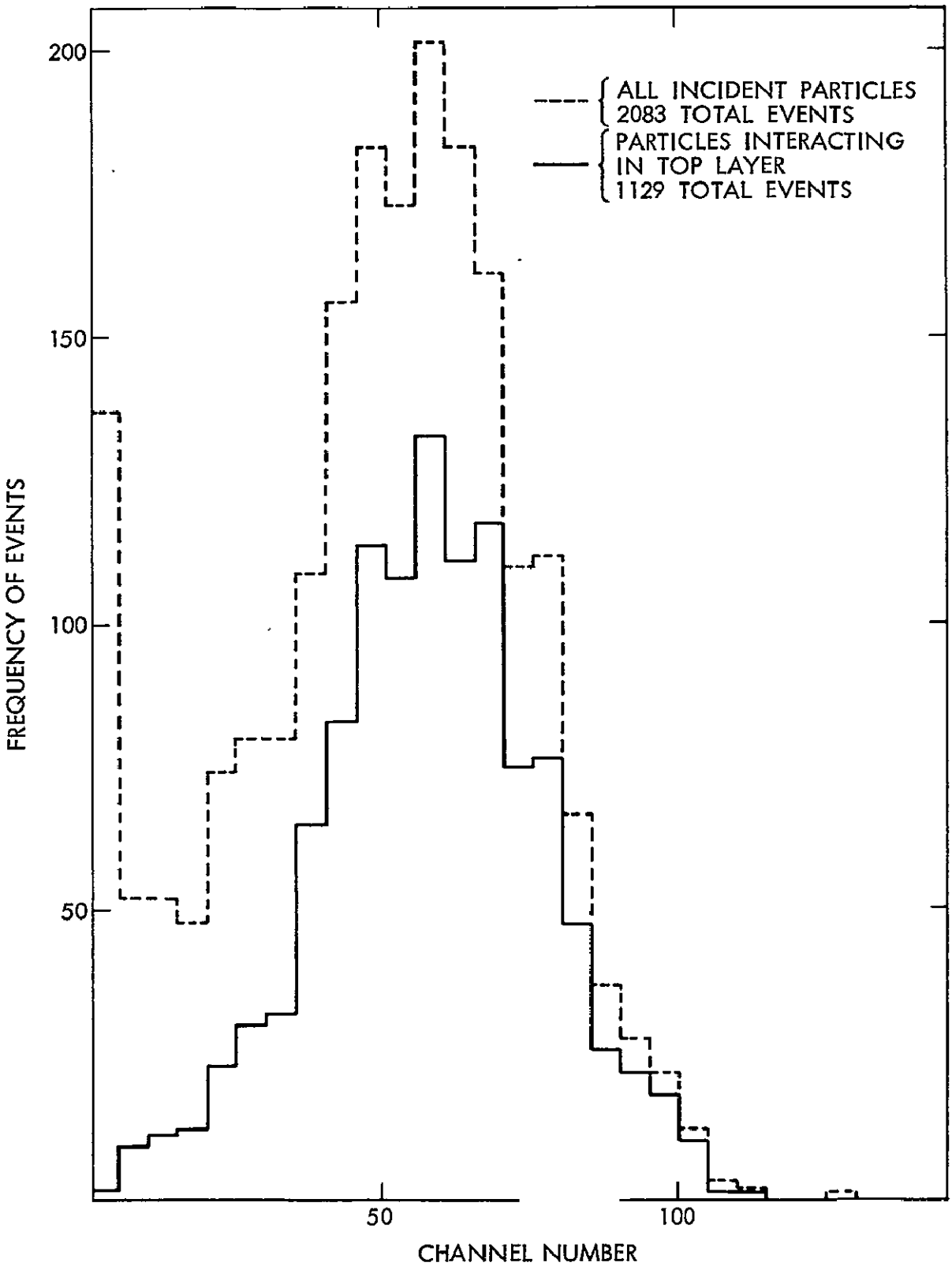

Figure II-11. Calibration measurements with 28 GeV/c protons with an iron ionization spectrometer of 2.5 λ total depth.

should be sufficient for energy measurement. It has been shown in previous work (Schmidt et al., 1969) that a spectrometer with a depth of roughly 2.5λ (inelastic) of iron can be used to measure the energy of high energy particles. Figure II-11 shows the results of calibration measurements with 28 GeV/c protons for the small spectrometer just mentioned. The solid histogram is the pulse height spectrum for events interacting in the top layer of the spectrometer. Since any changes in cross section with energy are expected to be slow, this accuracy (~35%) should be sufficient, and furthermore, it is attainable in 2.5λ of the total 5λ depth of the proposed spectrometer.

b. Multiplicity, Inelasticity, and Nuclear Disintegration Energy

Besides the inelastic cross section, the parameters which have the largest effects on the nuclear-electromagnetic cascade development are the multiplicity, inelasticity, and nuclear disintegration energy. Therefore, it is important to establish the mean values and fluctuations of these parameters. In order to accurately extrapolate the accelerator energy calibration of the ionization spectrometer to cosmic ray energies, one must know the dependence on primary energy of each of these parameters for interactions occuring in heavy absorbers (such as in the ionization spectrometer absorber).

The tungsten spectrometer in conjunction with the CsI(Tl) sections can be used to obtain valuable information about these nuclear interaction parameters, both from the accelerator calibration exposures and from the flight data. For

the most part, only the mean values of these parameters will be determined. Their distributions can be measured only at the accelerator energies.

Information about the multiplicity and the nuclear disintegration energy can be obtained from interactions occuring in the CsI (T1) section of the apparatus. The CsI (T1) section is comprised of five separate layers, each 1 radiation length in thickness. CsI (T1) is sensitive to the disintegration energy, which appears in the form of nuclear evaporation fragments. Neutrons carry about one third of the disintegration energy. The charged fragments are mostly heavily ionizing particles with very short path lengths in CsI (T1). Therefore, one will be able to identify the layer of CsI (T1) in which the interaction occurs. The output signal from that layer will be a measure of the nuclear disintegration energy for the interaction. Therefore, the dependence of the energy of nuclear disintegration on primary energy can be well established at accelerator energies. Information at higher primary energies can be obtained from the cosmic ray interactions in the CsI (T1) section during the flight of the experiment in balloons and the HEAO satellite.

The output signal from the CsI (T1) layer immediately below the one in which an interaction occurs will provide information about the multiplicity of charged particles produced in the interaction. The variation of the multiplicity with energy can be obtained reliably at the accelerator energies. Any changes at high energies, such as the decreasing dependence on energy suggested by

Malhotra (1963) should be detectable from the spectra of cosmic ray particles encountered during the flight.

It is difficult to make any unambiguous measurements of the inelasticity of the interactions with the apparatus planned. However an estimate of the amount of energy appearing in neutral mesons can be obtained from the energy in the electromagnetic component from the first interaction. Current experimental results strongly favor charge independence and so one can estimate the mean elasticity as a function of primary energy. Tungsten is a favorable material for this measurement because the radiation length is small compared to the interaction length. The electromagnetic cascade from the first interaction would tend to build up a maximum, where their energies can be reliably measured, before cascades from later interactions have been produced. Uncertainties in the location of the first interaction do not have a large effect on inelasticity measurements by this method, unless the inelasticity is significantly dependent on the multiplicity of the interaction.

c. Effect of the Speculative X-Process and Quarks on Energy Measurements with the Ionization Spectrometer

It has been suggested by Keuffel et al. (1969) and others that an "X-process" may exist at muon energies above 10^{12} eV in which a fraction of the energy is given directly to muons. This could occur directly or through the channel of a very short-lived particle which rapidly decays into muons before there is an

appreciable chance of its suffering a nuclear interaction. Such muons would deposit very little of their energy in an ionization spectrometer resulting in an underestimation of the energy of the primary particle. The results from other experiments do not confirm the results of the Utah group. One may regard the Utah analysis as giving an upper limit on the magnitude of the hypothetical X-process. According to their analysis, approximately 2% of the muons with energy above 10^{12} eV come from the X-process. The result with 10^{12} eV muons corresponds to a primary energy of about 10^{13} eV. Since these muons correspond to 10^{13} eV primaries, on the average less than 2% of the secondary energy is invisible to the spectrometer from this process. This would have a negligible effect upon determining energy spectra up to 10^{13} eV, since the anomalous events would be thrown into lower energy bins where there are already much larger numbers of normal events. This argument can be extended to primaries at least up to 10^{14} eV, since the center of mass energy in nucleon-nucleon collisions is only a factor of 15 greater. No case is known at lower energies where a process with a high energy threshold (usually due to high secondary particle mass) completely takes over and suppresses reactions with lower thresholds. Also the trend of the Utah results indicates the relative number of secondaries from the X-process may be decreasing at the highest muon energies observed.

The collection area of this experiment is such that only a few cosmic ray particles with energies appreciably above 10^{14} eV could be expected to enter the apparatus during a year of satellite operation, so it is a moot question whether

the energies of these few events would be faithfully estimated. Therefore, it can be concluded that over the useful range of the proposed spectrometer for measuring cosmic ray particle intensities, 10^{10} - 10^{14} eV, its performance would not be significantly affected by the possible existence of an "X-process."

There is also a possibility that at high energy an incoming proton might diffraction dissociate into its hypothetical three constituent quarks. Each of these quarks would have a quark-nucleon inelastic cross section which is about one third of the corresponding proton-nucleon cross section. If the quark mass were much greater than that of the nucleon, only a small fraction of the quark's kinetic energy would be lost in each collision. If this were to happen, the nuclear mean free path for producing pions and other secondaries would become longer and smaller fraction of the energy would be deposited in the spectrometer. It seems very unlikely that such a phenomena will significantly affect the spectrometer in the 10^{10} - 10^{14} eV region because: (1) the existence of quarks is generally regarded as not established in spite of numerous searches and (2) the negative results of many quark search experiments make it unlikely, if they exist, that they are copiously produced in the 10^{10} - 10^{14} eV region.

III. EXPERIMENTAL APPROACH

A. GENERAL DESCRIPTION

The apparatus described here has been developed over the last few years on balloon borne models by the GSFC and the LSU-MPI groups. The proposed satellite version is shown schematically in Figure III-1. The center section is the ionization spectrometer, charge detection modules are at either end, and spark chambers are shown as the directional detectors in this diagram. The tungsten modules shown in the middle section of the two-ended detector assembly comprise about 2/3 of the total weight. In order to make optimal use of this payload and the spinning nature of the satellite (the ends are alternately occulted by the earth), the two ends are identical so that the telescope operates continuously.

The ionization spectrometer consists of the 12 tungsten modules and the CsI(Tl) layers on either end. The total spectrometer is 5.5 nuclear mean free paths (λ) (135 radiation lengths X_0).

A tungsten module is shown in Figure III-2. It is 0.42 interaction mean free paths (10.4 X_0) thick. Pilot Y scintillator, 1/4-inch thick, is placed every 3.8 radiation lengths to sample the cascade particles. These scintillators are "double-wedge" shaped to provide directional information.

The top section of the ionization spectrometer is a totally active module consisting of 5 radiation lengths of CsI(Tl) arranged in optically independent,

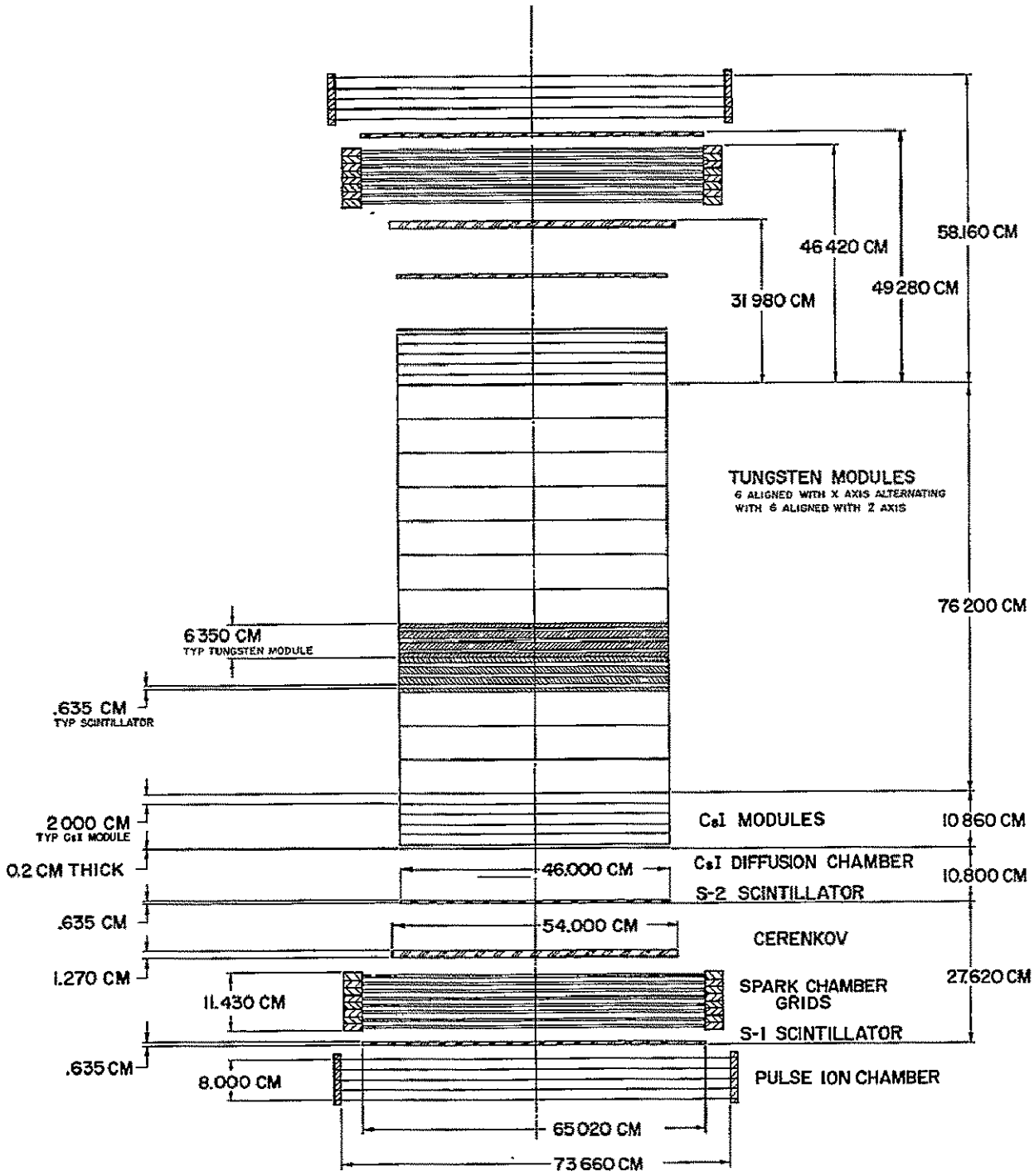

Figure III-1. Schematic diagram of experiment showing dimensions.

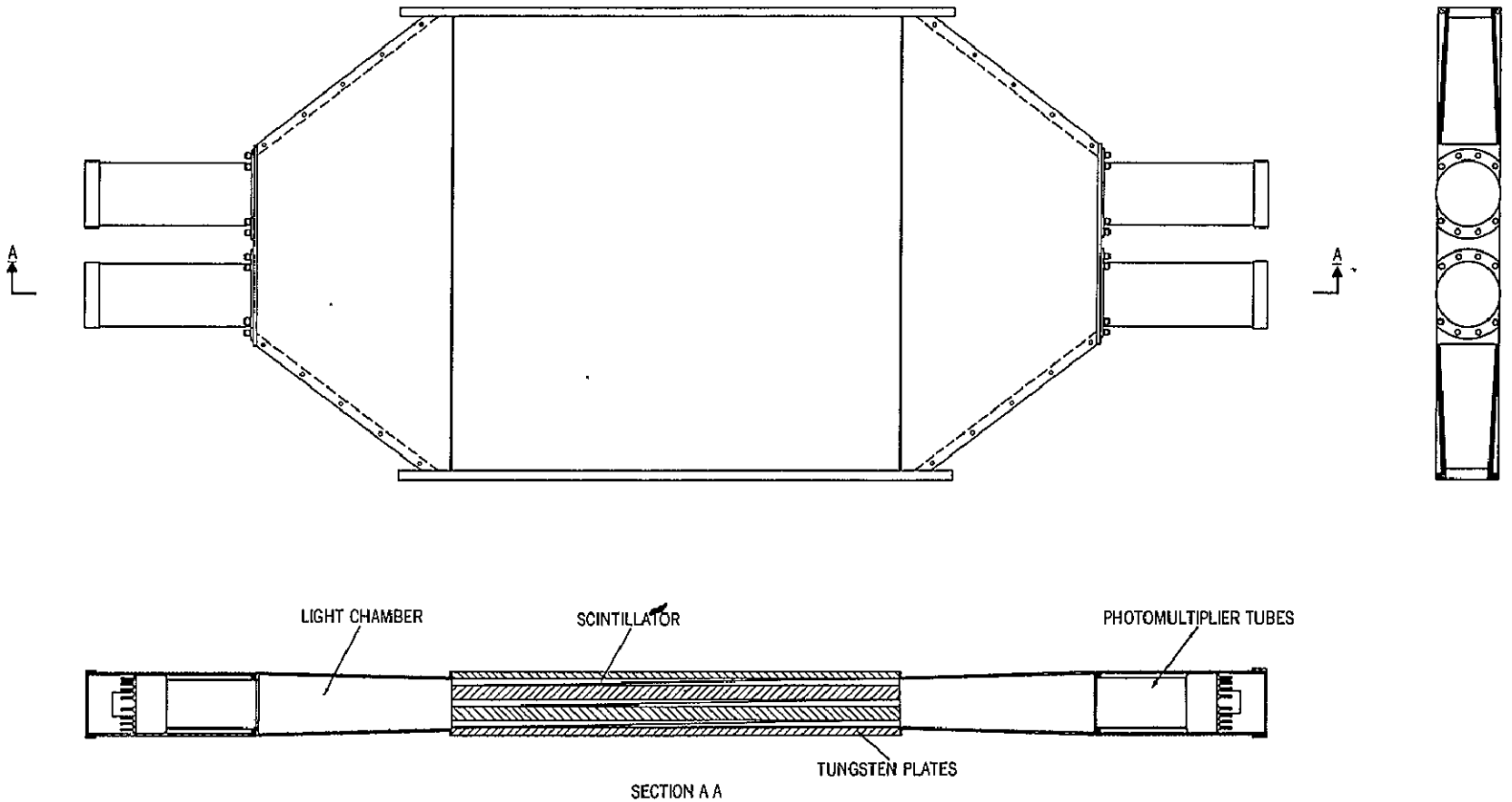

Figure III-2. Schematic diagram of one of the 12 individual modules comprising the ionization spectrometer.

1-radiation length thick slabs. Signals from these modules are used to aid in distinguishing between incident electrons and protons. Nuclear interactions which take place in this section can be examined in significant detail. The charge-defining modules are situated at the two extreme ends of the detector. The main geometry of the telescope is defined by the plastic scintillators S-1 and S-2. The Cerenkov response is proportional to Z^2 of the incident particle and provides a very linear signal over the whole charge range. The Cerenkov velocity threshold is used to reject low energy background particles. The diffusion chamber contains a 3-mm thick layer of CsI(T1), the light signal from which is collected efficiently by diffuse reflections in the light chamber. The outer element is a pulse ion chamber which responds to the very heavy nuclei. The directional detector shown in Figure III-1 is a wire spark chamber composed of 8 x-y grids.

The considerations which influenced the design of the ionization spectrometer are discussed in detail in the next section. The proposed calibrations of the instrument are also described. In Section C the design and functions of the charge module are presented. The CsI(T1) module of the ionization spectrometer is discussed in Section D. The trajectory defining system is examined in Section E.

B. ENERGY MEASUREMENTS – IONIZATION SPECTROMETER

The direct measurement of primary energies becomes increasingly more difficult in the ultra-relativistic range. Many of the physical processes vary like the logarithm of the energy and so exceedingly broad band devices are needed to measure this slow variation with energy. The most straight-forward technique is the ionization spectrometer originally proposed by Grigorov et al. (1958). This method is essentially a "three dimensional" version of the techniques developed for studying extensive air showers. Briefly, nuclear interacting particles are incident on an appreciable mass of condensed matter. Through a series of nuclear interactions the primary particle loses its energy to secondary particles which are mostly pions. These interact further contributing to the development of the nuclear cascade. The neutral pions all decay rapidly into gammas whose energy is dissipated in electromagnetic cascades. If the spectrometer is sufficiently thick, most of the initial kinetic energy of the primary particle is thus converted to ionization, and by sampling this ionization at frequent intervals it is possible to determine the total primary energy.

This method of measuring energy is not unique and other methods such as the transition radiation detectors have exciting possibilities for the future. Within the framework of this experiment the ionization spectrometer has been chosen as the best currently available technique for the whole energy range 10^{10} to 10^{14} eV. The considerations which have gone into its design are discussed in the subsequent paragraphs.

1. Design Optimization

The material composition, the physical size, and the geometrical configuration of the ionization spectrometer are determined by the following considerations:

(1) The total available payload weight;

(2) The accuracy with which energy of the cosmic ray primaries is to be measured; and

(3) The geometrical factor sufficient to investigate the expected cosmic ray flux.

The proposed ionization spectrometer has been designed to optimize energy resolution and geometrical factor under the constraints imposed by the maximum weight and space available to the projected experiment.

For a detector of uniform cross sectional area, a, and length, L, the geometrical factor, GF, is given by

$$GF \approx a^2/L^2 \quad (\text{for } L^2 \gg a).$$

This can be expressed in terms of the weight, W, to which the detector is constrained and the properties of the detector material: the length T of the detector in gm-cm^{-2} and the mean density, ρ, in gm-cm^{-3}. Since $a = W/T$ and $L = T/\rho$,

$$GF \simeq \frac{W^2 \rho^2}{T^4}.$$

Since the weight is independently constrained, the geometrical factor is optimized by choosing the material with the largest ρ^2/T^4. First let us consider how T depends upon the choice of material.

For any particular detector material, the desired energy resolution fixes the minimum acceptable T. The energy resolution is determined by the percentage fluctuations in the signal output from the active layers of the ionization spectrometers. Fluctuations of two types can occur: in the fraction of energy going into nuclear disintegrations and in the energy escaping through the bottom. The percentage fluctuations are smaller, the larger the number of nuclear interactions lengths along the path of the incident particle.

Both the column density (gm/cm^2) per interaction length and the number of interaction lengths necessary to achieve a particular energy resolution vary with detector material. The GF is maximized when T is minimized. The value of λ increases slowly with atomic number, favoring absorbers of low atomic number. On the other hand, because the inelasticity increases in heavier materials, the number of interaction lengths necessary to achieve a particular energy resolution decreases with increasing atomic number (W. V. Jones, 1970). These two effects tend to cancel and as a result, the column density necessary to achieve a given energy resolution is only weakly dependent on the detector material. For example, it increases by less than 25% in going from iron to tungsten.

In a detector composed of an absorber-scintillator sandwich, the energy resolution depends not only on the total amount of absorber material, but also on the spacing of the scintillator layers (Gillespie et al. 1970). Since much of the primary incident energy is partitioned into electromagnetic cascades, the sampling of the ionization energy must occur frequently enough that the electromagnetic cascades do not build up and die out between the detection layers. In Figure III-3 a and b the percentage fluctuations in the total number of particles detected is shown as a function of the thickness of the absorber material for both iron and tungsten, for four different primary energies. These figures are from Monte Carlo calculations by W. V. Jones (1970) in which the iron and tungsten are sampled every 2 and 4 radiation lengths, respectively. In the thicknesses required for the same energy resolution, about 6λ of iron and 5λ of tungsten, these correspond to 30 samplings in iron and 32 tungsten. The scintillator layers tend to dilute the density of the total detector, so the number of samplings should be no more than is necessary to achieve an energy resolution consistent with the performance of the rest of the instrument. Samplings each 4 X_0 in 5λ of tungsten gives ~20% energy resolution for 100 GeV protons. The resolution is better by about a factor of two for α-particles and should improve even more for heavier nuclei.

The geometrical factors, calculated for three different absorber materials for the allotted weight and for fixed energy resolution, are shown in Table III-1. The best choice for optimizing the geometrical factor is tungstern because of its

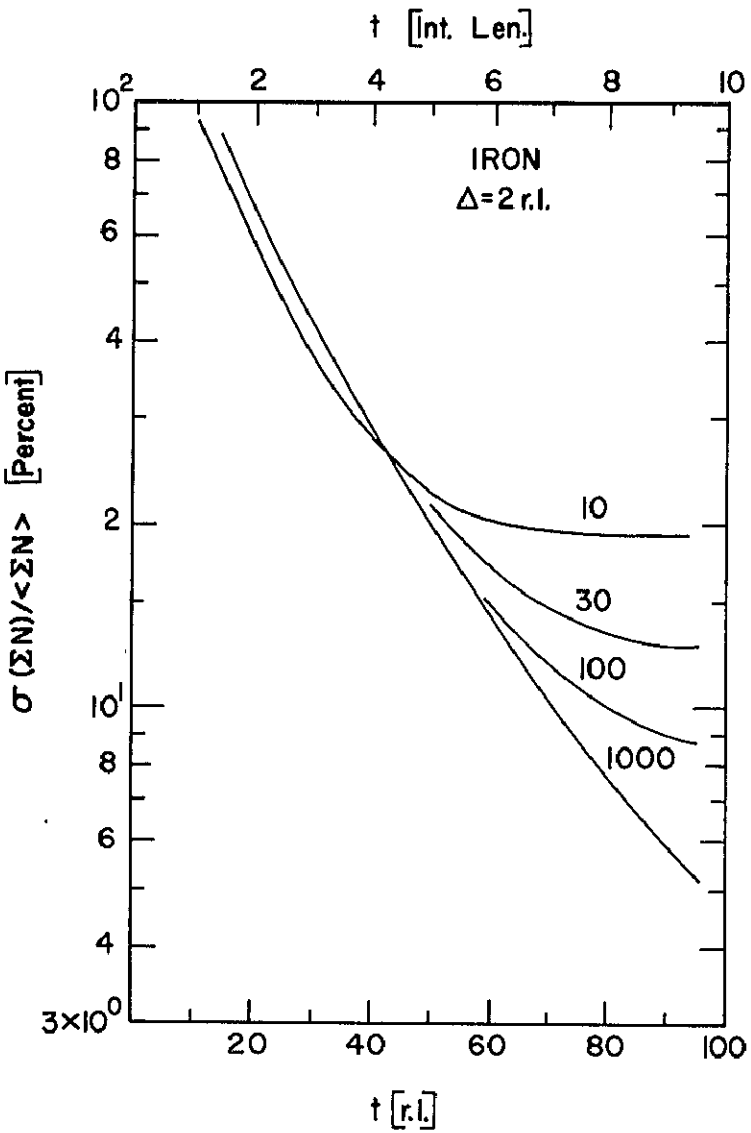

Figure III-3a. Relative standard deviations of the total number of particles ΣN recorded by an iron spectrometer of total depth t and sampling layer spacing Δ. The numbers beside the curves give the primary energy in GeV.

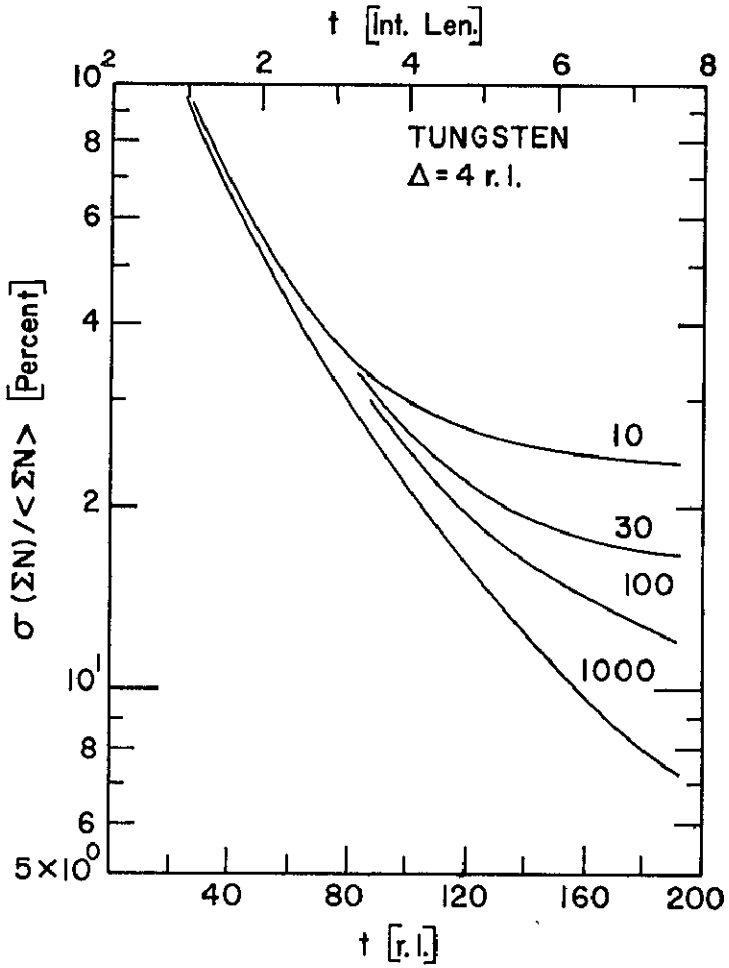

Figure III-3b. Relative standard deviations of the total number of particles ΣN recorded by a tungsten spectrometer of total depth t and sampling layer spacing Δ. The numbers beside the curves give the primary energy in GeV.

Table III-1

COMPARISON OF GEOMETRICAL FACTORS FOR DIFFERENT MATERIALS

Absorber Material	N[a]	λ gm-cm^{-2}	ρ gm-cm^{-3}	ρ_{eff}[b] gm-cm^{-3}	Relative Geometrical Factor
Tungsten	5	189	19.3	13.0	1.0
Iron	6	127	7.9	7.4	0.82
Glass	7	100	2.5	2.5	0.13

[a]Approximate number of nuclear interaction lengths needed to achieve less than 20% fluctuations for 100 GeV incident protons.

[b]The effective density of spectrometer plus sampling layers assuming one sample every 4 radiation lengths.

extremely high density. However the dilution of the scintillators reduces the gain considerably. Tungsten has an additional advantage over iron (copper is slightly better than iron) because of its large ratio λ/X_0. This aids greatly in separating electrons from protons and is advantageous for studying the inelasticity (Section II G).

Under the severe payload constraints of space flight, the weight in the spectrometer should be utilized as effectively as possible. A variety of scintillator arrangements have been suggested to use all the detector surface on the perimeter of the space craft. It has been found, however, that for a payload in the 6000 lb. class, so much of the weight is tied up in support structure, gondola, charge detectors, etc., that the most efficient geometry is two ended.

Several alternative geometries for the spectrometer are considered in Appendix 2. These considerations show that a "thin square" configuration, in

which all four sides are used is a close competitor in optimizing the geometric factor. However, the geometry for the energy measurement is complicated, and geometric effects would be introduced for which it would be difficult to compensate. While the directional measurements from the spectrometer (Section III-D) might have to be sacrificed, this alternative represents an attractive possibility for future experiments.

2. Calibration

The measurement of the energy of a primary particle using an ionization spectrometer is simple in principle. In a sufficiently deep spectrometer nearly all of the primary particle's energy is ultimately converted into ionization energy losses which can be measured. However, in practice there are a number of complications which must be taken into account. These are:

(1) Spectrometers have limited physical dimensions. Therefore, one must correct for energy leakage out of the sides and bottom of the instrument.

(2) Not all energy losses within the spectrometer are measured. In particular, the energies involved in nuclear disintegrations are essentially unmeasured in the sandwich-type device proposed here and only partially measured in a totally active (TANC) device. The energies of neutrons from such disintegrations are not measured with either type of device.

(3) In a sandwich-type detector the ionization is sampled by a material which is different from the primary absorber. A transition effect (Pinkau, 1965) is thus introduced because of the differing critical energies of the sampling medium and the primary absorber. Because of these considerations, several corrections must be made to the measured energy deposition in the spectrometer. These corrections are in general energy dependent.

These corrections are obtained by calibrating the instrument using known particles (protons and electrons) with known energies. The response of the instrument is then obtained as a function of incident energy. This has been done up to primary energies of around 30 GeV for a shallow iron spectrometer (W. V. Jones et al., 1969).

For high energy cosmic ray experiments, one needs to know the spectrometer response and the appropriate corrections at higher energies than those available at accelerators. Hence, one must somehow extrapolate the accelerator calibration results to higher energies. The extrapolation is most appropriately made by employing a Monte Carlo model of the nuclear-electromagnetic cascade in the spectrometer. This model is based upon all the available data on high energy interactions from emulsions and from mountain top experiments. The model is first applied to the particular spectrometer whose response has been determined at an accelerator. The parameters are adjusted until the calculated spectrometer

response agrees with the response observed with accelerator beam particles. This adjusted model is then used to calculate spectrometer properties at higher energies.

This Monte Carlo method has already been used extensively by W. V. Jones at the Max-Planck Institut and Louisiana State University in order to extend the accelerator calibration of an iron-absorber spectrometer to the higher energies observed in the cosmic rays. Figure III-4 shows a comparison of his three-dimensional calculations and the accelerator measurements with 10 GeV/c protons. This figure shows the frequency distribution (histograms in intervals of one particle) for the number of particles present in the 2.5 mean free path thick spectrometer. Each module contained two scintillators spaced 4 X_0 apart in the iron absorber. The agreement of the calculations with the measurements is quite satisfactory. Similar agreement was obtained for 20.5- and 28-GeV/c primary protons. Some further indication of the reliability of Jones' Monte Carlo model is shown in Figure III-5, where the calculations for 8 GeV/c protons in 3.5λ NaI are compared with measurements by Hofstadter (1969) for 8 GeV/c pions. In the calculations it was assumed that 1/3 of the nuclear disintegration energy was measured in the totally active NaI absorber. The calculations also agree with the burst size and lateral spread of the cascade particles measured in the Kiel air shower experiment at a depth of 10λ in a concrete absorber (Trümper, 1970).

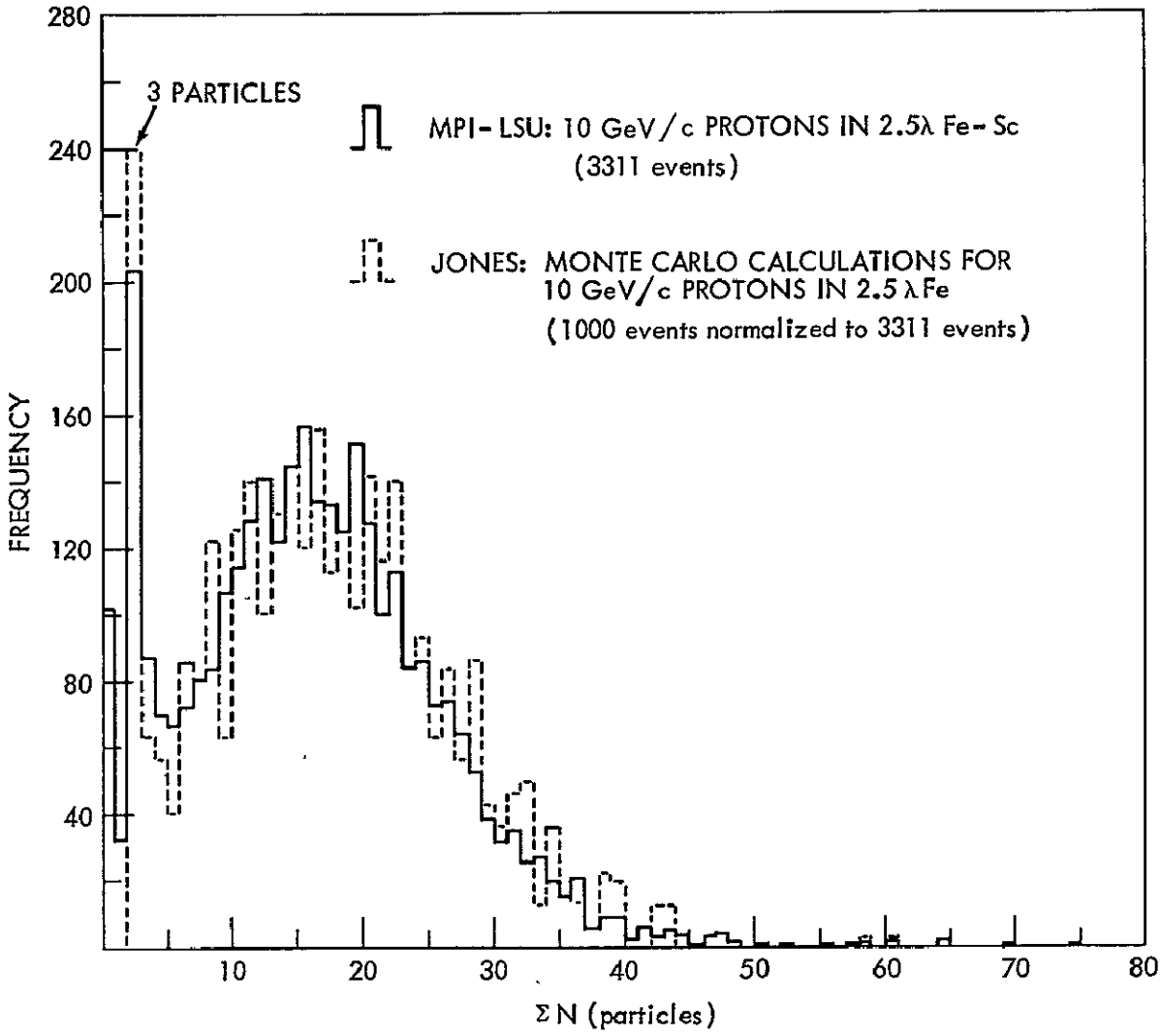

Figure III-4. Comparison of Monte Carlo calculations and accelerator measurements for the energy resolution of 10 GeV protons in an iron spectrometer.

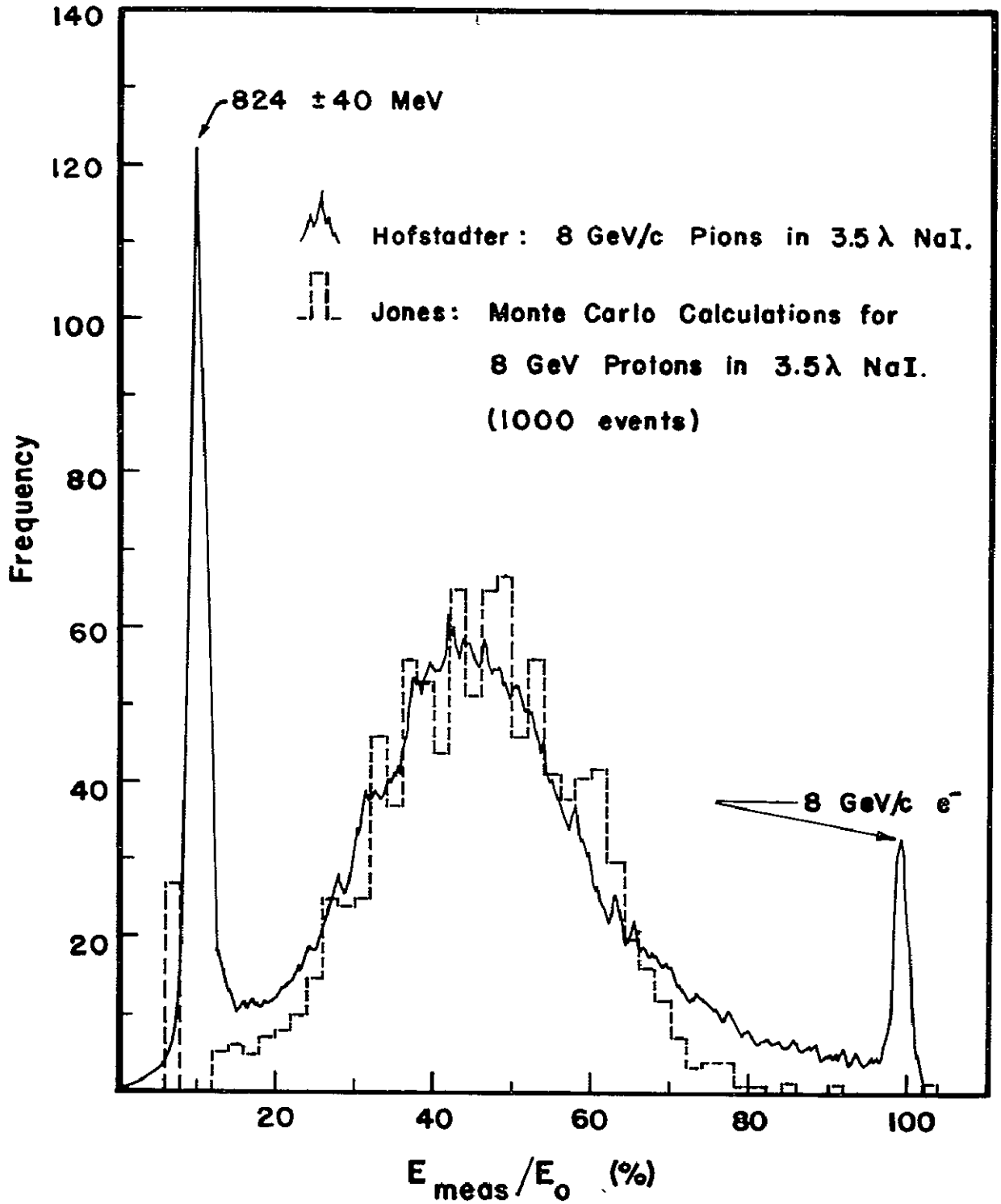

Figure III-5. Comparison of the energy resolution predicted by Monte Carlo calculations for 8 GeV protons in CsI with measurements made on 8 GeV/c pions.

Although the Monte Carlo calculations appear to be in good agreement with the measurements at low energies, one cannot be sure the agreement will still be good at very high energies or in other absorbers very different from iron and NaI. It is always possible for example that the Monte Carlo model used could have compensating errors which lead to apparent agreement with measurements. Thus it is highly desirable to perform extensive calibration studies of the proposed spectrometer at accelerator energies.

The Monte Carlo calculations suggest that systematic changes in resolution above energies of 100 GeV are small and predictable. It is fortunate that the National Accelerator Laboratory to be constructed at Batavia, Illinois, will be available well before the HEAO launch data for calibrating the experiment. It will provide a beam of 500 eV in a low current mode (most appropriate for the expected calibration) which will be used to verify the high energy Monte Carlo extrapolations. In the proposed calibration the parameters which most strongly affect the cascade development can be studied in detail. The following investigations are planned.

(1) The energy dependence of the spectrometer response will be determined.

(2) The inelasticity and the interaction cross-section will be measured at different energies using different absorber materials, e.g. Cu, Fe, W, and CsI (and TlCl if possible).

(3) The lateral and longitudinal cascade development will be studied.

3. Other Devices

The ionization spectrometer is by no means the only device which may be used to measure energy. Other possibilities have been considered and are compared with the ionization spectrometer. The energy resolution and its relationship to the experimental objectives are considered for TANC counters, superconducting-magnet spectrometers, and transition radiation detectors.

TANC counters: "Total Absorption Nuclear Cascade" (TANC) counters are usually meant to denote a special class of ionization spectrometers in which energy dissipation anywhere within the detector contributes to the output signal. A spectrometer which is constructed entirely of scintillating material is the most proven technique, but the output signal might also be a sonic vibration or Cerenkov light.

In the optimization of the spectrometer design discussed above it was shown that the achievement of maximum density is of paramount importance. The requirement that most of the primary energy be dissipated within the spectrometer fixes its thickness in the neighborhood of 800 to 1000 gm-cm^{-2}. For the region of the periodic table above and including iron, this thickness is almost independent of atomic number, A.

In Table III-2 the geometric factors associated with various spectrometer materials are compared assuming constant total weight and constant length, T, in gm-cm^{-2}. It can be seen from the table that the only close contender to the

Table III-2

COMPARISON OF DENSITIES AND RELATIVE GEOMETRY FACTORS OF SPECTROMETER MATERIALS

Material	Average Density	Relative Geometry Factor
<u>This Proposal</u> W - 945 gm-cm^{-2} 36 Plastic Scintillators - 24 gm-cm^{-2} CsI - 85 gm-cm^{-2}, half on each end	11.0	1.00
<u>Scintillator</u>		
NaI	3.67	.11
CsI	4.51	.17
TlCl	7.0	.41
<u>Cerenkov Radiators</u>		
Lead Glass - 970 gm-cm^{-2} CsI - 85 gm-cm^{-2}, half on each end	4.5	.17
PbF_2 - 970 gm-cm^{-2} CsI - 85 gm-cm^{-2}, half on each end	7.66	.48

tungsten-scintillator sandwich design among the scintillators is the recently announced TlCl (Rosette et al., 1970). As can be seen from Figure III-6, 5 λ of TlCl should have significantly better energy resolution than the proposed spectrometer. If the TlCl could be grown in large pieces at reasonable ($\sim 2.5 \times 10^5$ cm^3 would be needed) it might be considered as a substitute for the proposed spectrometer design. This high density scintillator would provide a significant

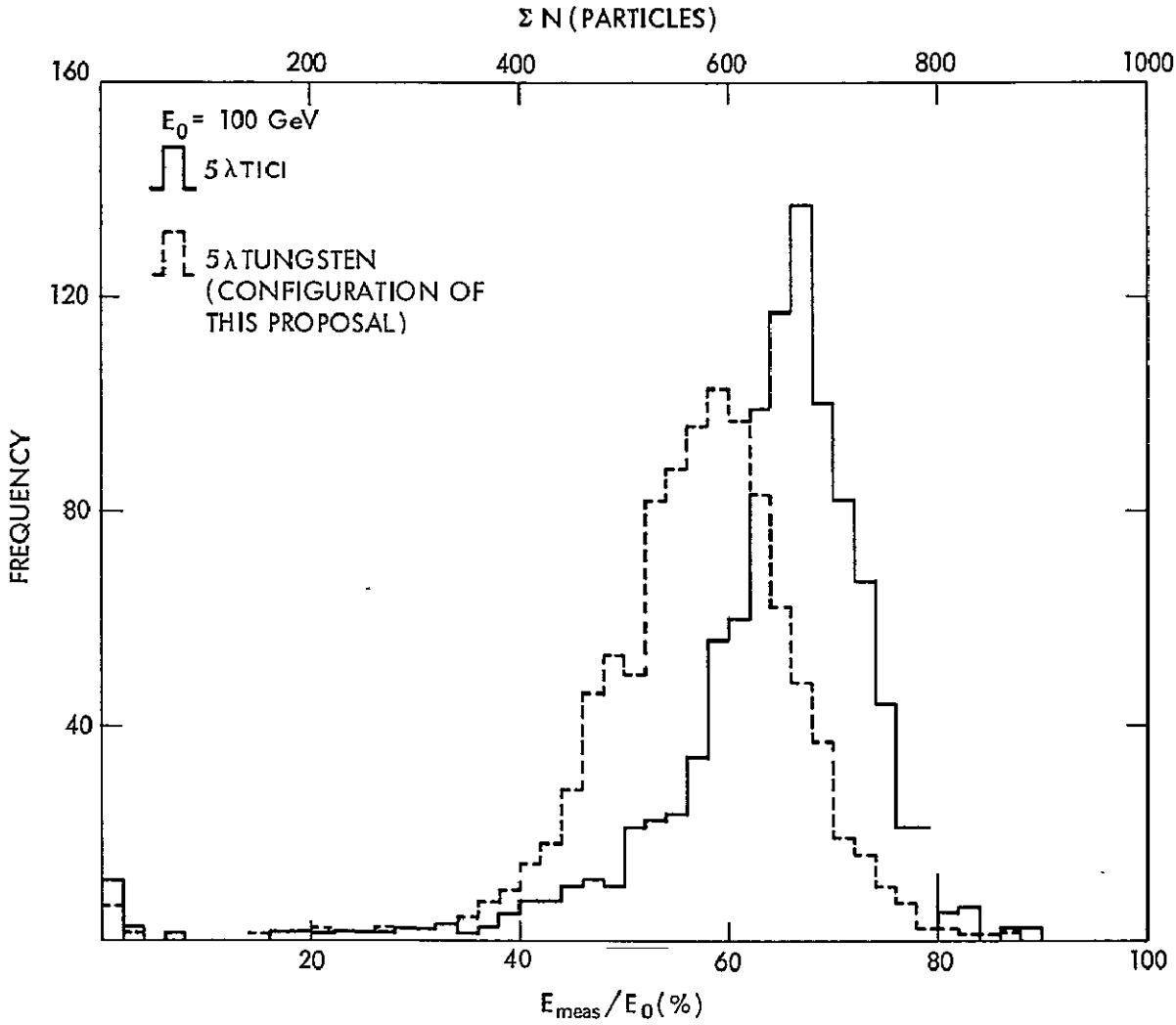

Figure III-6. Energy resolutions at 100 GeV primary energy predicated by Monte Carlo calculations for the 5λ tungsten spectrometer proposed and for a 5 λ TICl totally active spectrometer. The top scale gives the sum of particles for the tungsten spectrometer while the bottom scale gives the percent primary energy deposited in TICl.

improvement in energy resolution over the proposed tungsten-scintillator sandwich spectrometer at the same thickness, however its reduced density would reduce the geometric factor.

Superconducting Magnet Spectrometers: A magnetic spectrometer offers certain unique advantages, such as allowing one to distinguish e^+ from e^- and $\bar{p}$ from p, which are not possible using the ionization spectrometer. Since a magnet-spectrometer system also measures momentum, one must consider whether it could completely replace the ionization spectrometer approach. In order to make quantitative comparisons with a superconducting magnet and supporting cryogenic system having roughly the same mass as the proposed spectrometer, the magnet in the proposal by Alvarez et al. (1969), which they estimate to weigh 10,000 lbs. with its cryogenic support system, has been scaled down a factor of two in radial dimensions, but left the same in coil thickness. This reduces the weight by roughly a factor of 4, but allows the central field and superconductor current density to remain essentially unchanged. The outside coil diameter would be 1 meter. The average $\int Bdl$ is reduced a factor of 2 to about 15 kilo-guass-meters. The geometric factor would be of the order of 1 m^2-ster. If we assume the rest of the detector system of their proposal to also be scaled down a factor of 2 in linear dimensions to an outside diameter of 1.8 and a length of 1.3 m, then the energy resolution which may be achieved are given in Table III-3.

Table III-3

COMPARISON OF IONIZATION SPECTROMETER AND SUPERCONDUCTING MAGNET SPECTROMETER RESOLUTIONS

Device	Useful Energy Range / Energy Resolution
Ionization Spectrometer (This Proposal)	10^{10}-10^{14} eV $\frac{\Delta E}{E} \approx 25\%$ over entire range
Superconducting Magnet Spectrometer (see text)	(a) 10^{10}-10^{11} Ev if $\frac{\Delta E}{E} \leq 25\%$ and detector resolution = ±.1mm (b) 10^{10}-10^{13} eV if $\frac{\Delta E}{E} \leq 25\%$ and detector resolution = ±.001mm

Table III-3 indicates that a superconducting magnet spectrometer in the 2000-3000 lbs. weight class would fall short by a factor of 10^3 to cover the useful energy range of the ionization spectrometer if the detector position measuring resolution is ± 0.1 mm. A resolution of ±0.1 mm is already somewhat better than that generally achieved with large area wire spark chambers. It is evident that a magnet spectrometer system cannot begin to approach the energy range of the ionization spectrometer until a number of serious technological problems are solved: (a) detectors with square meters of area must be developed with spatial resolutions $\sim$±1 micron whose output can be telemetered back to Earth; (b) the $\int$Bdl obtainable with a given weight magnet system must be improved; and (c) a cryogenic system capable of working reliably for long periods in space must be developed. At the present time the useful range of

magnetic spectrometer is in the range 10^{10} to 10^{11} eV, and extending beyond 10^{12} eV will be difficult within the next 2 or 3 years. While studying anti-particle to particle ratios over this range would be most interesting, the compromises to other objectives of this proposal are prohibitive. There are interesting possibilities however for future space station experiments in which a super conducting magnet operates in conjunction with an ionization spectrometer.

Transition radiation detector. There has been much discussion and investigation of the possibility of utilizing transition radiation (Yuan 1968), photons emitted when a charged particle crosses a discontinuity in dielectrics, to measure $\gamma = E/Mc^2$ of a high energy particle. This possibility stems from the fact that the energy spectrum of photons emitted has a shape similar to a bremmstralung spectrum, but with an upper photon energy limit which is proportional to γ. For $\gamma = 10^3$, the upper photon energy limit is $\sim$50 keV. In order to obtain response proportional to γ for 10^{10} to 10^{14} eV protons the transition radiation photon detector must totally absorb photons over a 10^4 dynamic range from 0.5 keV to 5 MeV. Since the photons are emitted close to the line of travel of the charged particle, the photon detector must discriminate against the ionization energy loss of the charged particle which is also passing through it. Yuan (1970) has operated a transition radiation device using electrons at $\gamma = 10^3$ in an accelerator beam, and he finds that even at this γ with a large number of transition surfaces, the number of detected photons one can expect is small.

There are two major problems which must be overcome before this detector could be considered as an alternative to the ionization spectrometer.

(1) A practical means of producing large numbers of photons over the range $\gamma = 10 - 10^5$ must be found.

(2) A way of efficiently detecting the photons produced with good signal to noise ratio over a 10^4 dynamic range in the presence of the incident charged particle must be found.

These would seem to be potentially achievable only at the highest γ's and so at this time cannot be considered as an alternative to the ionization spectrometer.

C. CESIUM-IODIDE SECTION

Recent disagreements between different experimenters on the intensity and shape of the primary electron energy spectrum were discussed in an earlier section. They point out the need for very careful experimentation with emphasis on good discrimination of electrons from the copious background protons. The disagreements in intensity estimates by different groups (e.g. see Anand et al., 1969, or Marar et al., 1969) could also involve errors in energy estimation. Detectors with event rejection from "anti-coincidence" counters may be rejecting good electrons when one of the copiously produced low energy x-rays finds its way into an "anti" where it can produce a Compton electron.

The arrangement of the CsI electron cascade section was shown in Figure III-1. The top scintillator is thin, 1 gm/cm^2, so that it can be used as a charge measuring detector before the particles start losing their identity due to either electromagnetic cascading or nuclear collision.

The remainder consists of five scintillators, each 1 radiation length thick and viewed through opposite edges by two photomultiplier tubes. Each of these layers is pulse height analyzed so that there are five pulse heights corresponding to the passage of a particle through this section. The scintillators have large light outputs (e.g., singly charged relativistic particles lose $\sim$11 MeV) and so the resolution is limited only by Landau fluctuations and geometric effects. The geometric effects can be corrected by the use of proper calibration in conjunction with the trajectory of the particle.

The first tungsten modules (both ends) instead of having the signals from their three samples added, will have each scintillator pulse height analyzed separately. This will give further differential information on the longitudinal cascade development near shower maximum.

The average electromagnetic cascades and the location of the scintillators which sample the energy deposited are shown in Figure III-7.

The incident electrons develop electromagnetic cascades, in the CsI (Tl) scintillators. When they enter the tungsten part of the spectrometer, the

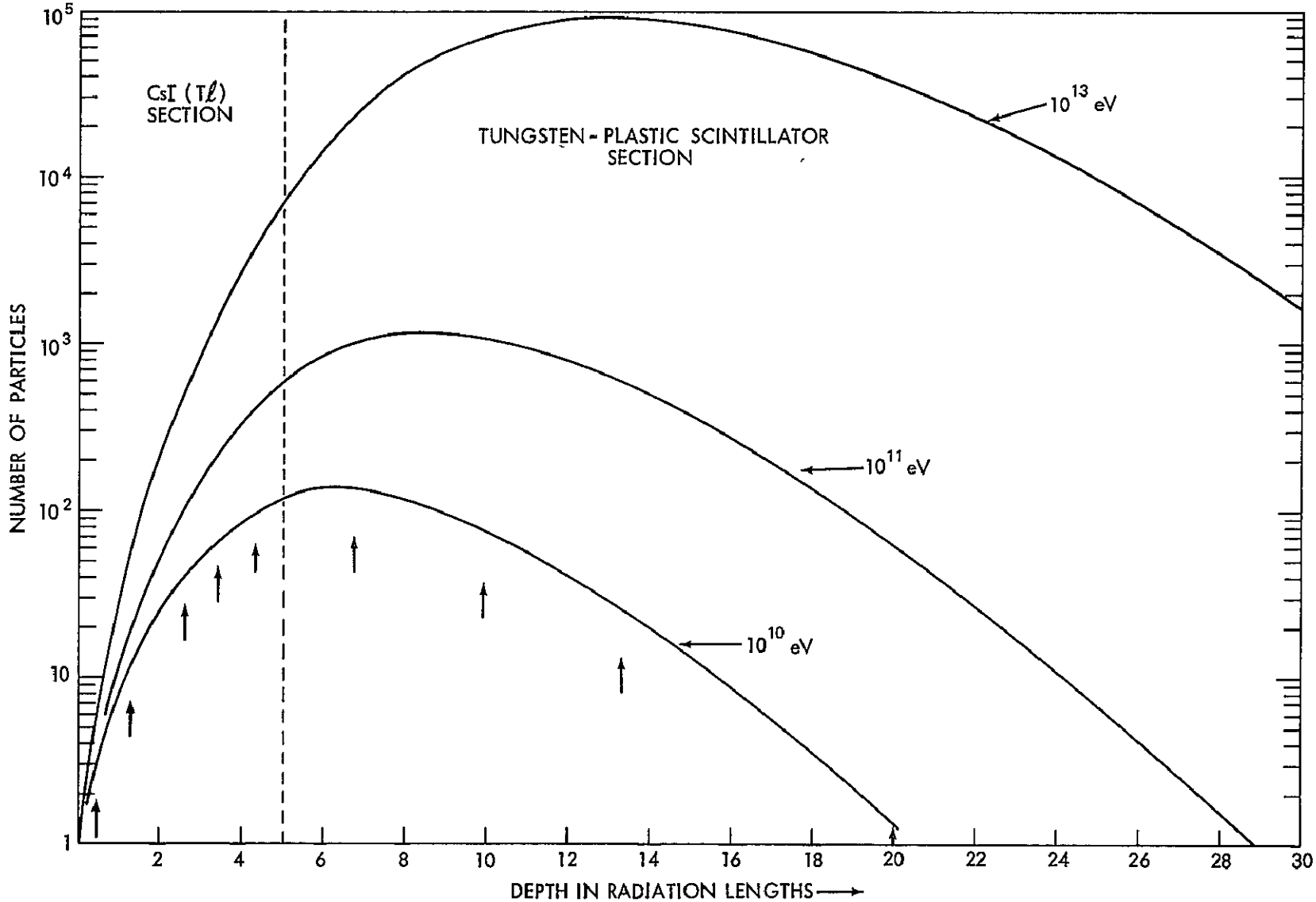

Figure III-7. Electron showers. Arrows indicate the location of scintillators which sample the shower.

development of the cascade continues through shower maximum until the cascade is completely absorbed. The tungsten is 125 radiation lengths deep and hence is able to completely stop all pure electromagnetic cascades. This will be exceedingly important in distinguishing electrons from cascades genetically related to nucleons. These events, for the same total energy deposited in the spectrometer, will have ionization losses distributed throughout the spectrometer. The electron measurements made to date from balloons have been done using substantially fewer radiation lengths. This reliance on the early part of the development of electron cascades has made the measurements subject to masquerading events from the copious proton background.

A copious "background" of protons is present. Some of these masquerade as electrons by producing one or more neutral pions in an interaction near the top of the spectrometer. The instrument is designed to make this imitative phenomenon as small as possible. The separation is more difficult the nearer the top of the spectrometer a particle interacts. From accelerator studies of shower fluctuations (Silverberg et al., 1970) it is known that electron-induced showers develop rapidly and have apparent origins within 2.5 radiation lengths of the top of the detector 98% of the time. For this reason, a totally active CsI section has been used as the initial section of the ionization spectrometer in order to "see" as many of the interacting protons as possible.

Proton interactions can be distinguished from purely electromagnetic cascades by the presence of heavily ionizing tracks. The number of heavy prongs is referred to as N_h in emulsion literature. These heavy prongs include the knock-on protons and the evaporation particles (black tracks). The energy of disintegration of the target nucleus goes into these heavily ionizing prongs localizing the energy of nuclear disintegration. The works of Jain et al. (1965) and Murzin (1969) have shown that $N_h \approx 8$ and is essentially constant from about ~30 GeV to ~3000 GeV. The spectrum of these particles is peaked at lower energies and so the nuclear disintegration energy of ~1 GeV is localized at the point of interaction. The pions take away the inelastic part of the energy and propagate the nuclear cascade. On the other hand a primary electron and its associated shower particles will produce a signal corresponding to at most a few hundred MeV during their passage through one radiation length. This difference between the nuclear and electromagnetic interaction is used to provide discrimination against protons simulating electrons.

As a quantitative measure of the effectiveness of this method an estimate of the contamination follows. The probability of interaction by a proton in a CsI block 1 radiation length thick is ~0.05. A proton in an interaction changes an average about 1/6 of its energy into the photon mode (Fowler and Kidd, 1967). So the protons competing with electrons have an energy ~6 times that of the electrons. The fraction of the protons which can simulate an electron

is

$$R = \frac{I_P(>E)}{I_e(>E_0)} \left[1 - e^{-2.5 X_0/\lambda}\right] \quad (1 - D)$$

where D is detection efficiency, I_P and I_e are the integral energy spectrum or protons and electrons. $E \approx 6E_0$ and X_0 and λ are respectively the radiation lengths and proton mean free paths.

It is rather difficult to get an exact value for D. However, D approaches unity for larger values of the nuclear disintegration energy. The spectrum of the heavily ionizing particles (Powell et al., 1959) has a most probable value of about ~10 MeV and has a negative exponent at higher values. Murzin and Sarcheva (1969) estimate an average value of 165 MeV for the heavily ionizing tracks. In the case of CsI which is reasonably linear in its response to low energy particles, one can expect all the energy released in evaporation tracks, and low energy N_h tracks to be detected close to the point of interaction. In one radiation unit of CsI protons of energy ~80 MeV will stop. The spectrum of N_h tracks is biased in favor of lower energy particles. The electrons of 100 GeV in one radiation length develop on an average 10 particles or deposits about 100 MeV. From the estimates of Grigorov et al. (1959), one can assume that in a nuclear disintegration about 1 GeV is deposited in heavily ionizing tracks. If all events in the literature with $N_h > 3$ are assumed to be due to collisions with the complex nuclei, then the presence of a nuclear disintegration will be detected with a probability of at least 0.7. This is undoubtedly a conservative

estimate because the CsI is also sensitive to all the low energy nuclear fragments with high efficiency. This is considerably better than what can be achieved with an electron cascade unit in which the cascade develops in an opaque, high-Z material such as tungsten or lead.

This method of separation will be useful over a geometric factor of about 1000 cm^2-ster because the later part of the shower is not important in the energy determination. Over the more restricted geometry of the complete spectrometer more complete separation of the proton background can be obtained.

The highest anticipated electron energy is 10^4 GeV and this shower will stop in about 50 radiation lengths. Cascades initiated by protons, for which the same total energy is deposited in the spectrometer, will have ionization losses distributed throughout. The lack of any signal from the remaining spectrometer, in conjunction with the directional information, will allow unambiguous electron proton separation.

The CsI section has other functions in the experiment. In the case of particles which have not suffered a nuclear collision it provides redundant dE/dx measurements which can help in achieving greater accuracy of charge identification. When an interaction does take place, its location can be identified and used for evaluating the accuracy of energy determination. The effects of interactions in nearby material on charge composition studies can be measured.

About 20% of the proton interactions (and a proportionally larger fraction of the interactions due to heavier primary particles) will take place in this section of the spectrometer. The nuclear physics which can be done with this section might be quite interesting and has been discussed.

The distribution of the interactions for any particular particle gives the mean free path in CsI, a compound whose nuclei have almost similar Z and A. It will also be possible to study the nuclear disintegration energy (energy going into heavy prongs) with the total energy of the particle. Any energy dependence in the disintegration of the nucleus could be studied.

D. CHARGE DETECTION

An important aspect of this experiment is the charge composition data. It has been pointed out that very little information is available above 20 GeV to compare with the extensive low energy data.

The difficult but realistic goal set for the design of this charge module was $Z \pm 0.5$ for $Z = 26$ increasing to ± 1 at $Z = 40$ and ± 2.5 at $Z = 80$.

The ability to realize this goal is determined by three main factors:

(1) the intrinsic statistical fluctuations in energy loss in the detector and the subsequent conversion of that energy to light;

(2) photo-electron statistics;

(3) and all the geometrical effects which produce variations in the light produced and collected.

Since the aim is to determine charge within ±1/2 a charge for nuclei up to and including Fe (Z = 26) signal resolution of ±4% is required.

In Figure III-8 a summary of the intrinsic resolutions for a thin detector is presented. The dashed line represents the separation between charges and the points represent full widths at half maximum (FWHM) calculated from the Landau distributions for a single detector. Note that at 8.4 GeV the FWHM exceeds the separation for Z > 22. At high energies the problems extend well down to Z = 16. This is further worsened by the skewness of the distribution becoming more extreme at higher energies. This is shown in Table III-4 where the probability of a Z of 25 simulating the ionization of other charges is given. (For reference purposes, the energy lost by an Fe of these energies is about 1.3 GeV in a 1/4" plastic scintillator.) This table illustrates that while the FWHM does not get worse at higher energies the distribution becomes more skewed making possible an error of 1, 2 or even more charges.

This problem is resolved by two considerations. First, the fluctuations which produce the Landau distribution are caused by the production of very high energy knock-on electrons. These knock-on electrons have sufficient range to leave the detector, reducing the skewness of the distribution. Secondly, an equilibrium tends to be set up so that as many knock-ons enter the element from above as leave

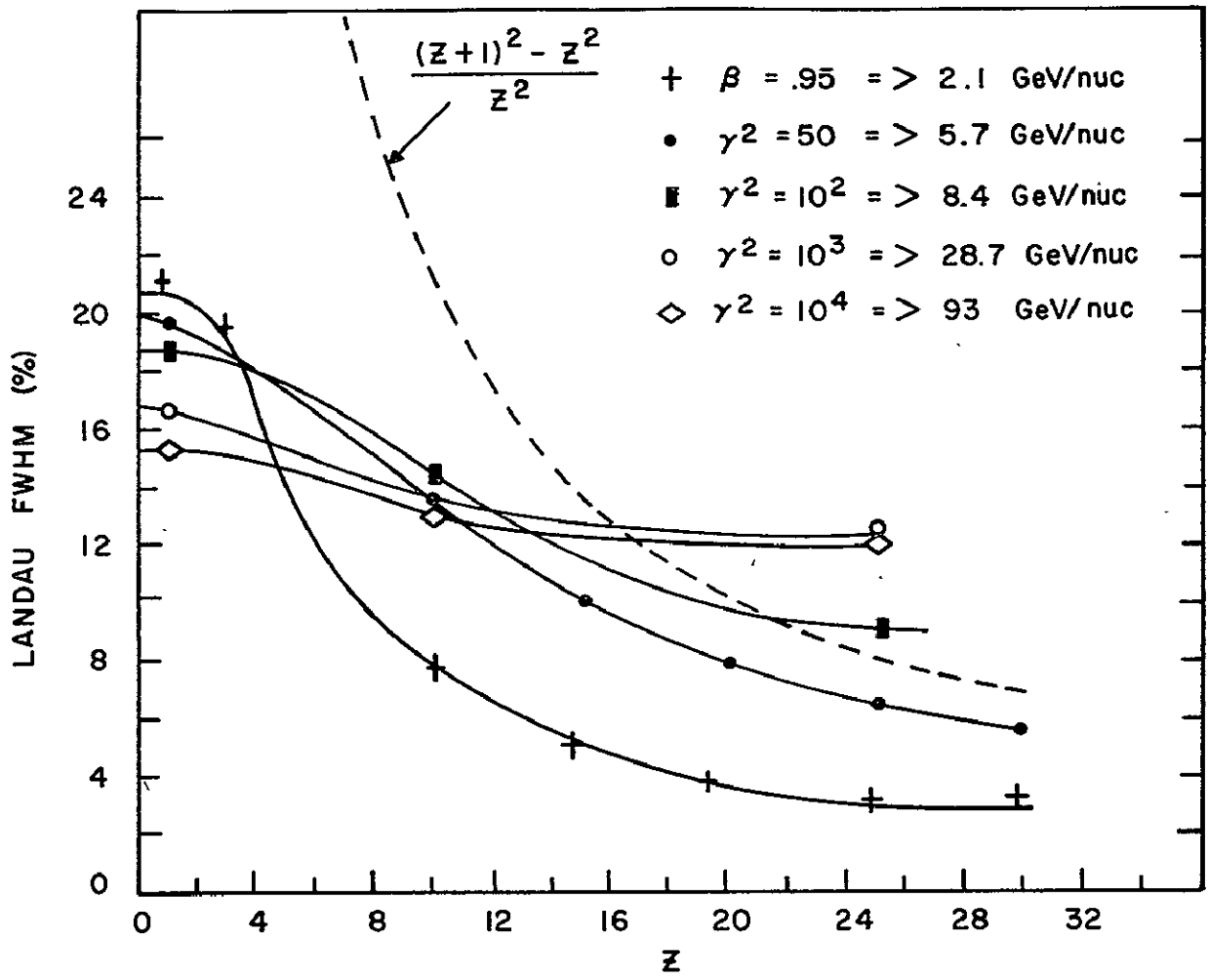

Figure III-8. Landau half widths as a function of particle charge for various energies.

Table III-4

SOME STATISTICS ON LANDAU DISTRIBUTIONS FOR RELATIVISTIC IRON NUCLEI

Energy (GeV/nuc)	$\gamma = \frac{E}{mc^2}$	E_t (MeV)*	P(<24.5)	P(<25.5)	P(25.5 - 26.5)	P(26.5 - 27.5)	P(>27.5)	f_{out}**
5.7	7.1	50	.03	.13	.02	0	0	0.8%
8.44	10	10^2	.01	.26	.10	.01	0	3.5%
28.7	31.4	10^3	.12	.52	.31	.14	.07	10.4%
93	100	10^4	.12	.57	.37	.22	.15	15.5%

*E_t is the maximum energy which can be transferred to a single knock-on electron.
**f_{out} is the fraction of energy into electrons with range greater than the detector thickness.

through the bottom, tending to smooth out fluctuations. In order to completely eliminate this problem, multiple charge measurements are made in all regions of the charge spectrum. If, as is shown in the last column in the table, the effect of energy loss from the crystal should reduce the response at high energies it will be possible to measure the energy dependence of the effect.

The magnitude of these various effects will be the subject of a Monte Carlo study in the near future. At any rate, because one wishes to operate at the limit of the intrinsic resolutions, the variations in pulse height due to systematic effects must be reduced to a few percent.

A schematic layout of the charge determination section is shown in Figure III-9. There are five elements for charge determination, all of which have theoretical responses proportional to charge squared at relativistic velocities. The plastic scintillators marked S1 and S2 define the particle acceptance cone of the telescope. These scintillators are viewed edge on through adiabatic light guides. The Cerenkov radiator marked C aids in the rejection of low energy particle background from interactions in the spectrometer. They correspond to particles which produce gray tracks in interactions in nuclear emulsions. The top CsI layer is designed to be thin to insure another charge measurement before the particle interacts. The remaining 5 CsI layers can be used for charge measurements until the particle interacts (total thickness is 0.25 λ). The fifth charge measurement is made in the parallel plate ion chambers at the top. They

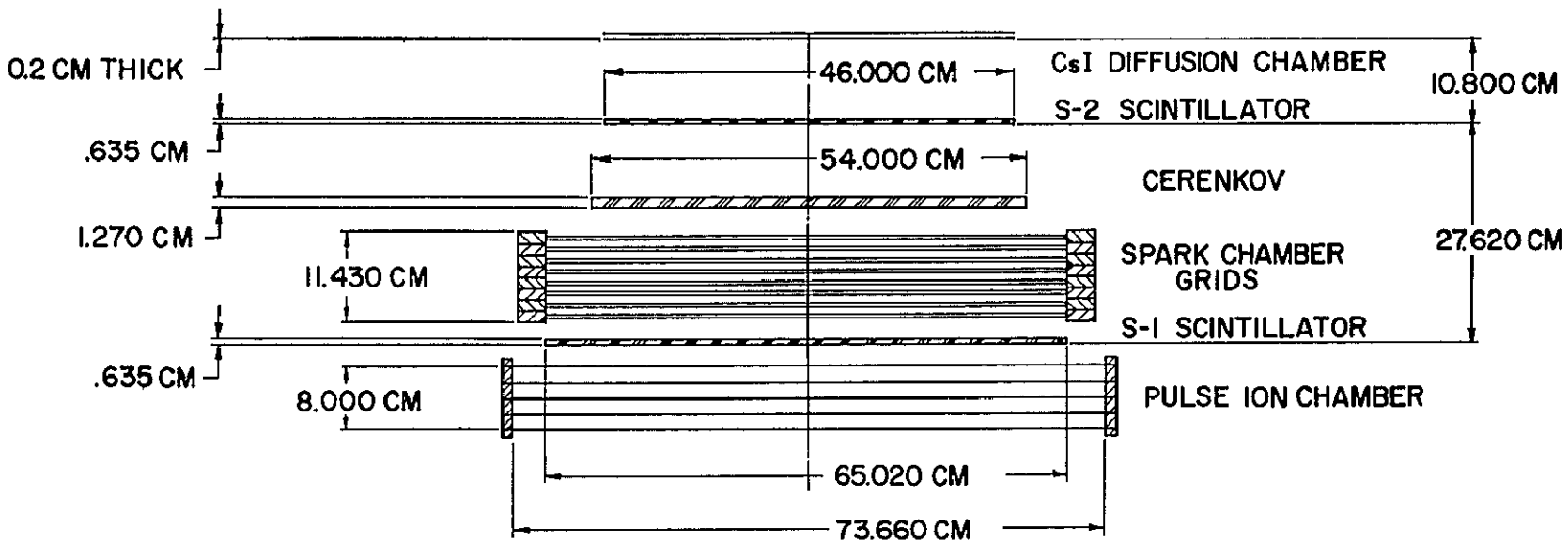

Figure III-9. Schematic diagram, charge detection section

will have a threshold at $Z \approx 20$ and extend up into the VVH region of the charge spectrum.

Each element is considered separately in the following paragraphs.

1. The Plastic Scintillators, S1 and S2

These scintillators define the acceptance geometry of the telescope and provide fast coincidence pulses for making decisions on accepting and rejecting events. Earlier measurements (Webber and Ormes, 1967) on Ne102 indicated that a substantial nonlinearity was present in these scintillators so that the response was proportional to Z rather than Z^2. This had the effect of reducing the separation of iron from its adjacent charges from 8% to 4%. However, more recent experience has shown that the nonlinearities are not nearly so serious with the Pilot B material. Further balloon tests will be done to compare Pilot Y, noted for its good transmission properties, and Pilot M, a solvent bondable scintillator. It is desirable to use Pilot M for the high g loads and vibration specifications that the rocket will place on the instrument. The adiabatic Lucite light pipes can be solvent bonded to Pilot M making a joint almost as strong as the material itself. The response is quite uniform over the large area of these detectors. Figure III-10 shows the variations in response for a 50 cm × 50 cm scintillator.

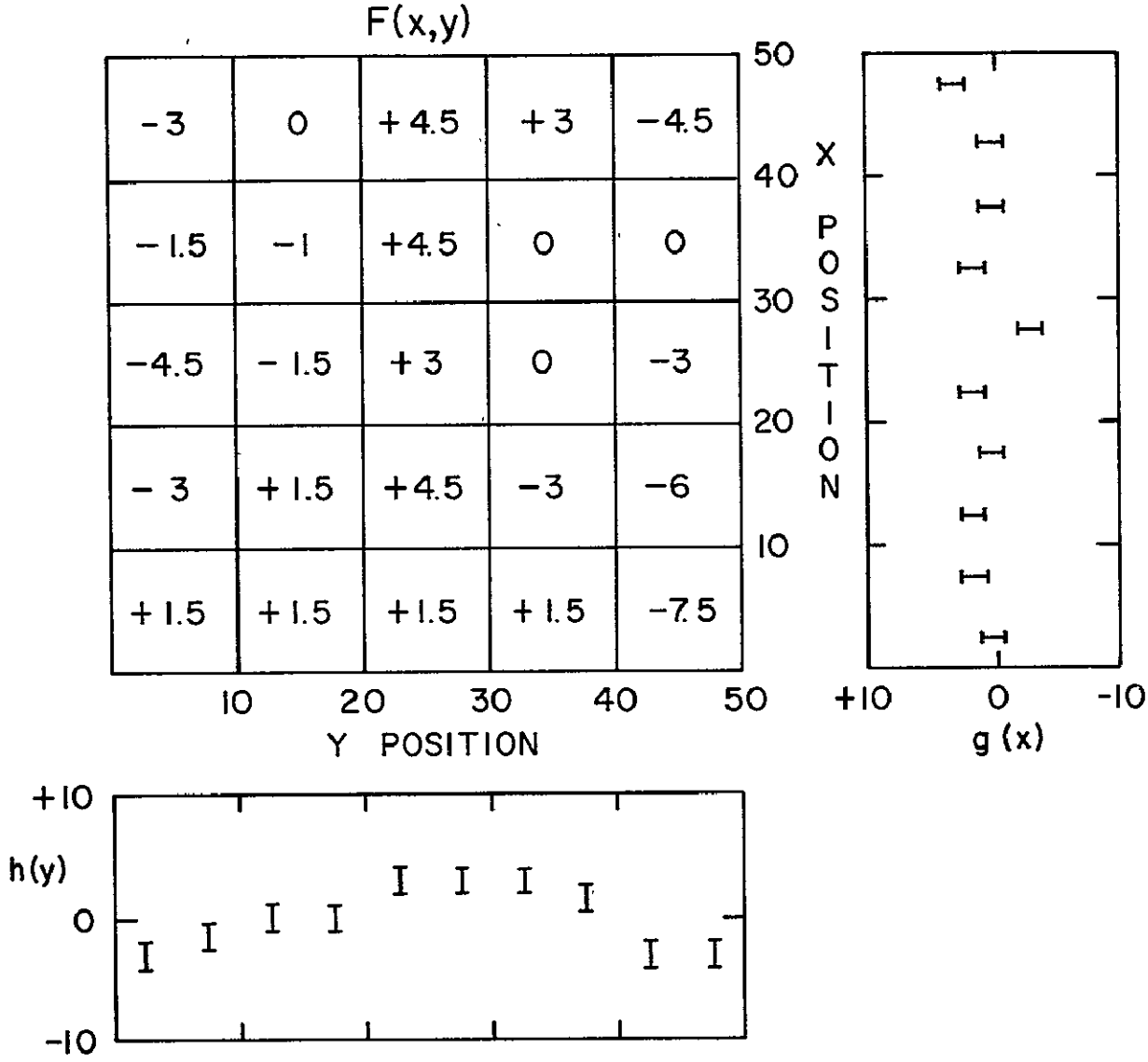

Figure III-10. Percentage deviations from mean response as a function of position for plastic scintillator.

2. Cerenkov Radiator

The inclusion of a Cerenkov radiator in the charge module has two main advantages. Along with CsI counter, it is expected to remain linear (αZ^2) in its response to charged particles at high Z. However, the Cerenkov radiator will not respond to slow, heavily ionizing particles which might simulate a high Z event. Also, a Cerenkov counter offers the possibility of sensing whether a particle has passed downward or upward through it. This directional response will help in eliminating events whose primary enters the side of the spectrometer and gives rise to a secondary traveling through the charge module.

A gas Cerenkov radiator has a high threshold and is useful in separating electrons from protons. However its use was excluded from consideration for two reasons. The detector would have to operate at several atmospheres pressure in order to respond uniformly to protons and nuclei with energies as low as 10 GeV/nucleon. The size would have to be large, 5 to 10 feet in each dimension, in order to generate a sufficient number of photons. This would necessiate a strong pressure vessel, the walls of which would break up many of the heavy nuclei, particularly the very heavies. The effective geometry factor would be small, resulting in considerable loss of data.

For indices of refraction above those of gases, there are no materials which are transparent and stable at room temperature and low pressure suitable for Cerenkov radiators until one reaches n = 1.33. Here liquids such as water exist

and at n = 1.5 solids such as Plexiglas are available. With indices of refraction in this range, the intrinsic response to protons from 10^{10} to 10^{14} eV varies only by about 1%. If n = 1.5, particles with $\beta < 0.67$ produce no signal, which would eliminate response to evaporation protons with T < 320 MeV.

The main technical problems with a Cerenkov counter using a Plexiglas radiator, such as is illustrated in Figure III-11, is that the number of optical photons emitted is small and their directions of emission are related to the direction of the incident particle. The thickness of the radiator must not greatly exceed 1 gm/cm^2 in order to avoid the too frequent breakup of heavy nuclei. At the thickness of this counter, 1.36 gm/cm^2, a primary relativistic cosmic ray with charge Z traversing the counter at an angle θ with respect to the normal to the counter will emit approximately 335 Z^2 sec θ photons in the spectral range visible to photomultiplier tubes (Ritson, 1961). Typical bialkali photocathode efficiencies are now 25%, so 84 ϵ Z^2 sec θ photoelectrons would be produced, where ϵ is the light collection efficiency. Experiments indicate (Coryden-Petersen et al., 1969) that sufficient collection efficiency can be achieved to resolve each Z.

The Cerenkov radiation is emitted in a conical wave front whose direction makes an angle, arc cos (1/n), with respect to the particle direction. Part of the radiation is totally internally reflected at the surfaces of the radiator and is "piped" to the edges, and most of the remainder immediately escapes at

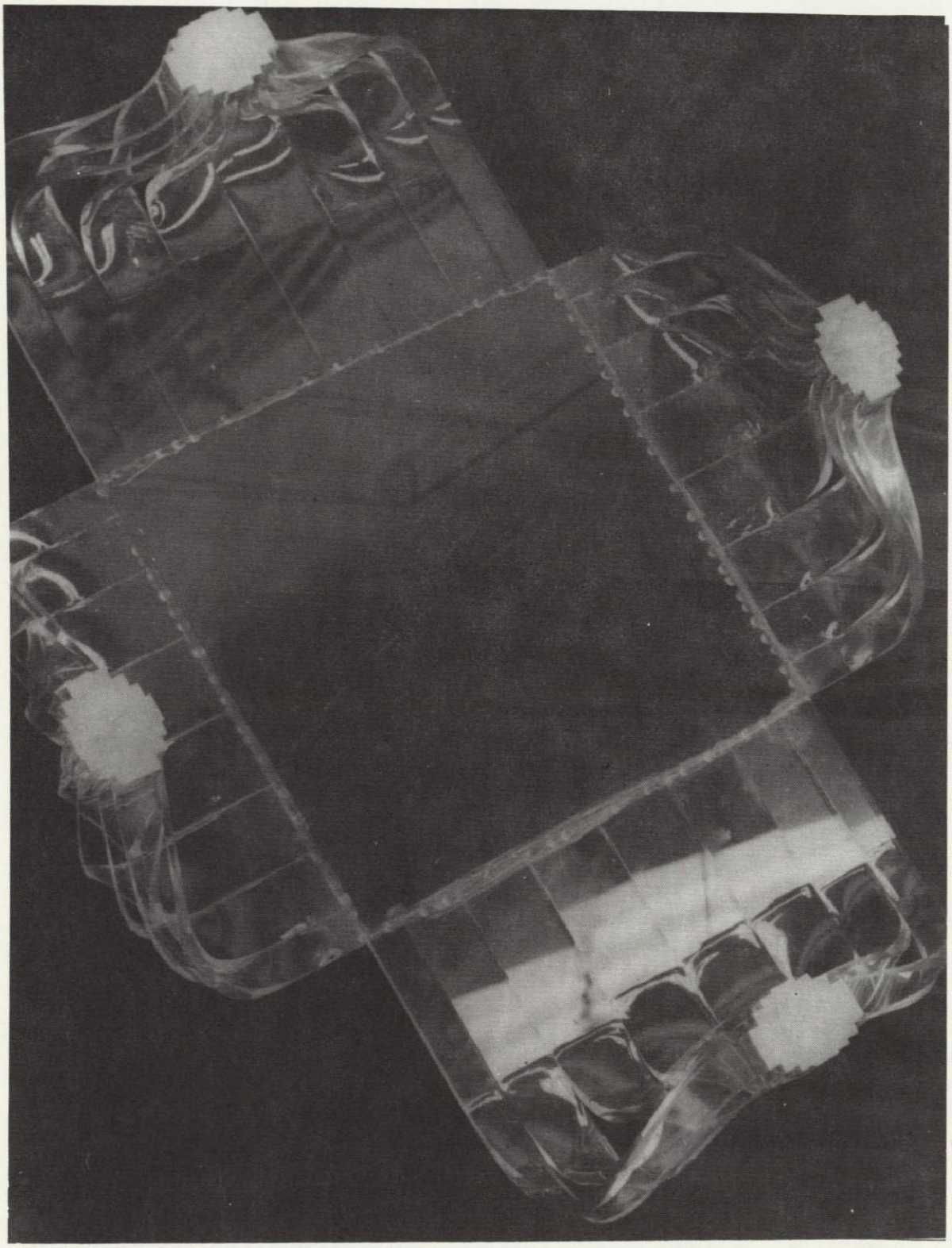

Figure III-11. Balloon Cerenkov detector with adiabatic light guides.

the first radiator boundary encountered. The light which immediately escapes serves as an excellent indicator of the particle traversal direction, whereas the internally reflected light is more efficiently delivered to the photomultiplier tubes. The fraction immediately escaping can be greatly increased by applying a satin finish, rather than a highly polished finish, to the plane surfaces of the radiator. The escaping photons can be collected either from a white-walled light diffusion chamber or by inserting thin sheets of Plexiglas containing a wavelength-shifting fluor. A portion of the wavelength-shifted light would suffer total internal reflection in the sheet and would be efficiently conducted to the photomultiplier tubes. Developmental work utilizing various combinations of internally reflected and escaping light will be carried out to arrive at an optimum Cerenkov counter design which will give good photoelectron statistics as well as the direction of traversal. Two separate measurements of the Cerenkov output will be made, one of the totally internally reflected light as viewed through photomultipliers and the second of the escaping light viewed in a white light box.

A preliminary version has been flown on balloons (Ormes et al., 1969) in which the totally internally reflected light was collected. Angular variations greater than expected have been found and are not understood. Nevertheless the compensations can be measured directly and applied to obtain useful charge information.

3. Pulse Ion Chambers

An additional charge measurement will be made in the range Z = 20 to Z > 100, with a set of four large area pulse ionization chambers which will cover the entire aperture of the instrument. The chambers will be made of parallel foil electrodes stretched across insulating frames. Each chamber will have a 2-cm gap filled with Xenon at 1 atmosphere pressure. The total amount of material presented to the cosmic ray flux will be less than 0.15 gm/cm^2.

Each of the four ionization chambers will make an independent dE/dx measurement of the incident particle. The chambers will be operated in coincidence with the main charge module and the ionization spectrometer which will result in a number of significant advantages:

(a) The main charge module and the ionization chambers will supplement each other in the charge range Z = 20 to Z = 35. This will aid in resolving individual charges in this range and in particular will help to separate the charges above Z = 26 from the relatively abundant iron.

(b) The knowledge of the trajectory and energy of the VVH nuclei will eliminate the effect of most of the ion chamber pulse-height variations for a given charge. The major remaining contributions to pulse-height variations are due to Landau fluctuations. Landau probability distributions have been calculated for a number of selected charges. Based on these distributions, analysis of the four independent pulse heights gives an average resolution of

$\Delta Z = \pm 1$ at $Z = 25$ and $\Delta Z = \pm 2.2$ in the minimum region. This is sufficient to separate $Z = 25$ from $Z = 26$ nuclei and $Z = 27$ from $Z = 28$.

(c) Since an independent measurement of the energy of the incoming nucleus will be made, it is possible to measure the energy dependence (relativistic increase) of the specific ionization loss in the gas of the ionization chambers (Halpern and Hall, 1940 and 1948; Sternheimer, 1952 and 1956; and Murphy, 1958), eliminating this as a source of error in the charge measurement. The distribution of dE/dx as a function of energy can also be used to estimate the error measurements on higher charges for those cases in which no energy information is obtained.

(d) Ovsenions have been raised (Doggett et al., 1952; Semikoz, 1956; and Tomlet et al., 1956) that the specific ionization may vary not as Z^2 at high charges. This is associated with a breakdown in the Born approximation at large values of Z. A statistical comparison of the Cerenkov counter and the ionization chamber measurements should show any significant departures from the Z^2 dependence of the specific ionization.

4. The CsI Scintillator

The main purpose of a thin CsI(Tl) is to have a completely linear charge measurement to supplement the plastic scintillators and provide another

dimension to the charge measurement. Because of its large density and its similarity to the electron cascade section it has been placed at the bottom of the charge detection section.

This CsI is viewed by four photomultiplier tubes looking into a white light chamber from the four corners. The chamber walls are painted with diffusively reflecting white paint (TiO_2).

5. Pulse Height Compensations

The opening angle of the charge module is about 75°, and so there are large path length variations in the pulse outputs. These have to be compensated by the knowledge of the trajectory as defined by the direction devices. (The direction measurements are discussed in the following section.) This technique is quite powerful and is presently being employed successfully for balloon flight data.

As an example of the geometric compensations, Figure III-12 shows the pulse height variations of carbon with zenith angle. As can be seen from this figure, sec θ is a good representation (within 2%) for the two plastic scintillators S1 and S2.

In the case of CsI the agreement is not good beyond 40°. This discrepancy can be understood in the following manner. The CsI scintillator is placed in a box painted white with photomultipliers at the four corners. The tubes face the

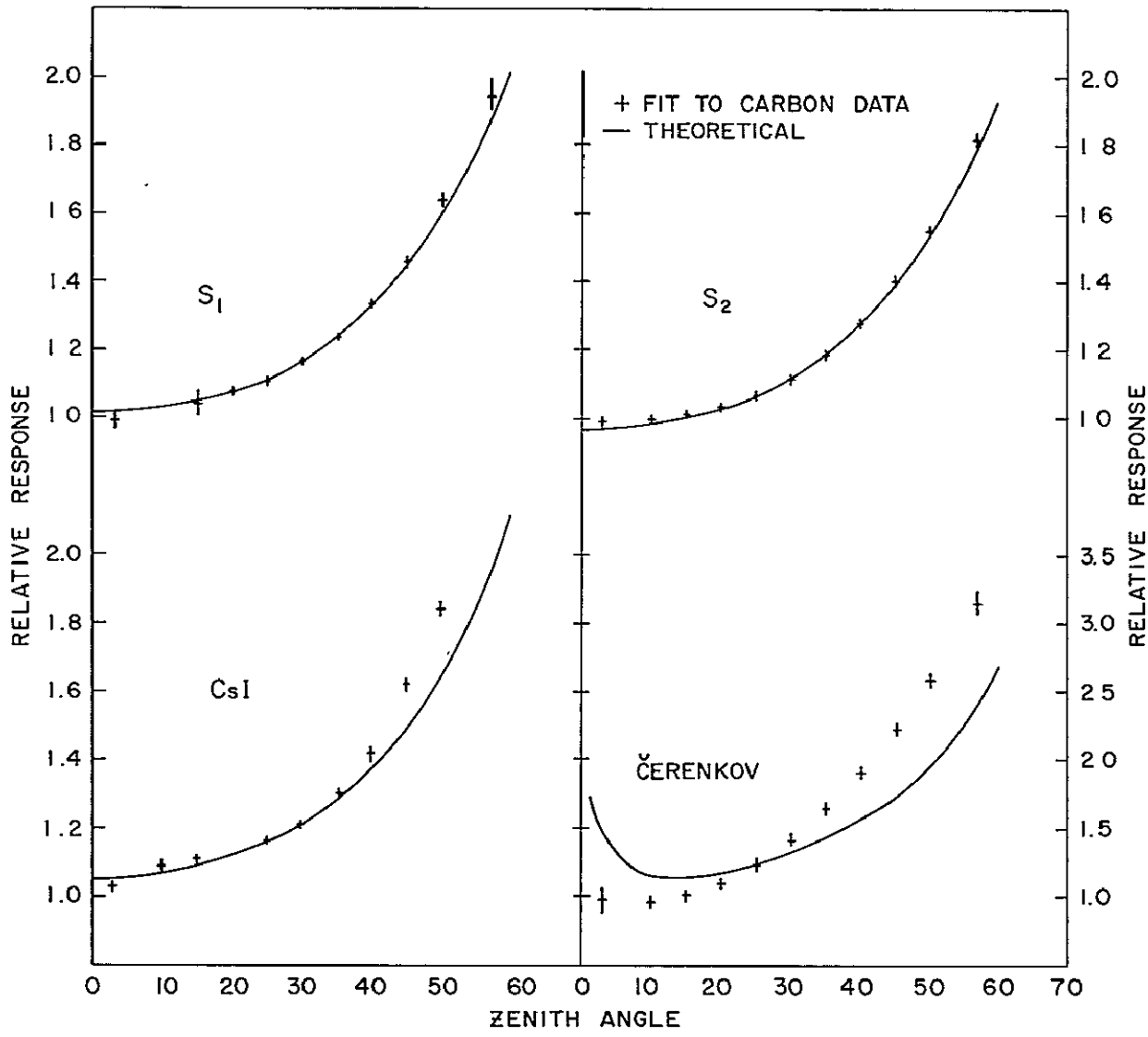

Figure III-12. Pulse height variations with zenith angle for different detectors. Note the different scale on the right hand side for Cerenkov.

white surfaces opposite the CsI and are arranged so that they do not view the scintillation direction. Light which comes from a spot near the tubes is collected more efficiently than light from the center. In fact when the detector is divided into nine squares, the center square is found to produce about 15% less signal than the average from the other areas. This affects the response as a function of zenith angle because extreme trajectories cannot pass through the central region. The enhancement at large zenith angles is due to trajectories which come nearer to photomultipliers and thus produce larger light pulses. The less extreme trajectories are distributed much more equally across the area of the detector.

Figure III-13 shows charge histograms for the experiment being flown currently at NASA (Ormes, et al., 1970). Figure III-14 shows histograms from the work of the Danish Institute group (Corydon-Petersen, et al., 1969) using Cerenkov counters in conjunction with spark chambers. The resolution exemplified by these raw data histograms is comparable with that obtained by Teegarden et al., (1969), Figure II-6, with much smaller detectors. This demonstrates the power of the directional compensation technique for obtaining good resolution using large geometrical factor equipment.

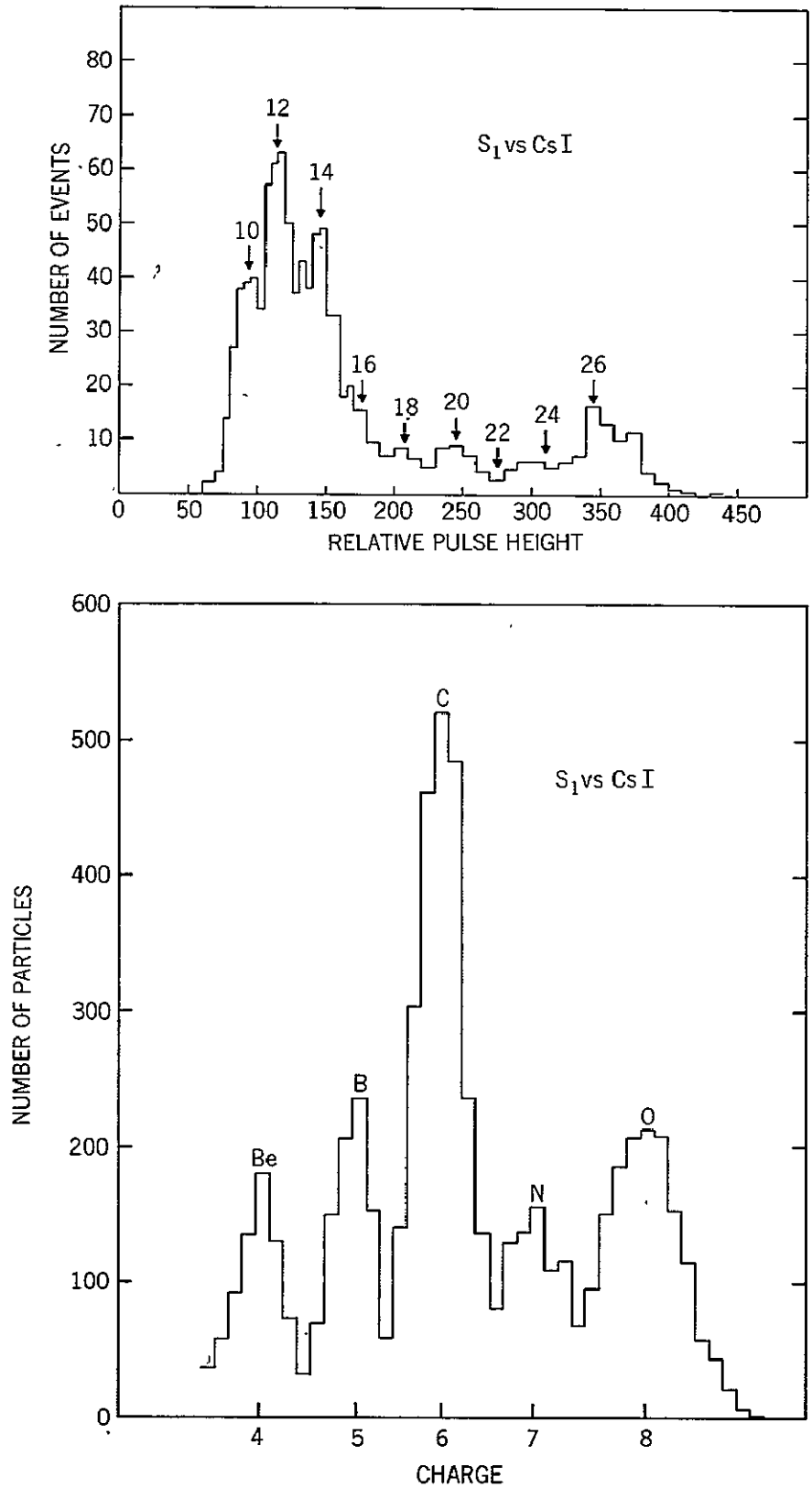

Figure III-13. Charge distributions obtained from balloon Flight 28 April, 1969.

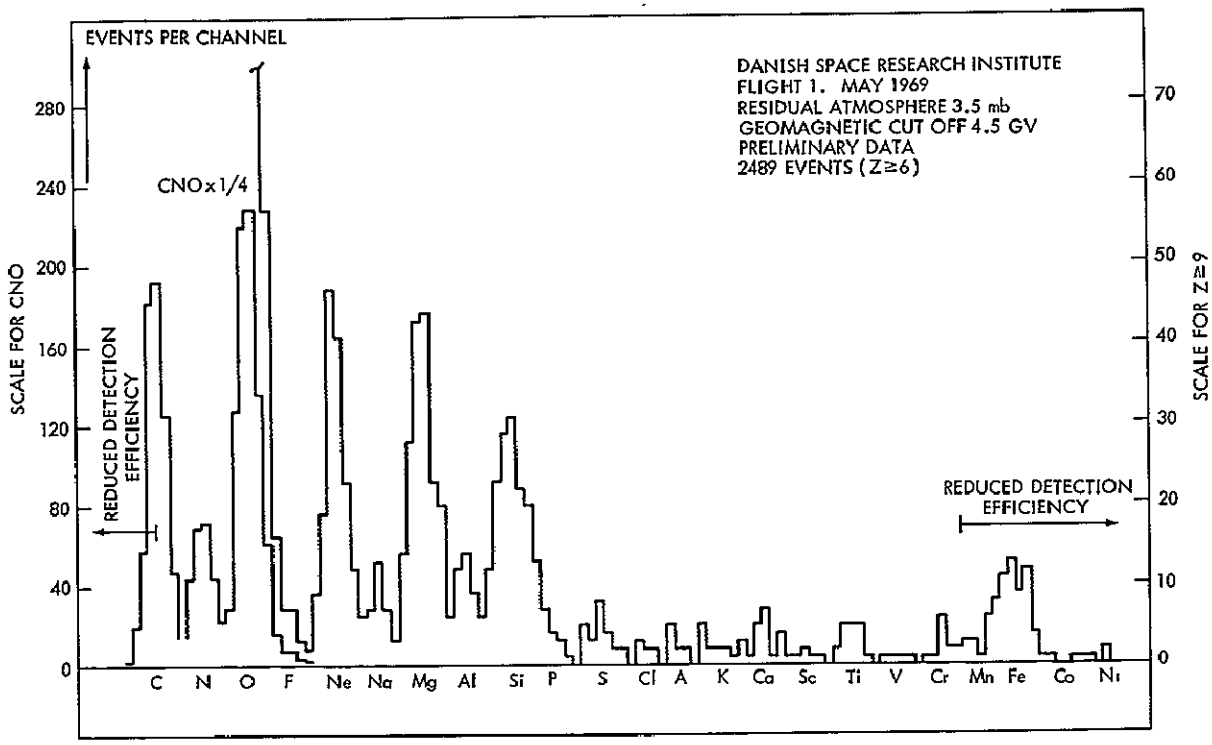

Figure III-14. Charge distribution obtained by Danish Space Research Institute Group.

E. TRAJECTORY DEFINING SYSTEM

For precise energy and charge determination it is necessary to know the trajectory of the incident particle through the charge identification unit and the spectrometer. One of the difficulties with the determination of the energy spectrum in Grigorov's experiments on the "proton" satellites was the lack of the precise knowledge of the geometric factor of the telescope. The energy deposited in the spectrometer does depend on the incident direction, and there is appreciable probability for part of a cascade shower to escape through the sides of the spectrometer. For absolute intensity measurements, it is necessary to know if the particle penetrates the whole spectrometer, or leaks out through the side. In order to measure the energy of each particle accurately, the exit point from the spectrometer should be determined to within ±1/4 mean free path. This implies an angular resolution of ±.5° required from the spark chambers.

Also, for achieving good charge resolution with large area detectors, it is necessary to apply corrections to the pulse heights based on the trajectory of the particle. These corrections have to be known to better than a few percent if unique charge identification in the region of $Z \sim 26$ is to be achieved. Also, background events from spacecraft structures may enter the equipment and simulate a complex nucleus. Especially for low abundance nuclei such as fluorine, it is necessary to eliminate these types of background.

The study of directional anisotropies (in the energy range $< 10^6$ GeV) have been performed with instruments with very wide opening angles such as neutron monitors and meson telescopes. These instruments in general have a tendency to smooth out anisotropies located in angular regions smaller than the opening angle of the instrument (Somogyi, 1968). Also, most of these ground based measurements do not have any useful information regarding the primaries that generate them. Even if, for example, heavy primaries are considerably more anisotropic than the proton component, this would not be detected from existing measurements.

In this experiment, the trajectory of the incident particles will be defined to within ±.5° for protons and approximately 1° for heavy particles (spark chamber version). With supplementary information from the spacecraft attitude data and the long exposures that are possible with satellites, a detailed search for anisotropies of different charged components and different energies could be made. This objective is unattainable from ground based experiments or balloon-borne experiments. The HEAO spacecraft scans the sky once in 6 months. Thus a reasonably complete coverage of the celestial sphere (not obtainable with any ground based monitor relying on the rotation of the earth for scanning the sky) can be achieved.

It is planned to get accurate trajectory information from the use of either of two alternate systems:

(1) digitized multiwire spark chambers; or

(2) multiwire proportional counters.

There will be a backup system making use of wedge-scintillators inside the spectrometer to get an estimate of the direction of energy flow in case of a failure of the main trajectory measurement. All three of these techniques have been developed for possible use in high energy experiments and are described in detail in this section.

The proposed spark chamber system was originally designed for γ-ray astronomy by Fichtel and his collaborators at GSFC. It has been flown successfully in balloon flights and considerable experience in interpreting data dealing with cosmic ray charge composition has been obtained.

A track produced by a carbon nucleus is shown in Figure III-15 together with the least squares best fit to the direction defined by the set cores. Figure III-16 shows the observed zenith angle distribution of carbon nuclei obtained during a 24 hour balloon flight at an atmospheric depth of 10 gm/cm^2 in April 1969. The solid curve is the theoretical distribution expected from an isotropic flux at the top of the atmosphere. The good agreement illustrates the excellent angular resolution which can be obtained over a wide range of incident angles with digitized wire spark chambers. Also, as a result of these flights, several new ideas to make the spark chambers more suitable for the objectives of the experiment have been generated. These design improvements are

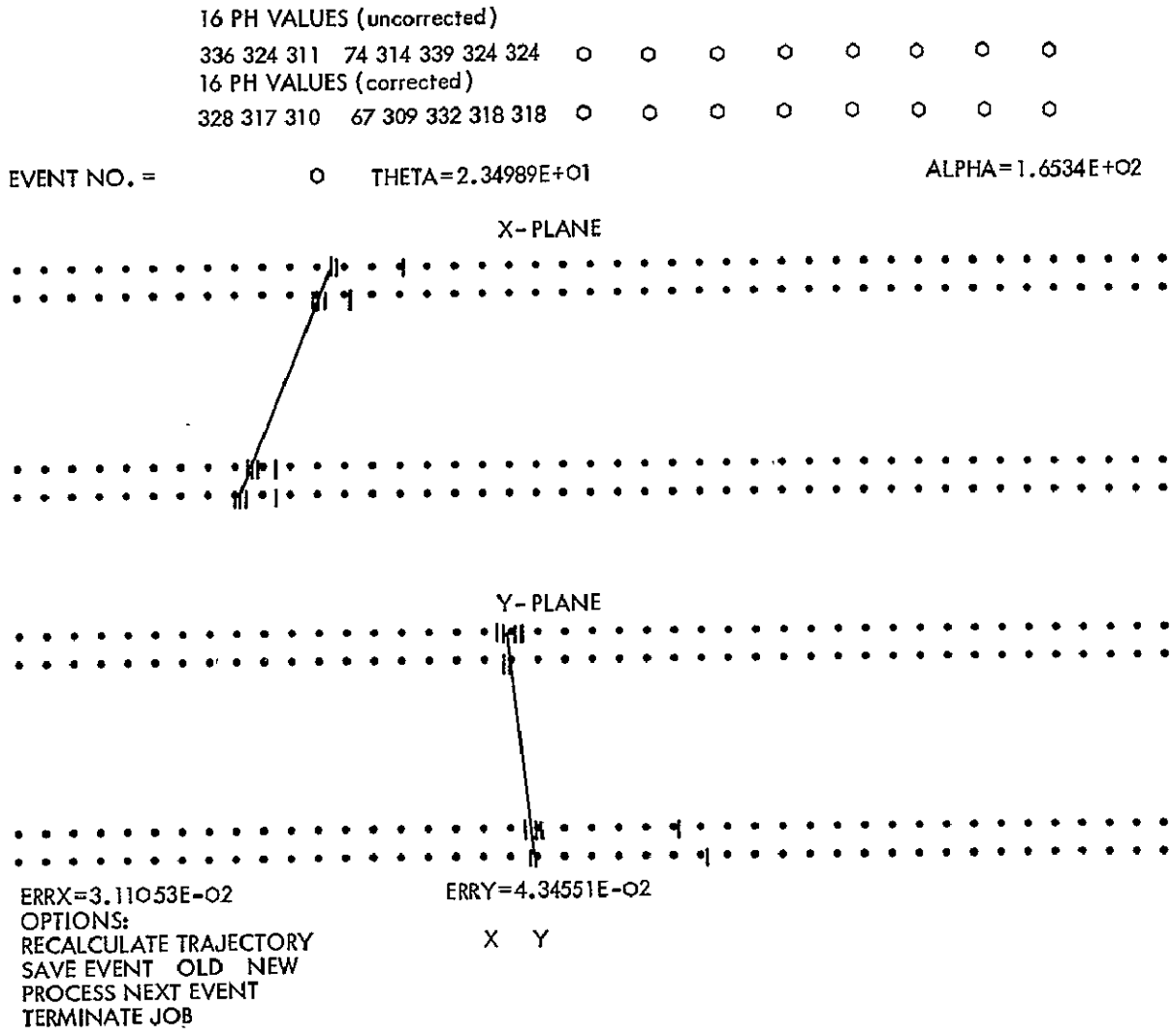

Figure III-15. A computer-generated graphical display of a carbon nucleus track.

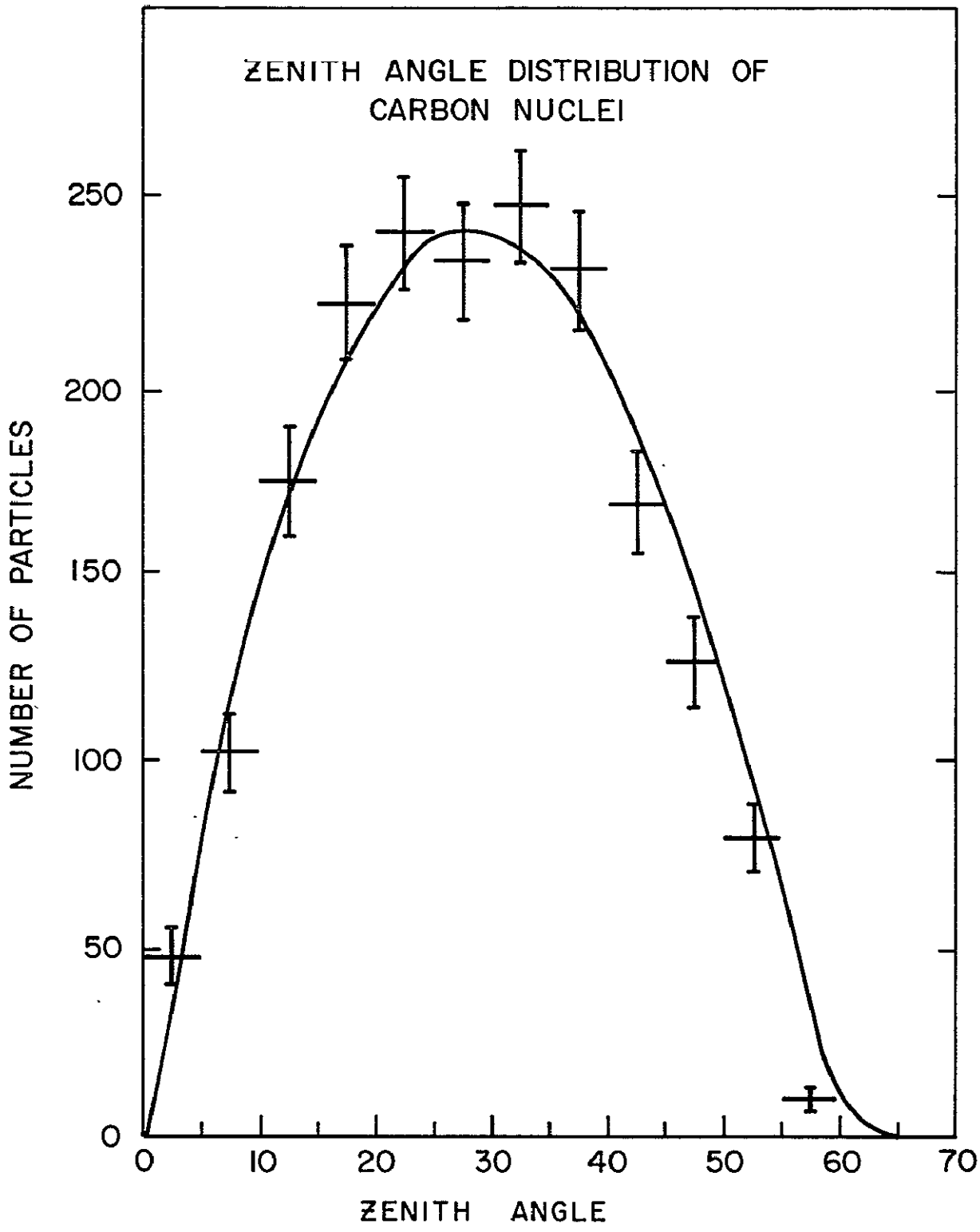

Figure III-16.

described in the instrumentation section. The problems and possible solutions associated with the application of the spark chamber to a satellite instrument with a lifetime of ~2 years are also discussed.

The alternative trajectory definition system is being pursued because of recent improvements in the performance of wire grid proportional counters (Charpak, 1968). The proportional counters appear to have attractive advantages in the long lifetime of the counter gas and in the accurate trajectory determination for high Z particles. Although they have not yet been tested in balloon flights, the proportional counters will be developed and tested in parallel with the spark chamber system.

1. Spark Chambers:

In this section, the systems currently being flown on balloons by the GSFC and MPI groups are described. The description is followed by a discussion of the problems which have come to light in the extension of the system for prolonged use in a satellite and for charge spectrum studies. The various solutions and improvements which are under development for the problems are also pointed out in detail.

Spark Chambers in use at the Present Moment: The digitized wire spark chambers have been developed for space flight application by Ross et al. (1969). The spark chambers (50 cm × 50 cm) based on the above developmental work have been successfully flown in balloon flights by the γ-ray Astronomy

and High Energy Cosmic Ray groups of the Goddard Space Flight Center. The γ-ray Astronomy group is planning a one year survey of the sky for γ-ray sources in an experiment in SAS-B satellite. As the whole spark chamber system has been conceived for ultimate use in a satellite, many of the mechanical design problems, materials selection problems, etc. have already been anticipated. Also Pinkau's group at the Max-Planck-Institut in Munich has been working with digitized spark chambers as well as with optical ones. Optical spark chambers were flown on balloons in connection with the LSU-MPI ionization spectrometer experiment and in connection with an MPI experiment for the detection of solar neutrons (Heidbreder et al. 1970). Digitized spark chambers have been developed for a gamma ray experiment to be flown on COS-B satellite. These are wire spark chambers of size 30 cm $\times$ 30 cm having core readout. Presently (May 1970) a group from MPI is in Palestine, Texas, for balloon flights of an experiment incorporating these chambers.

Principles of Operation: The spark chamber system is modular in concept; each module consists of two wire planes mutually orthogonal (along x, y directions) with 200 wires in each plane spanning 50 cms. When the spark chamber is triggered a high voltage pulse ($\sim$3 KV) is applied between the two grids. The low resistance path along the trajectory of the traversing particle causes an electrical break-down and a spark develops between the wires in the two planes. Each wire is connected to a ferrite core, which is set by the current associated with the spark. Thus for each event there is an x and y coordinate from each

module. The readout system (Ehrmann et al., 1967) interrogates the cores and passes on the coordinates to the digital data handling system. The system is designed to have good multiple track efficiency, so complex events can be recorded quite well.

Spark Chamber Modules: Each module at present has an effective area of 50 cm × 50 cm and is constructed by stretching 0.18 mm-diameter Be-Cu wires over a frame of glass-bonded mica. It is proposed to extend this construction to have an effective area of 64 cm × 64 cm by having 256 wires per plane instead of the present 200 wires per plane. The spacing between the wire grids is 4.0 mm and the distance between wires in the same plane ~2.5 mm. The ferrite cores and some of the associated electronics for core interrogration are located on shelves attached to the sides of the module.

In the satellite experiment, it is planned to use 8 modules. With efficiencies of 98% for minimum ionizing particles, the probability of a particle missing three planes is negligible. The trajectory of all particles can be obtained with high efficiency (±1 mm).

Container: The spark chamber modules and its electronics are kept inside a gas container, designed such that cosmic rays passing through encounter a minimum amount of matter (less than 1 gm/cm^2). The flats are of thin aluminum sheets (1/20"). The gas used is 90% Ne, 10% He, and traces of Argon and Ethanol. A number of pressure relief valves and other safety devices and gauges are used

for determining changes of pressure and temperatures and monitoring purposes. The present design, enclosing the entire electronics associated with the spark chamber inside a metal shield, has proved useful in preventing noise from high voltage pulses interferring with the pulse height analysis. Careful shielding, grounding and routing of signal cables have enabled operation with 1 millivolt pulses at the PM tube preamplifiers.

High Voltage Pulsers: The modules are driven by Edgerton, Germhauser, and Greer (E.G. & G) Krytrons (k N-2). The krytrons are triggered by an avalanche transistor-circuit. Each module has its own discharge capacitor to minimize problems of energy robbing between modules. Krytrons have lifetimes limited both by the number of triggers and by the steady erosion by a keep-alive current ($\sim 100\,\mu$ A). It is believed that krytrons, as presently developed, are not suitable for long lifetimes associated with a satellite experiment. In the next section, problems posed by the requirements of the satellite experiment and some approaches to their solution are discussed.

Problems of Reliable Spark Chamber Operations for Periods of Years:

At present, the lifetime of a spark chamber is limited by

(1) the purity of the gas mixture;

(2) high voltage pulsers - krytrons, spark gaps; and

(3) random failure of readout electronics.

Of these three, the last item is taken care of by good design, and redundant systems of high reliability. This already exists and is expected to be quite satisfactory.

The problems due to the gas mixture are of a different nature and have to be faced in any prolonged use of the spark chamber. The spark chamber modules have been designed to keep the outgassing from the different components inside the spark chamber from developing into a serious threat. The γ-ray astronomy group at Goddard has kept a chamber filled for four months and at the end of this time they could not find any deterioration in the operational behavior of the chamber. Any problems connected with outgassing from the chamber components will be tackled by providing a gas replenishment system which refills the chamber afresh on command. This need not be done (on the basis of Goddard experience) more than a few times during the life of the satellite. The associated monitoring of the contents of the gas chamber with a sensitive mass-spectrometer is also under development. The problems of the destruction of the quenching agent (ethanol) by the radiation belt do not appear to be serious for the HEAO orbit. When the gas mixture deteriorates, it usually results in lowered efficiency. By applying a higher voltage, one can regain a higher efficiency of operation.

Krytrons, at present, have a useful life at 7×10^6 counts or ~1 month at a keep-alive current of 100 μA. Currents less than 100 μA cause a delay larger than 40 nsec and hence are not too suitable. The solution of providing banks of krytrons to be switched by command is possible for extending the life of the spark chamber, though not necessarily an optimum or elegant one. E.G. & G. have recently developed a spark gap with a lifetime of 10^7 counts. The problem of keep-alive current lifetime, which is so severe for krytrons does not exist for spark gaps. Also the deterioration of spark gaps is of such a nature that even after 10^7 counts, if sufficient energy could be made available to the source triggering the spark gaps, the lifetime could be extended. Development is under way for achieving a lifetime of 10^8 counts for the spark gaps by suitable energy sources for H-V trigger circuit. For a two year lifetime the number of triggers for the spark chamber would be $\sim 3 \times 10^8$ triggers. Therefore, by provision of banks of spark gaps triggered on command, it should be possible to have a useful lifetime of ~ two years for the spark chamber system.

Improvements for Complex-Nuclei Detection: In an experiment to detect particles with Z = 1 to 30 or more, the knock-on electrons produced by the heavier nuclei can cause a problem in the identification of the trajectory of the complex nuclei (Ormes et al., 1970). The probability of producing a knock-on increases as Z^2; and with an efficiency of ~98% for detection of singly charged particles, the problem becomes a serious one. The detectors are large and for good charge resolution, it is necessary to apply corrections for differences in

detector response as a function of position. A knowledge of the trajectory of each incident high Z nucleus, therefore, is essential.

In Figure III-17, the efficiency of the spark chamber as a function of delay between application of high voltage pulse and the passage of the particle is given. It is seen that the efficiency for detecting singly charged particles falls to 10% after 3 μsecs. For the high Z, however, the efficiency still remains close to 100% as recombination has not removed the ions completely and sufficient numbers remain for the spark to take place. So, by adjusting the delay based on the information of the charge detecting sensors, it is possible to get an unambiguous trajectory for high Z particles alone. This system will be tried in a future balloon flight.

Evidence that this concept may work could be derived from a balloon flight with optical spark chambers carried out by the MPI group. In one of their balloon flights with an ionization spectrometer and optical spark chambers (Schmidt et al., 1969) the gas mixture in a 4 gap spark chamber became bad during flight. This caused single minimum-ionizing particles to remain undetected while alpha-particles and nuclei with higher Z were still detected reliably.

Another result of these balloon flights was that although the multiple spark efficiency of this chamber was very good (up to seven sparks per gap at 99% efficiency) the primary tracks of high Z particles in a sufficient number of gaps

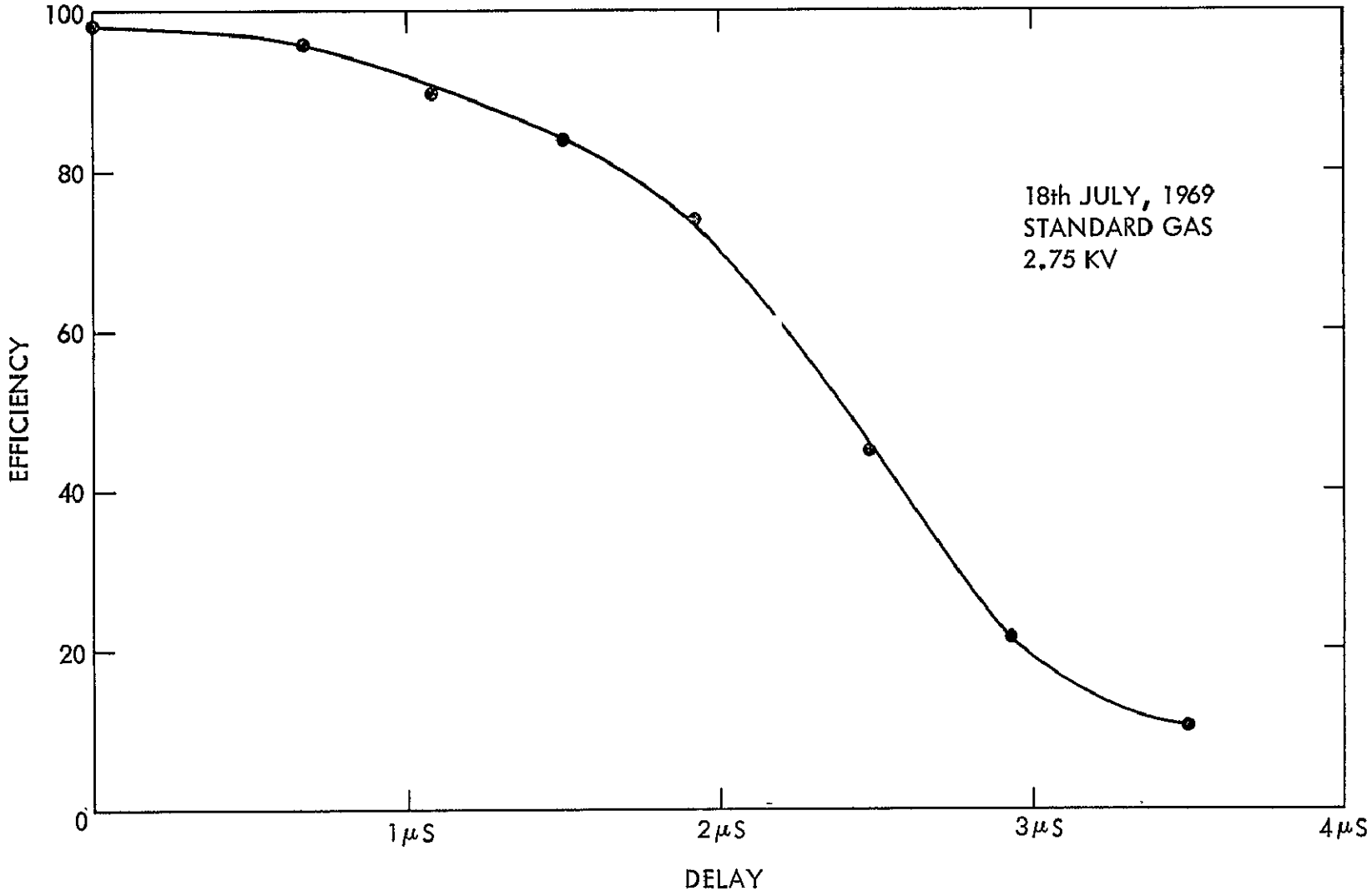

Figure III-17. Efficiency of the spark chamber as a function of the delay time between the passage of the ionizing particle and the application of the high voltage.

could be reliably found among the secondaries. This was done using 10 gaps, and in a sample only 3 gaps were used. It worked sufficiently well so that tracks could be followed into an emulsion stack and all of them were found there (Goza et al., 1970). Therefore, in the six gap wire spark chamber proposed here, it appears possible that the primary track can be found among the secondaries. Which approach to the problem is more efficient will be determined from balloon flights prior to final construction of the apparatus.

2. Multiwire Proportional Counters:

General: The feasibility of multiwire proportional counters for the trajectory measurements is being investigated to replace the spark chambers. Proportional counters of several geometries have been built at Marshall Space Flight Center. Those of the type developed by Charpak's group (1969) at CERN seem the most suitable, since they are able to record multiple trajectories efficiently.

The main advantages of the proportional counters over the wire spark chambers are their expected lifetime and reliability and their capability of discriminating against δ rays produced by heavy particles which will be discussed below. The disadvantages of position sensitive proportional counters for the application is that the position resolution is strongly coupled with the power consumption of the counter system.

The accuracy required for the trajectory measurements with a resolution of .5° in this experiment can be achieved at a power consumption comparable to

that of the spark chambers by arranging the location of the position detectors in the charge modules as shown in Figure III-18. Currently, counters are being developed which are suitable for this geometry.

Two of the x-y planes are located on top of the ionization chamber system and two x-y planes below the first plastic scintillator (spaced 25 cm apart). The counters will utilize 256 wires per x-y plane.

The individual counters will have a thickness of 1 cm and be filled with a Xenon CO_2 mixture at 1 atm. Each x-y plane consists of two insulating frames with an area of approximately 74 × 74 cm. Across the top and bottom of each frame, wire mesh will be stretched which serves as the cathodes, while two independent planes of parallel wires located in the center plane of each frame serve as anodes. The top counter system shares its gas volume with the ionization chambers. The lower two x-y planes have their own gas system for redundancy.

Mode of Operation: A minimum ionizing Z = 1 particle produces about 300 ion pairs in 1 cm of Xenon at 1 atmosphere. With a gas amplification of 5×10^2 about 2×10^{-14} coulombs per pulse are collected sufficient to enable the use of relatively simple preamplifiers with noise figures around 10^4 electrons for 20 pf input capacitance.

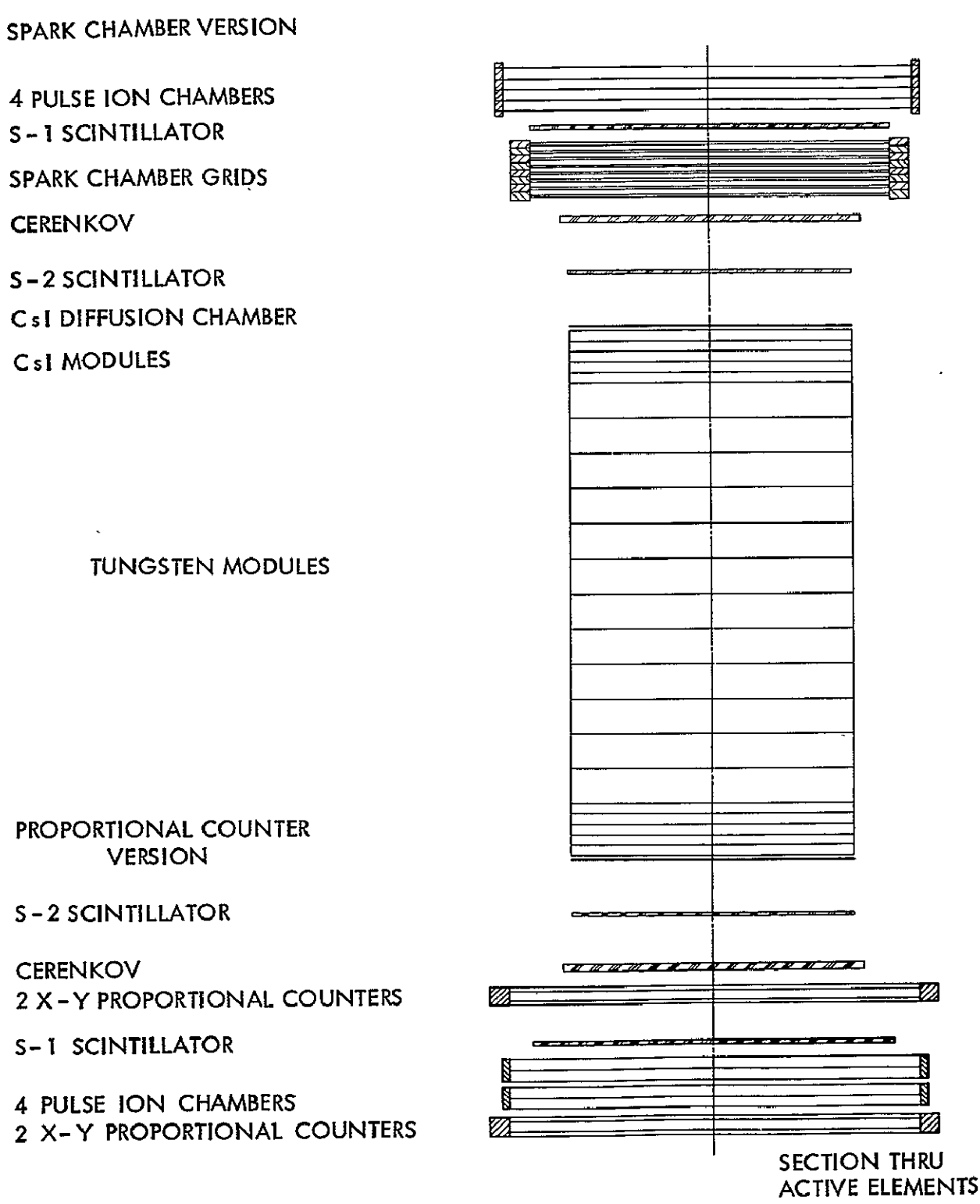

Figure III-18. Diagram of the cosmic ray experiment with the spark chamber apparatus shown on the upper end and the proportional counter apparatus shown on the lower end.

Figure III-19 shows the positional resolution obtained with such a counter by the MSFC group. These data were taken with an Fe 55 X-ray beam .3 mm wide, normally incident on the chamber and driven perpendicular to the wires in .6 mm steps. The counter had a thickness of 1 cm and a wire spacing of 5 mm.

At a gas gain of 5×10^2, space charge limitations will cause the signal to depart from Z^2 dependence at some charge above Z = 4, depending upon the length of anode over which the discharge is spread. This, of course, is of no consequence for the trajectory measurement since for that one needs only a signal above a certain discriminator level but not the absolute pulse height.

A desirable characteristic of the proportional counter assembly is the possibility of discriminating against δ rays produced around the path of heavily ionizing particles. With two discriminators following the amplifiers, it appears to be possible to virtually eliminate the effects of δ rays, Compton electrons, and shower-produced particles on the position resolution for high Z particles. If one discriminator were set for minimum ionizing Z = 1 particles and the other set for $Z \approx 3$, the trajectory measurement made by the upper discriminator would not be degraded by the above effects, since the energy deposit by δ rays on adjacent wires would seldom exceed 45 KeV. Two series of flip-flops would store the position information, as compared to the ferrite cores for the spark chambers, and the flip-flops would be read by the scanning electronics.

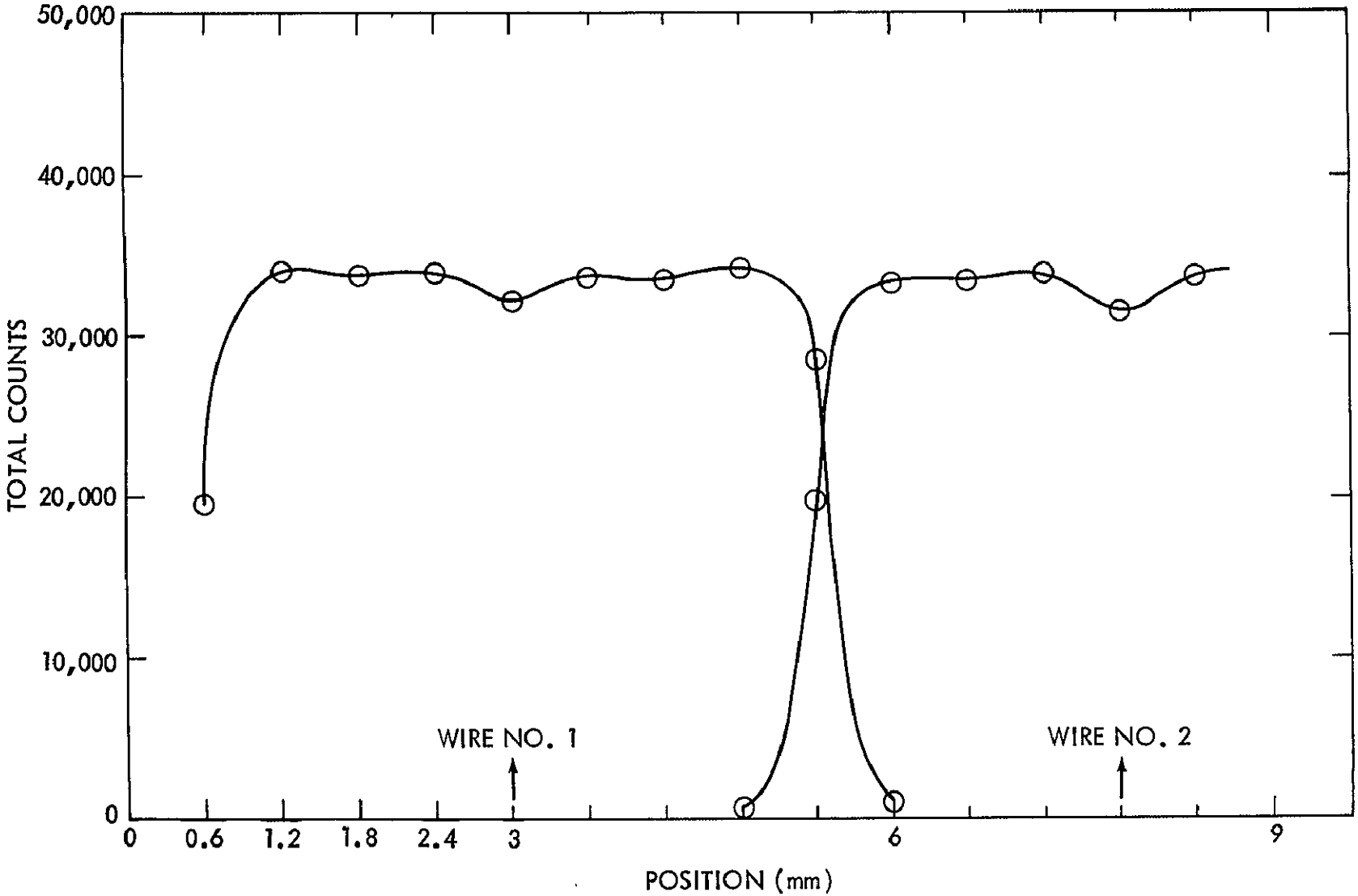

Figure III-19. Response of the wire proportional counter as a function of position shown for two adjacent wires.

Lifetime and Reliability: The lifetime of a proportional system is expected to exceed the lifetime of a spark chamber. In the proportional counter there is far less wear of the counter gas and no high voltage pulsing system. Assuming that the counters can be shut down during the passage through the South Atlantic Anomaly, a sealed gas system may yield a lifetime of 2 years with no refill. A gas supply system for refilling the counters (see spark chamber section) would then be a backup system only.

The addition of $\approx 10\%$ CO_2 to the Xenon filling will make the counter gas relatively insensitive to contamination. It should also be noted that electronegative gas contamination initially degrades the energy and time resolution of the counters, but these are not very critical in this application. Therefore, the life of the proportional counters for this application may be extended by raising the supply voltage on command, when the gas becomes contaminated to the extent that the pulse height decreases.

Limitations due to quenching gas dissociation and other effects associated with the total number of counts generally occur for Xenon-CO_2 counting above 10^{12} counts/cm^3. This limit should not be reached if the counter is shut down during passages through the South Atlantic Anomaly.

Redundancy of the Proportional Counter System: Two counter systems (top and bottom) are proposed that operate from separate gas supplies. Each

wire plane within one system will have its own HV supply, and each wire will have a separate amplifier and discriminator.

With all subsystems operating, the position resolution of ±.25 mean free path length for the exit point of a proton will be achieved. With the inner two systems failing a resolution of ±.5 mean free path will be achieved; with the outer systems failing ±.75 mean free path; and with either the top or bottom system failing an accuracy of ±1.5 mean free paths will be possible. In all failure modes the position information can be obtained by evaluation of the scintillator wedge position data.

Present Status of the Proportional Counter Development: Detailed studies of the behavior of proportional counters are being made with regard to the following areas:

(1) study of counter construction materials with regard to outgassing;

(2) effects of gas contamination from outgassing and dissociation of the quenching gas;

(3) space charge effects for very high Z particles;

(4) low power amplification and readout systems; and

(5) Monte Carlo calculations of the anticipated response including δ ray effects.

A balloon flight of a charge module consisting of a multiwire proportional system for position measurement, 4 ion chambers, and a Cerenkov counter is planned for the fall of 1970. The response of high Z particles and the δ-ray discrimination technique will be examined in detail on the balloon flight.

3. Wedges:

In a satellite experiment it is always worthwhile to have redundant devices for measuring all significant parameters. The direction of each incoming particle is extremely important to both the energy measurement and also to the charge determination. The direction of an incident charged particle can be determined by the scintillators in the spectrometer. If the scintillators are wedge shaped, then the light output depends on the thickness of the wedge at the particles point of incidence and hence on the distance of the particle trajectory from one edge of the scintillator. In the case of particle cascades the number of particles must be known for normalization, hence a double wedge of constant total thickness must be used. Pinkau et al. (1969) have shown that it is possible to measure the direction as well as the total energy content of electron induced cascades with a system of double wedges between absorber material.

In Figure III-20 the method of measurement is demonstrated. Photomultiplier tubes look into the end faces of a double wedge scintillator and yield signals A and B upon traversal of a charged particle at distance y. Then if S is the signal per unit path length of a charged particle, the signals A and B can be expressed as:

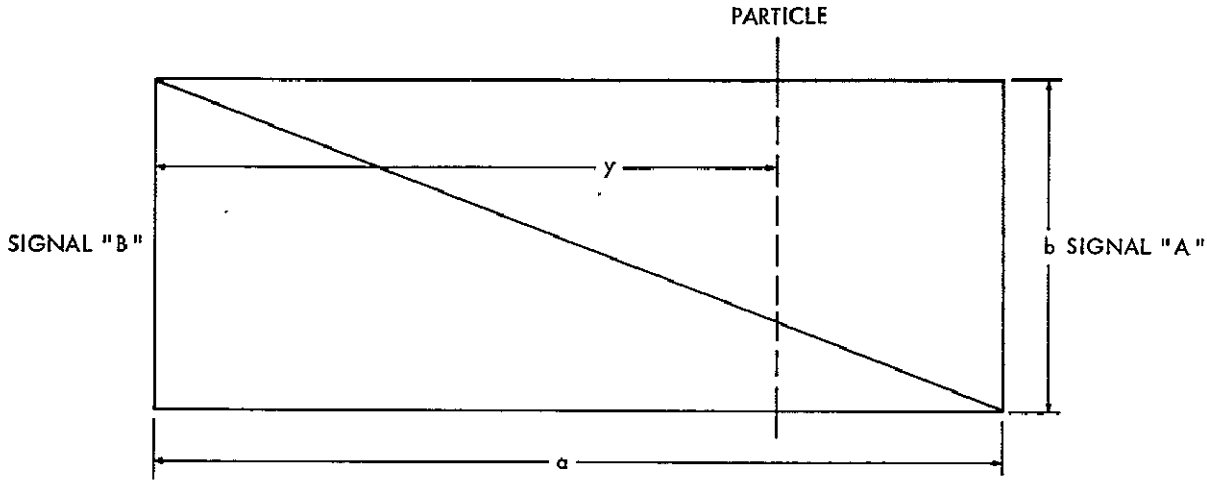

Figure III-20. Section drawn through a pair of wedge-shaped scintillators indicating the responses used to determine the location of the ionizing-particle.

$$A = Sy.b/a,$$

and

$$B = S(a - y)b/a,$$

where a and b are the dimensions of the scintillator. Now the quantity,

$$Q = A/(A+B) = y/a,$$

is a measure of y independent of S. In the case of k particles at the distance y_i (i = 1, 2. . .k) the equations are:

$$A = S(b/a) \sum_{i=1}^{k} y_i,$$

and

$$B = S(b/a) \sum_{i=1}^{k} (a - y_i).$$

Hence:

$$Q = \frac{1}{ka} \sum_{i=1}^{k} y_i = \frac{1}{a} \bar{y},$$

where

$\bar{y}$ is the center of gravity of the shower. So, as long as the shower axis (direction of momentum of primary) coincides with the center of gravity of charged particles at any given depth of cascade development the position of the shower axis can be determined.

Pinkau et al. (1970) used scintillator wedges of size 22 × 116 mm. The error in the determination of the shower axis at 2 to 3 radiation lengths absorber depth was $\Delta\bar{y} = \pm 9$ mm for 2.3 GeV primary electrons and $\Delta\bar{y} = \pm 6$ mm for 5.3 GeV electrons. In the proposed spectrometer the scintillators of one module, viewed by one PM tube, have a total thickness comparable to that used by Pinkau et al., but the lateral dimensions are about four times as large. Thus, the expected error in the present case would be ± 36 mm and ± 24 mm at the energies stated. Assume 40 mm in the worst case; then from top to bottom of the spectrometer, 74 cm deep, the angular resolution would be a few degrees. The orientation of the wedge-shaped scintillators will be arranged so that alternate modules provide x and y coordinate information, i.e., there will be five x measurements and five y measurements for cascades penetrating the inner 10 modules of the spectrometer. In the case of failure of the spark chamber this would represent an adequate replacement.

IV. INSTRUMENTATION

A. ELECTRONICS AND DATA HANDLING SYSTEM

This experiment is designed to measure the properties of cosmic rays over a large range in charge and energy. This requires a very large dynamic range electronics system and will produce over 1000 bits/event. With this large bit rate one would quickly saturate the spacecraft telemetry system. However, the steeply falling nature of the energy spectra under observation solves this dilemma. Each event will be assigned a priority, with the priority increasing with the charge and also with the energy of the particle. A buffer storage capable of handling several events will be the interface between this experiment and the spacecraft data handling system. Events will be fed to the telemetry on a priority basis, and the lowest priority event awaiting readout will always be subject to being replaced by an event of higher priority should one occur. Priority will be reorderable by command should a failure or other anomaly occur which might affect the system. In this way very plentiful events will be randomly sampled while rare events will all be saved.

So that it can operate as a reconfigurable instrument, a broad range of command capabilities will be necessary to meet any possible contingencies.

To achieve increased reliability redundancy has been provided in all crucial areas with no real penalty in weight and with minimized power penalty. The

provision of suitable rate data will enable the complete reconstruction of the incident energy and charge spectrum without any bias due to the priority system.

The discussion of the electronics will be divided into seven subsections:

(a) A major element will be the coincidence trigger system which selects events, classifies them, and assigns them priorities.

(b) The analog section, which will require a dynamic range of 10^5, consists of the P. M. tubes, preamplifiers, and the gating system.

(c) The pulse height analyzer section will digitize the analog pulses.

(d) The directional readout interrogates the memory of the spark chamber or proportional counter to determine which wires have been activated.

(e) The digital data handling system will format the data and act as the control interface to the spacecraft readout systems.

(f) The experiment will be monitored by occasional readout cycles devoted to housekeeping, rate, and calibration data.

(g) A command implementation section will receive and decode commands from the spacecraft and reconfigure the experiment accordingly.

For the purposes of discussion, the modules will be identified in the order that they are seen by the incident particles. For example, W_1 is used to mean the output from the first tungsten module the incident particle sees. Two electronics systems will be employed, one associated with each end. This optimal use of the spinning spacecraft leads naturally to the redundancy of two complete

electronics systems. The two systems and their basic subsystem are shown in Figure IV-1. The interrelationships of the various subsystems are shown in more detail in Figure IV-2.

Each of the electronic subsystems will be considered separately.

Coincidence: Figure IV-3 shows the basic trigger requirements for selecting events. All particles will be required to pass through the plastic scintillators S_1 and S_2, forming a master coincidence. Events will be classified as belonging to one of the following "modes" of triggering:

(1) E Mode: Electrons, which cannot be separated from protons in the charge module, will be required to give a pulse indicating that at least a 10 GeV electron shower is present in the first tungsten module W_1. This module is 10 radiation lengths thick with three separate samples taken at 6.7, 9.9 and 13.3 radiation lengths. These three thresholds are indicated by the arrows in Figure III-7 and are designed to be 90% efficient for detecting 10 GeV protons based upon Monte Carlo studies of the cascade fluctuations. If any of the three pulse heights falls below the level indicated, the event will be rejected. The CsI layers are not used in the coincidence requirements because of their slow rise times. This requirement is relatively insensitive to proton interactions (Silverberg et al., 1970). The protons which masquerade as electrons will be further tagged by the response of the remainder of the spectrometer and will be eliminated in the data analysis stage.

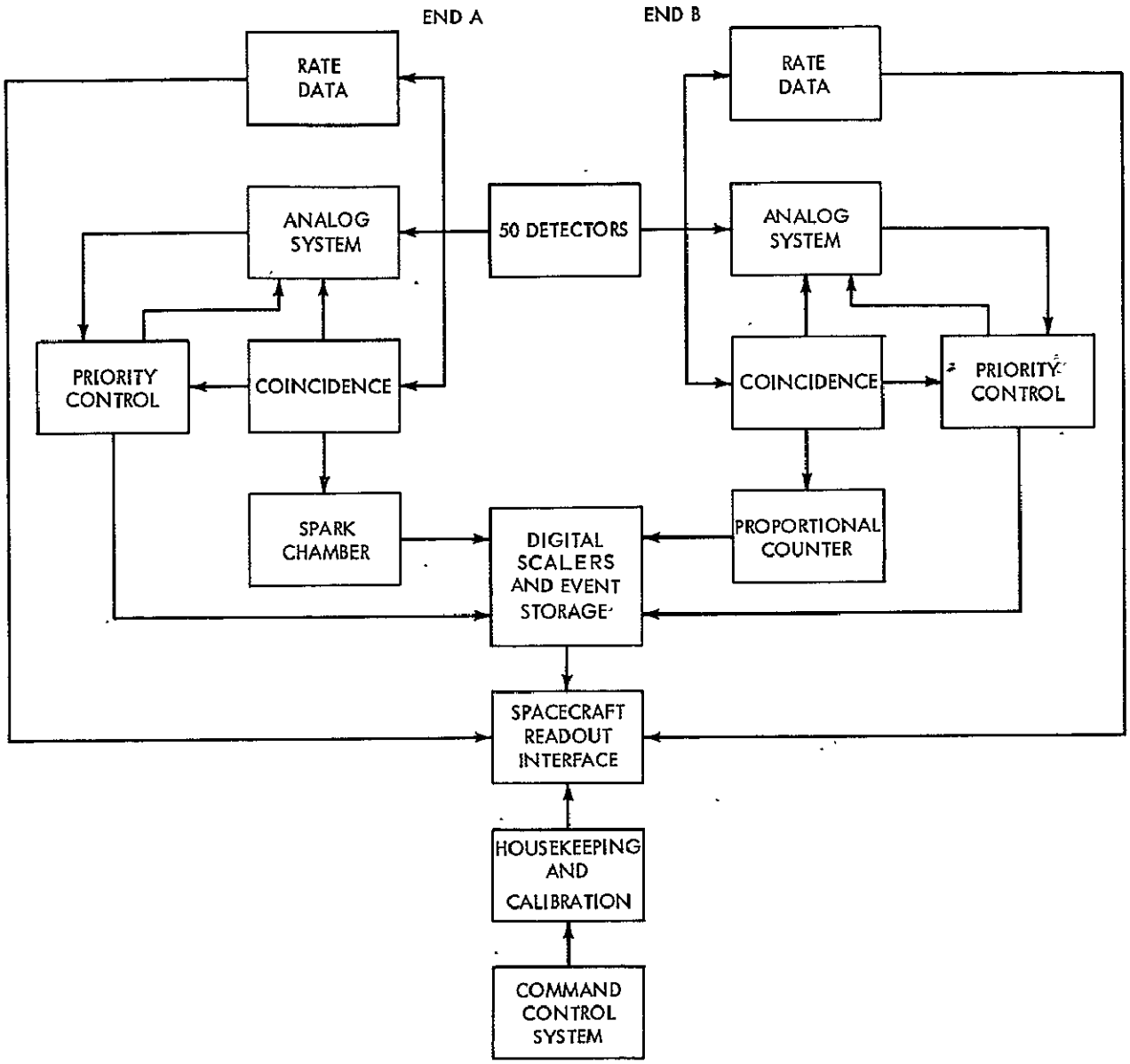

Figure IV-1. Electronics block diagram, overall system.

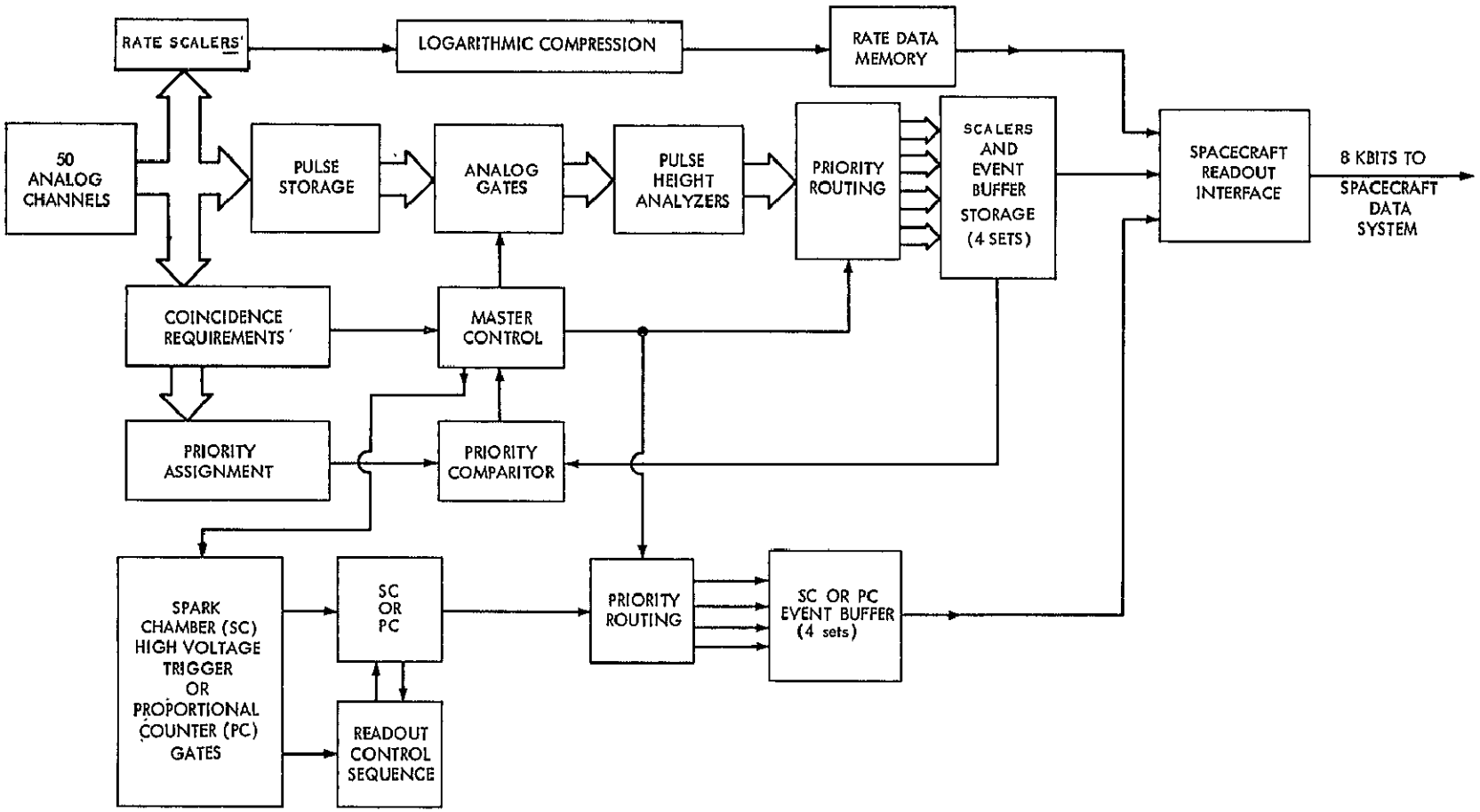

Figure IV-2. Detailed subsystem interface.

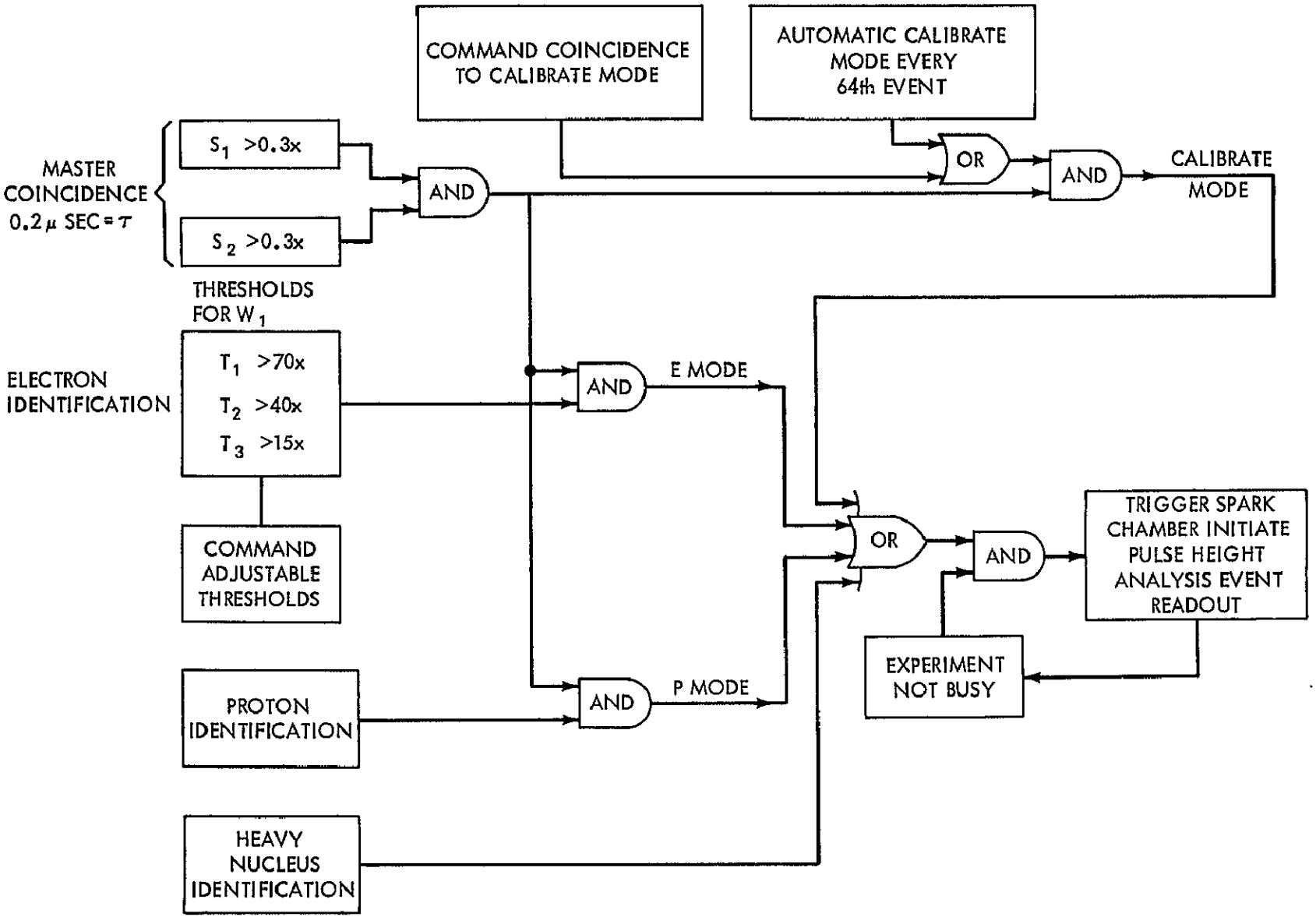

Figure IV-3. Coincidence logic.

(2) P Mode. Protons and helium nuclei will be identified by the criteria shown in Figure IV-4. A pulse will be required from the tungsten spectrometer which indicates an energy deposit greater than a threshold energy E_t in the spectrometer. In addition, a substantial energy deposit will be required in the n^{th} $(6 < n \leq 12)$ module where n is command adjustable.

(3) Z Mode. The heavy nuclei will be identified by their large pulses in the two plastic scintillators and the Cerenkov detector as shown in Figure IV-5. These heavy nuclei are rare enough that all particles passing through this geometry can be accepted, and so no minimum energy deposit is required from the spectrometer. A low Z mode operates between pulse heights of 7 and 20 times those of minimum ionizing, singly charged particles. These correspond to vertically incident Li and Be nuclei. However, from balloon flight experience, it is found that significant numbers of large angle alpha particles can also satisfy these requirements and so the low Z geometry is "stopped down" by the additional requirement of a moderate pulse height in W_1. Furthermore, it has been found that a significant background of events occur in which S_1 and S_2 give pulse height values inconsistent by more than a factor of 4. These events constitute an unwanted background and are eliminated by the simple requirement shown. If S_1 and S_2 are 20 × minimum and the Cerenkov is 6 × minimum then the event is acceptable as a high Z particle.

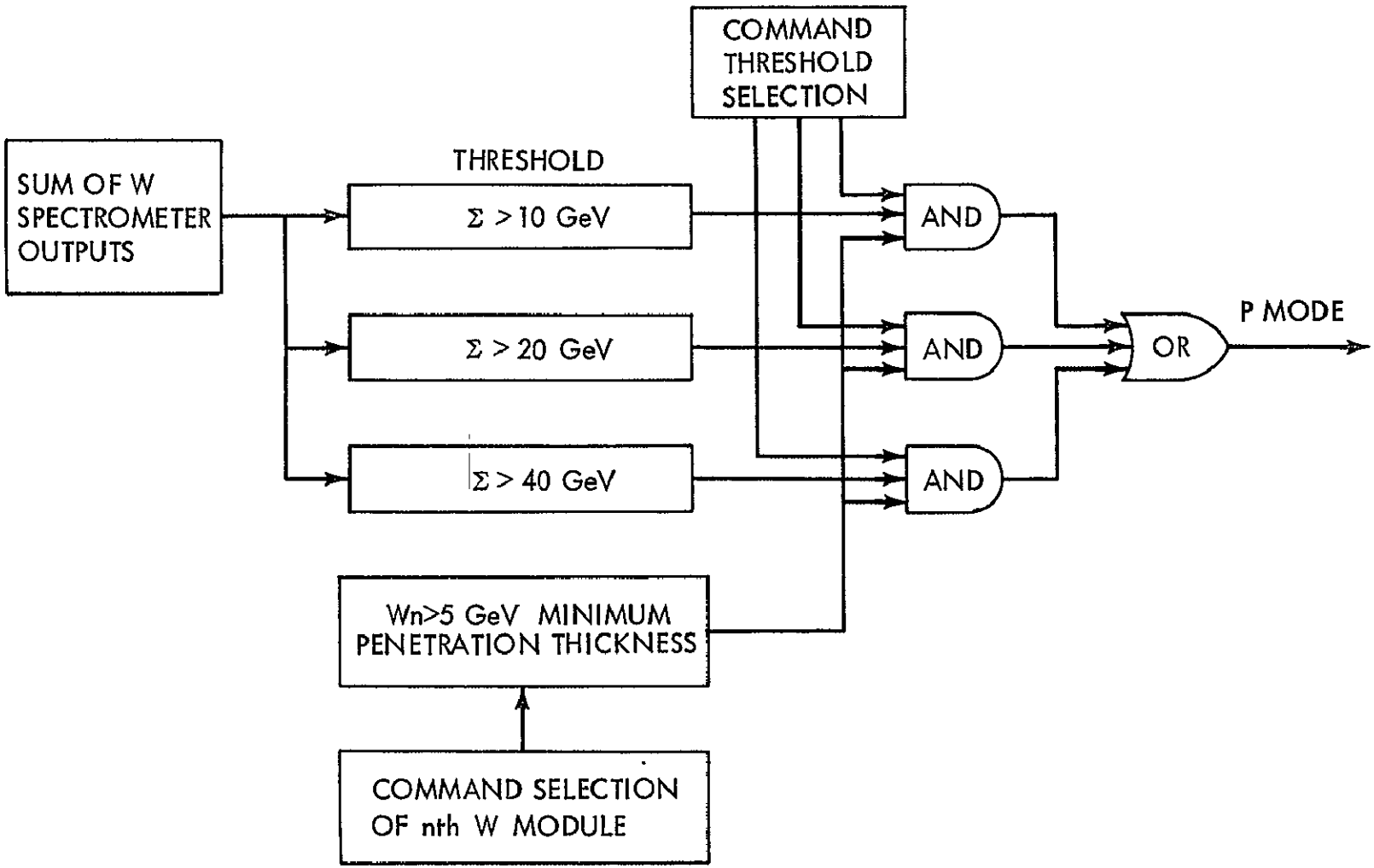

Figure IV-4. Proton and Helium identification logic.

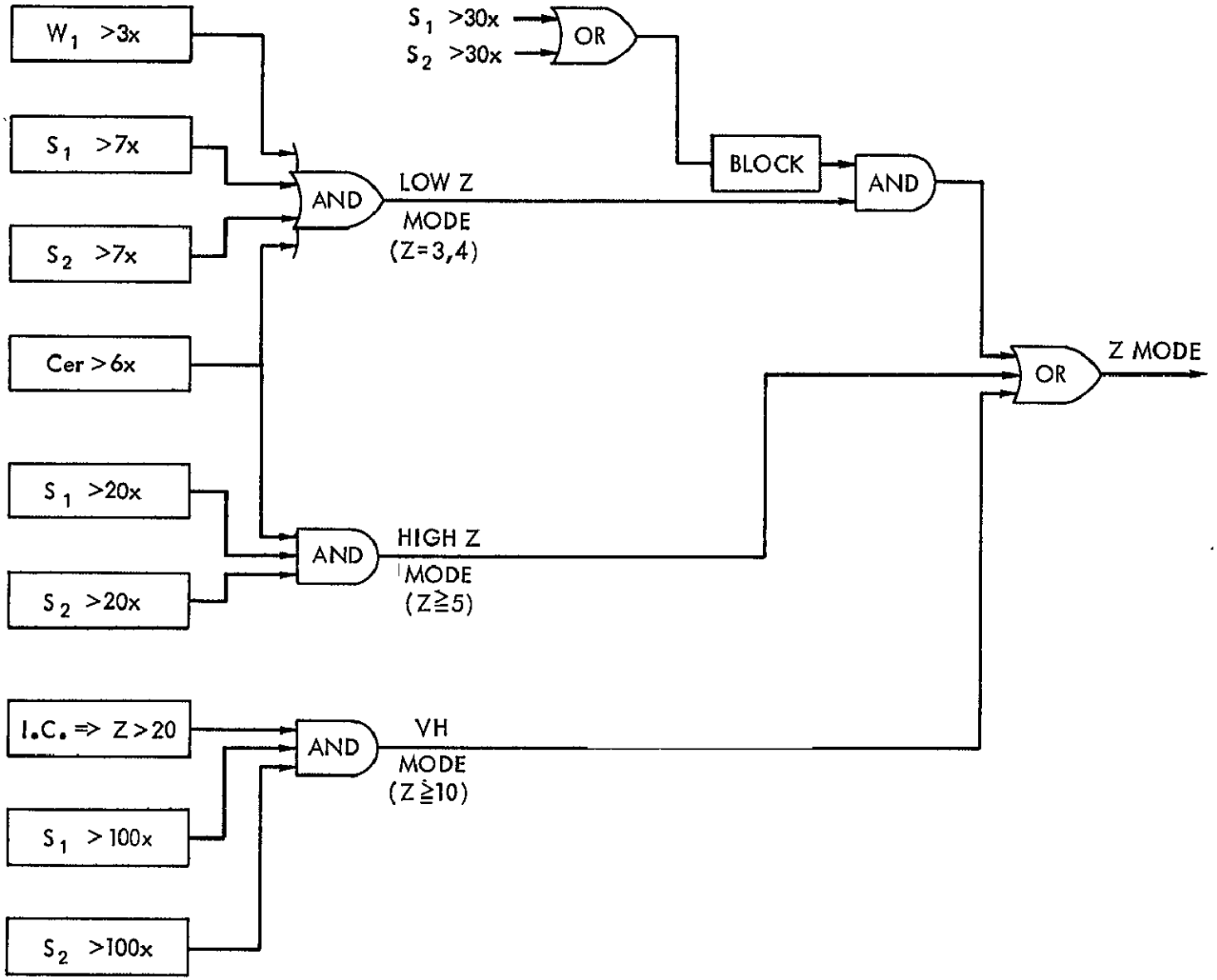

Figure IV-5. Heavy nucleus identification logic.

A complement to the high Z mode is a VH mode of larger geometric factor which requires only a coincidence between the scintillators, S_1 and S_2.

(4) Calibrate Mode. Every 64th event, all the threshold requirements are relaxed and the first available cosmic ray event passing through S_1 and S_2 is analyzed. This gives a random sampling of the background and is most useful as a data analysis aid.

These modes give a total counting rate of 10 - 20 counts/sec. The coincidence requirements will be command modifiable by the addition or subtraction of various requirements so that in the event of a malfunction or unexpected trigger rate, the situation can be rectified. For example, in Figure IV-4 commands are explicitly shown which could modify the energy threshold requirements from the tungsten modules or change the triggering geometry.

(5) Priority Scheme. The rarity of events can be related directly to the mode of triggering and to the response of the spectrometer. The priority assignment will have sixteen levels and will be defined by the matrix shown in Table IV-1. It is similar to a scheme developed for use on IMP-I (Cancro, 1969). This will result in 8 kbits/sec of data, an optimum and desirable bit rate. However, in case the spacecraft constraints dictate a lower data rate the priority scheme will adapted to make a more suitable selection of events.

The gradation is fastest in energy because of the steep spectra. This priority matrix can be reordered to emphasize certain features by reassigning by command the priority of a given trigger mode.

Table IV-1

EVENT PRIORITY ASSIGNMENT

Particle Energy	Trigger Mode	P	C	Low Z	High Z	E	VH
	Priority	0	2	3	4	5	6
10 GeV	1	1	3	4	5	6	7
10^2 GeV	2	2	5	5	6	7	9
10^3 GeV	4	4	6	7	8	9	10
10^4 GeV	8	8	10	11	12	13	14

The priority selection of events is shown schematically in Figure IV-6. The priority comparator operates in the following manner. There are four events in buffer storage, all with a priority rating. The highest priority event is being read out by the spacecraft. Another event occurs and is assigned a priority. its priority is lower than that of the stored events, then it is analyzed. If its priority is higher than any of the events in the buffer, the current event is read into the buffer containing that event with the lowest priority. Any of the four buffer channels which fails can be eliminated by command. This acts as a hedge against some unexpected background in some mode swamping the counting rate of all others. This system builds upon a technique developed first for a Pioneer experiment (Cancro, 1969a).

Analog section: Each of the detectors will be viewed by 2 or more photomultipliers giving a redundant tube for every detector in the event of failure. RCA ruggedized venetian blind type tubes with bialkali cathodes will be used in

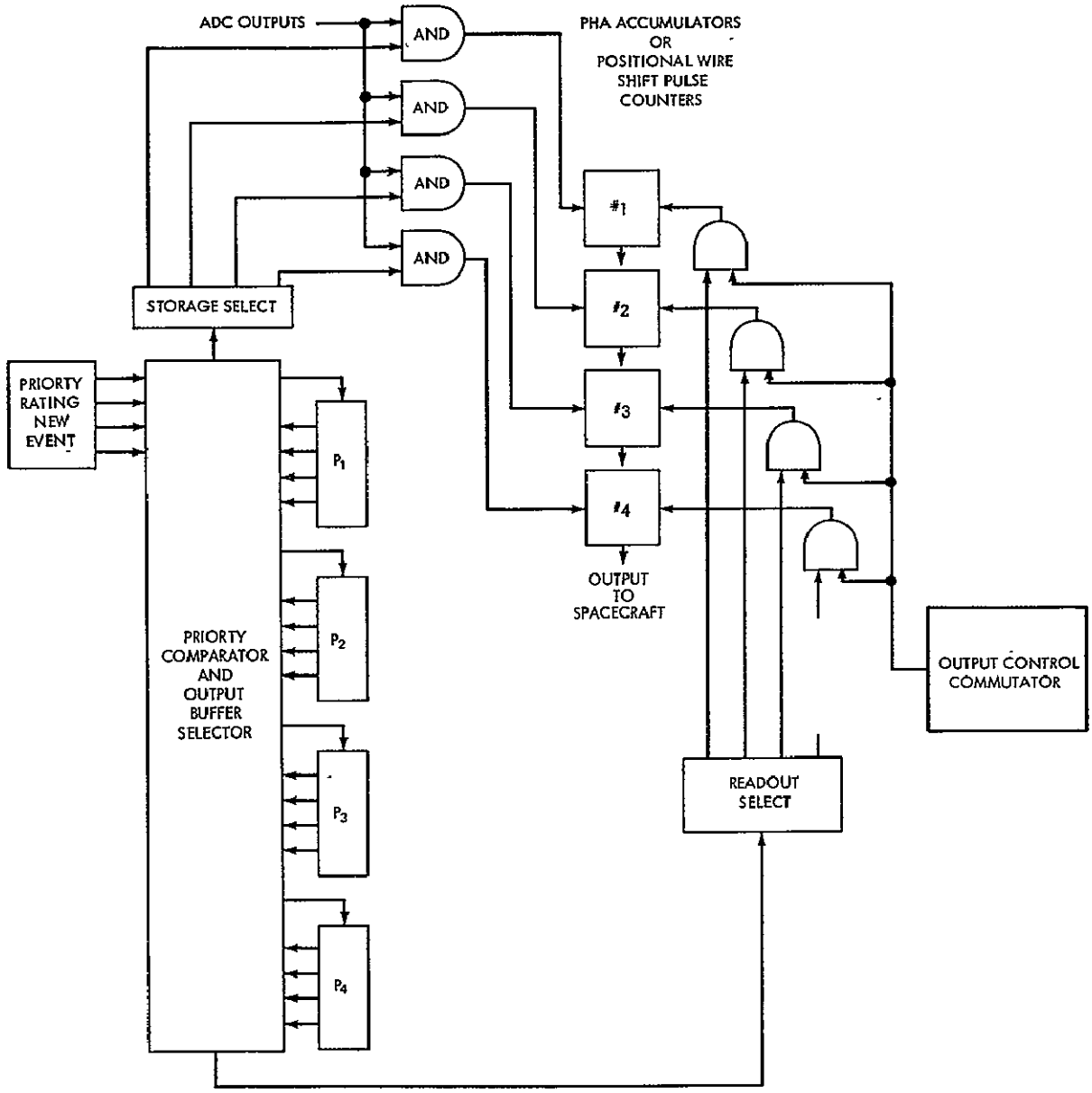

Figure IV-6. Priority selection logic diagram.

most cases. Table IV-2 gives a summary of the photomultiplier tubes, the pulse height analyzers and their uses. The signals from the two photomultipliers on each module will be added. In the event of failure a loss of gain will occur and more geometric corrections will be necessary to the pulse heights, but the detector will not be lost completely.

The 10^5 dynamic range required of the experiment presents the only major problem for the electronics. The ideal solution involves a logarithmic amplifier to be the first element seen by the pulse from the photomultiplier tubes. This alternative is shown in Figure IV-7. Such an amplifier suitable for space flight use does not exist.

Development work on the logarithmic systems will be conducted in the next year. The dynamic range of the subsequent electronics is determined by the desired accuracy.

In a logarithmic system

$$\text{Channel No. out} = k \log_{10} (\text{pulse height})$$

$$k = \frac{\text{number of channels}}{\text{decades of pulse height}},$$

the fractional width of each channel w is given by

$$\log w = \frac{1}{k}.$$

In this case, 5 decades are required and they can be fed into a 10 bit scaler (1024 channels) giving a channel width of 1.15%, an accuracy which easily exceeds that which is obtained from the ionization spectrometer and is perfectly

Table IV-2

SUMMARY OF ANALOG COMPONENTS

Detector	Number of PM Tubes per Module	Number of Modules × Number of Ends	Number of Channels per Module	Number of PM Tubes	Number of PHA Channels
S_1	2	1 × 2 = 2	1	4-5"	2
S_2	2	1 × 2 = 2	1	4-3"	2
C	8	1 × 2 = 2	2	16-5"	4
CsI Charge	4	1 × 2 = 2	1	8-5"	2
CsI Electron Cascade	2	5 × 2 = 10	1	20-2"	10
W_1	6	1 × 2 = 2	3	12-2"	6
W Spectrometer	4	10 × 1 = 10	2	40-2"	20
Ion Chambers		4 × 2 = 8	1		8
				104	54

Remarks

Totals: 28-5", 4-3", 72-2"

S_1 - Adiabatic light pulses

S_2 - Adiabatic light pulses

C - Two parts, one for charge, one for direction

CsI Charge - Light Diffusion Chamber

CsI Electron Cascade -

W Spectrometer - Ratio of two outputs from wedge shaped scintillators gives particle direction in Spectrometer.

W_1 - First and Last W modules

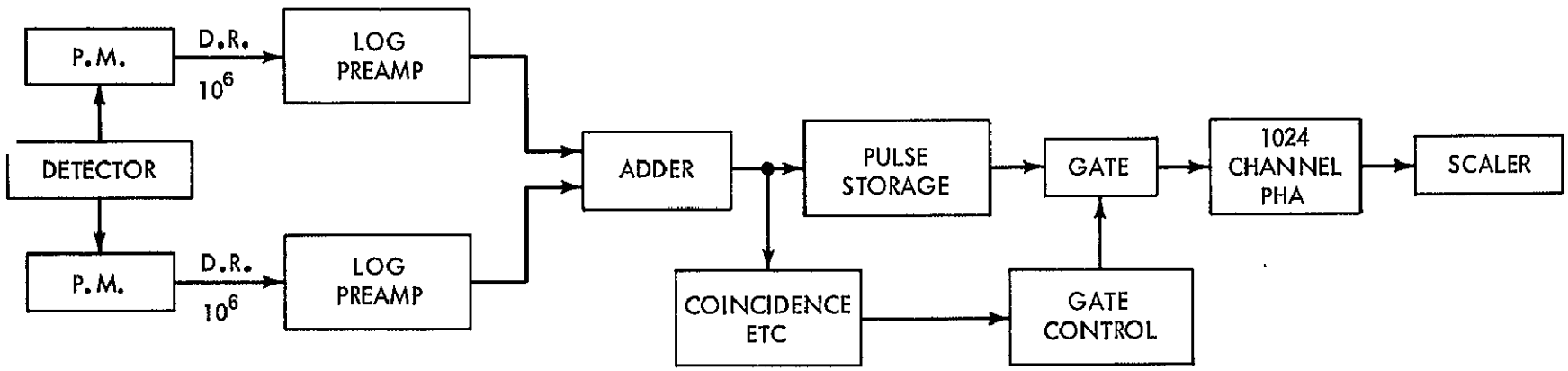

Figure IV-7. Logarithmic analog system.

adequate for the charge detection section. Thus the 10^5 dynamic range is converted into a 10^3 dynamic range, a much more manageable dynamic range.

There are several approaches to attaining such a logarithmic element. One attractive possibility is to use the PM tube itself. By adding all the dynode preamplifier outputs and by limiting the output voltages to a constant value, a stepwise linear system would be attained which would closely approximate a logarithmic response.

If this extended dynamic range cannot be attained in a single preamplifier, a system utilizing two photomultiplier outputs as shown in Figure IV-8 could be used. In this case each preamp has a range of 10^3. The reduced dynamic range causes a significant increase in complexity.

In the event that logarithmic preamplifiers are not developed a fall back design exists. This is outlined in Figure IV-9 and makes use of four separate photomultiplier outputs. This alternative involves considerably more complex circuitry.

Pulse Height Analyzers: The pulse height analyzers, gates, and gain selection circuits are all standardized in modular form and are qualified for space flight use (Cancro, 1969b). The pulse height analyzer is shown in Figure IV-10. These systems utilize gain switching and have been flown on IMP satellites. The alternative method of having each pulse height analyzer look at more than one stored pulse (using long term pulse storage) has been considered. This has the disadvantage that very high digitizing frequencies must be employed to

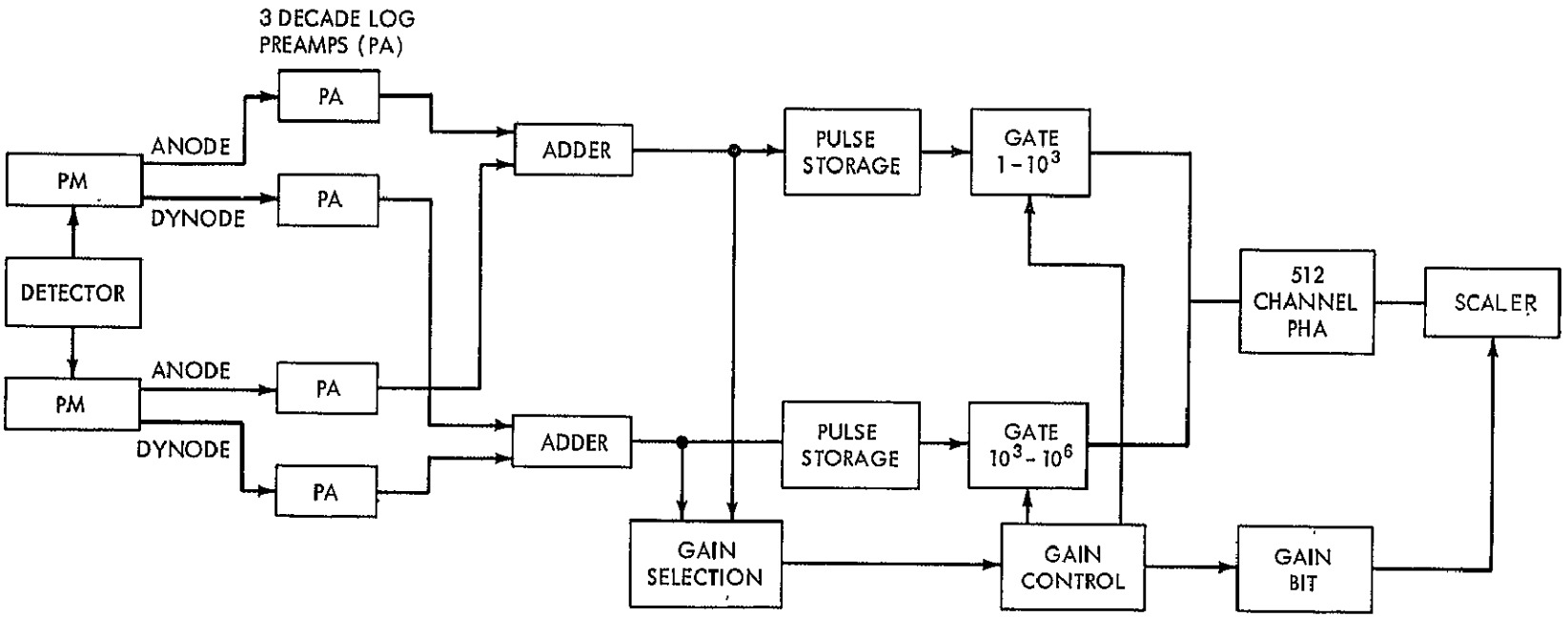

Figure IV-8. Dual range logarithmic analog system.

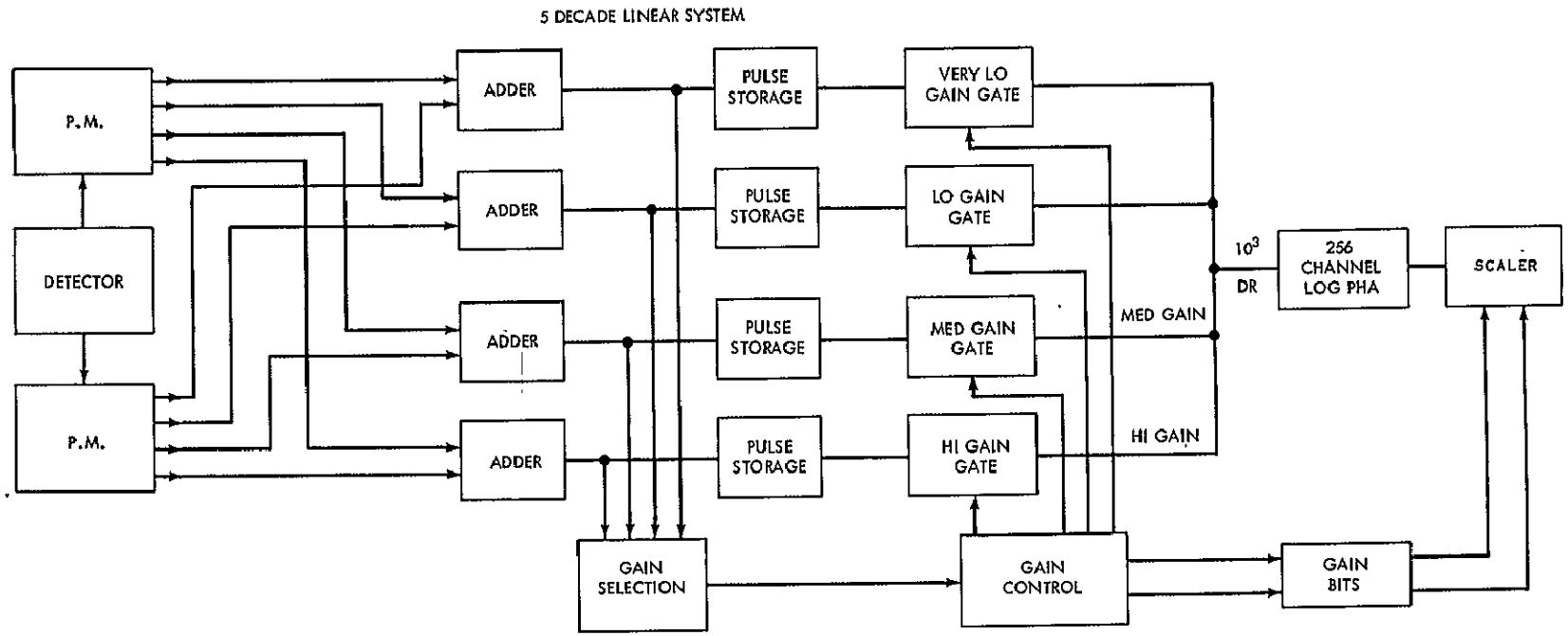

Figure IV-9. Large dynamic range linear analog system.

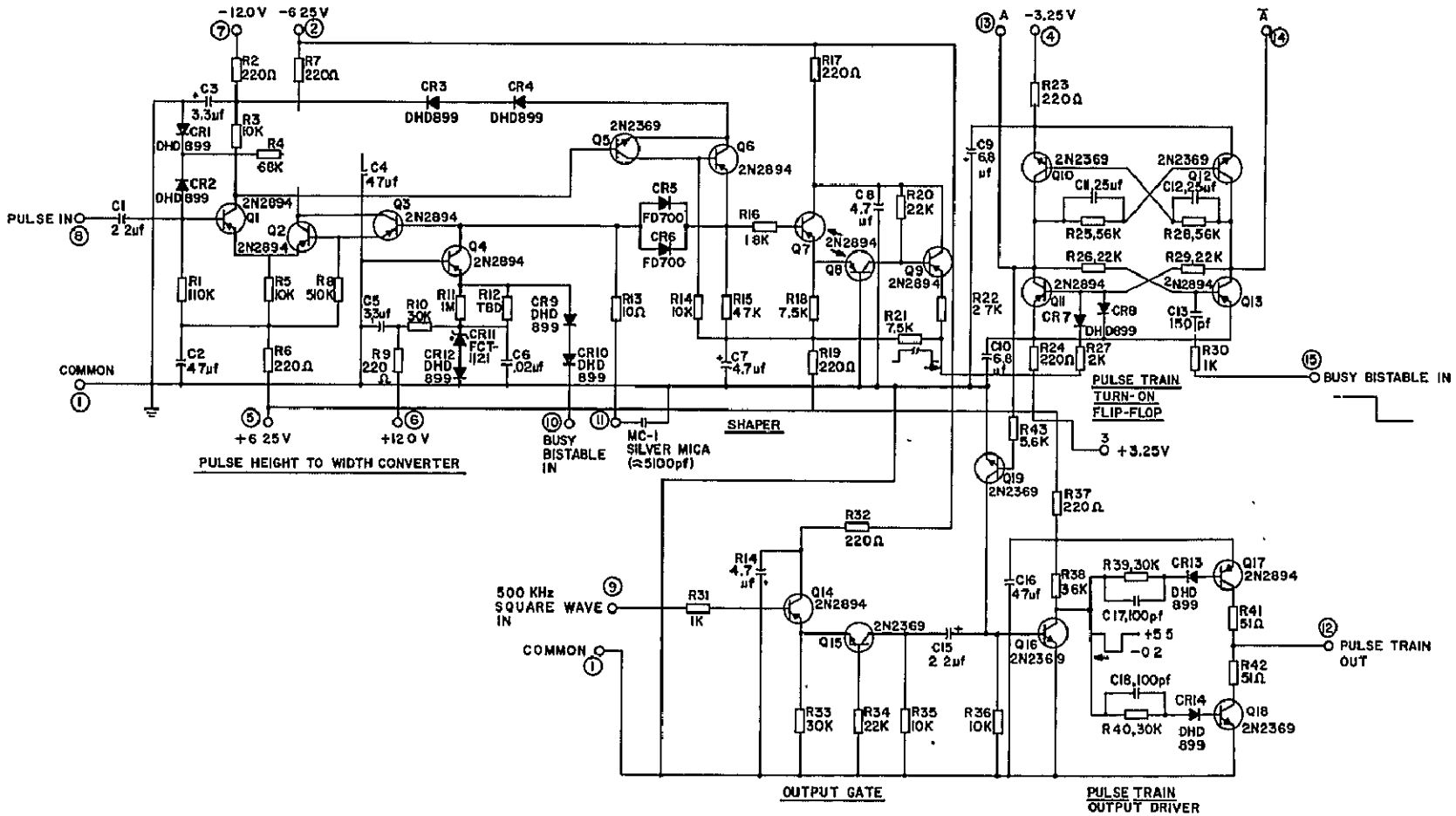

Figure IV-10. Pulse height analyzer.

keep the dead time low. This would be incompatible with the low power requirements of the scaling circuits and the digital output buffers.

Positional Wire Readout:

The spark chambers have been adapted from those developed by the γ-ray astronomy group at Goddard and discussed previously. The readout and electronic systems have been discussed in various publications (Ehrmann, et al., 1967) and have been found adequate for this purpose. In the balloon tests so far conducted the core readout efficiency was less than 100% but in a manner which has not prohibited track identification. This situation has since been remedied by improved sensitivity.

The readout of the spark chamber involves the direct digitization and digital storage of the input information. Each of the grid wires threads a magnetic core, which in turn, receives and contains its datum of information when the high voltage is pulsed to the chamber plates. The cores are normally in the quiescent or "reset" state between operations. Spark current in a wire "sets" a core, and the "readout" act of determining which cores have been set by the events resets the cores.

The core readout circuits can be described as follows. The total spark chamber system contains 16 decks of 256 wires each. This provides 8 x, y pairs of coordinates and makes up a system containing $(256 \times 8 \times 2) = 4096$ wires. Each 256 core tray is made up of a matrix of 8 sense lines, 8 current pulsers and 4 grounding circuits. The cores are sensed in a serial order so

that the position of the set core is given by the 8 bit core number. A ninth bit differentiates between x and y, and 10, 11, and 12th bits give the deck number.

The readout is accomplished by the following sequence of events. After an event occurs the first 8 cores of the first tray of the x array are read into a shift register. The shift register is then advanced until either a set core is found or until all eight bits have been examined. If a set core is found, its address (which resides in a register) is recorded, and shifting continues. After the eight sensing circuits have been examined the next current pulser interrogates the next eight cores and shifting continues. This process is continued across the tray until all 256 cores have been interrogated. This process clears all the set cores for the next event.

Several alternative readout schemes have been considered. The most obvious alternative implies the transmission of $16 \times 256 = 4096$ bits of information per event. The scheme used is far more efficient because it relies on the fact that a typical event being detected in the chamber will set 30 or 40 cores. Since each core requires 12 bits of data to be localized, the transmission of the location of only those set cores requires approximately $40 \times 12 = 480$ bits, a saving of almost a factor of 10.

A further reduction in the amount of data transmitted can be effected (since the chamber is scanned across each tray and many sparks spread to more than one wire) by simply adding two bits to the address of a set core. If adjacent

cores are set the number of adjacent cores is transmitted. This reduces the data transmitted by more than 33% based on an analysis of balloon flight results.

The spark chamber will be read out into the output buffer simultaneously with the pulse height analyzer data. Two limitations to the recycling time exist. First is the speed at which cores can be scanned, and the second is the high voltage capacitor recharge time. Work is presently being done on both these factors to reduce the dead time.

The alternative trajectory definition system using wire grid proportional counters will have a readout system which is basically similar to that of the spark chamber. In the spark chamber system the temporary storage element used is a magnetic core, in the proportional counter system it is a semiconductor bistable device. The number of wires in both systems is similar but the proportional counter system will have twice the number of storage elements, corresponding to the two discriminators which sense whether a singly charged or multiply charged particle passed near each wire. The upper level (multiply charged particle) storage should have fewer stored bits than the lower level (singly charged particle) storage. (It would reduce the data readout requirements if only the high levels storage is read out.)

Consequently the readout considerations mentioned above apply equally well to the proportional counter system.

Digital data system: The digital data handling system will program the outputs of the pulse height analyzers into a suitable format and control the scanning of the spark chamber for set cores. It will order events in the experiment spacecraft buffer for transfer to the spacecraft data-handling systems. It will insert event identification numbers into the readout pattern, edit out unnecessary data (e.g. PHA outputs of zero), number the analyzer outputs, etc. For handling data of this type, unique integrated circuits have been developed at GSFC (White and Lokerson, 1970). Two of these "bugs" will have direct applicability to this experiment. In Figure IV-11, an accumulator with buffer storage is shown which would act as the memory device. The experiment will contain 208 (4 sets of 52) of these units to handle the pulse height data and a comparable number for the positional data. A second "bug" shown in Figure IV-12 will be used for all the rate data. It contains a 24 bit counter with a logarithmic compressor to a 12 bit output word.

Calibration, Rate, and Housekeeping: Occasionally the data system will switch the experiment into a calibrate mode of operation in which calibration data, rate, and housekeeping data will be read out in place of the normal output. Light sources (scintillators doped with α particle sources) on or near the face of each photomultiplier tube will be used to calibrate the detector. Coincidence

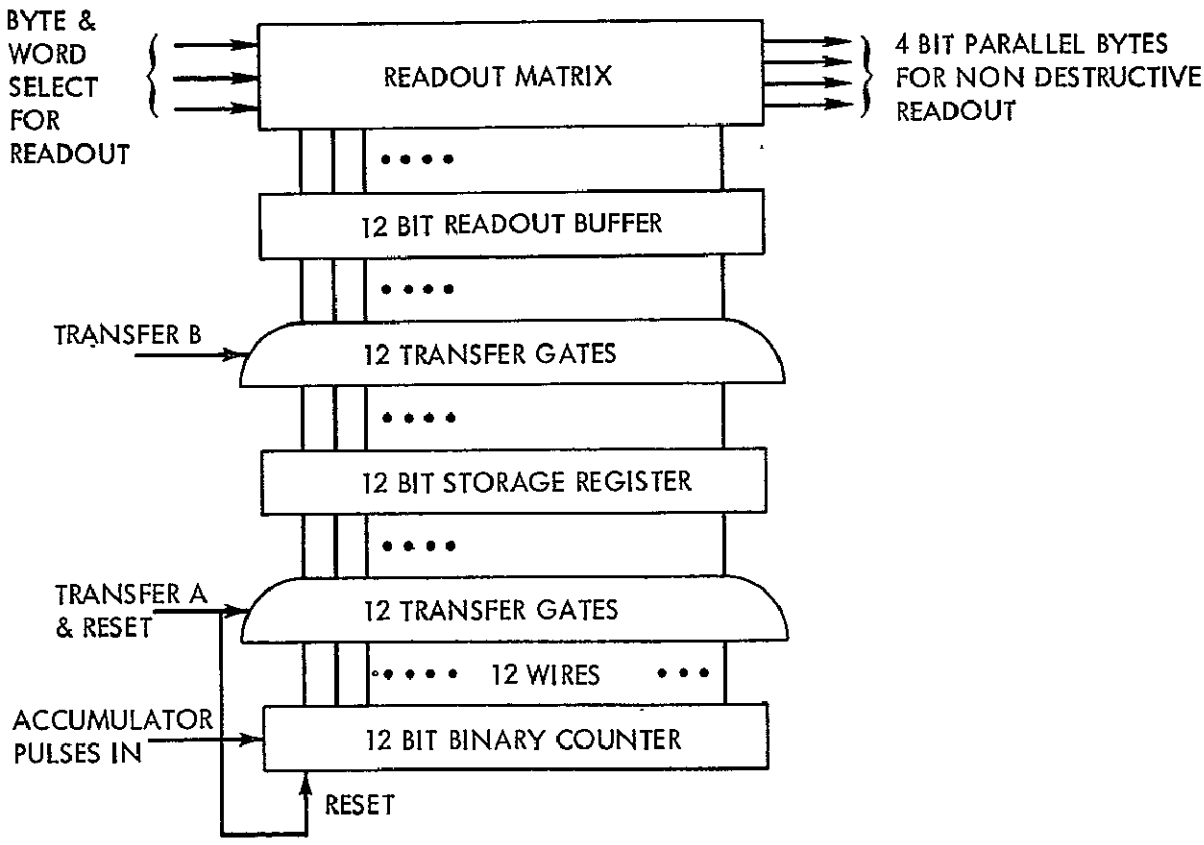

Figure IV-11. Twelve bit accumulator with temporary storage and buffered readout storage.

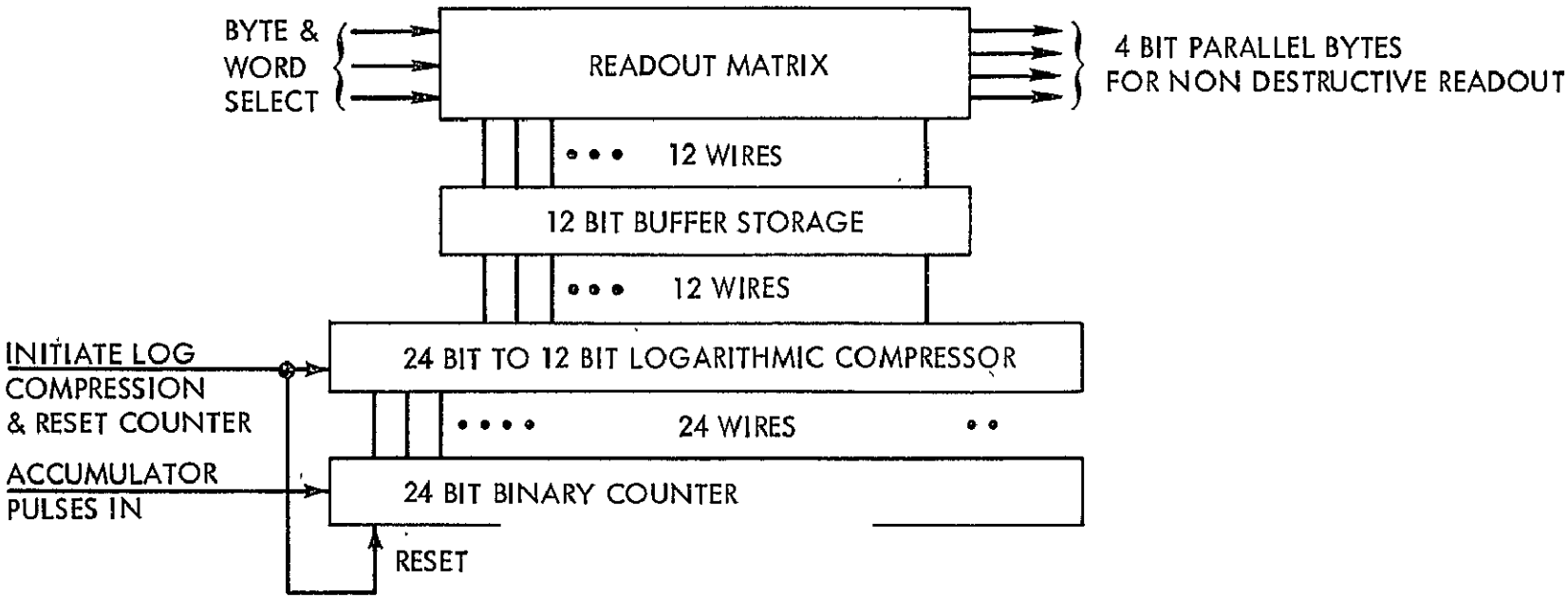

Figure IV-12. Rate data accumulator.

requirements will be relaxed and each detector will be pulse height analyzed. The pulse height distributions from each photomultiplier will be transmitted. This will allow the detectors to be monitored from the ground for gain drifts, and other failures. In addition, the housekeeping cycles will read out the necessary voltages, temperatures, pressures, etc. to monitor the operation of the instrument. Of critical importance will be the monitoring of the gases of the positional detectors and the ion chambers. A small mass spectrometer will be placed in each gas to monitor its composition. Rates of all thresholds, partial coincidences, rejected events, and over-ridden events will be scaled in order to monitor performance and to correct fluxes.

Commands: Based upon information learned from the above performance monitors, commands will be sent from the ground which will reconfigure the experiment in light of the ground information. Commands will be required to do the following:

(1) Switch to redundant circuits in the event of failure.

(2) Reconfigure the coincidence requirements by removing or adding different detectors and/or threshold levels to given coincidence modes.

(3) Reassigning priorities.

(4) Changing threshold energies by switching in different threshold circuits.

(5) Changing or purging gases in spark chamber and the proportional counter.

(6) Switching into a calibrate mode of operation.

(7) Turning power off and on various subsystems and/or the whole experiment.

(8) Switching to calibrate mode and commanding housekeeping data to be transmitted to ground for diagnostic purposes.

(9) Changing the high voltage of the directional detector and/or switching in new spark gaps.

These functions are estimated to require at least 16 - 5 bit command words and 128 discrete on-off commands.

Ground Support Equipment: The ground support electronics and checkout equipment for this experiment would be exceedingly complicated if it were to consist of specialized equipment. It will be handled far more easily and flexibly by a small digital computer. In addition, this approach is the most economical. The main problem is one of memory capacity to handle the large amount of data generated per event. Ground support equipment for balloon flight instruments have been designed with a basic concept similar to the above consideration and found to be very useful for decisions regarding the performance of the equipment.

Testing and Redundancy: The electronics systems to be used are standard space flight qualified units. They will be tested individually and again as an integrated unit in order to insure proper operation.

The experiment is multiply redundant. The experiment has separate electronics on different ends. Two photomultipliers view each detector. Four event output buffers are used, etc. As can be easily seen, a multiplicity of failures can occur and the experimental objectives can still be met.

The spacecraft electrical requirements are as follows:

1. Power: 50 watts continuous
2. Voltage: The 28 - 33 volts raw power from the spacecraft will be converted and distributed within the experiment.
3. Telemetry: The experiment will trigger at the rate of 10 - 20 events/sec and will produce 1000 - 1200 bits/event. This will be converted to a bit rate of 8 kbts/sec or less of continuous data (see priority scheme).
4. Commands: 16 - 5 bit command words and 128 discrete on-off commands will be minimal for operating this sytem. Redundant circuitry will be selected, on-off switches for shutting down all or part of the experiment, gas changes will be initiated and the laboratory will be reconfigured by ground command.
5. Time Information: Spacecraft time should be available for identification of event times to the nearest millisecond.

B. MECHANICAL SYSTEM

The structural and mechanical components of the High Energy Cosmic Ray experiment consist of housings for the various modules, a number of high density

moderating plates interspersed between plastic scintillators, a support structure, a pressure vessel, a gas purging system, and miscellaneous electronic equipment packaging. The stack-up of sensor modules in this double-ended experiment is as follows:

1. Pulse Ion Chamber
2. S-1 Scintillator
3. Spark Chamber
4. Cerenkov Counter
5. S-2 Scintillator
6. Cesium Iodide Diffusion Chamber
7. Five Cesium Iodide Modules
8. Twelve Tungsten Modules
9. Five Cesium Iodide Modules
10. Cesium Iodide Diffusion Chamber
11. S-2 Scintillator
12. Cerenkov Counter
13. Spark Chamber
14. S-1 Scintillator
15. Pulse Ion Chamber

The geometrical relationships of these elements are shown in Figures IV-13 and IV-14.

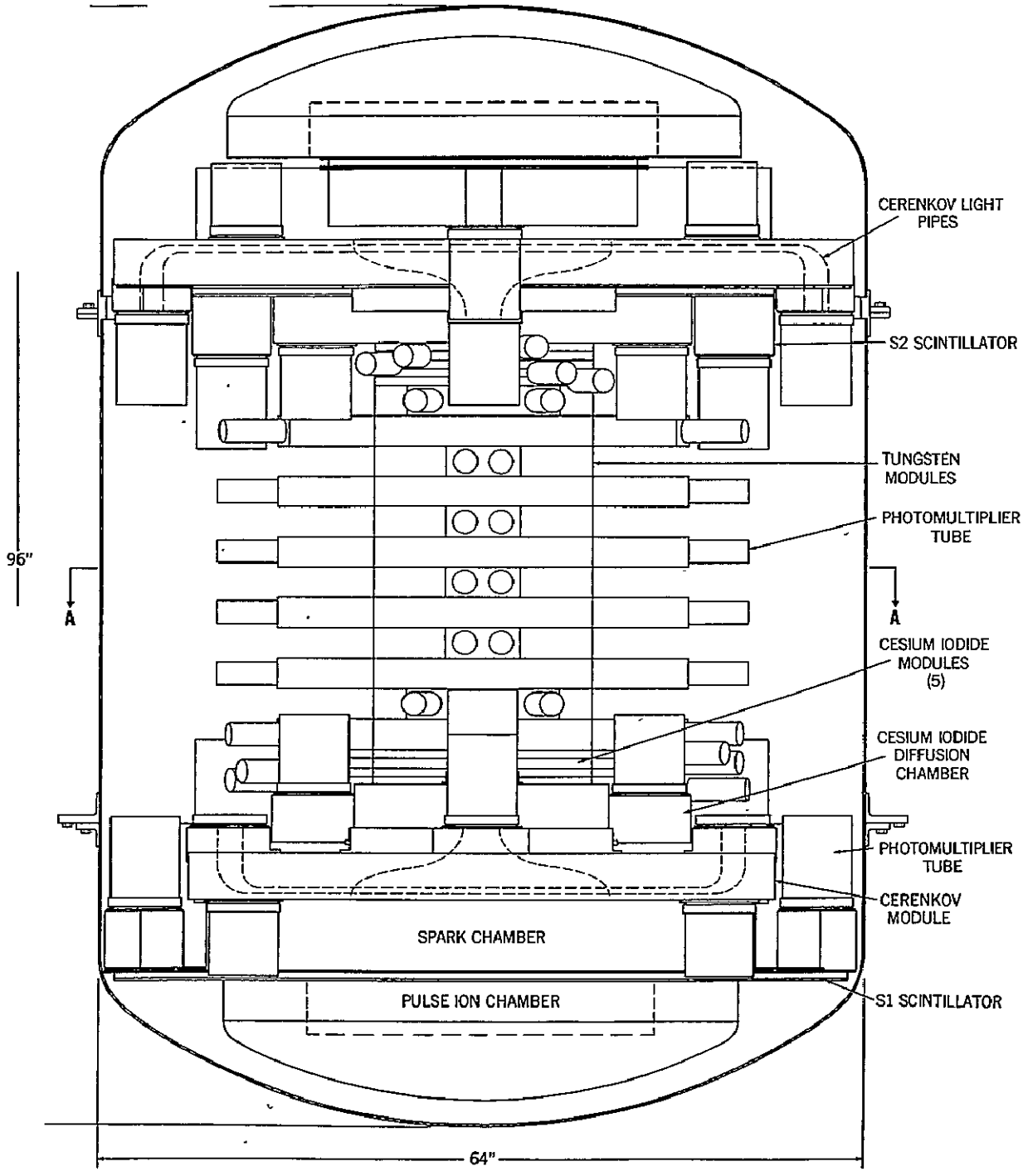

Figure IV-13. High energy cosmic ray experiment, side view.

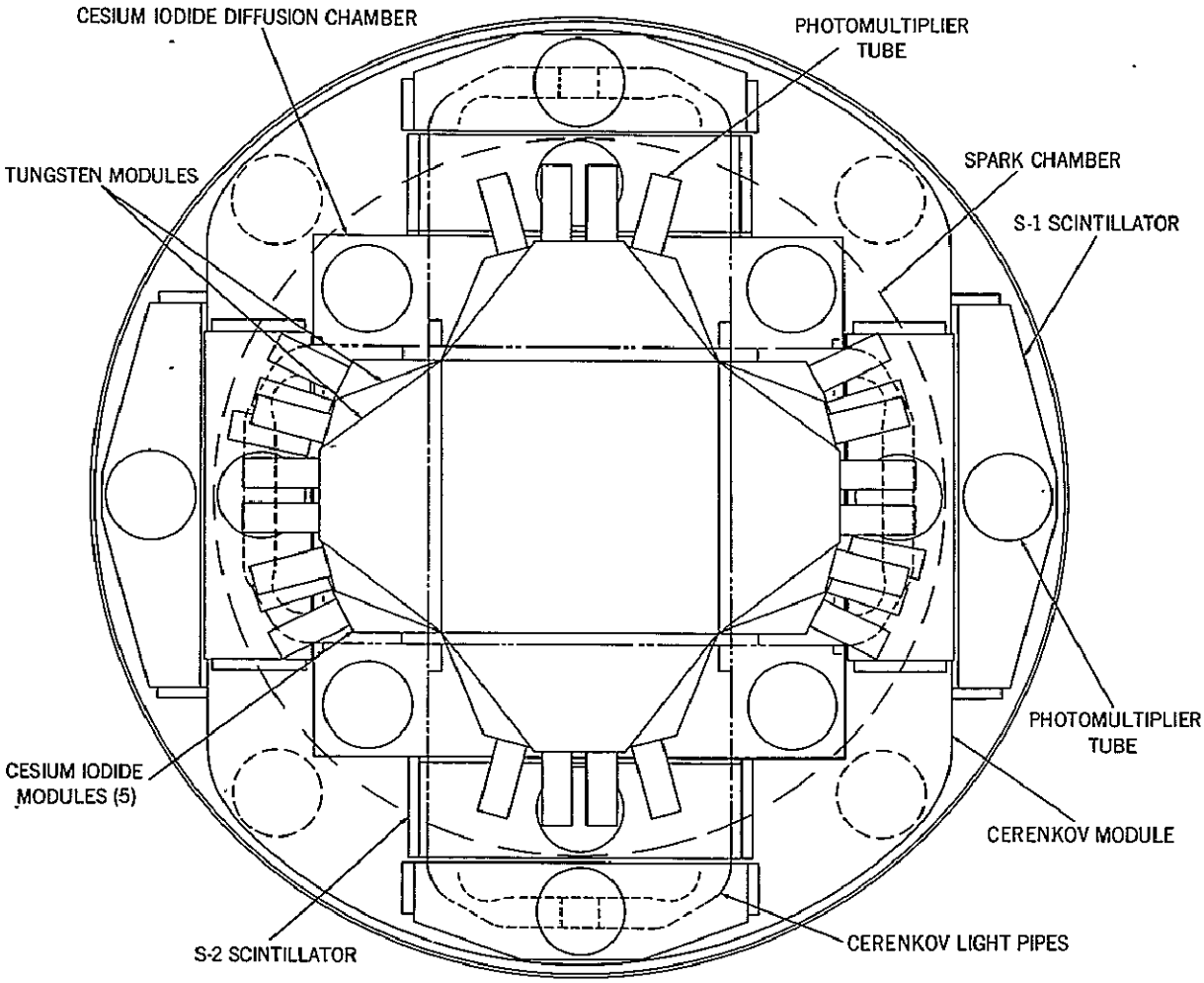

(section A-A)

Figure IV-14. High energy cosmic ray experiment, top view.

Tungsten Modules:

The tungsten modules are made up of four (4) tungsten plates with a plastic scintillator sheet between each pair. These plates are bolted to two side plates of aluminum, which provide the structural frame for each module and the connection into the primary support structure. On each of the two remaining sides of the module, an aluminum light transmission chamber is attached. Each of these is equipped with two photomultiplier tubes housed in aluminum cans which view the edges of the plastic scintillator sheets. Each outer tungsten plate is .289 inches thick and each inner one is .578 inches. The plastic scintillator sheets are made so that each consists of two wedges with alunimum foil between. Light from one wedge will therefore only travel to the phototubes on its side of the module, thus providing position information regarding a particular cosmic ray particle. See Section III B for more detailed explanation of the operation of the tungsten modules.

Cesium Iodide Modules:

The cesium iodide module consists of a square aluminum frame which supports a block of cesium iodide, and two light transmission chambers with a photomultiplier tube on each. The cesium iodide is 18 inches square and 2 centimeters thick. Because the module is only .787 inches thick and the photomultiplier tube assembly is over 2.0 inches in diameter, the positions of the photomultiplier tubes on the light transmission chambers are staggered from

one module to the next. This allows each tube assembly to overhang its light chamber without interference.

Cesium Iodide Diffusion Chamber:

The diffusion chamber is an aluminum sheet metal box approximately 4 inches high and 35 inches square. On the inside it contains a 3 mm thick sheet of cesium iodide, 50 cm square. It has four photomultiplier tubes viewing into the box, near the four corners. The inner surfaces of the box are painted white for maximum light reflection.

S-2 Scintillator:

This unit is an aluminum housing for a sheet of plastic scintillator with plastic light pipes. The scintillator is .250 inches thick and 19 inches square. A series of lucite light pipes are adhesive-bonded to two of the edges of the sheet. Each bundle of light pipes leads to a photomultiplier tube in an aluminum can. The overall width of this unit is 22.75 inches and length is 48.25 inches. The housing is .875 inches high at the center with a cover box at each end for the light pipes.

Cerenkov Counter:

The Cerenkov counter is in an aluminum chamber which houses a .500 inch thick Cerenkov scintillator. The scintillator is 21.2 inches square and has light pipes extending outward from all four edges. Each bundle of light

pipes terminates at one of four photomultiplier tubes. In addition, the inside of the chamber is painted white, similar to the diffusion chamber, so that light may be reflected into four additional photomultiplier tubes which are located near the four corners of the scintillator, viewing into the box. The main chamber is 62 inches long, 49 inches wide, and 4 inches high. Four boxes, 2-1/4 inches high, are mounted on top of the main chamber to provide for the light pipes and their photomultiplier tubes. Each tube is mounted in a can.

Spark Chamber:

The spark chamber structure is primarily a gas tight, low pressure vessel which provides a proper gas environment for the high voltage wire grids. It contains a set of eight wire grid frames and the associated electronic components. The gas is a mixture of neon and argon with a small percentage of alcohol. The chamber is a short cylinder 6 inches high and 48 inches in diameter. In order to minimize the interactions of the incident cosmic ray particles, the upper and lower surfaces are made as thin as possible. The "windows" as they are called have been made of .020 aluminum on units successfully flown on balloons. Similar windows may be used on the proposed spark chambers. However, because of requirements for gas replenishment in flight, with attendant pressure variations, other window materials and thickness will be investigated. Also while present balloon flight spark chambers have had flat windows (since they did not have to replenish the gas) it is intended to investigate the possibilities of curved windows which could tolerate greater pressure loads. The seals used

on existing spark chambers have been "O" rings. Since the required diameters of the main seals are large, (about 30 inches), it may be found that acceptable leak rates for long duration space flight cannot be obtained reliably with "O" ring seals. In this event the main joints will be designed with metal to metal seals similar to those successfully flown on Explorer 17 and Explorer 32. On these spacecraft a copper shear gasket joint 30 inches in diameter was used. The total helium leak rate of these spacecraft, which included nineteen other similar sealed ports, was less than 1×10^{-6} std. cc/sec. This leak rate would be permissable for the spark chambers for this mission. A spark grid is shown in its chamber in Figure IV-15.

S-1 Scintillator:

This unit is similar to the S-2 scintillator assembly except that it is slightly longer and wider. This provides a larger scintillator, which is necessary from the standpoint of the entry cone angle. The total length is 62.75 inches and the width is 27.1 inches.

Pulse Ion Chamber:

The pulse ion chamber is somewhat similar to the spark chamber in that it is a gas tight low pressure vessel. This unit however contains a different gas (Xenon) which does not degrade and therefore does not have to be replenished. It contains a series of high voltage plates suitably mounted in the chamber. It also must have thin "windows" top and bottom to minimize the interactions of cosmic ray particles.

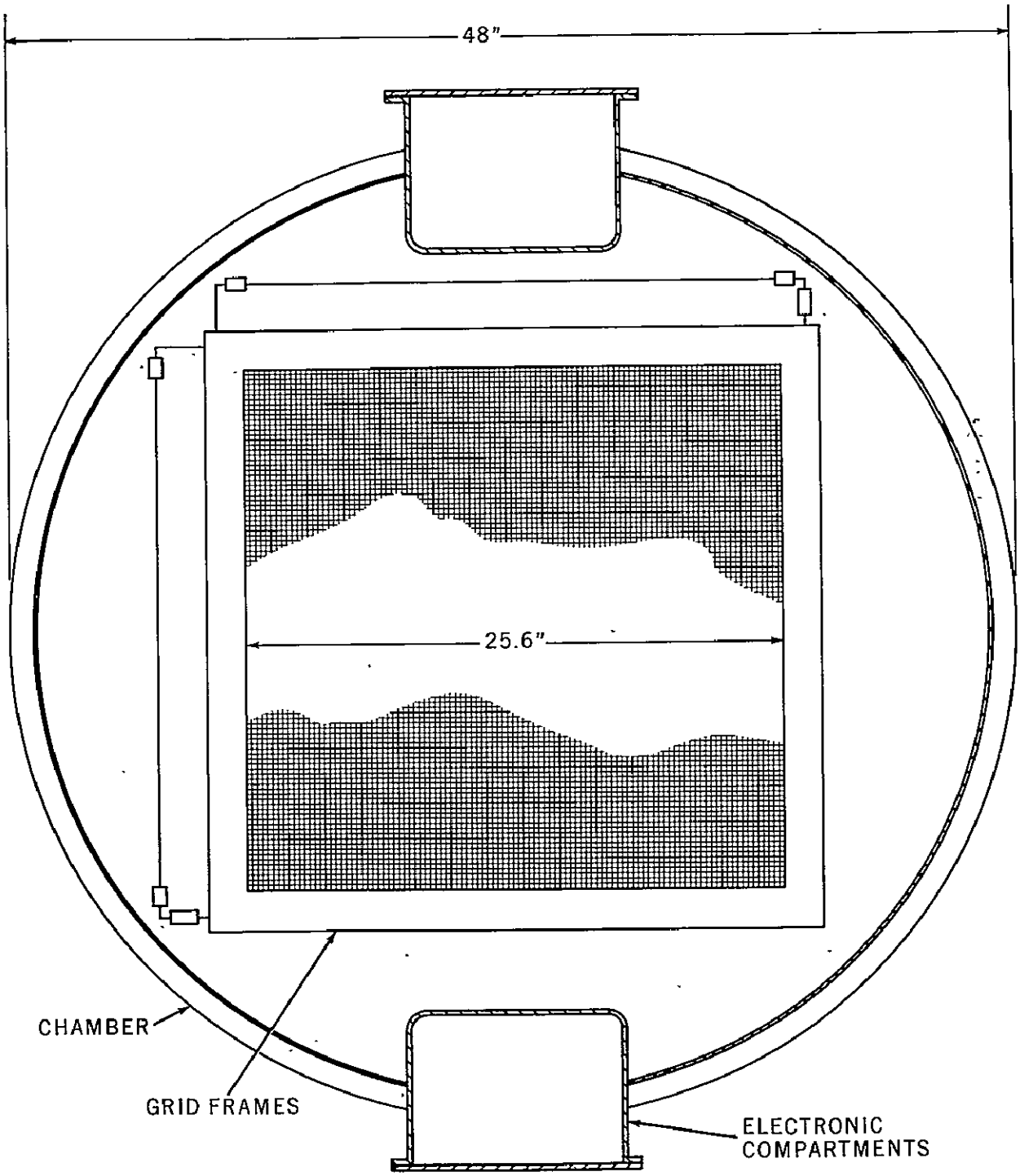

Figure IV-15. A spark chamber grid in its container.

Gas Replenishment System:

Tests with existing spark chambers that have been flown on balloons have shown that the alcohol constituent in the spark chamber gas is gradually decomposed by the sparking action. Over a short duration flight this poses no problem. On a spacecraft flight however where the experiment is intended to operate for a year or more it will be necessary to replenish the gas in the chamber after several months of operation. To provide this capability a pressurized gas system is included in the design of the experiment. A schematic diagram of the system is shown in Figure IV-16. It consists of two spherical supply tanks and the required plumbing lines, fittings, valves, regulators and miscellaneous components needed to change the gas in the spark chambers by command from the ground. Sufficient gas is contained in the tanks for at least four flushings. Two tanks are included in the system with cross-feed capability, so that either spark chamber can be filled from either tank, thus providing redundancy in the event of one tank failure.

In this experiment the spark chamber is just one sensing element in the complete stack. Since the total height is limited by spacecraft size, the spark chamber must be relatively flat. This results in flat or nearly flat windows. These flat windows of thin material are unable to withstand the pressure differential that would exist across them if the inside was pressurized to 1 atmosphere while the outside was at vacuum, or if the chamber were evacuated while 1 atmosphere of pressure existed on the outside of the spark chamber.

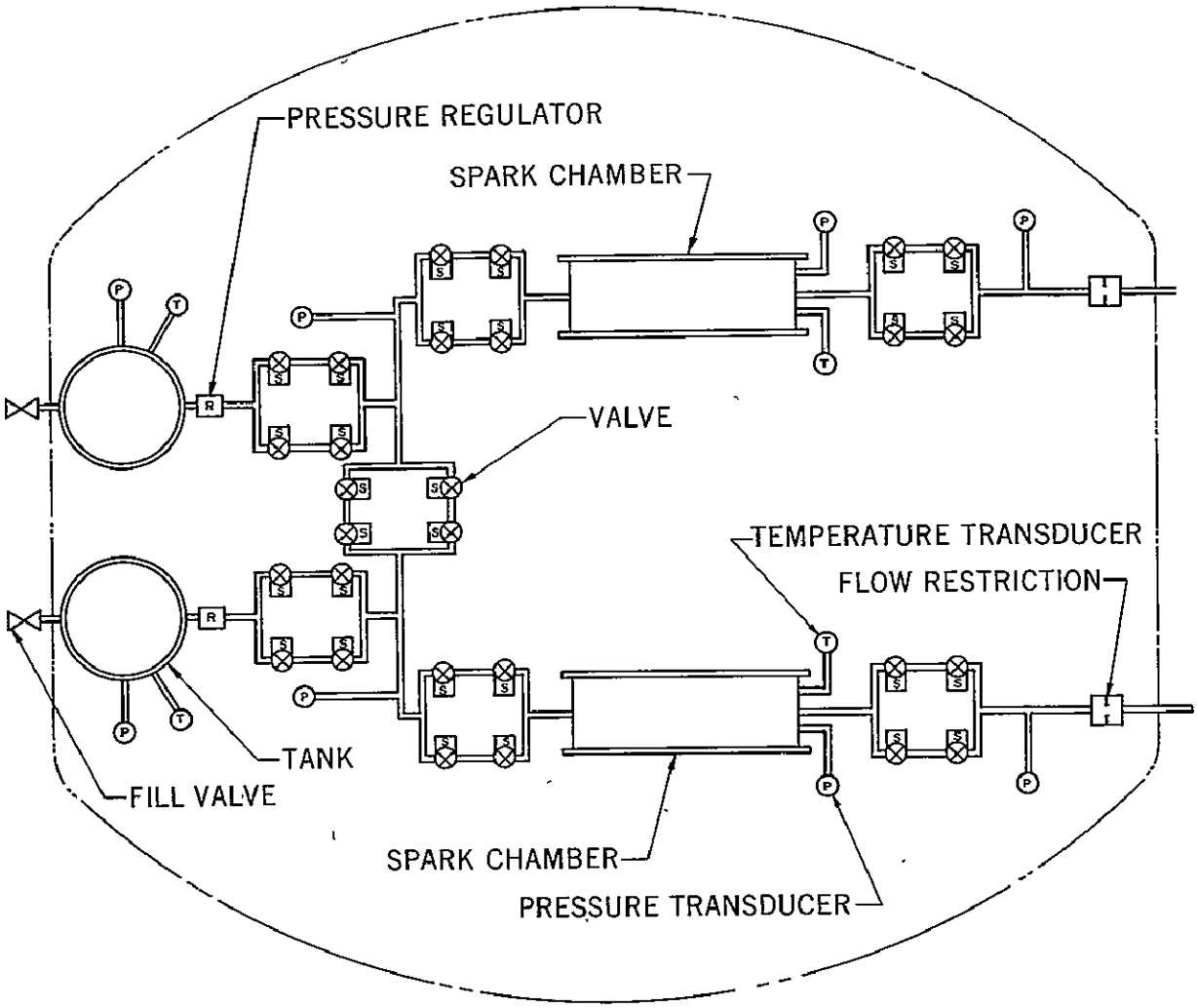

Figure IV-16. Gas refill system.

The first condition would exist during normal operation if the experiment was not housed in a pressure vessel. The second condition would exist with the present design during spark chamber gas elimination if the chamber was completely vented to space. In order to effect a change of gas when needed in the spark chamber, the present design makes use of a slow bleed or flow restriction in the vent line. This will enable a nearly constant pressure to be maintained in the chamber while it is being slowly purged. It requires a pressure regulator on the incoming line to maintain the pressure of the inlet gas at 1 atmosphere. A flow restrictor somewhat similar to this was used successfully on Explorer 32. In that case the requirement was for a restrictor that would produce a bleed rate slow enough so that spacecraft pressure would decrease at approximately 1 atmosphere in 48 hours when the valve was opened. This is considered to be a more stringent requirement than that needed for the spark chamber.

The gas pressurizing system is installed inside the main pressure vessel to minimize through fittings and increase reliability. Fill valves are located externally so that the system can be filled and checked out after the experiment is installed in the spacecraft. It is expected that the final filling of the system would take place on the launch gantry. The entire gas pressurizing system is intended to be based on existing components such as valves, regulators and tanks that have been previously qualified on other space flights.

Pressure Vessel:

The entire experiment is housed in a pressure vessel that provides an environment of 1 atmosphere of nitrogen. This gas environment serves two main functions, it prevents arcing and corona problems with high voltage leads and it eliminates a large pressure differential across the spark chamber and ion chamber windows. The pressure vessel is a cylinder with two domed ends. It has a diameter of 64 inches and a length of 96 inches. This length fits within the spacecraft dimension across the flats. The domes are secured by bolted flanges with "O" ring seals. Thickness of the domes is critical for the same reason as the spark chamber window, to minimize interactions of cosmic rays. If made of aluminum the domes would be in the order of 0.100 inches thick. Studies will be performed to determine if a lower value of mass per unit area can be achieved with titanium. A micrometeorite bumper will be incorporated if penetration probabilities warrant this.

Internal Structure:

A truss structure inside the pressure vessel supports the experiment. Four column members at the corners of the tungsten modules provide direct support for these units and indirectly for the other components. The truss members carry loads through to heavy rings at the wall of the pressure cylinder. These rings provide attach-points into the spacecraft structure. Secondary structural members are used to support the ends of the photomultiplier tubes and other items which are cantilevered and in need of additional support. This structure is shown in Figures IV-17 and IV-18.

12. Handling Dolly:

To position the experiment for assembly and checkout, a handling dolly similar to one presently in use at Goddard for the IMP I spacecraft will be designed. This will provide rotation of the experiment about two axes and enable access to any portion.

Weight estimates of the various components are summarized in table IV-3.

Table IV-3

WEIGHT AND MOMENTS OF INERTIA

Item	Weight each	No.	Total Weight
a. Pulse Ion Chamber	60 lbs.	2	120.0 lbs.
b. S-1 Scintillators	30	2	60.0
c. Spark Chambers	160	2	320.0
d. Cerenkov Counters	50	2	100.0
e. S-2 Scintillators	30	2	60.0
f. Diffusion Chambers	40	2	80.0
g. Cesium Iodide Modules	46	10	460.0
h. Tungsten Modules	318	12	3816.0
i. Pressure Vessel, incl. Struct.	900	1	900.0
j. Gas press. syst.	38	1	38.0
k. Electronics, set	80	1	80.0
			6034 lbs.

Moments of Inertia are estimated to be as follows:

I_x = 460 slug ft.^{2} (launch axis)

I_y = 290 slug ft.^{2} (instrument axis)

I_z = 460 slug ft.^{2} (spin axis)

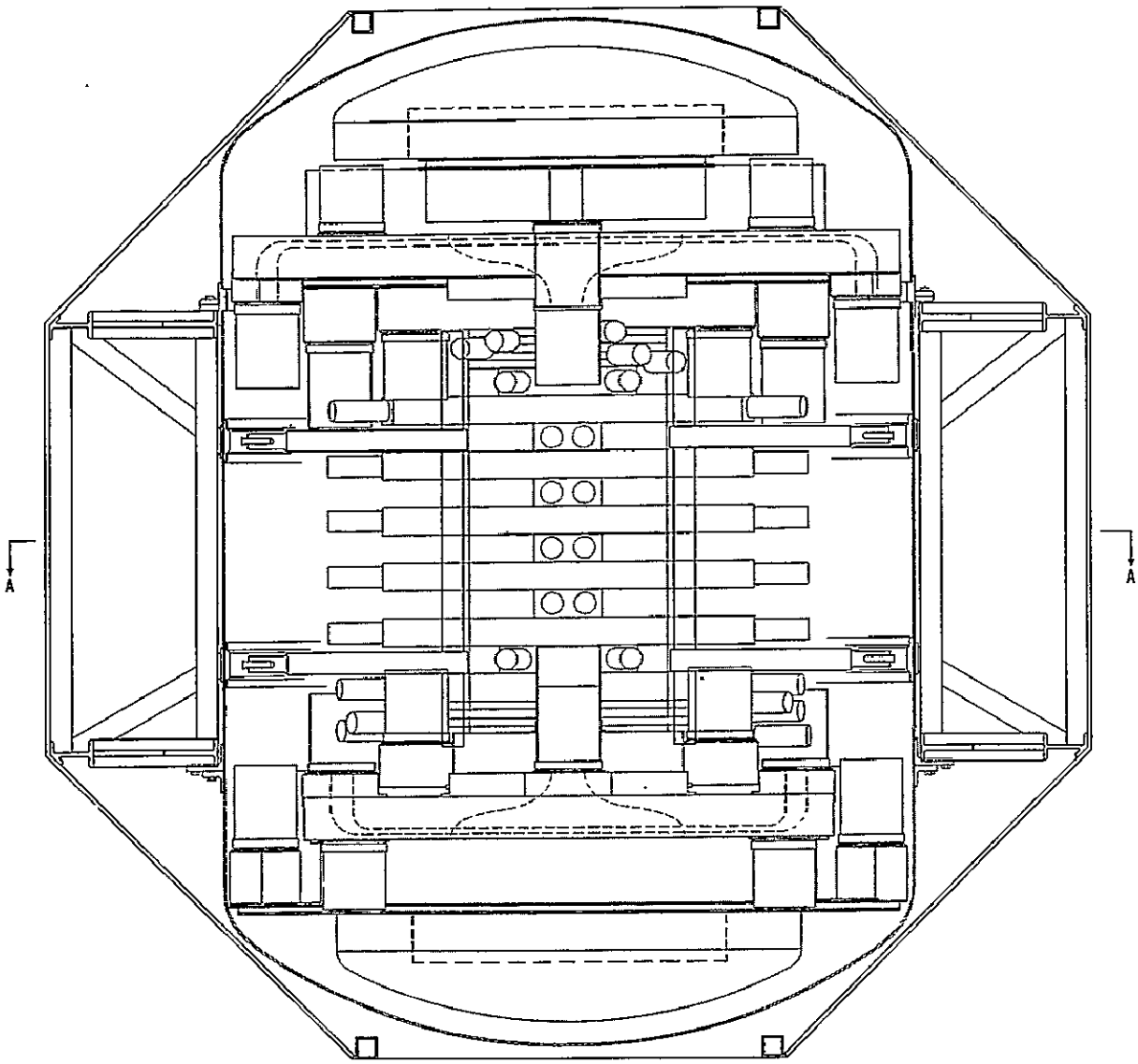

Figure IV-17. Support structure, side view.

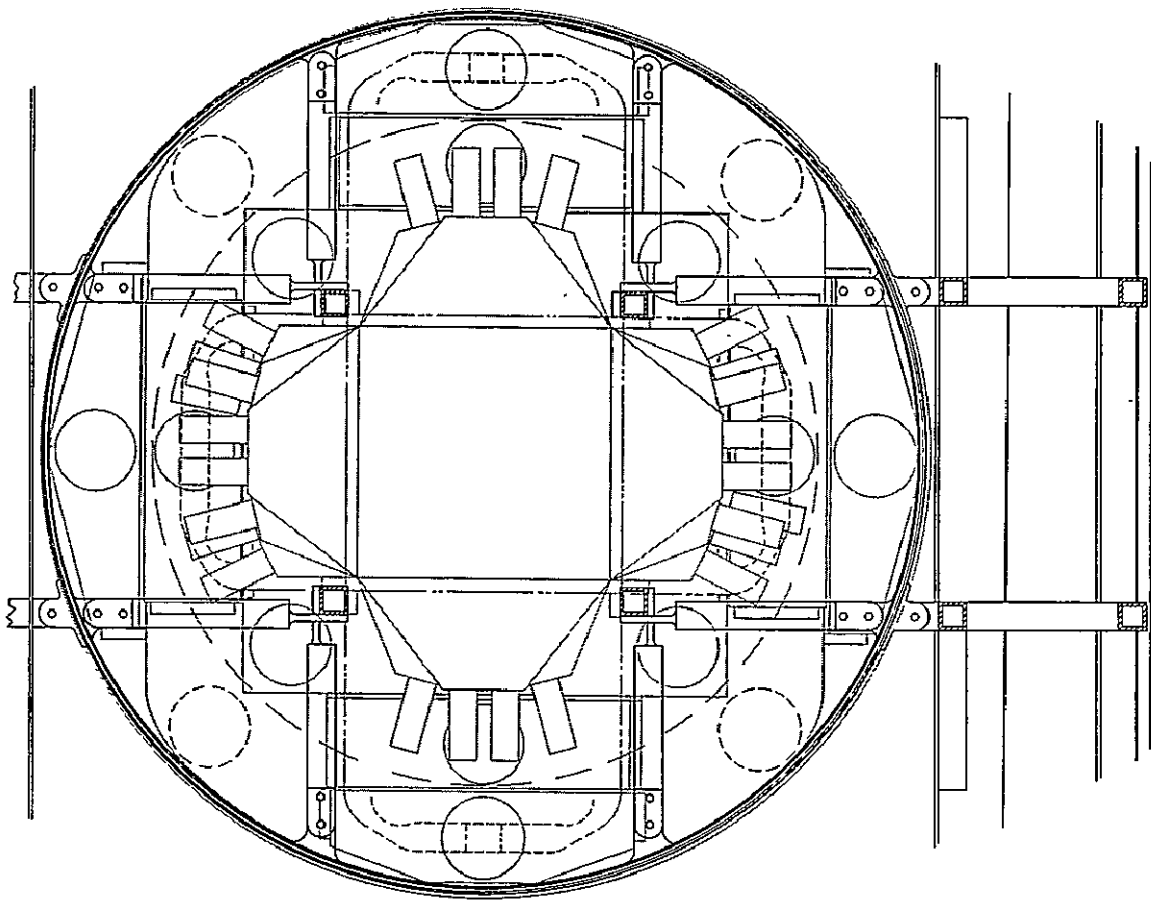

Figure IV-18. Support structure, top view.

It should be noted that this proposal has been written towards a design weight of 6000 lbs. If more weight were available to this experiment it would be put into the spectrometer section, and the geometric factor increases like the square of the weight allotted in this design. This gain is rapid and is accomplished by merely changing the dimensions of the spectrometer. No additional changes would be required to take advantage of any increased allotment.

The spacecraft mechanical requirements are as follows:

1. Weight: 6,000 lbs.
2. Size & Shape: Cylinder; 100 inches long, 64 inches in diameter.
3. Field of View: 2 ends ± 60°.
4. No pointing required.
5. Aspect information to ± 2°.
6. Accessibility: Normal for servicing.
7. Thermal ± 20°.
8. Meteorite: Experiment will be enclosed in a gas-tight container which also provides meteorite protection.
9. South Atlantic Anomaly: Experiment will have automatic shutdown capability.
10. No other experiments should be within field of view.
11. Mechanical structure not in field of view.
12. Local spacecraft structure will have to be mated to the experiment support system which will carry the weight from the spectrometer through the gas container wall.
13. It is expected to be located near the center of rotation of the spacecraft due to the large payload weight.

V. CONCLUSIONS

A. SUMMARY REMARKS

Breakthroughs in information on cosmic rays have been, in the past, associated with major technical developments. The development of constant level plastic balloons, saw the discovery of heavy elements and the fact that the relative abundance of the elements in the universe and cosmic rays seem to be somewhat related. The differences between the two abundances such as the over-abundance of Li, Be, B in cosmic rays were of great astrophysical consequence and led to many new experiments. The dawn of the space age, with its eccentric satellites and sophisticated detector developments, ushered in a decade of activity in which the low energy cosmic rays have been studied extensively. As a result, models of interstellar propagation with path length distributions, multiple sources, etc. have greatly enhanced our understanding of cosmic ray phenomena. It is noteworthy that, as soon as very large area detectors were flown, very heavy nuclei and possible transuranic elements were discovered. The correlations of exciting discoveries with new technical developments have been very significant indeed!

The HEAO is a major new opportunity with a capability of placing heavy and complex payloads in a near earth orbit. This proposal has outlined some of the studies that one could profitably carry out with this mission. If the past is any

guide to the future at all, this new step in cosmic ray experimentation will result in unexpected discoveries of great value. It is difficult to conceive of any step in science as an isolated act. One experiment leads to another – a better and more sophisticated attempt to answer questions raised. Some of the possible future developments for extending and expanding upon the measurements proposed here are outlined in the following section.

B. FOLLOW-ON EXPERIMENTS

The merits of a proposed experiment are not determined solely by the significance of its scientific objectives and its technical feasibility. The proposed research is also related to the capabilities and resources it develops for the experiments which might logically follow it. Second generation experiments which evolve from the work proposed here might be distinguished by greater sophistication, resolution, or energy range; or by any combination of these factors.

An immediate second generation backup of a similar design could be flown to repeat and perhaps improve upon some of the details of the measurements, especially in the event of a greatly reduced lifetime of the first spacecraft. It would preferably follow the first spacecraft by sufficient time (~2 years) that improvements learned from the first flight could be incorporated before the design had to be frozen. After a somewhat greater time delay, the information obtained from the presently proposed experiment should permit significant advances in experimental technique and design.

Advances in sophistication: This proposal is based upon a considerable body of experience with similar techniques in cosmic rays at mountain and balloon altitudes and in accelerator beams up to 30 GeV and upon state-of-the-art apparatus design. However, even with further balloon altitude and accelerator studies, the best techniques of dealing, for example, with very energetic heavy nuclei may not become clear until the results have been obtained from the presently proposed experiment. The ionization energy loss of these highly relativistic, high Z particles cannot be simulated exactly in the laboratory, and balloon flights may be too limited in payload weight and exposure time to provide enough data and experience. Because of the necessity of such extrapolations from our present experience, it is reasonable to expect that while the results of the proposed experiment will be of high quality, they will lead to suggestions for further refinements in design for the second generation.

For extending the range of the measured spectra to higher energies, one possibility is to explore the use of the transition radiation detector. At these energies there are a large number of X-rays emitted because of the linear dependence on γ. The situation is further improved for heavy nuclei because the emitted transition radiation depends on the square of the charge of the incident particle. However, because of the steep cosmic ray energy spectra, electrons at the same gamma are much more plentiful than protons. These electrons will constitute a background which must be removed. For example, if the integral spectral indices of electrons and protons are the same at very high energies

the number of electrons is 1% of the number of protons at the same energy. Then at the same γ electrons will be about 760 times as abundant as protons. These electrons can be rejected by causing their showers to develop in a large-area, thin ionization spectrometer, two faces of which are covered by transition radiation detectors. A layer of tungsten four radiation lengths deep and 10^4 cm^2 in area would weigh roughly 500 lbs. The electrons would be very effectively removed. Since some fraction of the protons would be rejected also, a correction would have to be made for such protons.

Increases in available payload; weight, size, and power: In order to increase the energy range studied in cosmic ray experiment, the product of the counting rate of the experiment and the exposure time must increase. In the earliest balloon flights, this product was in the range of 10^4 cm^2-ster-sec. More recent balloon experiments have had exposure factors of 10^6 cm^2-ster-sec. The increased exposure time in the early satellite work brought this figure to 10^8 cm^2-ster-sec, while the experiment proposed here will have an exposure factor of 10^{10} cm^2-ster-sec. Hopefully, the success of the early HEAO flights will encourage the authorization of scientific satellites of still greater payload such as those now encountered only in the manned-spacecraft flights. If such flight opportunities were to develop, a substantially improved version of the experiment in this proposal could be flown. For example, if the ionization spectrometer weight could be increased from the 2000 kg in this proposal to 10,000 kg, it

could be an isotropically sensitive, totally active, 5λ- diameter sphere of high density scintillator, subdivided into a large number of blocks, each viewed by a tiny, directly attached, semiconductor photodiode instead of photomultiplier tubes. This arrangement would allow as much as a factor of 100 increase in the area-solid angle geometry factor. The energy spectrum measurements could then be extended by another factor of 20 higher in energy, and the sensitivity of charge composition measurements could be improved by a factor of 10. The increased geometry factor would be valuable for the study of directional anisotropies and increase the sensitivity of time variations studies of high energy components of primary cosmic rays. The study of the detailed energy spectrum and charge composition of the VVH component would become a meaningful proposition.

Greater available power, as well as payload, might permit operation of an ionization spectrometer in combination with a superconducting magnet and/or a liquid hydrogen target. But until results from the present experiments are available, the desirability of the various detector combinations cannot be ascertained, and a detailed consideration of the merits of such combinations is clearly beyond the scope of this proposal. It is certain however, that any of these second generation developments would build directly upon the scientific data and technical experience obtained from carrying out the experiment in this proposal.

APPENDIX 1

A High Energy Nuclear Interaction Experiment for HEAO

Quantitative measurements of total elastic and inelastic cross sections and differential elastic cross sections for p-p collisions at very high energies might directly answer several questions about high energy interactions: How do scattering cross sections and amplitudes behave as infinite energy is approached? For example, does the total cross section in p-p collisions approach zero, a finite constant, or no limit (i.e. oscillate) at infinite energy? Does the width of the diffraction scattering peak in p-p collisions approach a finite constant, or does it logarithmically shrink toward zero as the energy increases? Proton collisions with complex nuclei can not be expected to conclusively answer these questions, so frequently asked by elementary particle theorists, because of the added complexities of both experimental and theoretical analyses and interpretations.

A liquid hydrogen target for a satellite p-p interaction experiment would have two serious disadvantages: (1) The required cryogenic equipment would add appreciably to the weight, power consumption, complexity, and cost of the experiment. (2) The elastic diffraction p-p scatters, which account for about 1/4 of the total cross section, would not be observed because the laboratory scattering angle of the high energy proton becomes too small to detect and the low energy recoil proton stops and remains undetected inside the liquid hydrogen for any reasonable choice of target mass and dimensions.

A high pressure hydrogen gas target offers the possibility of detecting the recoil proton by simultaneously serving as an ionization chamber. However, in order to obtain the recoil proton kinetic energy from its ionization, a large number of anode wires would be required in order to separate the recoil proton contribution from the ionization of the high energy proton and to distinguish recoil protons from knock-on electrons by rough angle and range information. For high pressure hydrogen targets weighing $\sim$ 180 lbs. (including pressure vessel), only about 1/2 gm/cm^2 of range in hydrogen is available to stop the recoil protons, which allows about 50% of the elastic scattering recoils to escape without yielding the accurate energy measurement necessary to obtain the 4-momentum transfer of the event. In order to accept 75% of the elastic events, the target plus pressure vessel mass would have to be increased to about 700 lbs. and 90% acceptance would require more than 1800 lbs. Another drawback of a high pressure hydrogen target for satellite experiments is the low ratio of hydrogen mass to total target mass (including pressure vessel), typically $\sim$ 1/25 for a safety factor of 5 in the stress of the pressure vessel. All of the above considerations are independent of the size of the high pressure hydrogen target, and are dependent only upon the choice of total mass and safety factor. Further technical development of the hydrogen gas target and ion chamber is clearly desirable for use when low experiment weight becomes less of a premium, but other alternatives might be more suitable for early satellite flight opportunities.

The alternatives to liquid or high pressure hydrogen targets to produce p-p interactions are hydrogen-containing compounds. The chemically stable solid containing the most hydrogen appears to be polyethylene, $(CH_2)_n$, which contains almost twice as many hydrogen atoms per cm^3 as liquid hydrogen, and the ratio of hydrogen mass to total target mass is 1/7. The advantage of having a high density of hydrogen is usually more than offset by the disadvantage of having carbon present to produce undesirable background events. The carbon background is particularly a problem when it can only be subtracted statistically, which has usually been the case in cosmic ray experiments. However, it is proposed to separate the elastic p-p scattering events kinematically from the background of p-C events, and to partially separate the p-p inelastic events on the basis of their distinguishing characteristics.

The elastic scattering events would give especially valuable information concerning the high energy behavior of scattering amplitudes, as a curve of $d\sigma/dt$ as a function of s, the c.m.s. energy squared, and of t, the 4-momentum transfer squared, would be obtained for the forward diffraction scattering peak. This data would not only exhibit how the $d\sigma/dt$ distribution depends upon s, showing whether or not it continues to shrink with increasing energy, but the extrapolation of the $d\sigma/dt$ curve to $t = 0$ gives a good approximation to the total cross section. This assumes that α^2, the square of the ratio of the real to the imaginary part of the forward scattering amplitude, remains small at very high energies, which all current theoretical models predict. If enough events could be obtained,

the real part of the forward scattering amplitude could be directly measured, hence α could be determined, from observation of Coulomb interference in the $d\sigma/dt$ vs. t curve in the region of $|t| = .005$ $(BeV/c)^2$. Typical $d\sigma/dt$ curves taken at accelerator energies can be found in the literature (Foley et al., 1963; and Bellettini et al., 1965). The dependence of $d\sigma/dt$ on t is observed to be closely exponential, the area under the curve corresponding to about 9 mb for p-p elastic scattering. The p-p inelastic cross section is about 30 mb. These numbers are expected, at most, to change gradually with increasing energy. This proposal would determine σ_{total} both from $d\sigma/dt$ extrapolation to zero and from $\sigma_{elastic} + \sigma_{inelastic}$.

A recent Serpukov experiment (Beznogihk et al., 1969) has demonstrated the feasibility of measuring the $d\sigma/dt$ distribution by observing the angle and energy of proton recoils from a thin polyethylene target, and the experiment shows that the p-p elastic scatters are clearly separable from the background of interactions in carbon. Application of this approach to a cosmic ray experiment is made easier by the fact that, at high energy, kinematic relations of laboratory kinetic energy, T, and recoil laboratory angle, θ, as functions of s and t simply become functions t, alone:

$$= \frac{|t|}{2M}$$

$$\theta \cong \text{arc.tan} \frac{2M}{|t|^{1/2}}$$

where M is the recoil proton mass. The first equation is exact for any elastic scattering, and the second is valid at energies high compared to the particle masses. The above equations tell us that all proton recoils from elastic high energy scattering must lie on a single curve of θ vs. T, which provides the basis for a separation for carbon background events. As the measurement of recoil kinetic energy also measures t, a histogram of the data can be plotted to directly give $d\sigma/dt$ vs. t. Since any changes with energy are expected to be gradual, a spectrometer measurement of the energy of the outgoing high energy scattered proton would provide s with sufficient precision for each event.

A schematic diagram of the proposed experimental arrangement is shown in Figure A-1. The counters and spark chambers below the spectrometer are a cosmic ray charge identification unit of fairly standard design which, in combination with the spectrometer shared with the p-p interation experiment, measures the composition and energy spectrum of primary cosmic radiation. The p-p interaction experiment spark chambers A, B, and C above the spectrometer would be triggered and all the counter pulse heights would be recorded each time the spectrometer signaled an energy deposition above some preset threshold in coincidence with counter signals 1 and 2 or 3 and 4. Normally, a p-p or p-C interaction within the solid angle of the spectrometer would produce pulses in all four counters, 1, 2, 3, 4, but the less stringent coincidence requirement 12 might allow one to observe charge exchanges of antiprotons and annihilations of positrons. The 34 coincidence would be sensitive to primary cosmic ray γ-rays,

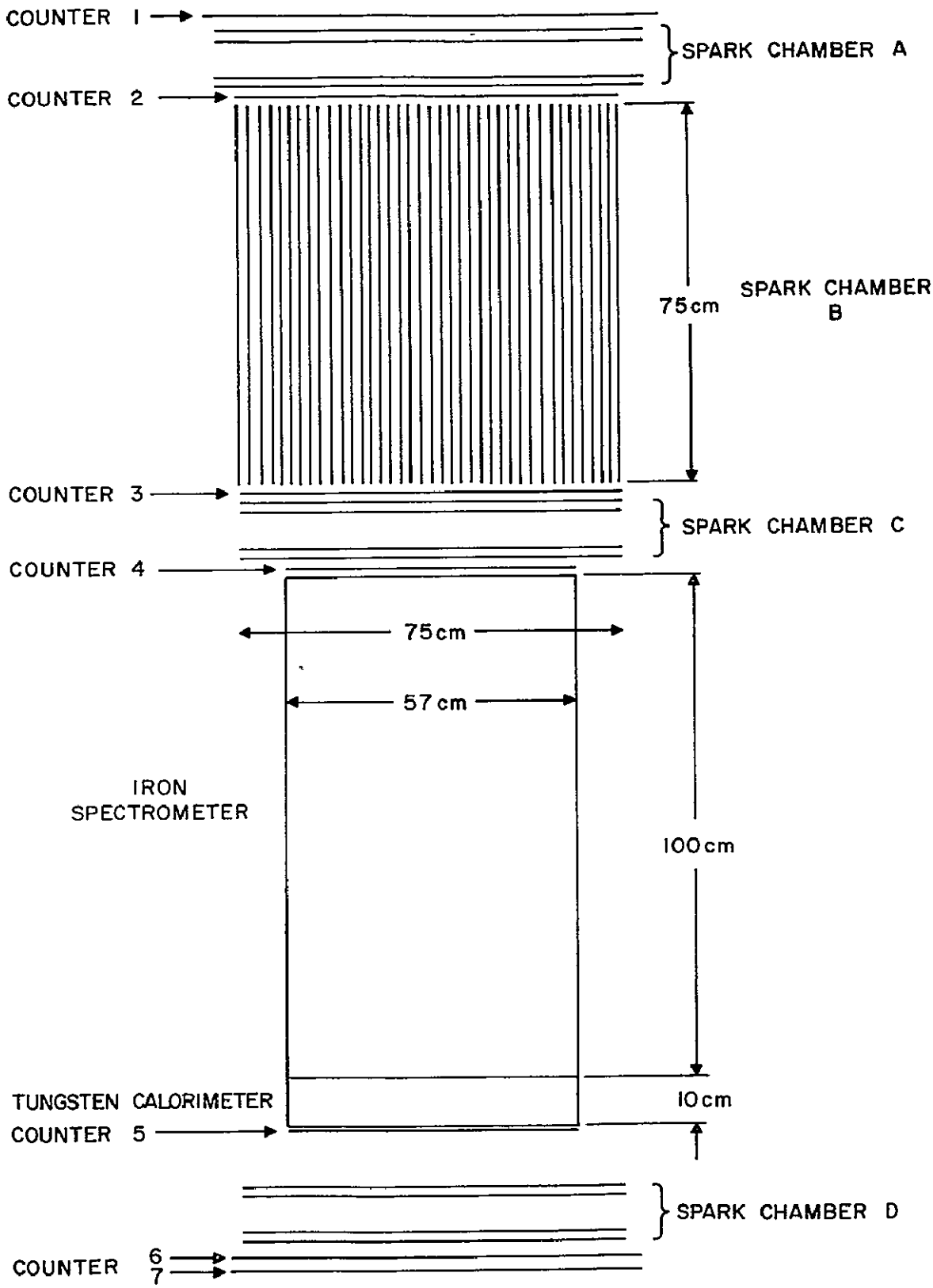

Figure A-1. Arrangement to measure p-p interaction cross sections (upper module) and cosmic ray spectrum (lower module).

if any of these components are present in sufficient numbers at energies above several GeV. Excessive triggering rates on events with energies near the low end of the region of interest would be avoided by sampling only definite fractions (such as 1 event of every 8) of the lower energy events. It probably would be desirable to be able to separately control in binary steps the sampling ratios for several bands of spectrometer energy pulses by ground control.

The pulse height of counters 1 and 2, possibly supplemented by a Cerenkov counter pulse height, would serve to identify the charge, Z, of the incoming cosmic ray particles, so that some data on the relatively infrequent α-particles and heavy nuclei intensities and interactions would be obtained to supplement the main cosmic ray experiment at the other end of the spectrometer. The pulse height of counters 3 and 4 would, in combination with the information from spark chamber C, determine the number of charged secondaries from inelastic p-p and p-C interactions. The secondaries from high energy events will often lie very close together so that separate tracks cannot be resolved by spark chamber C, but the counter pulse height can still be relied upon to give the number of secondaries with good statistical confidence, assuming that all are minimum ionizing.

Digitized spark chambers A and C would consist of four x-y measuring gaps, each, to determine the particle trajectory before and after interaction, if any, in the plates of spark chamber B. Spark chamber B would contain ~100

vertically oriented narrow (1/4 to 3/8 in.) gaps. Approximately 3/4 of the thin plates would be $(CH_2)_n$; the remainder would be carbon plates to allow a determination of the carbon background to be subtracted. It might be advantageous to grade the plate thicknesses, with, say, thinnest plates near the center to obtain more uniform statistics over a wide range of t. The plates would have a total thickness of 15 gm/cm^2, of which the hydrogen would be ~ 2 gm/cm^2, and target mass would be 84 kg. The unconventional vertical plate orientation is necessary to permit clear observation of recoil protons, which are ejected with angles close to 90° with respect to the high energy proton track. Even with this orientation, about 1/2 of the events will be missed or discarded because the recoil proton direction is too nearly parallel with the plates for satisfactory sparks. The spark positions can probably be most satisfactorily recorded with a TV-type vidicon scanning system, since 100 wire chamber gaps might introduce too much extraneou material and equipment complexity. Wide-gap spark chambers viewed by vidicons might be an alternative design for spark chambers A and C, with a possible advantage that multiple tracks might be better resolved.

Part of the plates in the interaction chamber would be carbon to permit a CH_2-C background subtraction of carbon inelastic events in order to obtain the total inelastic cross section on hydrogen. The statistical errors which seem implicit in this procedure will be considerably reduced by the fact that this subtraction need only be done for events with an even number of charged secondaries, since an odd number of charged secondaries can come only from a carbon

event. Also, except for the elastic scattering recoil protons, virtually all other slow protons stopping in a few gm/cm^2 of material must come from carbon interactions, so these events can also be removed before making the subtraction.

In order to estimate event rates, the following table summarizes the target and nuclear interaction experiment parameters:

Wt. of target:	84 kg.
Overall target chamber size:	75 × 75 × 75 cm.
Average target thickness, C:	13 gm/cm^2
Average target thickness, H:	2 gm/cm^2
Effective H thickness for elastic p-p:	1 gm/cm^2
Probability of p-p inelastic collision:	.037 assuming [illegible] mb.
Probability of p-p elastic collision:	.005 assuming 1 gm/cm^2 and 7 mb.

Assuming a geometric factor of 489 cm^2-ster, the following number of p-p events would be obtained in one year:

Energy lower limit (eV)	p-p inelastic events	p-p elastic events
10^{11}	4.3×10^5	6×10^4
10^{12}	1.1×10^4	1.7×10^3
10^{13}	210	31

For comparison, a gas hydrogen target with the same total mass of pressure vessel and hydrogen gas of 84 kg. would have an average target thickness of 1.3 gm/cm^2 of hydrogen, an effective thickness for elastic p-p events of about 0.7 gm/cm^2, and an average total wall thickness (2 walls) of 11 gm/cm^2 of titanium. The above rates would correspondingly be reduced by a factor $\sim 2/3$ for operation with similar geometries. Technological considerations appear paramount in choosing between the two approaches.

APPENDIX II

Optimization of the Geometrical Configuration of the Ionization Spectrometer

The spatial configuration of the ionization spectrometer was designed to maximize the counting rate for incident particles having a path length in the detector greater than 5λ of tungsten. The size of each detector shape considered was constrained to remain within the weight limitation for this experiment. The entire perimeter of the spacecraft, except for support structure, is available as sensitive viewing area to the cosmic ray flux. Three different configurations, each making use of as much perimeter viewing areas as the weight and energy resolution constraints allow, were considered. For comparison the three shapes are shown in Figure 2-1. They are:

a. a rectangular parallelepiped with two square viewing faces, each 46×46 cm^2, separated by a length of 76 cm;

b. a rectangular parallelepiped with four rectangular viewing faces, each 76×20 cm^2, separated by a length of 76 cm;

c. a hexagonal parallelepiped with three rectangular viewing faces each 44×29 cm^2, separated by a length of 76 cm.

The geometrical factor for each of the three configurations was calculated using a Monte Carlo simulation of an isotropic incident flux. The results are

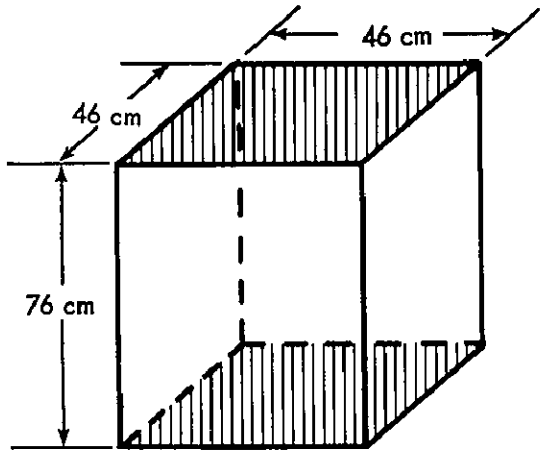

(a)

2 SQUARE VIEWING FACES

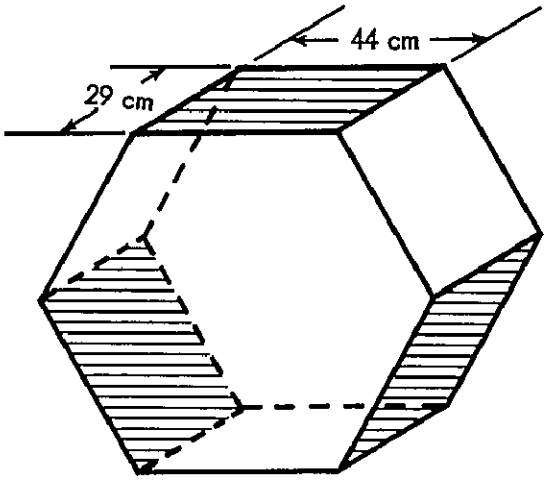

(b)

3 RECTANGULAR VIEWING FACES

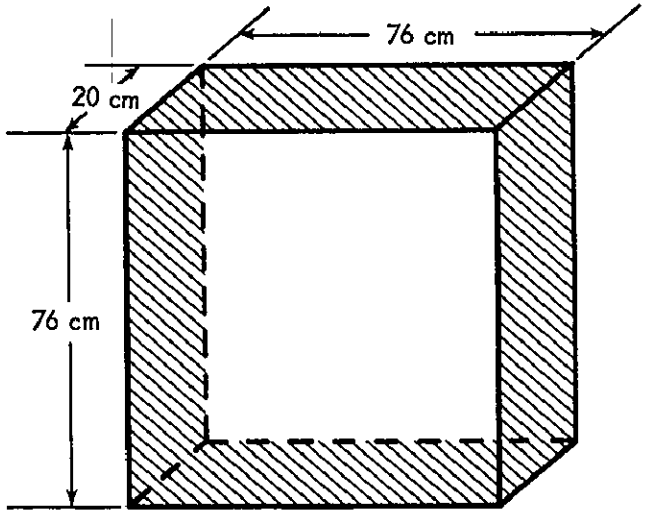

(c)

4 RECTANGULAR VIEWING FACES

Figure A-2. Three alternate spectrometer shapes.

shown in the following table. For comparison, results are also given for minimum acceptable path lengths of 3λ and 4λ.

Table 2

Detector	Geometrical Factor cm^2 - sterad		
	3λ	4λ	5λ
(a) Rectangular (2 faces) 76 × 46 × 46	1.6	1.3	1.00
(b) Rectangular (4 faces) 76 × 76 × 20	1.5	1.1	0.90
(c) Hexagonal (3 faces) 76 × 44 × 29	1.4	0.98	0.55

As can be seen from the above table, the rectangular detector with two square faces, configuration (a), makes the most efficient use of the maximum weight which can be employed. Configuration (b) is a close competitor which is handicapped primarily by the asymmetry (76 × 20 cm^2) of the viewing faces. However, configuration (a) has the overriding advantage that the arrangement of the scintillators is straight-forward and simple, and only two charge determination modules and two direction modules are needed.

Spectrometer designs utilizing the entire perimeter of the detector have been suggested by Pinkau et al., (1968). These scintillator configurations could be developed to enable optimum use of greater weight allotments should they

become available. For instance, if the weight available to the experiment were to increase by about a factor of 2.7, a cube could be constructed, 76 cm on an edge. Scintillators could be arranged in the tungsten in two perpendicular planes, each parallel to one pair of the four viewing faces of the detector. This detector would have the same mean density as the spectrometer presently proposed. Its geometrical factor for path lengths greater than 5λ would be larger by a factor of 12.8. For an increase in weight of about a factor of 6, a hexagonal detector could be optimized for an increase in geometrical factor of a factor of 35.

These designs present interesting possibilities and complications. The advantages they offer are the capabilities to reach higher energies in the particle spectra and to achieve better statistics in the measurement of heavy particle abundances, time variations, and spatial anisotropies. The difficulties encountered would be in the use of wedge-shaped scintillators to provide position measurement redundancy and in the previously straightforward interpretation of the scintillator response as a function of position in the spectrometer. These problems are by no means insurmountable and lead to the conclusion that the more complex designs deserve further study.

APPENDIX 3

A METHOD OF MEASURING THE COSMIC RAY CHARGE COMPOSITION BETWEEN 10^{10} AND 10^{14} eV

J. F. Ormes,* V. K. Balasubrahmanyan, F. B. McDonald, & R. D. Price

NASA/Goddard Space Flight Center
Greenbelt, Maryland

Abstract

We wish to report the details of an experiment to measure the charge composition of the primary cosmic radiation from Z = 1 to about 50 in the energy range 10^{10} to 10^{14} eV. A large geometry factor of ~7500 cm^2ster is necessary to measure intensities at the low flux levels of these particles. The necessary charge resolution can be obtained using 1/2 m x 1/2 m square detection elements in the following manner. The linearity properties of CsI scintillators and Cerenkov detectors make them ideal for primary charge identification. Further charge information and a fast coincidence pulse will be obtained from two geometry defining plastic scintillators. The fast coincidence pulse will trigger a digitized spark chamber which will provide sufficient directional and positional information so that resolutions comparable with much smaller area detectors can be obtained. The energy of the incident particles is determined using total energy spectrometers. The module for examining electromagnetic cascades consists of six tungsten-scintillator elements, each of one cascade length thickness and each pulse height analyzed. The energy of incident nucleons is measured in the 20 elements of an iron-scintillator ionization calorimeter. It has a total depth of 3.5 nuclear interaction mean free paths.

INTRODUCTION

Cosmic rays are an important source of astrophysical information as they bring us samples of material from outside the solar system. They range in energy from 10^7 to 10^{20} eV and so they contain information about some of the very energetic phenomena which take place in the universe. The astrophysical questions on which cosmic rays can shed some light include the important problems of the origin, acceleration and propagation of the particles themselves. The experimental observables include the relative abundance of the different nuclear species, the energy spectra of the nuclear components and the electrons, the time variations (or their absence) and the anisotropies in their arrival directions.

The low energy end of this spectrum ($\lesssim 10^{10}$eV) has been extensively studied, and the ultra high energy end is accessible only to indirect study through extensive air showers. Grigorov et al (1967) have made an attempt to study the energy region 10^{10} to 10^{14} eV with total ionization calorimeters carried in the Soviet "Proton" satellites. The experimental effort to be described in this paper is designed to follow up this pioneering effort with improved equipment. Our aims include greater energy accuracy, an unambiguous flux determination and the addition of charge and mass resolution. From these measurements, the energy dependence of the charge and mass composition of the radiation in this range can be determined, and further insight can be gained into the origin and propagation of cosmic rays and related astrophysical problems.

The experiment can be conveniently divided into three problem areas: (1) charge identification over the range $1 \leq Z \approx 90$ and mass separation of electrons from protons, (2) the energy measurement over a dynamic range of 10^4, and (3) event collection to obtain reasonable statistical accuracy.

DETECTOR SYSTEM

Event Collection

Starting with the third of these problems, recall that the number of events observed is proportional to $A_n t$, where A_n is the area solid angle product or geometrical factor of the telescope and t is the time of observation. The experiment must be conducted at the top of the atmosphere and so let us optiminstically assume that a balloon borne experiment can be kept aloft for 20 hours. Typical fluxes encountered will be 10^{-2} particles/m^2 ster sec (eg., protons $> 10^{13}$ eV, the sum of all nuclei heavier than He above 2 or 3 x 10^{11} eV and electrons $> 3 \times 10^{11}$ eV) and to measure this flux level in 20 hours with 5% accuracy a geometrical factor A_n of 1/2 m^2 ster is needed.

In order to obtain this large a geometry the instrument has been designed using square elements 1/2 meter on a side. This represents a 4 or 5 fold increase in area over previously used detectors, and in order to obtain charge identification the resolution must not deteriorate with this increase.

In order to extend the energy spectrum data to high energies for individual charges, it is necessary to place the equipment outside the atmosphere for extended periods. We are designing

*NAS-NASA Postdoctoral Resident Research Associate

the instrument so that it is suitable for future placement on board a satellite for a period of the order of one year.

Charge Identification

One of the major purposes of the experiment is to measure the charge composition of the cosmic radiation. The "charge identification module" which will accomplish this is shown schematically in Figure 1. The plastic scintillators, on the top and the bottom in order to define the geometry, are viewed edge on by two 5" photomultiplier tubes through adiabatic light guides. A third dE/dx measurement is made in a CsI(Na) mosaic which consists of 9 square pieces 17 cm on a side. The light from this detector is sampled by two 5" P.M. tubes looking into a light chamber painted with diffusively reflective white paint. Such a diffusion chamber is used so that the response will be independent of the spatial position of the particle traversal. A final pulse height measurement is made in a 1/2 inch ultraviolet transmitting Lucite Cerenkov radiator. This highly directional light is transmitted to the edges of the crystal by total internal reflection and then is collected through adiabatic light guides by four 5" photomultipliers. The CsI(Na) measurement should be linear (αZ^2) up to a $Z \approx 30$ or 40, however the plastic scintillators are known to be non-linear and increase like Z beyond Z about 6 or 8 (Webber and Ormes, 1967). The Cerenkov light output is known to be linear up to Z = 20 and is expected to be linear over the whole charge spectrum.

In addition to their other functions, the plastic scintillators provide a fast trigger pulse for three wire grid spark chambers with digital readout. The chambers to be used are ones which have been developed for gamma ray astronomy at Goddard Space Flight Center (Ehrmann et al, 1967 and Cline et al, 1967). Three (x, y) coordinate pairs will be measured to determine the trajectory of the particle through the apparatus. This will make possible corrections for the path length and the positional variations in the light produced by each individual particle. It will also make possible an accurate determination of the geometry factor of the telescope for high energy particles and will identify events initiated by more than a single primary particle.

The plastic scintillators have been tested and resolutions of 45% full width at half maximum (FWHM) are consistently obtained using sea level mu mesons (Balasubrahmanyan et al, 1967). This resolution could be improved to 30 or 35% when the spark chamber information on location and direction of the incident particles is used in the analysis.

Preliminary tests show that for the CsI(Na) crystal mosaic and diffusion chamber the light collection efficiency is independent of photomultiplier location, and that resolution of 50% is possible for singly charged particles. The resolution is presently photon dominated and so will improve with increasing charge.

The Cerenkov detector is the most difficult to scale up in size. In the first place one is restricted to thicknesses such that only about 330 useful photons are produced by a singly charged particle. In the past thin Cerenkov detectors for cosmic ray work have been constructed so that the highly directional light produced by the cosmic rays was incident directly on the photomultiplier cathode directly. This limited the size of Cerenkov counters to the available photomultiplier tubes. We have attempted to construct thin large area counters where the Cerenkov light is transported by the highly efficient process of total internal reflection. For a 1/2" ultraviolet transmitting lucite plate 1/2 meter square with four adiabatic light guides feeding four 5" photomultiplier tubes, we obtain the distribution shown in Figure 2 from sea level muons. The signal is clearly above noise and the FWHM is about 170%. The use of the spark chamber to define the particle trajectories could result in the decrease of the spread due to the large size of the detector. The considerable proportion of this resolution which is due to photon statistics should improve when particles of higher charge are incident on the detector system. This principle of constructing Cerenkov counters could be extended to even larger sizes and the final limit will be set by the absorption length of light in the medium ($\approx$ 2 meters). In the range of iron nuclei where the Cerenkov counter will be important for the charge determination, the FWHM due to photon statistics is expected to be about the same as the separation between charges ($\approx$8%).

This four dimensional system should provide adequate charge identification information to yield $Z = \pm 1$ up to charge 30.

Total Energy

The total energy of the particles will be measured by the method of total ionization calorimetry. Sometimes called total energy spectrometry, the method has been described in detail by Grigorov et al (1958) and more recently by Murzin (1965).

Since we wish to apply the method to both electrons and nucleons, the calorimeter is designed in two parts, both shown in Figure 3. The first part, of high Z material, is used to separate out the electrons from a proton background thirty times as intense by developing an electromagnetic cascade. The second part consists of 3.5 nuclear interaction mean free paths of iron, sufficient matter for a nuclear cascade to develop. (This section will be increased to 7 m.f.p. in the future to provide enough matter to absorb 90% of the incident energy. Present balloon technology has set the limit of 3 1/2 m.f.p.'s. The weight of the balloon payload is of the order of 1000 lbs/ m.f.p.)

The electron identification is achieved and its energy is measured by sampling the number of particles in the cascade at intervals one cascade length apart. In each module, following a cascade length of tungsten, is a plastic scintillator viewed through air coupling by two three inch photomultipliers. The pulse height from the phototubes will be proportional to the number of particles. The total thickness of six cascade units enables one to trace the shower development through its rapid buildup. As the shower enters the nuclear cascade iron modules, seven more samplings of the electromagnetic shower are made equally spaced throughout the 35 radiation lengths of iron. This will completely absorb a 2×10^{12}eV electron. It is anticipated that the electron shower development will be calibrated on the 2×10^{10}eV SLAC electron beam.

Because the nucleon interaction mean free path is 30 times the electron radiation length in tungsten, only 20% of the nucleon beam will suffer its first interaction in the six radiation lengths, and so the protons will be separated from the electrons by the relatively much slower development of the showers. Once in the iron module, the ratio of m.f.p. to radiation length drops to 10, but still the electron showers will develop much more rapidly than the proton ones. The energy spectrometer is divided into modules 1/2 mean free path thick. Within these modules 3 scintillators are placed providing a sampling of the cascade every 1/6 mean free path. Each module is viewed by two photomultiplier tubes whose outputs are added and pulse height analyzed. The pulse heights are proportional to the average signal from the three samples. This large number of samples is necessary in order to reduce the importance of the fluctuations in the shower development. In this way the energy can be determined to ~20%, providing a calibration can be made. Calibration is planned on the 30GeV AGS at Brookhaven and is anticipated at 10^{12} eV at the University of Michigan high altitude facility proposed to be built at Echo Lake on Mt. Evans, Colorado (Jones, et al, 1967).

The development of electron and proton induced showers of various energy is shown in Figure 4.

The tungsten and iron modules have been tested in the laboratory and found to be quite adequate. With 1/2 meter square modules viewed edge on by air coupled photomultipliers, resolutions of FWHM <100% are consistently attained on sea level muons. Further analysis shows that only 40% is due to spatial and other intrinsic effects, and the rest is due to photoelectron statistics. As the number of particle increases, the resolution will quickly improve to 40% which is as good as that obtained on much smaller crystals.

Electronics

In order to have an acceptable data transmission rate and spark chamber repetition rate, it is necessary to electronically select only those events which are of particular interest. The requirements for accepting an event and pulsing the spark chambers are shown in Figure 5. This eliminates events due to low energy protons and helium which have been extensively studied.

In Figure 6 a block diagram of the electronics is shown. In addition to the features usually illustrated by such diagrams, this is shown in order to emphasize the redundancy which has been built into the experiment to avoid a catastrophic failure. For example, there are two photomultipliers looking at each detection element. There are two complete and independent data readout systems, on-board tape recording and telemetry. The whole philosophy of this redundancy is motivated by the aim never to come away from a flight using a 30×10^6 ft^3 balloon with no data at all because of a catastrophic electronic failure.

In order to cover the charge range from 1 - 90 and the 10^{10} to 10^{14} eV energy range a dynamic range of 10^4 is needed. Figure 6 illustrates the two ways in which this dynamic range is obtained. In the case of the charge module, a 256 channel analyzer is used in conjunction with two changes in gain, each by a factor of 8. This places the changes at Z = 12 and Z = 34, charges where the cosmic ray abundances are conveniently low. In the case of the energy modules, four decade logarithmic amplifiers are used with 128 channel analyzers. This yields a differential range of 6.5% per channel. Since the electronics have an intrinsic error of $\pm$ 1 channel, the pulse height is measured to $\pm$ 6.5%. This is quite sufficient since the energy can only be measured to the nearest 20% because of fluctuations in the cascade shower process.

The analog to digital converters to be used are similar to those which were used by the Goddard group (Jones et al, 1966) and have required no important change in design.

The 36 photomultipliers, the 17 pulse height analyzers and the readout logic should operate on about 45 watts of battery power. The telemetry and the on-board recorder should require another 5 volts, and hence the whole system should operate on around 50 watts. This implies 80 pounds of batteries for a 20 hour flight allowing a factor of 2 safety margin.

The counting rate of interesting events will be about 10/sec and with 150 pulse height bits and 150 spark chamber bits/event, 3 kilobits is the minimum allowed bit rate. It is compatible with present Goddard tape recorder systems. This rate is also consistent with the spark chamber triggering capabilities. This will yeild about 7×10^5 events for a 20 hour balloon flight.

Conclusion

The major technical problems to be faced appear to be logistical ones. Having a two or three ton experiment which also has the mobility necessary for a balloon experiment is clearly a

problem. One must be able to perform linearity checks on 20 ADC systems in a reasonable time which suggests a complex ground support system. The data analysis will clearly have to be computerized as one balloon flight will produce 10^8 bits of pulse height information alone. This will have to be correlated with another 10^8 bits of positional information from the spark chamber. These are problems of quantity rather than quality and should be solvable.

In going then from the first balloon system to the projected satellite system no major problems are anticipated. The technology certainly exists, and a satellite flight of one year should allow us to go a factor of 500 lower in flux or to 2×10^{-5} particles/m^2ster sec. This should make possible a measurement of the L/M ratio above 10^{13} eV and should extend direct measurement of the proton component to 10^{15} eV. These particles have a radius of curvature of about a light year, and studies of the anisotropies of cosmic rays should tell us something about the structure of the interstellar magnetic fields.

References

1. Balasubrahmanyan, V. K., McDonald, F. B., and Ormes, J. F., "A Proposal for the Study of High Energy Cosmic Rays," Goddard Report X-611-67-468.

2. Cline, T. L., Fichtel, C. E., and Kniffen, D. A., "Proposal to Pursue High Energy Gamma Ray Astronomy Using a Digitized Spark Chamber on an Explorer," Goddard Report X-611-67-135.

3. Ehrmann, C. H., Fichtel, C. E., Kniffen, D. A., and Ross, R. W., "A Magnetic Core Digitized Spark Chamber for Space Science Experiments," Goddard Report X-611-67-267.

4. Grigorov, N. L., Murzin, V., and Rapoport, I., Soviet Phys., J.E.T.P., 7, 348, 1958.

5. Grigorov, N. L., Nesterov, V. E., Rapoport, I. D., Savenko, I. A., and Skuridin, G. A., "The Study of the High Energy Cosmic Ray Particles with the "Proton" Satellites," Proceedings of the Tenth International Conference on Cosmic Rays, Calgary, 1967.

6. Jones, L. W., Mills, F. E., and Cork, Bruce, "Proposal for an Ultra High Energy Cosmic Ray Physics Facility," University of Michigan, ORA-67-1588-P1, 1967.

7. Jones, L. L., Ludwig, G. H., Stilwell, D. E., Trainor, J. H., and Way, S. H., "OGO-E Cosmic Radiation - Nuclear Abundance Experiment," Proceedings IEEE 13th Nuclear Science Symposium, 1966.

8. Murzin, V. S., "The Ionization Calorimeter," Progress in Cosmic Ray Research, in press 1965

9. Webber, W. R., and Ormes, J. F., Minnesota Tech. Rept. CR-94, 1967.

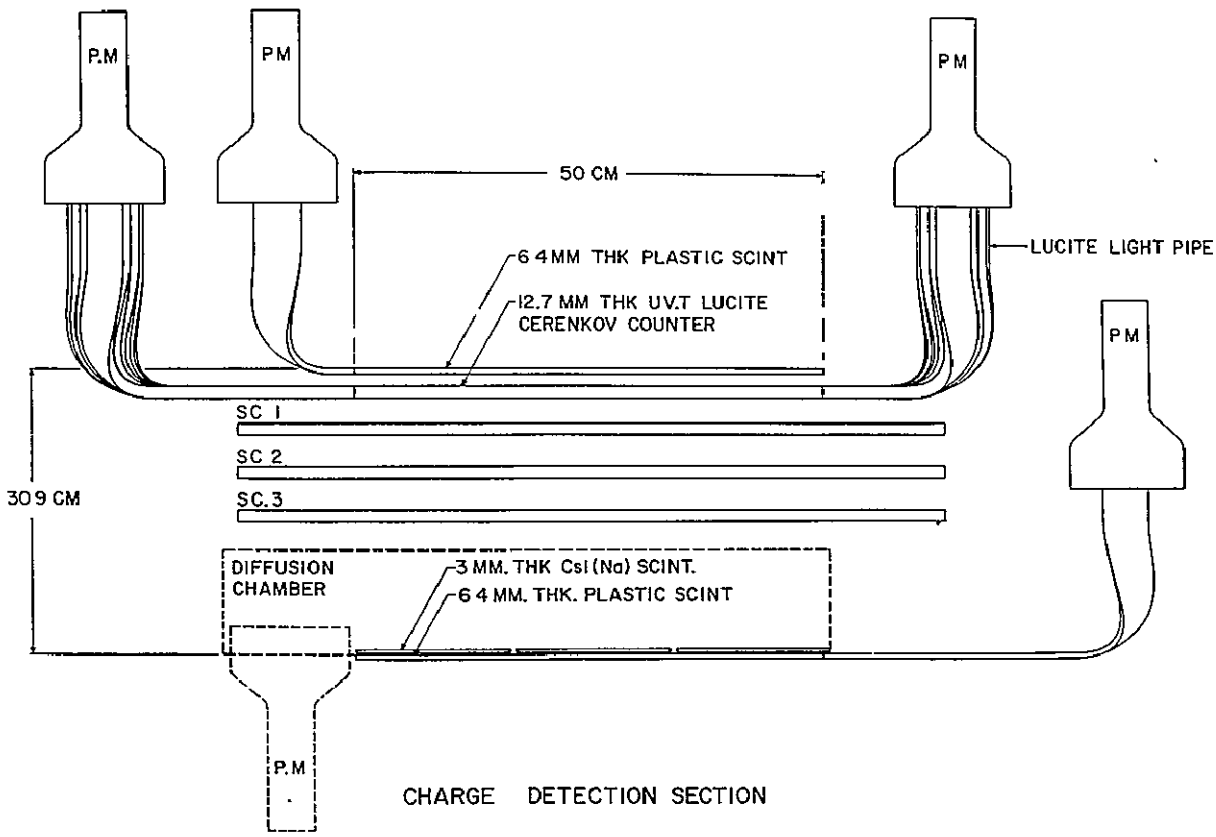

Figure 1. Charge identification module. This view shows the two geometry defining plastic scinitillators, the Cerenkov detector, the three spark chambers and the CsI (Na) scnitillator.

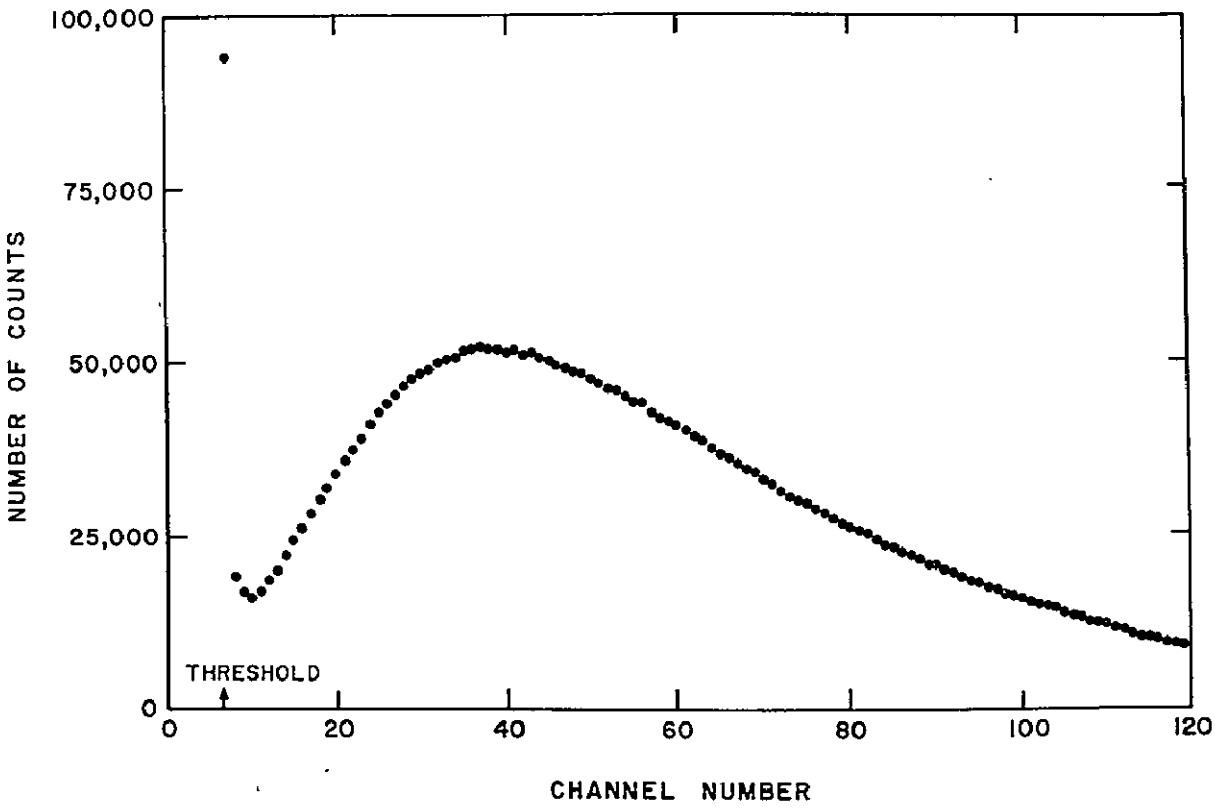

Figure 2. Pulse height distribution obtained with a 1/2-meter square Lucite Cerenkov detector 1 1/4 cm thick. The radiator is viewed edge-on by four 5"- diameter photomultipliers through adiabatic light guides.

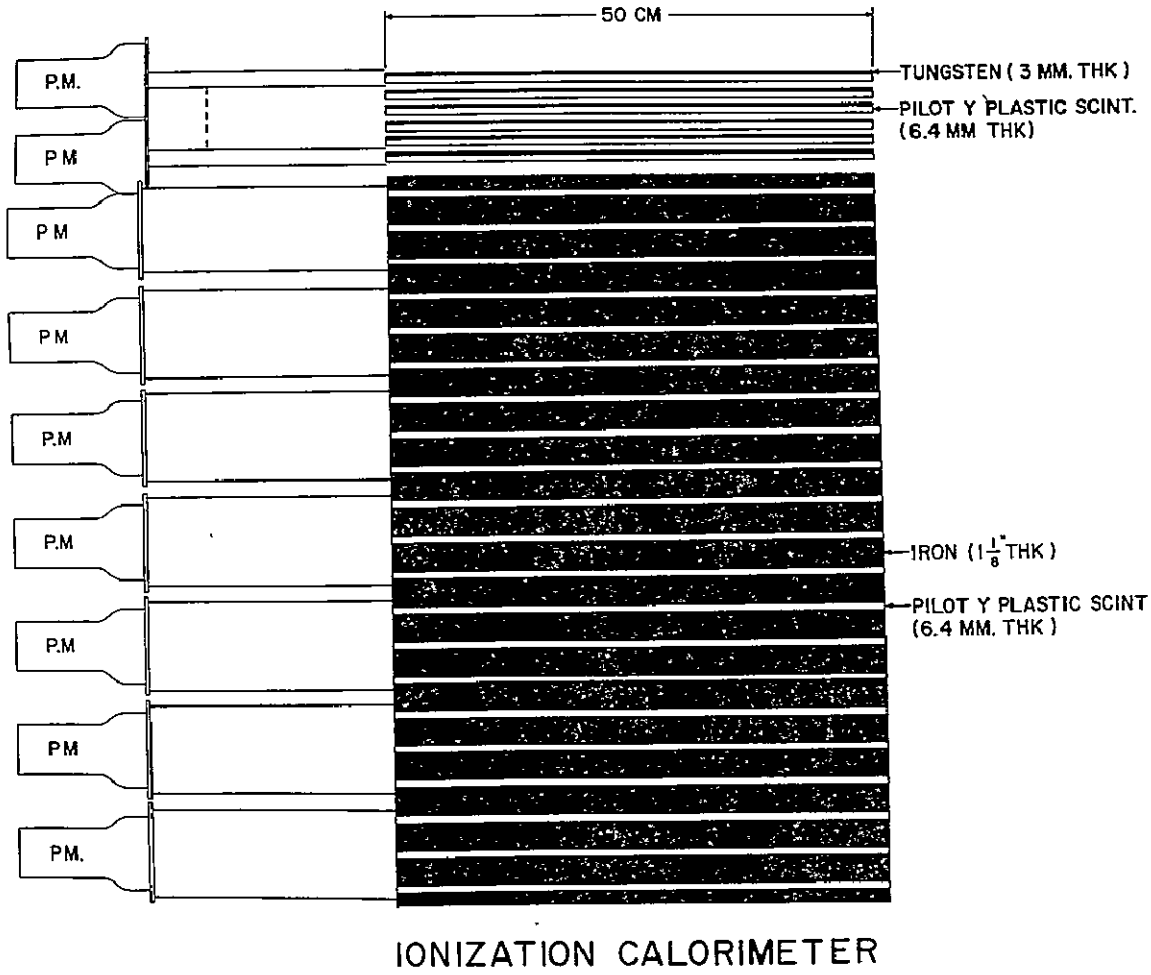

Figure 3. The total ionization calorimeter. The electron cascade section consists of six pieces of tungsten, 1 radiation length thick, followedby Pilot Y plastic scintillators. The nuclear cascade section consists of seven modules, each containing 1/2 a nuclear mean free path of iron and 3 Pilot Y scintillators.

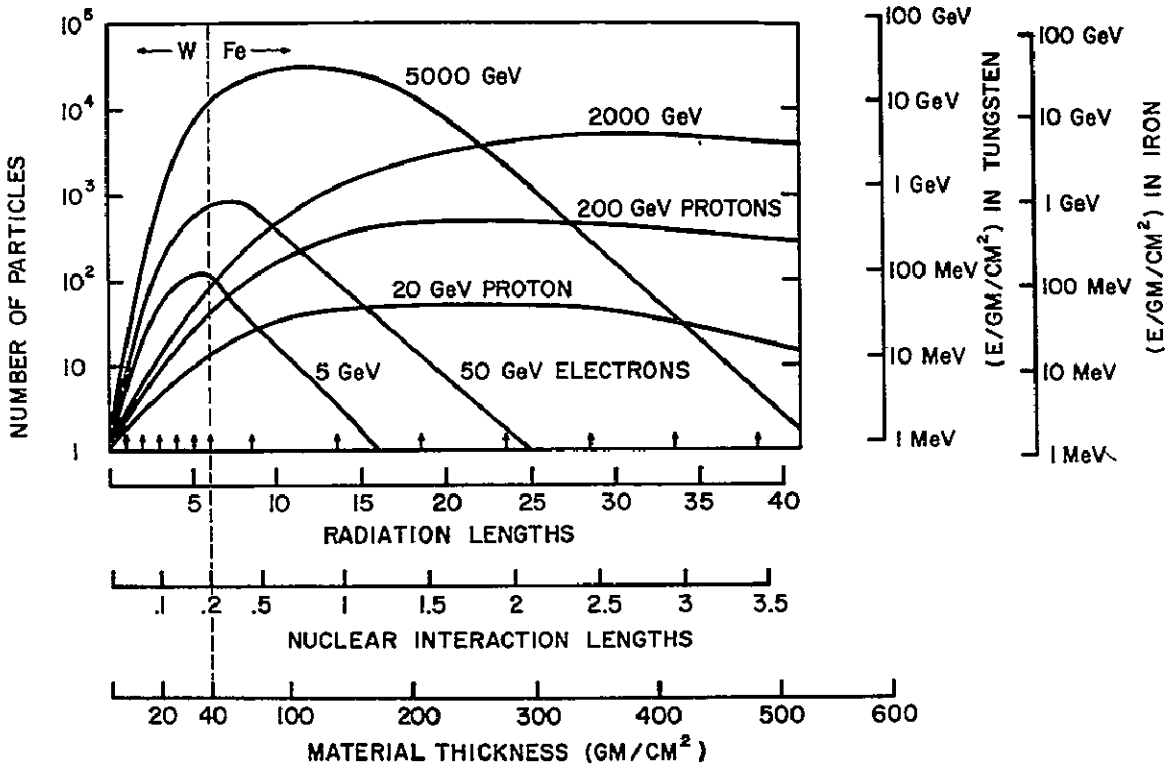

Figure 4. Comparison of the number of particles at various depths in the shower for electrons and protons. Note that electron showers develop and decay away more rapidly then those for protons. The proton shower curves shown here represent the expected average behavior of a large number of events, but for any individual event there will be large fluctuations.

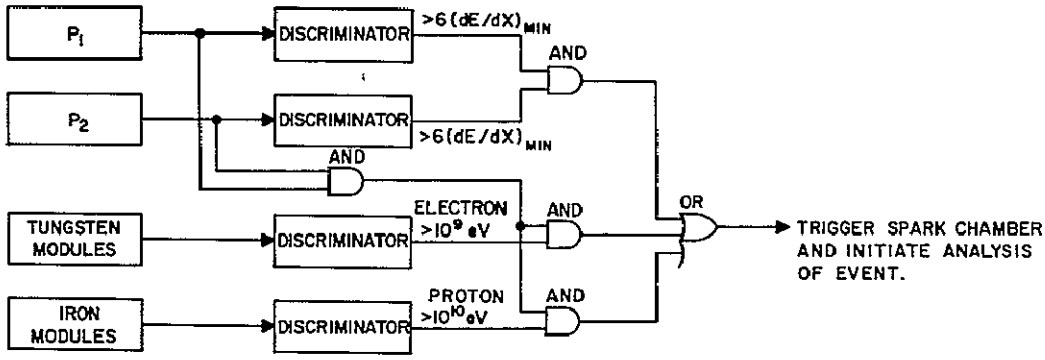

SCHEMATIC DIAGRAM OF EVENT SELECTION REQUIREMENTS

Figure 5. Trigger requirements for the system. For charges $Z > 2$ all events are accepted. The minimum energy requirements for electron and for nucleon showers prevent the system from being overloaded with unwanted events.

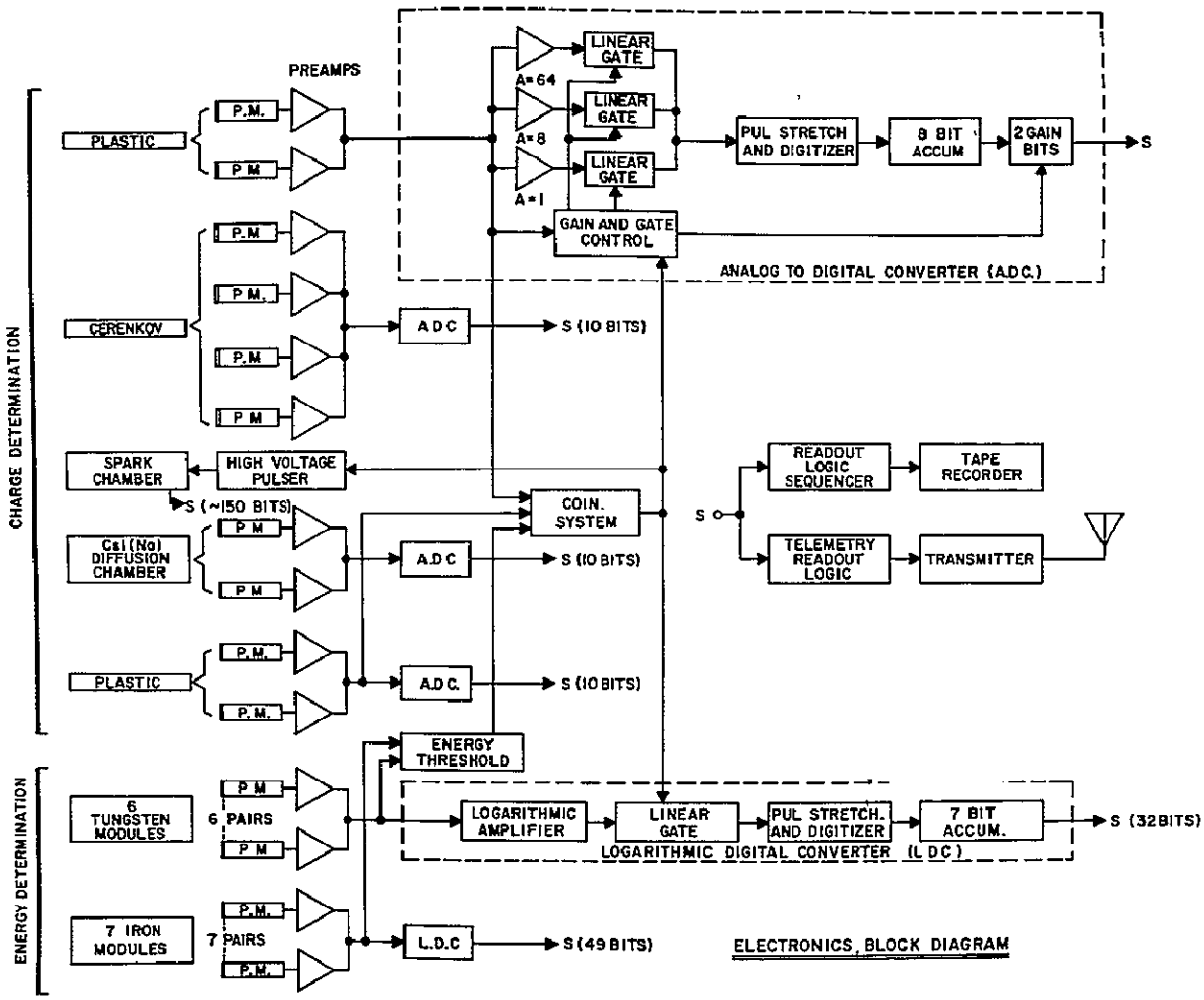

Figure 6. Bloak diagram of the electronics for the experiment.

REFERENCES

Ables, J. G., K. G. McCracken, and U. R. Rao, Proc. IX Intern. Conf. Cosmic Rays, London, 208 (1965).

Agrinier, B., Y. Koechlin, B. Parlier, J. Paul, J. Vasseur, A. Russo, L. Scarsi, Proc. XI Internat'l. Conf. Cosmic Rays, Budapest, OG-71 (1969).

Aizu, L.,and M. Koshiba, Suppl. Prog. Theor. Phys. 31, 150 (1964).

Alexander, J. K., L. W. Brown, T. A. Clark, and R. G. Stone, Astronomy & Astrophysics, to be published (1970).

Anand, K. C., R. R. Daniel, and S. A. Stephens, Nature 217, 25 (1968).

Anand, K. C., R. R. Daniel, and S. A. Stephens, Proc. XI Internat'l. Conf. Cosmic Rays, Budapest, OG-41 (1969).

Anand, K. C., R. R. Daniel, S. A. Stephens, B. Bhowmik, C. S. Krishna, P. C. Mathur, P. K. Aditya, and R. K. Puri, Proc. IX Intern. Conf. Cosmic Rays, London, 1, 362 (1965).

Axford, W. I., Planetary & Space Sciences 13, 115 (1965).

Balasubrahmanyan, V. K., D. E. Hagge, G. H. Ludwig, F. B. McDonald, 1966, J. Geophys. Res. 71, 1771 (1966).

Balasubrahmanyan, V. K., J. F. Ormes, M. J. Ryan, R. F. Silverberg, and R. D. Price, Bul. Am. Phys. Soc. 15, 589 (1970), to be published.

Barrett, P. H., L. M. Bollinger, G. Cocconi, Y. Eisenberg, and K. Greisen, Rev. Mod. Phys. 24, 133 (1952).

Beedle, R. E., J. A. Lezniak, J. A. Rockstroh, and W. R. Webber, Proc. XI Internat'l. Conf. Cosmic Rays, Budapest, OG-22 (1969).

Beznogihk, G. G., A. Buyak, K. I, Iozchev, L. F. Kirillova, T. K. Markov, V. A. Morozov, V. A. Nikitin, P. V. Nomokonov, M. G. Shafranova, V. A. Sviridov, Truong Bien, V. I. Zayachki, N. K. Zhidkov, L. S. Zolin, S. B. Nurushev, and V. L. Solovianov, Physics Letters 30 B, 274 (1969).

Blanford, G. E., Jr., R. L. Fleischer, P. H. Fowler, M. W. Friedlander, F. Klasinore, J. M. Kidd, G. E. Nichols, P. B. Price, R. M. Walker, F. P. Wetel, and W. C. Wells, Proc. XI Intern. Conf. Cosmic Rays, Budapest, paper OG-79 (1969).

Bleeker, J. A. M., J. J. Burger, A. J. M. Deerenberg, A. Scheepmaker, B. N. Swanenburg, and Y. Tanaka, Can. J. Physics 46, 522 (1968).

Bradt, H., M. LaPointe, and S. A. Rappaport, Proc. IX Intern. Conf. Cosmic Rays, London, 2, 651 (1965).

Bradt, H., and S. A. Rappaport, Phys. Rev. Letters 22, 760 (1969).

Brecher, K., and P. Morrison, Phys. Rev. Letters 23, 802 (1969).

Brownlee, R. G., S. A. David, A. J. Fisher, L. Horton, L. Goorvich, P. C. Kohn, C. B. A. McCusker, A. Outred, A. F. Parkinson, L. S. Peak, M. H. Rathgeber, M. J. Ryan, and M. M. Winn, Proc. XI Intern. Conf. Cosmic Rays, Budapest, paper EAS-5 (1969).

Burbidge, E. M., G. R. Burbidge, W. A. Fowler, and F. Hoyle, Rev. Mod. Phys. 24, 547 (1957).

Cancro, C. A., Trans. Nucl. Sci. 16, 90 (1969).

Cancro, C. A., Nucl. Instr. and Methods 73, 61 (1969).

Charpak, G., R. Bouclier, T. Bressani, J. Favier, and C. Zupancic, Nucl. Instr. and Methods 62, 262 (1968).

Cini-Castagnoli, G., M. A. Dodero, and L. Andreis, Can. J. Phys. 46, S839 (1968).

Colgate, S. A., and R. H. White, Proc. VIII Intern. Conf. Cosmic Rays, Jaipur, 3, 335 (1963).

Comstock, G. M., C. Y. Fan, and J. A. Simpson, Astrophys. J. 146, 51 (1966).

Corydon-Petersen, O., B. Dayton, N. Lund, K. Melgaard, K. Omo, B. Peters, and T. Risbo, Danish Space Research Institute, Denmark, preprint (October 1969).

Daniel, R. R., and S. A. Stephens, Proc. XI Internat'l. Conf. Cosmic Rays, Budapest, OG-102 (1969).

Daniel, R. R., and N. Sreenivasan, Nuovo Cimento 35, 391 (1965).

Daniel, R. R., P. J. Lavakare, and S. Ramadurai, Cosmic Ray Studies in Relation to Recent Developments in Astronomy and Astrophysics, Tata Institute of Fundamental Research, Bombay (November 1968).

Doggett, J. A., and L. V. Spencer, Phys. Rev. 103, 1956 (1957).

Durgaprasad, N., Ph.D. Thesis, Bombay Univ., 1964.

Earl, J., and A. Lenchek, Astrophys. J. 157, 87 (1969).

Earl, J., Bul. Am. Phys. Soc. 15, 564 (1970), to be published.

Ehrmann, C. H., C. E. Fichtel, D. A. Kniffen, and R. W. Ross, Nucl. Instr. and Methods 56, 109 (1967).

Elliott, H., T. Thambyahpillai, and P. S. Peacock, Imperial College of Technology, preprint (1970).

Fan, C. Y., G. Gloeckler, and J. A. Simpson, Can. J. Phys. 46, 548 (1968).

Fanselow, J. L., R. C. Hartman, P. Meyer, and P. Schmidt, Proc. XI Intern. Conf. Cosmic Rays, Budapest, paper OG-25 (1969).

Fanselow, J. L., R. C. Hartman, R. H. Hildebrand, and P. Meyer, Bul. Am. Phys. Soc. 15, 592 (1970), to be published.

Fleischer, R. L., P. B. Price, R. M. Walker, M. Mauretti, and G. Morgan, J. Geophys. Res. 22, 355 (1967).

Fowler, P. H., private communication (1970).

Fowler, P. H., and C. J. Waddington, Phil. Mag. 1, 637 (1956).

Fowler, P. H., R. A. Adams, V. G. Cowan, and J. M. Kidd. Proc. Royal Soc. 34, 39 (1967).

Fowler, P. H., V. M. Claphan, J. M. Kidd, and R. T. Moses, Proc. XI Intern. Conf. Cosmic Rays, Budapest, paper OG-111 (1969).

Garcia-Muñoz, M., and J. A. Simpson, Proc. XI Intern. Conf. Cosmic Rays, Budapest, paper OG-66 (1969).

Gillespie, C. R., R. W. Huggett, and W. V. Jones, Nucl. Instr. and Methods, in press (1970).

Goza, E. R., S. Krzywdzinski, and E. G. Stafford, Rev. Sci. Instr. 41 219 (1970).

Greisen, K., Ann. Rev. Nucl. Sci. 10, 63 (1960).

Grigorov, N. L., V. Murzin, I. D. Rapoport, Soviet Physics, JETP, 7, 348 (1958).

Grigorov, N. L., V. E. Nesterov, I. D. Rapoport, I. A. Savenko, and G. A. Skaridin, Proc. X Internat'l. Conf. Cosmic Rays, Calgary, 512 (1967).

Grigorov, N. L., V. E. Nesterov, I. D. Rapoport, I. A. Savenko, G. A. Skuridin, and A. F. Tikenkov, Proc. XI Intern. Conf. Cosmic Rays, Budapest, paper OG-99 (1969).

Grigorov, N. L., A. U. Podgarskaya, L. V. Poperkova, and Z. H. Sonelyeva, Ekspi Teoret. Fiz. 35, 3 (1959).

Hagge, D. E., V. K. Balasubrahmanyan, and F. B. McDonald, Can. J. Phys. 46, 539 (1968).

Halpern, O., and H. Hall, Phys. Rev. 57, 459 (1940).

Halpern, O., and H. Hall, Phys. Rev. 73, 477 (1948).

Heidbreder, E., K. Pinkau, C. Reppin, and V. Schönfelder, to be published.

Hofstadter, R., Science 164, 1471 (1969).

Jain, P., H. Glake, J. Rinoldo, and P. Bharadwaj, Nucl. Phys. 67, 641 (1965).

Jain, P. L., E. Lohrmann, M. W. Teucher, Phys. Rev. 115, 654 (1959).

Jones, F., GSFC Preprint X-641-70-129, to be published.

Jones, W. V., Phys. Rev. 187, 1868 (1969).

Jones, W. V., Phys. Rev., in press (1970).

Jones, W. V., K. Pinkau, U. Pollvogt, W. K. H. Schmidt, and R. W. Huggett, Nucl. Instr. and Methods 72, 173 (1969).

Kaplon, M. F., and D. M. Ritson, Phys. Rev. 88, 386 (1952).

Keuffel, J. W., J. L. Osborne, G. L. Bolingbroke, G. W. Mason, M. O. Larson, G. H. Low, J. H. Parker, R. O. Stenerson, and H. E. Bergeson, Proc. XI Intern. Conf. Cosmic Rays, Budapest, paper MU-31 (1969).

Kinsey, J. H., Astrophys. J. 158, 295 (1969).

Koshiba, M., E. Suda, and F. Takasaki, Can. J. Phys. 46, S561 (1968).

Lal, D., Proc. Indian Acad. Sci. 38A, 93 (1953).

Lezniak, J. A., T. T. von Rosenvinge, and W. R. Webber, Proc. XI Intern. Conf. Cosmic Rays, Budapest, paper OG-68 (1969).

Lietti, B., and J. J. Quenby, Can. J. Phys. 46, S942 (1968).

Long, C. E., M. S. Thesis, Univ. of Minnesota, unpublished (1968).

Malhotra, P. K., Proc. VIII Intern. Conf. Cosmic Rays, Jaipur, 5, 40 (1963).

Marar, T. M. K., P. S. Freier, and C. J. Waddington, Proc. XI Intern. Conf. Cosmic Rays, Budapest, paper OG-23 (1969).

Marsden, P. L., J. B. Crowden, R. Jakeways, and I. R. Calder, Proc. XI Internat'l. Conf. Cosmic Rays, Budapest, OG-38 (1969).

McCracken, K. G., and U. R. Rao, Proc. IX Intern. Conf. Cosmic Rays, London, 1, 213 (1965).

McDonald, F. B., Phys. Rev. 109, 1367 (1958).

Meldner, H., Arkiv Fysik 36, 593 (1967).

Meyer, P., Annual Rev. Astron. & Astrophys. 7, 1 (1969).

Murthy, P. V. R., Nucl. Instr. and Methods 63, 77 (1968).

Murzin, V. S., and L. I. Sarychena, NASA TTF-594 (1969).

Myers, W. D., Nucl. Phys. 81, 1 (1966).

Nikolsky, S. J., Usp. Fiz. Nauk. 78 (5), 365 (1962).

Nilson, S. G., Physics Letters 28B, 458 (1969).

Nishimura, J., E. Mikumo, I. Mito, K. Niu, I. Ohta, and T. Taira, Proc. XI Internat'l. Conf. Cosmic Rays, Budapest, OG-43 (1969).

O'Connell, R. F., and S. D. Verma, Phys. Rev. Letters 22, 1443 (1969).

O'Dell, F. W., M. M. Shapiro, R. Silberberg, B. Stiller, C. H. Tsao, N. Durgaprasad, C. E. Fichtel, D. E. Guss, and D. V. Reames, Proc. XI Intern. Conf. Cosmic Rays, Budapest, paper OG-85 (1969).

Oran, W. A., G. M. Frye, C. P. Wang, J. Geophys. Res. 74, 53 (1969).

Ormes, J. F., V. K. Balasubrahmanyan, R. D. Price, M. J. Ryan, and R. F. Silverberg, GSFC X-661-70-106; Trans. Nucl. Sci., in press (1970).

Ormes, J. F., and W. R. Webber, Proc. IX Internat'l. Conf. Cosmic Rays, London, 1, 349 (1965).

Ormes, J. F., and W. R. Webber, J. Geophys. Res. 73, 4231 (1968).

Parker, E. N., Interplanetary Dynamical Processes, Interscience, New York, (1964).

Parker, E. N., Astrophys. J. 142, 584 (1965).

Patel, D., V. Sarabhai, and G. Subramanian, Planet. Space Sci. 16, 131 (1968).

Peacock, D. C., J. C. Dutt, and T. Thambyahpillai, Can. J. Phys. 46, S788 (1968).

Pinkau, K., Phys. Rev. 139, 1548 (1965).

Pinkau, K., R. W. Huggett, and S. D. Verma, unpublished proposal (1968).

Pinkau, K., U. Pollvogt, W. K. H. Schmidt, R. W. Huggett, Proc. XI Intern. Conf. Cosmic Rays, Budapest, paper OG-61 (1969).

Pinkau, K., C. Reppin, and V. Schönfelder, Nucl. Instr. and Methods 49, 13 (1967).

Pollvogt, U., Ph.D. Thesis, Technische Hochschule München (1970).

Powell, C. F., P. H. Fowler, and D. H. Perkins, The Study of Elementary Particles by the Photographic Method, Pergamon Press, New York, (1959).

Price, P. B., R. L. Fleischer, D. D. Peterson, C. O'Ceallaigh, D. O'Sullivan, and A. Thompson, Phys. Rev. Letters, 21, 630 (1968).

Ramaty, R., D. V. Reames, and R. E. Lingenfelter, Phys. Rev. Letters 24, 913 (1970).

Rappaport, S. A., and H. V. Bradt, Phys. Rev. Letters 22, 960 (1969).

Reames, D. V., and C. E. Fichtel, Phys. Rev. 162, 1291 (1967).

Ritson, D. M. Techniques of High Energy Physics, Interscience Publishers, New York (1961).

Roelof, E., APS Division of Cosmic Physics, Washington, D.C. (April 1970).

Rogers, I. W., M. G. Thompson, M. J. L. Turner, and A. W. Wolfendale, J. Phys. Soc. 2, 365 (1969).

Rosette, K. H., M. R. Farukhi, G. R. Kramer, C. Swinehart, and R. Hofstadter, Trans. Nucl. Sci., in press (1970).

Ross, R. W., C. H. Ehrmann, C. E. Fichtel, D. A. Kniffen, and H. B. Ogdman, Trans. Nucl. Sci. 16, 127 (1969).

Rubstov, V. I., N. S. Svirjewsky, and V. I. Zatsepin, Proc. XI Internat'l. Conf. Cosmic Rays, Budapest, OG-39 (1969).

Schmidt, W. K. H., Ph.D. Thesis, Kiel Univ. (1969).

Schmidt, W. K. H., K. Pinkau, U. Pollvogt, and R. W. Huggett, Phys. Rev. 184, 1279 (1969).

Semikoz, V. B., JETP Letters 9, 3243 (1969).

Shapiro, M. M., and R. Silberberg, Proc. XI Intern. Conf. Cosmic Rays, Budapest, paper OG-88 (1969).

Shivanandan, K., J. R. Hauck, and M. O. Harwitt, Phys. Rev. Letters 21, 1460 (1968).

Silverberg, R. F., J. F. Ormes, and V. K. Balasubrahmanyan, to be published (1970).

Smith, L. H., Proc. X Intern. Conf. Cosmic Rays, Calgary, 506 (1967).

Somogyi, A. J., Annals of the IQSY 4, (1968).

Sternheimer, R. M., Phys. Rev. 91, 256 (1953).

Sternheimer, R. M., Phys. Rev. 103, 511 (1956).

Subramanian, G., and V. Sarabhai, Astrophys. J. 149, 417 (1967).

Teegarden, B. J., F. B. McDonald, and V. K. Balasubrahmanyan, Proc. XI Intern. Conf. Cosmic Rays, Budapest, paper OG-71 (1969).

Thambyahpillai, T., and J. C. Dutt, Proc. IX Intern. Conf. Cosmic Rays, London, 1, 257 (1965).

Trümper, J., private communication (1970).

von Rosenvinge, T. T., W. R. Webber, and J. F. Ormes, Astrophysics and Space Science 3, 4 (1969).

von Rosenvinge, T. T., Ph.D. Thesis, Univ. of Minn., to be published (1970).

Webber, W. R., Rapporteur paper, Proc. XI Intern. Conf. Cosmic Rays, Budapest, 1969.

Webber, W. R., and J. Kish, Bul. Am. Phys. Soc. 15, 620 (1970), to be published.

Webber, W. R., and J. F. Ormes, J. Geophys. Res. 72, 5957 (1967).

Wentzel, D. G., Astrophys. J. 156, 303 (1969).

White, H., and D. Lokerson, IMP-I Encoding System Interface Document, Code 711, GSFC/NASA (Feb. 1970).

Yuan, L. C., Bull. Am. Phys. Soc. 13, 555, 1968.

Yuan, L. C. L., Trans. Nucl. Sci., in press (1970).

NASA–GSFC COML., ARL., VA.